UNIVERSIDAD COMPLUTENSE DE MADRID
FACULTAD DE MEDICINA
Departamento de Microbiología I

TESIS DOCTORAL

Macrófagos en tolerancia inmunológica

MEMORIA PARA OPTAR AL GRADO DE DOCTOR

PRESENTADA POR

Patricia Conde San Román

Director

Jordi Cano Ochando

Madrid 2019

UNIVERSIDAD COMPLUTENSE DE MADRID

FACULTAD DE MEDICINA

Departamento de Microbiología I

MACRÓFAGOS EN TOLERANCIA INMUNOLÓGICA

MEMORIA PARA OPTAR AL GRADO DE DOCTOR

PRESENTADA POR

PATRICIA CONDE SAN ROMÁN

Dirigida por el doctor

Jordi Cano Ochando

Madrid, 2018

Macrófagos en tolerancia inmunológica

Patricia Conde San Román

Este trabajo ha sido realizado en la Unidad de Inmunología del Trasplante en el Instituto de Salud Carlos III, con ayuda de los proyectos SAF-2013-48834-R Y SAF2016-80031-R del programa estatal de Investigación, Desarrollo e Innovación orientada a Retos de la Sociedad en el marco del Plan Estatal de Investigación Científica-Técnica y de Innovación 2013-2016.

Para llegar a conseguir la realización de este trabajo han sido importantes muchas personas a las que debo mi agradecimiento:

En primer lugar a Jordi por permitirme trabajar a su lado desde los primeros momentos; casi como dice la canción "*en otra vida, en otro mundo, pero a tu lado*". Momentos personalmente duros llenos de inseguridad e inexperiencia pero a la vez con una enorme dosis de aprendizaje y trasmisión de conocimientos. Nunca se sabe cual va a ser el punto de inflexión en la vida que te haga cambiar de rumbo, y esos primeros momentos fue uno de ellos. Así que no tengo nada más que decir que *"prometo estarte agradecida".*

A mi pareja, compañero de viaje, por aguantarme y acompañarme durante tanto tiempo siempre con una sonrisa, la mejor de las terapias. Ya sabes que "*A veces tengo la cabeza como inerte, A veces tengo la certeza de tenerte Y me endulzaron las heridas con los peces Y tengo una pecera solo pa beberte"…*

A mis progenitores, que con tanto esfuerzo me han ayudado a construir uno de los pilares más importantes de la vida. *"Papá cuéntame otra vez ese cuento tan bonito…"* Me han contado y enseñado valores con los que construir un pensamiento crítico. En un mundo donde todo se compra y se vende, se manipula y se corrompe, la educación "sin títulitis" es imprescindible.

No quiero acabar sin dejar de recordar a familiares y amig@s*. "Hemen gaude, ta poztutzen naiz…*" La nostalgia y los buenos recuerdos siempre me llevan a ell@s. Crecimos y aprendimos; vivimos y nos hicimos mayores, "*ta berriz izango gara ZORIONTSU edozein herriko jaixetan. Lau teilatu gainean…"*

Eskerik asko denori, bihotzez maite zaituztet

“Enseñarás a volar

pero no volarán tu vuelo.

Enseñarás a soñar,

pero no soñarán tu sueño.

Enseñarás a vivir

pero no vivirán tu vida.

Sin embargo…

en cada vuelo,

en cada vida,

en cada sueño,

perdurará siempre la huella

del camino enseñado ”

M.Teresa de Calcuta

ÍNDICE

RESUMEN

En estudios previos llevados a cabo en el laboratorio (1) se identificó una población celular derivada de monocitos que se acumulaban en los órganos trasplantados durante tolerancia. La caracterización de este conjunto de células demuestra que fenotípicamente expresan CD11b, receptor del factor estimulante de colonias (CSF1), CD169 y glicoproteínas de superficie de complejo 6 de antígeno linfocitico, locus C (Ly6C) y/o locus G (Ly6G). Ambas proteínas Ly6 forman parte de la súper familia Gr-1. Ly6C se expresa en el 50% de las células T $CD8^+$, neutrófilos y monocitos tanto en médula ósea como en órganos linfoides periféricos y está sobre regulada por interferón alfa (IFN-α), IFN- β e IFN-Ɣ. (2). Por el contrario, Ly6G se expresa principalmente en granulocitos de medula ósea. El análisis genómico revela que estas células $CD11b^+CSF1R^+Ly6C^{lo}Ly6G^-CD169^+$ aisladas de órganos tolerizados corresponden a macrófagos supresores con capacidad de modificar la respuesta inmune favoreciendo un ambiente inmunodeprimido indispensable para la aceptación de los órganos. La función supresora de esta población celular se basa predominantemente en la capacidad de inhibir la proliferación in vitro de las células T $CD8^+$ y favorecer la inducción de las células T reguladoras (Treg). Uno de los mecanismos de acción de los macrófagos supresores propuesta en la tesis se lleva a cabo mediante la proteína de membrana específica de células dendríticas ICAM-3-grabbing non integrin (DC-SIGN, CD209a) implicada además en múltiples aspectos relacionados con la función inmune (3). Estructuralmente DC-SIGN es una proteína de transmembrana de tipo II con un dominio extracelular carbohidrato (CRD) cuya función es el reconocimiento específico de glicolípidos con alto contenido en manosa (Man), fucosa(Fuc) y N-acetil glucosamina (GlcNAc) presentes tanto en patógenos como en células y tejidos propios. DC-SIGN requiere de ligandos ricos en residuos Man y Fuc como Lewis X (Le^x) (4) para regular la función inmune de los macrófagos supresores. Esta interacción produce un aumento de interleuquina 10 (IL-10) y una disminución de citoquinas pro inflamatorias, contribuyendo al establecimiento de un ambiente tisular inmuno deprimido que favorece la tolerización de trasplantes (5, 6). El papel de DC-SIGN

tiene una doble cara ya que su interacción con células tumorales y patógenos les proporciona una vía de escape inmunológico. Dada su función de "receptor de adhesión" DC-SIGN brinda a los agentes infecciosos una vía de escape al sistema inmune mediante la internalización de estructuras glicosiladas presentes en las paredes celulares de algunos patógenos como el virus del VIH, Mycobacterium tuberculosis, Hepatitis C, etc. (7, 8). Distintos autores han demostrado también que DC-SIGN media la interacción de monocitos y macrófagos con las células tumorales vía Le^x favoreciendo la progresión tumoral (9). Le^x también denominado syalil- Lewis X o CD15 es un glicolípido de superficie rico en fucosa, ligando de DC-SIGN. Constituye uno de los grupos de antígenos de la sangre más importante y se acumula en los tejidos durante procesos inflamatorios y cancerígenos. Sabemos que la doble señalización mediante DC-SIGN TLR4 es indispensable para una producción óptima de IL10 (10). Acorde con ello, sugerimos que la inducción de la tolerancia en trasplantes mediados por macrófagos supresores vía DC-SIGN depende de dicha señalización simultánea con TLR4. Explorando el novedoso concepto de la "inmunidad entrenada" estudiamos una nueva vía para inhibir el rechazo al órgano trasplantado mediante el uso de nano particulas. Nuestro laboratorio ha desarrollado una nano terapia mTOR (mamalian target of rapamicyn) basada en nano partículas lipoproteicas de alta densidad (HDL) con afinidad especifica por los macrofagos capaces de evitar los cambios fenotípicos asociados con la inmunidad entrenada. Estos cambios fenotípicos se caracterizan por un aumento en la producción de citoquinas y chemoquinas pro inflamatorias como por ejemplo, TNF-ϒ, IL-6 e IL-1β. Inesperadamente observamos que la terapia inhibitoria de mTOR con rapamicina (mTORi-HDL) inducía la expresión de CD40 en los macrofagos reguladores. Por ello desarrollamos una segunda terapia con nano particulas basada en el bloqueo de la vía TRAF6 (TRAF6i-HDL) responsable de la señalización CD40-CD40L. Distinto experimentos in vivo mostraron que la administración sistémica de las nano partículas mTORi-HDL combinadas con TRAF6i-HDL favorecían supervivencia prolongada del órgano trasplantado.

SUMMARY

In previously work, our laboratory characterized a monocyte-derived cells population that accumulated in cardiac allograft during tolerance induction (1).This cells population co-expressed CD11b, colony-stimulating factor (CSF1), CD169 and the lymphocytic antigen surface glycoproteins complex 6, locus C (Ly6C) and locus G (Ly6G). Both Ly6 proteins belong to Gr-1 super-family. Ly6C is expressed in the 50% of $CD8^+$ T cells, neutrophils and monocytes in bone marrow (BM) and periphery lymphoid organs and it is upregulated by IFN-α, IFN- β e IFN-ɣ (2). On the contrary, Ly6G is mainly expressed in BM derived granulocytes. The gen array reveals that $CD11b^+CSF1R^+Ly6C^{lo}Ly6G^-CD169^+$ cells isolated from tolerized allograft are macrophages with an immune suppressive function based on the inhibitory capacity of T cell proliferation and favoring the regulatory T cells (Treg) expansion. Mechanistically we demonstrated that dendritic cell-specific ICAM-grabbing non-integrin (DC-SIGN, CD209a) is upregulated in $CD11b^+CSF1R^+Ly6C^{lo}Ly6G^-CD169^+$ cells, which is implicated in suppressive function and many other immune facet (3). Structurally DC-SIGN is a type II transmembrane protein with an extracellular carbohydrate recognition domain (CRD) with a strong affinity for high mannose (Man), fucose (Fuc) and N-acetylglucosamine (GlcNAc) glycolipids, localized in either pathogens or self-cells and tissues. DC-SIGN binds to carbohydrates containing Man or Fuc residues, such as Lewis x (Le^x) (4) to regulate the immune function in the suppressive macrophages. This binding enhance the interleukin 10 (IL-10) and decreases the proinflammatory cytokines production, maintaining a suppressive environment and favoring the allograft acceptance in transplantations (5, 6). DC-SIGN has a double cutting edge, providing an immune scape to pathogens and tumor cells. Because of his “receptor adhesion” capacity, provides a way to scape from immunity to the infection agents due to the internalization of the glycosylated structures localized on the cell wall of pathogens like, VIH, Mycobacterium tuberculosis, Hepatitis C, etc. (7, 8). Other authors have shown the interaction of monocytes and macrophages with tumor cells mediated by DC-SIGN, favoring the tumor progression (9). Le^x also named syalil – Lewis x or CD115 is a

glycolipid rich on fucoses and is one of the principal blood antigens which is accumulated on tissues during inflammatory and cancer processes. We know that DC-SIGN signaling crosstalk with TLR4 is required for the optimal IL-10 production (10). According to this, we suggest that induction of transplantation mediated by DC-SIGN^{+} suppressive macrophages depends on simultaneous TLR4 signaling. We also studied the novel "trained immunity" concept as a way to prevent allograft rejection using nano therapy. Our laboratory developed a mammalian target of rapamicyn (mTOR) nano immunotherapy based on high-density (HDL) nanoparticles to specifically target macrophages and prevent phenotype modifications associated with trained immunity. These phenotypic modifications are characterized by an enhanced of pro inflammatory cytokines like, TNFɣ, IL6 and IL1β. Unexpectedly, mTOR inhibitor rapamicyn (mTORi-HDL) therapy induces the expression of CD40 in regulatory macrophages. With this in mind we develop a second nano particles therapy consisting of blocking CD40 mediated TRAF6 signaling pathway (TRAF6i-HDL). We found that preventing macrophages' trained immunity phenotype trough systemic administration of specific mTORi-HDL in combination with TRAF6i-HDL nano immunotherapy resulted in indefinite allograft survival.

OBJETIVOS e HIPÓTESIS DE TRABAJO

El objetivo de esta tesis ha sido identificar y caracterizar la población celular de origen mieloide involucrada en la aceptación del órgano trasplantado durante tolerancia. Utilizando un modelo experimental murino de trasplante cardiaco, identificamos los factores que influyen en el desarrollo de los macrofagos supresores así como los mecanismos de acción durante tolerancia. Adicionalmente, investigamos la acción de la inmunidad entrenada de los macrofagos en los órganos trasplantados y exploramos el uso terapéutico de la nano terapia como herramienta de control in vivo sobre la función supresora de los macrofagos durante tolerancia.

CAPITULO I: Fenotipo, desarrollo y mecanismos de acción de macrofagos en tolerancia

Basándonos en nuestros resultados previos y sabiendo que el Gr-1 reconoce independientemente dos marcadores de superficie, Ly6C y Ly6G hemos caracterizado una población celular específica que se acumula durante tolerancia en los órganos trasplantados. En nuestro trabajo proponemos la hipótesis que los monocitos inflamatorios $Ly6C^{hi}$ infiltran el órgano trasplantado y se diferencian a macrofagos supresores $Ly6C^{lo}$. Esta conversión requiere el bloqueo de la vía co-estimulatoria CD40L-CD40 que resulta en una inhibición parcial de IFN-ɣ. Además, dicha conversión requiere obligatoriamente la presencia de CSF1, cuya acción sobre la polarización de los macrofagos (11) y la inducción de la función supresora (12) ha sido previamente demostrada. Mecanisticamente demostramos que DC-SIGN se encuentra sobre expresado en los macrofagos supresores $CD11b^{+}CSF1R^{+}Ly6C^{lo}Ly6G^{-}CD169^{+}$ y que se necesita una señalización simultanea de DC-SIGN mediante sus ligandos fucosilados y TLR4 para producir una cantidad óptima de citoquina supresora IL-10 asociada con la supervivencia de los órganos en trasplantes.

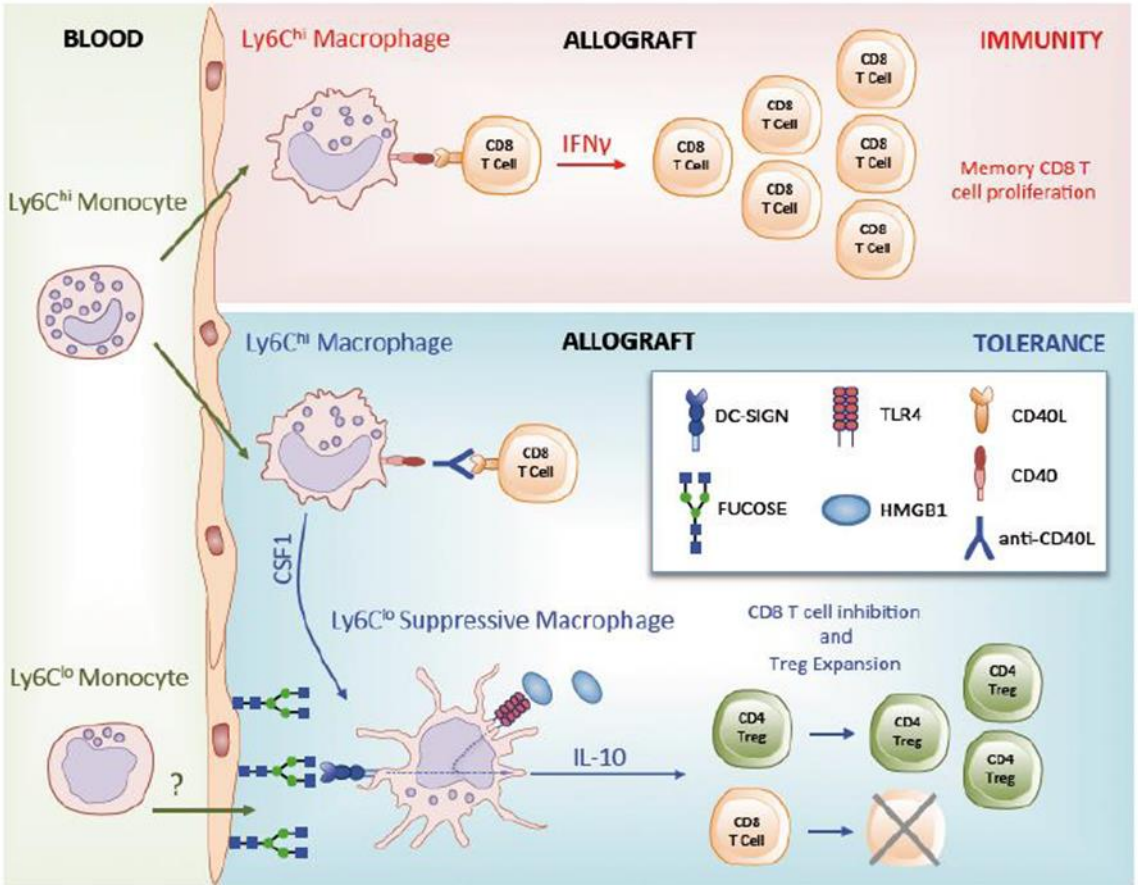
BLOOD
Ly6C^hi Macrophage
ALLOGRAFT
IMMUNITY
Ly6C^hi Monocyte
CD8 T Cell
IFNγ
Memory CD8 T cell proliferation
Ly6C^hi Macrophage
ALLOGRAFT
TOLERANCE
DC-SIGN
TLR4
CD40L
FUCOSE
HMGB1
CD40
anti-CD40L
CSF1
Ly6C^lo Suppressive Macrophage
CD8 T cell inhibition and Treg Expansion
Ly6C^lo Monocyte
IL-10
CD4 Treg
?

CAPITULO II: Nano inmunoterapia en tolerancia

El objetivo del segundo capitulo de la tesis ha sido estudiar el efecto de la nano inmunoterapia mTOR durante el trasplante de órganos. Conociendo la implicación de la ruta mTOR en la regulación de la inmunidad entrenada (13, 14) nos planteamos la hipótesis de utilizarla en nuestro modelo experimental de trasplante cardiaco como herramienta para inhibir la inmunidad entrenada en los macrofagos y prevenir los cambios epigenéticos y fenotípicos, responsables del rechazo del órgano. Con el objetivo de evitar la expresión nociva de CD40 por los macrofagos, se desarrolló una segunda nano inmunoterapia DC40-TRAF6 que consistía en el bloqueo de la vía co-estimulatoria CD40L-CD40.

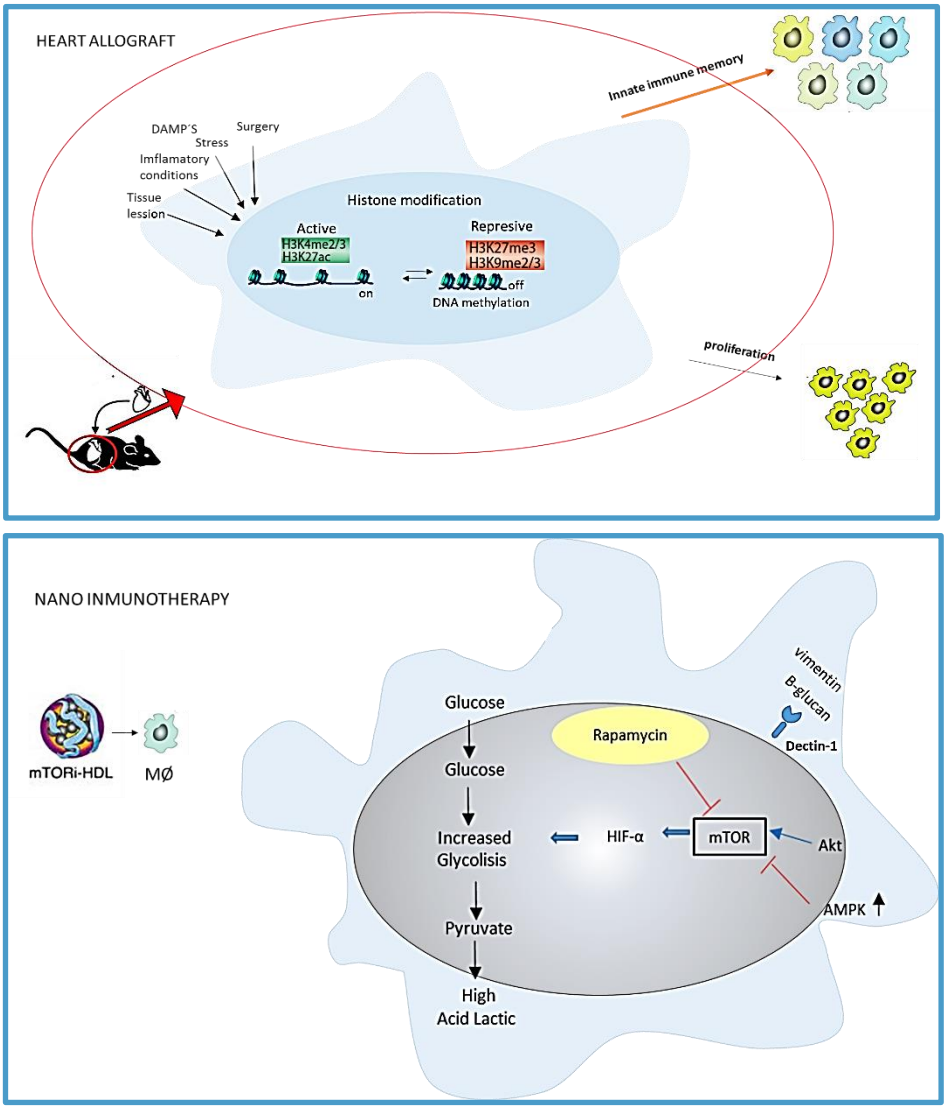

INTRODUCCIÓN

PERSPECTIVA HISTORICA

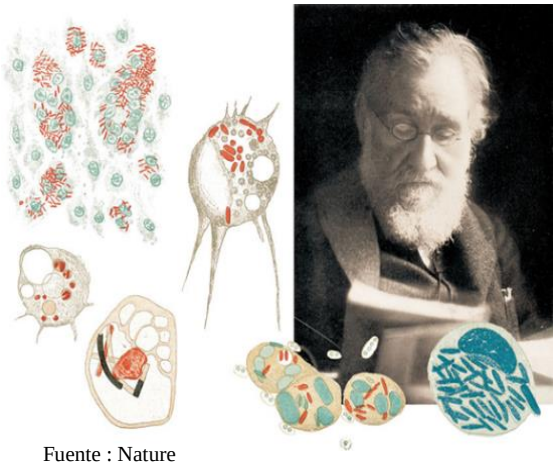

Fuente : Nature

El Sistema Mononuclear Fagocítico (SMF) fue descubierto hace más de un siglo por el premio Novel Ilya Metchnikoff (1882). Metchnikoff clasificó a las células del SMF en dos grandes grupos; los macrófagos, del Griego “grandes comedores” y los microfagos “pequeños comedores”, hoy conocidos como leucocitos. Atribuía a los macrófagos no solo la capacidad de fagocitar sino características muy importantes para el desarrollo, la homeostasia y protección del hospedador frente a infecciones, lo que hoy en día conocemos como “inmunidad innata” (15). A lo largo de la historia de la medicina el SMF ha sufrido varias redefiniciones y los macrófagos han sido denominados de distintas formas dependiendo de las diferentes opiniones sobre su función. Por ello existen multiples sinónimos que los definen como por ejemplo: eritrofagocito, célula pirrol, célula de la adventia, polyblasto, histiocito y clasmatocito.

Table 1. The reticuloendothelial system (RES) of Aschoff

Increase of phagocytic activity ↓	Endothelial cells		
	Fibrocytes		
	Reticular cells of spleen and lymph nodes	RES in a strict sense	RES in a wider sense
	Reticuloendothelial cells of lymph and blood sinuses, including Kupffer cells		
	Histiocytes		
	Splenocytes and monocytes		

fuente: Ital J Anal Embryol.

Fue Aschoff quien en 1924 desarrolló más ampliamente el concepto, describiendo distintos tipos celulares dentro del nuevo Sistema Reticulo endotelial (SRE). La clasificación de las células del SRE se basaba exclusivamente en su capacidad fagocítica,

constituyéndose dos grupos principales; células del SRE en un sentido estricto y células del SRE en un amplio sentido. Esta nueva clasificación excluía a las células endoteliales y fibrocitos debido a su baja capacidad fagocítica (16). En 1949 J.A Thomas (17) reintrodujo el termino Sistema Reticulohistiocitico (SRH) previamente propuesto por Volterra (18). Thomas clasificaba a las células del SRH no solo por su actividad fagocítica sino por su capacidad de favorecer la proliferación y el crecimiento celular. De esta forma incluía en la nueva clasificación todas las células capaces de adquirir un estado histiocitico, lo cual no solo se limitaba a las células del tejido conectivo sino que también incluían células del musculo liso y estriado, células óseas y células epiteliales. No fue hasta el año 1969 cuando se acuñó por primera vez el término de Sistema Mononuclear Fagocítico (SMF) para describir el concepto más moderno de lo que hoy en día conocemos. Durante la conferencia llevada a cabo en 1929 en Los Paises Bajos, un comité de expertos, en los que se incluyen Ralph van Furth, James G.Hirsch y Zanvil A.Conh, reestructuraron el concepto del SMF de acuerdo a características celulares como la morfología, función y cinética incluyendo tanto a las células altamente fagocíticas como a sus precursores (15). De esta forma el SMF quedaba constituido por monocitos y macrófagos bajo la creencia de que todos los macrófagos provenían de la diferenciación de los monocitos circulantes. Hipótesis inicialmente defendida por Carrel y Ebeling (19) que mediante una serie de experimentos con cultivos celulares sanguíneos observaban que las células responsables de fagocitar a otras células del propio cultivo eran fundamentalmente macrófagos derivados de los monocitos. Hecho que contrastaba con estudios posteriores donde afirmaban la existencia de macrófagos en organismos pluricelulares carentes de sistema circulatorio (20). Las nuevas técnicas desarrolladas por la época como la inmunoquímica, la radiografía de thimidina, la parabiosis y el microscopio electrónico ayudaron a desarrollar la nueva clasificación del SMF (21, 22, 23). En condiciones normales, las características morfológicas más específicas de estas células quedaban resumidas en los parámetros indicados en la siguiente tabla.

Characteristic [a]	Bone marrow promonocytes	Peripheral blood monocytes	Tissues	
			Free macrophages	Fixed macrophages
Cell diameter	14–20 μm	10–14 μm	10–25 μm	
Nuclear/cytoplasmic ratio	⩾1	∾1	<1	<1
Nucleus shape	folded or indented	reniform	reniform or oval	reniform or oval
nucleoli	+	+	+	+
DNA synthesis	50–70%	0–1%	0.5–3%	1.5–2.5%
Cytoplasm				
polyribosomes	+++	+	±	±
endoplasmic reticulum	+	+	++	++
Golgi complex	large	smaller	variable size	variable size
mitochondria	++	++	++ to +++	++ to +++
lysosomes	+	+	++ to ++++	++ to ++++
endocytic vesicles	+	+	++ to ++++	++ to ++++
Surface membrane				
ruffling	++	+++	++++	
microvilli	+	++	+++	+++
Functional properties				
adherence to glass	+++	+++	+++ to ++++	
pinocytosis	+	++	+++	+++
immune phagocytosis	++	+++	++++	++++

fuente:J Exp Med.

Según Ravinovich (1968,1973) y Conh (1968) los criterios para la caracterización funcional de los macrófagos, monocitos y pro-monocitos en un solo grupo se basaban en su alta capacidad fagocítica y su habilidad por adherirse firmemente a las superficies (24, 25, 26). El proceso de fagocitosis de las células del SMF consistía en dos fases: una inicial adhesión a la partícula a ingerir y su posterior digestión. Los autores defendían que el proceso de adhesión se llevaba a cabo mediante receptores específicos que los monocitos y macrófagos poseían en superficie, por lo que fueron denominados fagocitos “profesionales”. Característica que los diferenciaba de los “no-profesionales” como por ejemplo las células endoteliales y fibroblastos. La adhesión mediada por anticuerpos (Ab) fue denominada como fagocitosis “inmune”. Aparte de la clasificación morfológica y funcional del SMF los resultados de estudios sobre cinética llevados a cabo por Volkman y Gowams (27) ayudaron a mejorar la caracterización del SMF. Estos estudios describían como los fagocitos mononucleares se originaban de células precursoras albergadas en la médula ósea que luego eran

transportadas por el sistema circulatorio como monocitos y que finalmente llegaban a su órgano diana dando lugar a los macrófagos residentes (28,29). En los años 70, Steinman identificó las células dendríticas (CD) dando lugar a la "tercera célula" (30). Este hallazgo determino que el SMF no estaba confinado solo a monocitos y macrófagos como previamente se había propuesto, sino que estaba formado por tres amplios grupos celulares; macrófagos, monocitos (y células derivadas de monocitos) y CD.

MONOCITOS

Caracterizados por primera vez en 1990 por Naito et al (31), los monocitos, emergen del hígado fetal durante la fase embrionaria y se dispersan por la sangre colonizando la mayoría de los órganos (32). Con un fenotipo similar al monocito adulto, los monocitos fetales no expresan el receptor CFS1, poseen una alta capacidad de proliferación en los tejidos y expresan pocos genes relacionados con el reconocimiento de patógenos y la activación del sistema inmunitario. (31, 33). Recientemente ha sido identificado el precursor monocítico común (cMoP) el cual daría lugar a los monocitos y a células derivadas de monocitos. Una vez infiltran los tejidos los precursores pueden mantener el fenotipo durante homeostasis o diferenciarse a células con un amplio espectro fenotípico y funcional dependiendo del escenario en el que se encuentren. Las células cMop son linaje-negativas (LIN-), expresan CD117 (KIT) y el CFS1 (34). Los monocitos se dividen en dos subgrupos; monocitos clásicos Ly6C^{hi}, cuyo homologo humano son los denominados monocitos CD14^{+}, y monocitos no clásicos Ly6C^{low}, equivalente al humano CD14^{low}CD16^{+}. Los monocitos clásicos se pueden encontrar en circulación sanguínea y durante homeostasis en algunos órganos como; bazo, nódulos linfáticos, piel y pulmones, mientras que los monocitos no clásicos estarían localizados principalmente en los vasos sanguíneos y su función principal seria mantener la integridad del endotelio vascular (35). Un estudio reciente muestra que los monocitos Ly6C^{low} de vasos sanguíneos y tejidos son capaces de detectar el daño local mediante el receptor TLR7 favoreciendo la movilización de neutrófilos al punto específico

dañado. Además serían los encargados de limpiar los restos celulares resultantes de la necrosis focal (36). Aunque se cree que la mayoría de monocitos circulantes Ly6C^{low} se diferencian a partir de los Ly6C^{hi}, algunos autores defienden un origen distinto denominándolos macrófagos residentes de arterias (37). Los monocitos clásicos Ly6C^{hi} poseen una alta capacidad fagocítica y una habilidad para infiltrarse en los tejidos y órganos donde una vez extravasados se pueden diferenciar en distintos células fagocíticas mononucleares. Atendiendo a sus propiedades funcionales las células derivadas de monocitos Ly6C^{hi} se clasifican en dos grupos principalmente; CD derivadas de monocitos y macrófagos derivados de monocitos o células mieloides supresoras (MDSC). Aunque dada la plasticidad de las células del SMF y el consecuente solapamiento de funciones a veces estas clasificaciones pueden ser subjetivas. Por ello hoy en día todavía no existe un consenso claro en si las células derivadas de monocitos constituyen 2 líneas celulares ontogénicamente distintas o si son las mismas células que puedan adquirir unas u otras propiedades acordes al contexto en el que se hallen. Las células derivadas de monocitos pueden expresar CD11c y MHC II, pudiendo activar las células T y migrar hasta los nódulos linfáticos al igual que las CD clásicas. Además al igual que los macrófagos, pueden también expresar F4/80 y CD69 manifestando una alta capacidad fagocítica y de remodelación de los tejidos dañados. Modelos de estudio de homeostasis, han descrito los “monocitos tisulares”; monocitos circulantes que una vez extravasados en tejidos sanos no se diferencian ni a CD ni macrófagos. Estas células se localizarían en los órganos durante un tiempo limitado manteniendo el perfil de expresión genética típica de los monocitos (38).

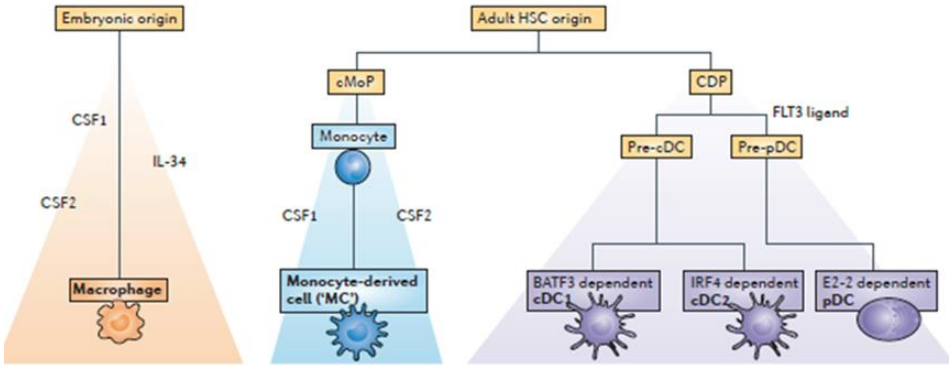

fuente: Nat Rev Immunol.

MACRÓFAGOS

Estudios actuales sobre la ontogenia, defienden un origen multifocal de los macrófagos, diferente a la corriente inicial sobre el origen único y exclusivo a partir de monocitos circulantes. A pesar de ello los monocitos clásicos Ly6C^{hi} siguen siendo descritos como los precursores definitivos de la mayoría de fagocitos mononucleares en órganos adultos y de los que dependen su aporte continuo en homeostasis (40). A pesar de describir los macrófagos y clasificarlos bajo un mismo nombre cabe destacar la gran plasticidad de estas células capaces de adaptarse específicamente a su órgano de residencia, origen y estado. Situaciones de daño tisular e inflamación complican aún más si cabe el escenario ya que las células del SMF experimentan cambios fenotípicos inexistentes durante homeostasis. Definir una ontogenia única y definitiva de los macrófagos es un reto para la inmunología debido entre otras cosas a la complejidad del sistema hematopoyético de los mamíferos que se desarrolla en diferentes etapas extra e intra embrionarias y de las cuales surgen los futuros linajes eritropoyéticos, mieloides y linfoides (33). La primera etapa de la hematopoyesis embrionaria se denomina hematopoyesis primitiva y se desarrolla a partir del mesodermo del saco vitelino dando lugar a los eritrocitos primitivos, megacariocitos y macrófagos. La segunda etapa, llamada hematopoyesis transitoria definitiva, surge del endotelio del saco vitelino y da lugar a precursores eritro mieloides (PEM), excluyendo células de origen linfoide (41). Una vez la circulación fetal está establecida, estas células con potencial eritro-mieloide, migran hacia el hígado fetal donde se diferencian en diferentes tipos celulares incluyendo los monocitos. La tercera y última etapa de la hematopoyesis es la denominada hematopoyesis definitiva. Surge del endotelio de la esplacnopleura embrionaria donde comienzan a generarse las células inmaduras del sistema hematopoyético. Estos precursores colonizan el hígado fetal y establecen la hematopoyesis definitiva diseminándose a la medula ósea fetal responsable de generar las células del sistema hematopoyético adulto (42). Estudios más recientes de fate-mapping proponen una nueva ontogenia en donde los PEM se desarrollarían en solo dos fases a partir del saco vitelino. La fase más temprana de los PEM daría lugar principalmente a macrófagos y progenitores primitivos sin intermediarios monocíticos

que expresan CSF1-R. Estos macrófagos serian totalmente independientes a la contribución de progenitores hematopoyéticos y serian considerados los precursores de los macrófagos residentes como la microglía, células de Langerhans, células de Kupffer y macrófagos alveolares (43). Una segunda fase, PEM tardía, daría lugar a macrófagos del saco vitelino y precursores que expresan el factor de transcripción c-Myb. Estas celulas migrarían al hígado fetal a través de la circulación dando lugar posteriormente a progenitores transitorios definitivos con un amplio espectro mieloide incluyendo los monocitos. Los PEM tardíos se proponen como los principales precursores de macrófagos residentes de la mayoría órganos adultos (32). La contribución de las células hematopoyéticas a la población de macrófagos residentes es tema de debate. Aunque al nacer todos los tejidos están poblados de macrófagos fetales, el grado de implicación posterior de sistema hematopoyético en la tasa de renovación de la población de estos macrófagos tisulares es controvertido y todavía bastante desconocido. Los mecanismos moleculares que hacen que un macrófago sea remplazado en un determinado tejido dependen no solo del órgano en cuestión sino del tiempo y del estado de dicho tejido. Incluso en el mismo estado basal, la cinética de diferenciación de un monocito a macrófago varía entre diferentes órganos y tejidos. Así pues, la vida media de un macrófago intestinal es de aproximadamente 4-6 semanas. Al igual que intestino, los macrófagos de la dermis y los de corazón tienen una vida media de 8 a 12 semanas y dependen constantemente de la movilización de monocitos de médula ósea adulta. Teniendo en cuenta la tasas de renovación, los tejidos adultos en homeostasis se pueden clasificar en, aquellos con capacidad de auto renovación que no requieren de la movilización de monocitos (cerebro, epidermis, pulmón e hígado), tejidos con una rápida tasa de renovación (intestino y dermis) y tejidos con una tasa de renovación lenta (corazón y páncreas) (33).

CLÍNICA DE TRASPLANTES DE ORGANOS

"Es evidente que los trasplantes alargan la vida. Pero sobre todo, añaden vida a los años" (44).

Desde que en 1905 se realizara la primera cirugía de trasplante en seres humanos, el trasplante de órganos ha sido el tratamiento de elección en la mayoría de los casos ante un fallo orgánico grave. A pesar del éxito considerable y creciente en el desarrollo de tratamientos de prevención del rechazo de órganos trasplantados, el factor limitante más importante del proceso es el tiempo de supervivencia de los órganos trasplantados. El tiempo medio de supervivencia es de 5 años, y solo el 54% de los trasplantes de hígado, riñón y pulmón alcanzan los 10 años. En España desde que se aprobara la Ley de Trasplantes, se llevan realizados más de 53.708 trasplantes de órganos. En este mismo periodo recibieron en nuestro país un trasplante de tejidos o células alrededor de 200.000 personas, lo que supone 43,4 donantes por millón de población (pmp) siendo España líder mundial en donación y trasplantes (44). La principal complicación de los trasplantes es la denominada "graft-versus-host disease" (GVHD) que deriva en una cronificación del órgano trasplantado y finalmente su rechazo (45). La GVHD es un desorden inmunológico que con el tiempo se traduce en fallo multi orgánico afectando al intestino, hígado, riñón, piel y pulmones. Solo el tratamiento prolongado con drogas inmunosupresoras evita el GVHD, condicionando a los pacientes a la aparición de serias complicaciones secundarias.

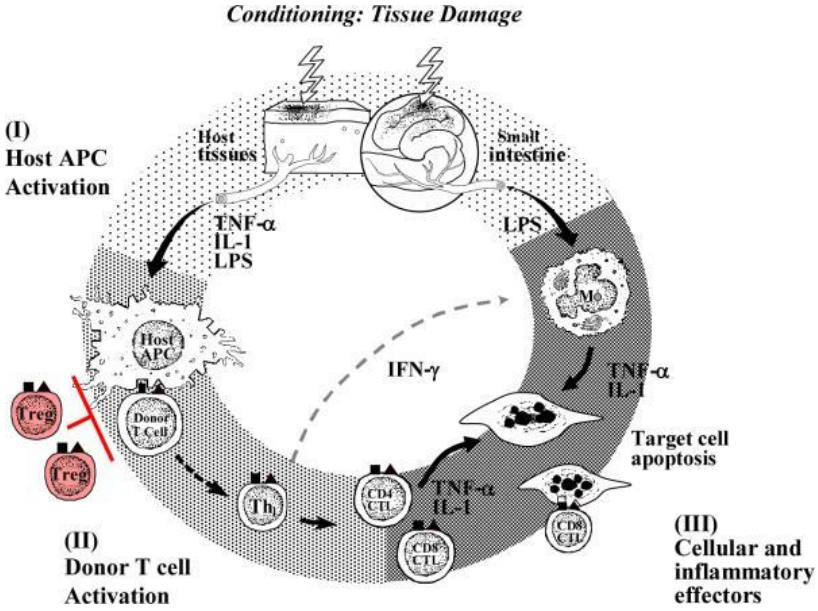

Fuente: Lancet (68).

La fisiopatología del rechazo a los trasplantes de órganos se basa en dos importantes situaciones. La primera, los mecanismos inflamatorios mediados por las células T del donante infusionadas en el receptor cuya función se adapta al medio extraño en el que se encuentran, proliferando y diferenciándose en respuesta a las células presentadoras de antígeno (APC) del receptor. Y la segunda, que el tejido del receptor es un tejido previamente dañado por enfermedades subyacentes (46,47). Los tejidos lesionados producen señales de alarma (Damage associated molecular pattern`s, DAMP`s), resultando en una mayor producción de citoquinas inflamatorias, quemoquinas y aumento en la expresión de moléculas de adhesión, antígenos MHC y moléculas co-estimulatorias en las APC del receptor. Consecuentemente, estas señales de peligro inducen un aumento en la activación, proliferación y migración de las células T del donante (47). La idea de que la amplificación de activación de las APC del receptor aumente el riesgo de rechazo del órgano trasplantado relaciona diversas situaciones clínicas con dicho riesgo, como por ejemplo, estados avanzados de enfermedad, historial de infecciones o enfermedades crónicas. Pese a los continuos logros y avances

en la clínica de trasplantes, los tratamientos actuales se basan en terapias con drogas inmunosupresoras inespecíficas prolongados en el tiempo que desembocan en enfermedades secundarias tales como fallos metabólicos, infecciones, incluso desarrollo de cáncer (48, 49,50). Aunque se han obtenido resultados prometedores en la clínica, el estado de tolerancia entendido como la ausencia de ataque inmune específico a un órgano extraño, es todavía impreciso y obliga a seguir investigando para desarrollar mejores protocolos.

ROL DE LOS MACRÓFAGOS EN TRASPLANTES

Históricamente los inmunólogos han tendido a desarrollar protocolos tolerogénicos basados en estrategias de control de las células del sistema inmune adaptativo como por ejemplo el bloqueo co-estimulatorio, la linfo-deplección y la inducción in vivo de células Treg (51,52). Los primeros en estudiar la implicación de las células derivadas de monocitos en un modelo de trasplante cardiaco en rata fueron Nicholas Tilney y Terry Strom en el año 1977 (53). Ambos demostraron la capacidad supresora de las células aisladas de trasplantes (donde los macrófagos constituían un 10% de la población celular total). La población celular fue analizada mediante ensayos de proliferación y los resultados demostraban que los las células adherentes (90%) aisladas de los recipientes tolerantes exhibían una mayor actividad supresora en comparación con las células no adherentes (15%) obtenidas de recipientes con rechazo. Análisis posteriores de las células adherentes aisladas de bazo confirmaron los anteriores resultados, sugiriendo qué los macrófagos derivados de monocitos infiltrados en órganos tolerantes poseían una alta capacidad supresora (53). William John Martin obtuvo resultados similares sobre la capacidad supresora de las células adherentes llevando a cabo distintos ensayos con suero anti-linfocitico (SAL/ALS). El primer ensayo media la habilidad del SAL en inhibir la formación de rosetas, el segundo determinaba la capacidad del SAL en provocar cito adherencia in vitro de los linfocitos a los macrófagos y el tercero cuantificaba la distribución entre hígado y bazo de células del timo pre incubadas en SAL e inyectadas posteriormente en ratón. El resultado de sus ensayos correlacionaba

directamente la modificación del patrón de distribución de las células del timo con la capacidad del SAL en deprimir la respuesta inmune y prolongar los injertos de piel (54). Es en 1979 cuando se atribuye específicamente a los macrófagos la función supresora en trasplantes de órganos en humanos (55). El estudio se llevó a cabo por Hyung M. Lee con 66 pacientes trasplantados y bajo tratamiento inmunosupresor en los que se obtenían células mononucleares del riñón trasplantado. Estas eran puestas en co-cultivo con células T citotóxicas de los donantes marcadas con Cromo (51Cr) y expuestas previamente a células diana del recipiente. El estudio concluía en que las células mononucleares aisladas del riñón trasplantado eran capaces de suprimir la lisis celular mediada por los linfocitos. EL porcentaje de lisis era determinada por la cantidad de 51Cr en el medio. Mas extensamente, los autores demuestran que la fracción de células adherentes dentro del conjunto de células mononucleares aisladas del riñón trasplantado contenía entre un 55-85% de monocitos y/o macrófagos. Complementando estos hallazgos, los autores llevaron a cabo un experimento posterior en mono Rhesus con un modelo de trasplante de piel. Los recipientes eran tratados con globulina anti-timocitos (ATG) durante 5 días tras los cuales se obtenían células mononucleares de sangre periférica (PBMC). Observaron que la fracción adherente de las PBMC reducía sustancialmente la proliferación linfocítica cuando eran añadidas a cultivos celulares, sugiriendo a los macrófagos supresores como parte mediadora en la función inmunosupresora inducida por el tratamiento con ATG (56). Kamada y colegas (57), llevan a cabo unos experimentos en un modelo de trasplante de hígado en rata en donde describen las dos fases en la que se desarrollaría la actividad supresora que implica a macrófagos y células Tregs medida en un ensayo de reacción leucocitaria mixta (MLR). Durante la fase temprana (4-30 días post trasplante) los macrófagos adherentes del bazo de recipientes tolerantes son los responsable de la función supresora mientras que durante la fase tardía (20 o más semanas post trasplante), las células supresoras T no adherentes, son las responsables de dicha función. A mediados de la década de los noventa Mybourgh y su laboratorio fenotiparon por primera vez la población celular supresora en un modelo de trasplante renal en primates no humanos. Los autores identificaron una población de monocitos

infiltrados en los órganos trasplantados que expresaban CD11b y que eran responsables de la supresión in vitro en ensayos MLRs (58). Los experimentos concluían en que la falta de estas células $CD11b^+$ se traducía en una pérdida de la capacidad de inhibir la proliferación y que además dicha capacidad supresora estaba mediada por algún factor soluble. Entrado el siglo XXI, Vanhove (59) describe una población $CD11b^+/Cd80/86^+$ $Sirp\alpha^+$ a la que atribuye una importante función durante tolerancia en modelos de trasplante renal en ratas. Observan que durante la tolerancia inducida mediante un bloqueo co-estimulatorio con anticuerpo anti CD28y anti CD3, las células $CD11b^+/Cd80/86^+$ $Sirp\alpha^+$ se acumulaban en los órganos trasplantados y que además las células obtenidas de sangre y médula ósea que expresaban CD11b y Sirpα, inhibían la proliferación in vitro de células T. En otro de sus trabajos (60), demuestra que la población derivada de monocitos que expresan CD11b, Cd80/86 y Sirpα es responsable de la producción de quimiocina CCL5 encargada de conducir a las células Treg hacia el órgano tolerizado. Distintos mecanismos de acción se han descrito como responsables de la función supresora de los macrófagos durante tolerancia. Utilizando un modelo de trasplante cardiaco en ratón (1), nuestro laboratorio fue el primero en demostrar la función indispensable de las células supresoras derivadas de monocitos en la prolongación de la tolerancia. En un modelo de trasplantes donde la tolerancia es inducida mediante el bloqueo de la ruta CD40L-CD40 y utilizando distintas técnicas de depleción celular como anticuerpos anti-Gr-1 y anti-Ly6G, ratones Cd11b-DTR (receptor de la toxina de Difteria), ratones MAFIA (macrophage Fas induced apoptosis) y liposomas de clodronato, los autores identifican una población celular $Cd11b^+CSF1R^+Gr\text{-}1^+$ que migra rápidamente desde la médula ósea al órgano trasplantado donde actúan inhibiendo la respuesta inmune adaptativa previniendo así el rechazo del órgano trasplantado y favoreciendo el aumento de células Treg. Recientemente nuestro laboratorio ha propuesto una nueva clasificación más completa de la población celular supresora aislada de órganos tolerizados. Hemos descrito nuevos marcadores fenotípicos y hemos proporcionado información novedosa sobre su desarrollo, origen así como nuevos mecanismos de acción implicados en la función supresora. Aunque los mecanismos de acción de los monocitos y macrófagos

en trasplantes de órganos no están claramente establecidos, una hipótesis que se proponen en la tesis es la posibilidad de que los macrófagos y monocitos de los órganos sufran un "entrenamiento" previo al trasplante que resultaría en la adquisición de un fenotipo pro-inflamatorio favoreciendo al rechazo del órgano trasplantado.

INMUNIDAD ENTRENADA

Recientemente se ha demostrado que las células del sistema inmune innato podían adquirir características previamente solo atribuidas a las células del sistema adaptativo. La memoria de la inmunidad innata es un proceso mediante el cual monocitos y macrófagos adquieren características funcionales tras una primera exposición ante microbios o componentes microbianos. Varios estudios han descrito como plantas y organismos invertebrados eran capaces de construir una respuesta inmune de memoria que les confería protección frente a reinfecciones (61). A este término se le ha denominado "inmunidad entrenada" (62). El fenómeno de inmunidad entrenada apareció tras la administración de la vacuna frente a la tuberculosis preparada a partir del bacilo Calmette-Guérin (BCG) (63). Descubrieron que la vacunación con BCG en niños no solo les protegía frente a la tuberculosis sino que aumentaba la respuesta de anticuerpos frente a otras infecciones (64), se producían menos casos de atopia (65) y evitaba la anergia frente a otros patógenos como la difteria y el tétanos, traduciéndose en una reducción drástica de la mortalidad infantil (66). Distintos experimentos llevados a cabo en ratones y humanos demuestran que la exposición a productos patógenos tales como, vacuna BCG (67), Candida albicans (C.albicans) (68) o componentes de la pared celular microbiana como el β-glucano (69), inducen un aumento en la producción de citoquinas y quimiocinas pro-inflamatorias (por ejemplo, TNF-α, IL-6 e IL-1β) cuando los monocitos son re-expuestos a un segundo estimulo. Este cambio en el fenotipo inflamatorio de los monocitos proporciona una robusta protección frente a una re-exposición. En el caso de infección por C.albicans, el laboratorio de Netea (68) realiza unos experimentos relevantes en donde la

administración de la vacuna BCG en ratones deficientes en células T y B les protege de una dosis letal de C.albicans. Los resultados reflejan un 100% de supervivencia en ratones vacunados frente a tan solo un 30% de supervivencia entre los ratones no vacunados. Hay que tener en cuenta que no solo los microbios son responsables de la inmunidad entrenada. Al igual que el β-glucano, la vimentina es un ligando endógeno del receptor de la inmunidad innata (PRR) Dectin-1. Ligandos exógenos y endógenos de estos receptores son clasificados como DAMPs y actúan como señales de peligro para el sistema inmune innato del hospedador. Tal y como anteriormente hemos comentado, el proceso de trasplante conlleva un lesión y daño tisular incluso previo a la cirugía. La vimentina es un filamento proteínico presente de forma normal en los vasos sanguíneos y fibroblastos que en condiciones de necrosis e inflamación se extravasa al medio externo. Existen evidencias de que la vimentina es responsable de la vasculopatía asociada al rechazo crónico en trasplantes cardiacos (70). Por ello podríamos suponerla como uno de los componentes endógenos responsables de inducir la inmunidad entrenada en trasplantes de órganos y favorecer el rechazo.

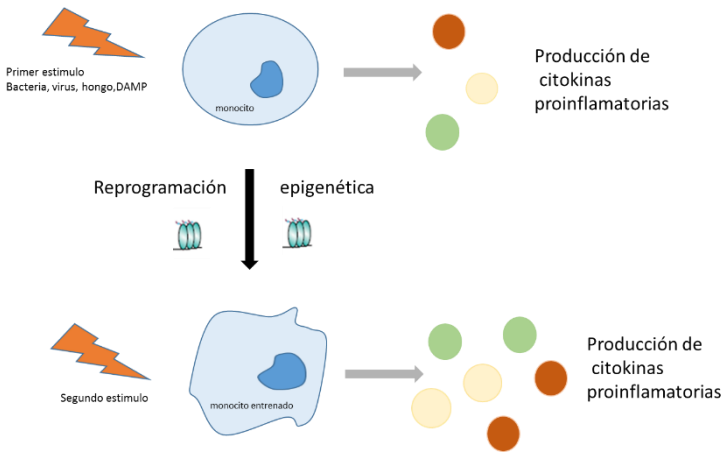

MECANISMOS DE ACCION DE LA INMUNIDAD ENTRENADA

Los mecanismos de acción implicados en el cambio fenotípico pro-inflamatorio de los macrófagos durante la inmunidad entrenada se deben principalmente a dos situaciones muy ligadas entre ellas; un cambio en el metabolismo celular y una reprogramación epigenética (71). Muchos metabolitos celulares actúan como cofactores para enzimas con una función esencial en la epigenética, por ello un cambio del metabolismo celular afecta directamente a la epigenética (67,72). La regulación epigenética se basa en modificaciones del ADN a nivel de histonas u otros componentes de la cadena, que sin llegar a alterar la propia secuencia del ADN alteran la estructura de la cromatina, favoreciendo o inhibiendo factores de trascripción. La acetilación de las histonas por ejemplo, produce un debilitamiento en la unión entre al ADN y las histonas provocando un aumento en la activación de la trascripción. Al contrario, la metilación de las histonas puede provocar tanto un aumento como un bloqueo de la trascripción dependiendo de la cantidad de grupos metilos que sean añadidos y el residuo de lisina que sea modificado. Distintos experimentos llevados a cabo por Saeed y colegas (71), concluyeron en que los cambios en la trimetilación de la lisina 4 en la histona 3 (H3K4) y la acetilación de H3K27 se asociaban con un aumento en la trascripción de los genes de citoquinas pro-inflamatorias responsables del cambio en el fenotipo de los macrofagos. El otro mecanismo clave responsable del cambio fenotípico en la inmunidad innata es el cambio en el metabolismo celular caracterizado por un aumento en la glicolisis aeróbica. La influencia del estado metabólico de las células del sistema inmune ha sido estudiada durante años. Se sabe por ejemplo que el fenotipo de las células T y los macrófagos varía dependiendo de su actividad metabólica y que tras su activación se produce un cambio del metabolismo basal de fosforilación oxidativa a una glicolisis aeróbica (73). Este cambio se define como “Efecto Warburg” (74). Los macrofagos M1 (clásicos) caracterizados por un perfil pro-inflamatorio dependen principalmente de un metabolismo glicolítico mientras que los macrofagos M2 (alternativos) con funciones inmuno reguladoras utiliza una ruta metabólica basada en la oxidación de los ácidos grasos (75). La vía mTOR es un mecanismo clave en facilitar la disponibilidad de nutrientes

y/o energía para los procesos metabólicos celulares tales como la síntesis de proteínas, glicólisis y lipogénesis “de novo” (76) y además está implicada en en la polarización de macrófagos (77). La actividad mTOR provoca un defecto en la señalización vía Akt que resulta en una disminución de IL-10 e IL-4, indispensables para la polarización de macrofagos M2 y un aumento en la respuesta inflamatoria (77). El bloqueo químico de mTOR restaura la actividad de Akt y la capacidad de conversión de macrofagos inmuno competentes a inmunosupresores.

INMUNIDAD ENTRENADA Y TOLERANCIA EN TRASPLANTES

Los monocitos y macrófagos tienen un papel principal en la inducción de la tolerancia en trasplantes de órganos. Ya que moléculas endógenas resultantes de lesiones y daño tisular pueden inducir el cambio de metabolismo y la reprogramación de los monocitos provocando un aumento en la respuesta inflamatoria es lógico suponer que dichos mecanismos sean relevantes en la tolerancia de trasplantes. Con ello en mente, nuestro laboratorio ha desarrollado una inmunoterapia basada en nano partículas de lipoproteínas de alta densidad (HDL) con afinidad específica a macrofagos. Debido a que la vía mTOR juega un papel importante en la regulación de la inmunidad entrenada en las células del sistema innato (62,71) y en la función de los macrofagos (77) creemos que su bloqueo pueda servirnos como herramienta para prevenir el rechazo al trasplante de órganos. En la construcción de las nano particulas hemos utilizado la rapamicina como agente inhibidor de la vía mTOR (mTORi), la cual, fue encapsulada utilizando una corona de fosfolípidos naturales y apoliproteína A-I (APOA 1).

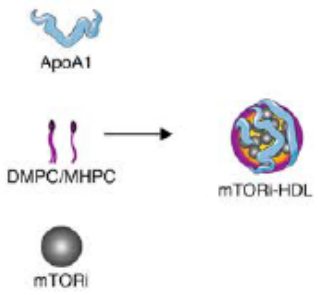

RESULTADOS

Los macrófagos supresores se acumulan durante tolerancia

Para identificar la población de origen mieloide acumulados durante la inducción de la tolerancia, utilizamos un modelo experimental de trasplante cardiaco en ratones cuyos haplotipos del complejo mayor de histocompatibilidad (MHC) eran totalmente incompatibles. Para ello usamos como recipientes ratones de la cepa C57/BL6/MaFIA ($CFS1R^{GFP+)}$ (H-2b) en los que trasplantamos el corazón de ratones BALB/c (H-2d). Utilizamos como recipientes ratones MaFIA ya que expresan constitutivamente la proteína verde fluorescente (GFP) bajo el promotor CFSR1 lo cual nos permite identificar más fácilmente las poblaciones de origen mieloide exclusivas del recipiente que se acumulan en el órgano trasplantado (78). En los experimentos preliminares se trataron 2 grupos de recipientes. El grupo tolerante tratado con anticuerpo anti CD40-L (clon MR1) y el grupo control tratado con anticuerpo anti inmunoglobulina G (IgG). Los datos confirmaron los resultados obtenidos en trabajos publicados previamente (79) donde se demostraba que el tratamiento con anti CD40-L favorecía la supervivencia del órgano trasplantado. Por el contrario, en el grupo control el rechazo se producía alrededor de los 10 días post trasplante (pt) (Fig.1A).

A

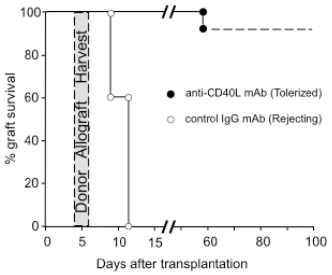

B

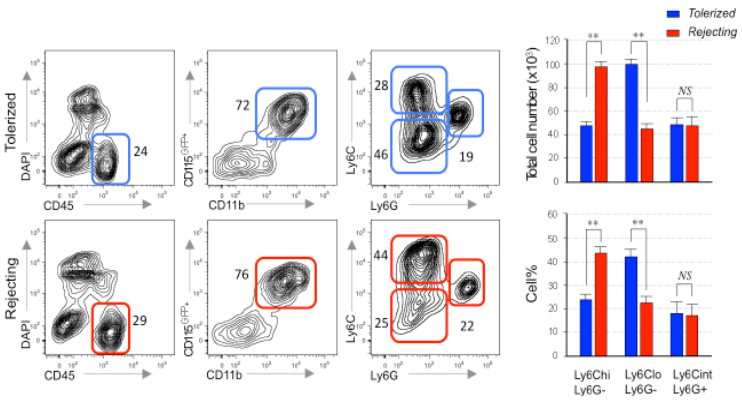

C

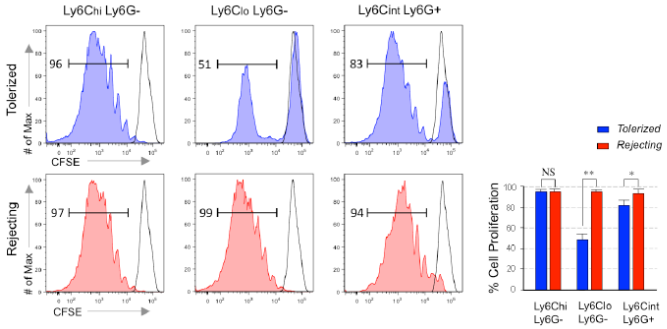

D

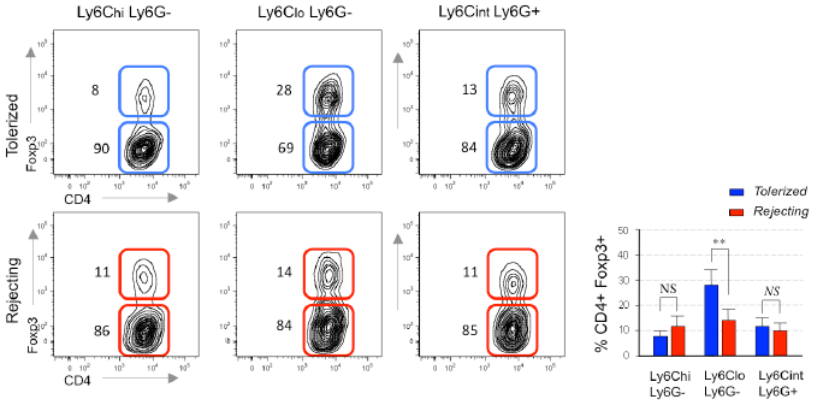

Figura 1: (A) Gráfica de supervivencia de órganos rechazados (grupo control tratados con Ac anti IgG) y órganos tolerizados (tratados con Ac anti CD40L) en recipientes de trasplante cardiaco heterópico (n=20 ratones/grupo). Los órganos fueron recogidos a día 5 post trasplante (pt). (B) Resultados de citometría en la expresión de Ly6C y Ly6G en las poblaciones de células mieloides obtenidas de los órganos trasplantados tolerantes y rechazos a día 5pt. El análisis de los resultados se representan mediante el error estándar de la media ± SEM (n=8 ratones/grupo). (c) Capacidad supresora in vitro de cada una de las poblaciones mieloides respecto a la proliferación de células T CD8⁺ .La proliferación fue cuantificada en base a la dilución del CFSE tras 96h mediante citometria de flujo. Los porcentajes de la proliferación celular fueron representados mediante ± SEM de la media de 5 experimentos independientes. (D) Expansión in vitro de células Treg. El análisis citométrico indica la expresión de Foxp3 en células T CD4⁺ tras 96h en co-cultivo con las distintas poblaciones mieloides. Los porcentajes de expansión de las Treg se representan mediante ± SEM de la media de 5 experimentos independientes.

5 días post cirugía los órganos trasplantados son recogidos y analizados mediante citometría de flujo. Seleccionando las células vivas $CD45^{+}CD11b^{+}CSFR1GFP^{+}$ y en base a la expresión de Ly6C y Ly6G distinguimos tres poblaciones mieloides (Fig.1B). El análisis cuantitativo revela una mayor frecuencia de células $CD11b^{+}CSF1R^{+}Ly6C^{lo}Ly6G^{-}$ y una menor proporción de células

$CD11b^{+}CSF1R^{+}Ly6C^{hi}Ly6G^{-}$ en los órganos de los grupos tratados con anti CD40-L comparados con el grupo control ($p \leq 0.01$). Sin embargo no se encontraron diferencias entre ambos grupos en cuanto a la frecuencia de células Ly6G. Para determinar la capacidad de supresión de las poblaciones mieloides, evaluamos la habilidad de cada una de las poblaciones en inhibir la proliferación in vitro de células $CD8^{+}$ estimuladas con anticuerpos anti CD3 y anti CD28 (Fig.1C). La población $CD11b^{+}CSF1R^{+}Ly6C^{lo}Ly6G^{-}$ aislada de los órganos tratados con anti CD40-L al contrario que la población $CD11b^{+}CSF1R^{+}Ly6C^{hi}Ly6G^{-}$, poseía una potente capacidad supresora. La población $CD11b^{+}CSF1R^{+}Ly6C^{int}Ly6G^{+}$ también pareció mostrar una ligera capacidad supresora. Sin embargo ninguno de las tres poblaciones aisladas de los órganos rechazados procedentes de los grupos control, con tratamiento anti IgG, mostraron capacidad de supresión alguna. Igualmente, evaluamos la capacidad de cada una de las tres poblaciones mieloides en favorecer la expansión in vitro de células $CD4^{+}Foxp3^{+}$ T reg (Fig.1D). Coherente con los resultados de supresión, solo las células $CD11b^{+}CSF1R^{+}Ly6C^{lo}Ly6G^{-}$ aisladas de los trasplantes de recipientes tolerizados promovían la expansión de las células Treg. De este modo la población celular $CD11b^{+}CSF1R^{+}Ly6C^{lo}Ly6G^{-}$ aisladas de órganos trasplantados de recipientes tratados con anti CD40L poseen muchas de las características asociadas a células supresoras derivadas de monocitos, incluyendo la capacidad de inhibir la proliferación de células T $CD8^{+}$ (80) y favorecer la expansión de células $CD4^{+}Foxp3^{+}$ T (81). Es más, la caracterización genética reveló que dicha población $CD11b^{+}CSF1R^{+}Ly6C^{lo}Ly6G^{-}$ acumulada en órganos tolerizados correspondía a macrófagos y no células dendríticas (82) (Fig.S1A). El análisis morfológico de estas células confirmaba también su origen monocítico (Fig.S1B).

Los macrófagos supresores son necesarios para inducir la tolerancia

Para caracterizar más a fondo las poblaciones de células derivadas de monocitos identificadas anteriormente, realizamos un análisis transcripcional. Los resultados revelaron que los macrófagos supresores $Ly6C^{lo}$ procedentes de recipientes tolerizados mostraban un aumento significativo en la expresión de algunos genes como CX3CR1,

F4/80, CD206 (receptor de manosa de macrófagos), CD68, CD172 (Sirp-α) y CD169. La citometría de flujo también nos confirmó la expresión de estas proteínas en los macrófagos supresores (Fig.2A). Para estudiar la función supresora in vivo de los macrófagos Ly6C^{lo} aprovechamos su diferencia de expresión en el marcador de superficie CD169 con la disponibilidad de unos ratones transgénicos que expresan el DTR unido a CD169, CD169-DTR (83). En los cuales podemos deplecionar específicamente los macrofagos supresores CD169^{+}Ly6C^{lo} mediante la administración de la toxina (DT) (Fig.S2A y S2B). Usando el mismo modelo experimental de trasplante cardiaco, trasplantamos corazones de BALB/c en recipientes tolerizados controles CFS1R^{GFP+} o recipientes tolerizados CSF1R$^{GFP+/}$CD169^{DTR} tratados con DT el mismo día del trasplante. 5 días pt examinamos las células infiltradas en el órgano mediante citometría de flujo. Los recipientes CSF1R$^{GFP+/}$CD169^{DTR} tratados con DT mostraban una reducción específica de los macrófagos supresores en comparación con el grupo control (Fig.2B). Advertimos también, que la depleción de los macrófagos CD169^{+}Ly6C^{lo} se asociaba con un aumento en células T activadas o de memoria CD8^{+}CD44^{hi}CD62L^{lo} (Fig.2C y 2D) y una disminución en el porcentaje de las células T reguladoras CD4^{+}Foxp3^{+} (Fig.2E).

A

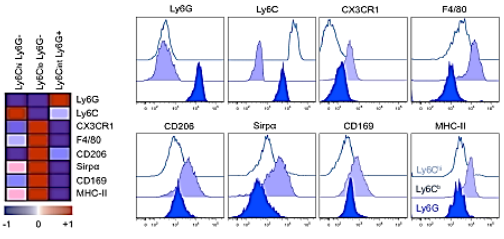

B

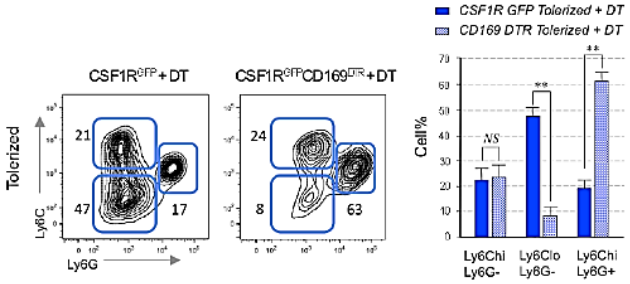

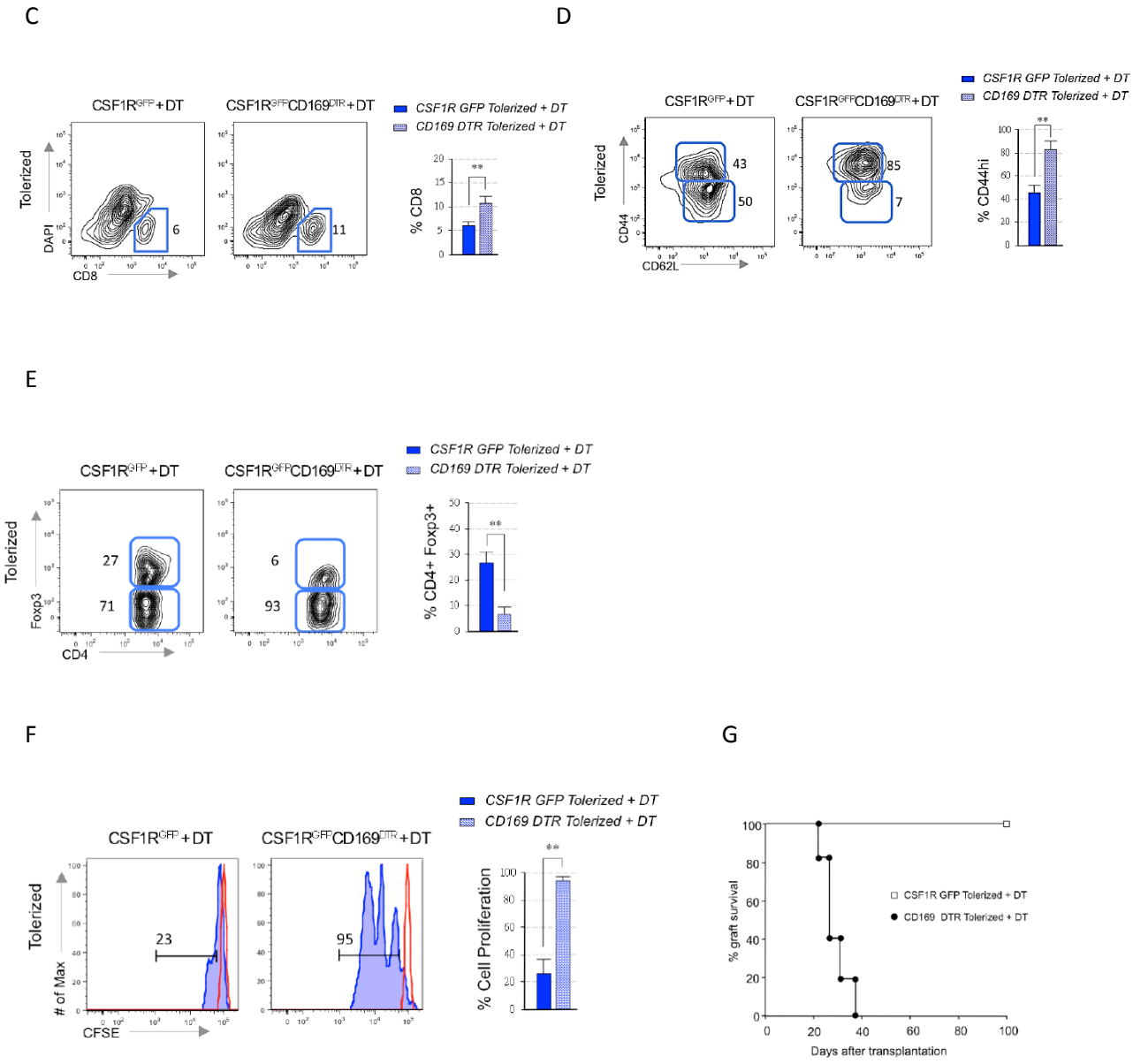

Figura 2: (A) Heatmap del análisis trasncripcional de marcadores mieloides con un diferencial de expresión de p≤ 0.05 entre las distintas poblaciones mieloides obtenidas de órganos tolerantes a día 5 pt. Representación de los marcadores en las distintas poblaciones mediante histogramas de citometria de flujo (n=3). (B) Resultados cito métricos de las poblaciones mieloides obtenidas a día 5 pt de órganos trasplantados en recipientes tolerantes CFS1R^{GFP+} o CSF1R$^{GFP+/}$CD169^{DTR} tras la administración de DT. Resultados de la media expresados mediante ± SEM (n=12 de 3 experimentos independientes). (C y D) Representación cito métrica de porcentajes y marcadores de memoria/naive CD44/CD62L de las células T CD8^{+} infiltradas en los órganos trasplantados tras la depleción de los macrofagos CD169^{+}Ly6C^{lo}. Resultados de la media expresados mediante ± SEM (n=12 de 3 experimentos independientes). (E) Representación cito métrica de porcentajes de expresión de Foxp3 en células T CD4^{+} infiltradas en los órganos trasplantados tras la depleción de los macrofagos CD169^{+}. Resultados de la media expresados mediante ± SEM (n=4 de 3 experimentos independientes). (F) Efectos de la depleción in vivo de los macrofagos CD169^{+} sobre la proliferación de células T. Las células T CD8^{+} marcadas con CFSE (5x10^{6}) fueron inyectadas en recipientes tolerantes CFS1R^{GFP+} o CSF1R$^{GFP+/}$CD169^{DTR}. La proliferación fue cuantificada en base a la dilución del CFSE tras 120h mediante citometria de flujo. Resultados de la media expresados mediante ±

SEM (n=4 de 3 experimentos independientes). (G) Efectos de la depleción in vivo de los macrofagos CD169$^+$ sobre la supervivencia de los órganos trasplantados en recipientes CFS1RGFP$^+$ o CSF1R^{GFP+}/CD169^{DTR} tolerantes (n=12 ratones/grupo).

Para comprobar que los macrofagos supresores CD169$^+$Ly6C^{lo} mantenían su capacidad inhibitoria in vivo, realizamos una trasferencia adaptativa de células T CD8$^+$ marcadas con CFSE en recipientes CD169^{DTR} tolerizados. Para valorar la proliferación de las células T CD8$^+$ realizamos un ensayo de proliferación en donde medimos la dilución del CFSE 5 días post administración de la DT (Fig.2F). Las células T CD8$^+$ no proliferaban cuando eran trasferidas a recipientes controles. Sin embargo si proliferaban en los recipientes transgénicos cuyas células CD169$^+$Ly6C^{lo} fueron depleccionadas. Observamos también que en los recipientes sin macrófagos supresores, se producía el rechazo al órgano alrededor de los 30 días pt a pesar del tratamiento tolerante con anti-CD40L (Fig.2G).

El bloqueo de CD40L inhibe la acumulación de macrofagos supresores

Aprovechando que las células mieloides expresan CD40, pero no CD40L (Fig.S3A y S3B) quisimos evaluar la implicación del tratamiento tolerogénico con anti-CD40L en las células derivadas de monocitos aisladas de órganos trasplantados. Utilizando el mismo modelo experimental, diseñamos un experimento en el que eludíamos los efectos directos del bloqueo de la vía co-estimulatoria administrando al mismo tiempo que el anti-CD40L un anticuerpo agonista anti-CD40. Los resultados revelaban que la co-administración del agonista favorecía la acumulación de macrofagos inmunogénicos Ly6C^{hi} en los órganos trasplantados (Fig.3A) y que además se correspondía con una disminución en la subpoblación de macrofagos supresores Ly6C^{lo}. Estudios previos (84) demostraban que el aumento de macrofagos Ly6C^{hi} mediado por CD40 podría deberse a un incremento en los niveles de IFNγ. Para tratar de demostrar la relación el aumento de Ly6C^{hi} mediados por IFNγ y la estimulación de la vía CD40-CD40L en nuestro modelo experimental, medimos la expresión IFNγ en los órganos de recipientes sin tratar, recipientes tolerizados y recipientes tolerizados tratados con el agonista anti-CD40 (Fig.3B). La PCR (polymerase chain reaction) cuantitativa mostraba una disminución

significativa de IFNγ en las muestras obtenidas de recipientes tolerizados comparados con los recipientes rechazados, cuyos valores eran muy parecidos a los recipientes a los que se co-administró el agonista anti-CD40. Para acabar de corroborar esta teoría, utilizamos para los trasplantes recipientes deficientes en el receptor CD40 (CD40 -/-, CD40KO) tolerizados y co-tratados con el agonista. Los resultados no mostraban un aumento de macrofagos Ly6C^{hi}ni una mayor expresión de IFNγ en los órganos trasplantados (Fig.3C). El análisis de supervivencia del órgano refleja una tolerancia mantenida en los recipientes CD40KO en comparación con los WT (Fig.3D).

A

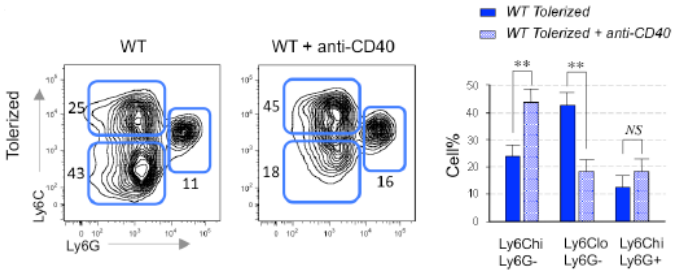

B

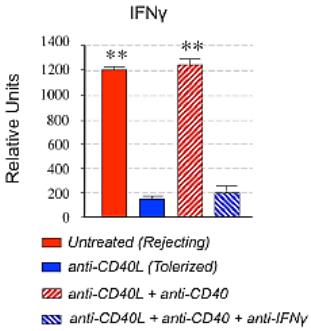

C

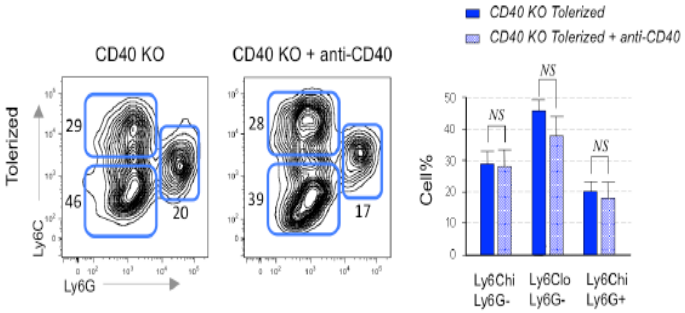

D

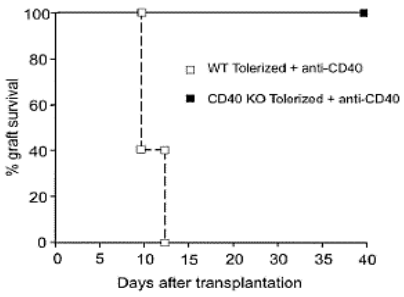

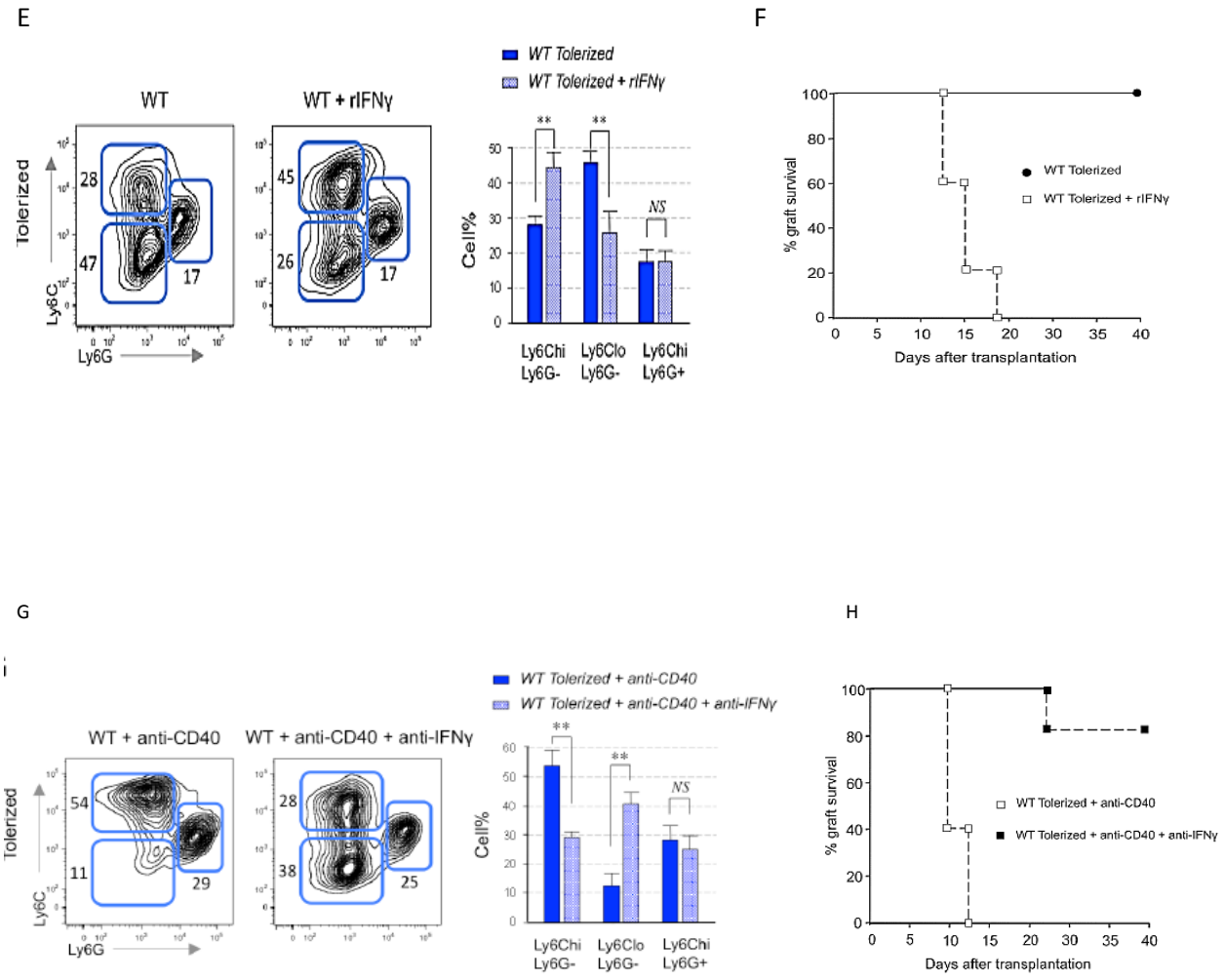

*Figura 3: Resultados de la citometria de flujo de las poblaciones mieloides en los órganos trasplantados de recipientes tolerantes WT con o sin tratamiento con el Ac agonista CD40. Resultados de la media expresados mediante ± SEM (n=4 de 3 experimentos independientes). (B) Expresión de IFNγ en los corazones trasplantados. Los órganos de cada grupo fueron recogidos a día 5 pt. El Ac agonista CD40 fue inyectado a dosis de 100 µg/ratón a día 0 y +1 pt. El recombinante IFNγ fue inyectado a $4X10^5$ unidades/día durante 10 días (n=4 ratones por grupo). Las muestras fueron analizadas mediante PCR cuantitativa y representadas en unidades relativas. Las barras graficas representan la media expresados mediante ± SEM de 3 experimentos independientes (**p ≤0.01). (C) Resultados cito métricos de las poblaciones mieloides de recipientes CD40 deficientes tolerizados con o sin tratamientos agonístico con Ac CD40. Resultados de la media representados mediante ± SEM (n=4 de 3 experimentos independientes). (D) Efectos de la señalización vía CD40 en la supervivencia del trasplante en recipientes tolerizados WT o CD40 deficientes (n=8). (E) Resultados cito métricos de las poblaciones mieloides en recipientes WT tolerizados y tratados con o sin IFNγ recombinante ($4X10^5$ unidades/día durante 10 días). Resultados de la media representados mediante ± SEM (n=4 de 3 experimentos independientes). (F) Efectos del IFNγ recombinante en la supervivencia del trasplante en recipientes WT tolerizados (n=8). (G) Resultados cito métricos de las poblaciones mieloides de órganos trasplantados en recipientes WT tolerizados co-tratados con Ac agonista CD40 con y sin IFNγ recombinante. Resultados de la media representados mediante ± SEM (n=4 de 3 experimentos independientes). (H) Efectos de la inhibición parcial de la expresión de IFNγ en la supervivencia del trasplante en recipientes WT tolerizados co-tratados con Ac agonista CD40 (n=8).*

Los datos obtenidos en los experimentos anteriores, indicaban que la tolerancia inducida por la administración de anti-CD40L era en parte mediada por el bloqueo en la producción de IFNγ. Para confirmar esta hipótesis en nuestro modelo de trasplante tratamos los recipientes, previamente tolerizados, con IFNγ recombinante observando un aumento en la población de macrofagos $Ly6C^{hi}$ y una disminución de los $Ly6C^{lo}$ (Fig.3E) resultando en un rechazo del órgano trasplantado (Fig.3F). De la misma forma, el bloqueo parcial de IFNγ en los recipientes tratados con el anticuerpo agonista anti-CD40 restablecía la población de macrofagos supresores $Ly6C^{lo}$ (Fig.3G) y restauraba la supervivencia del órgano trasplantado (Fig.3H).

CSF1 media el desarrollo de los macrofagos supresores

El análisis genético realizado anteriormente (Fig.S1A) mostraba un aumento en la expresión de CSF1R (CD115) en la población de macrofagos supresores $CD11b^{+}CSF1R^{+}Ly6C^{lo}Ly6G^{-}$, lo que nos sugería una posible implicación del factor de crecimiento CSF1 en el desarrollo de dicha población supresora. Medimos el CSF1 en muestras de corazones trasplantados advirtiendo una sobre-expresión en los recipientes tolerizados (Fig4A). Para investigar la función directa del CSF1 sobre el desarrollo de macrofagos $Ly6C^{lo}$, utilizamos como recipientes, ratones tolerizados y tratados con o sin anticuerpo neutralizador anti-CSF1. Los resultados obtenidos, demostraban que la administración del neutralizador de CSF1 provocaba no solo una reducción del número de $Ly6C^{lo}$ en los órganos trasplantados sino que además, puestas en co-cultivo disminuía la capacidad de expansión in vivo de células $CD4^{+}Foxp3^{+}$ reguladoras. Condiciones ambas, que dificultan la inducción a la tolerancia (Fig. 4B, 4C y 4D).

A

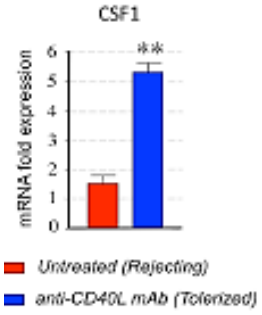
CSF1
mRNA fold expression
**
Untreated (Rejecting)
anti-CD40L mAb (Tolerized)

B

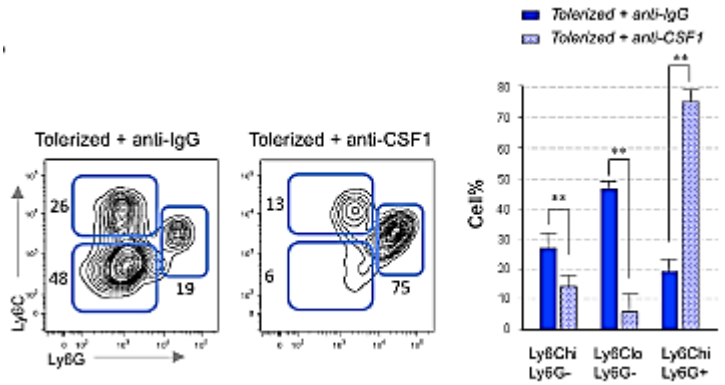
Tolerized + anti-IgG
Tolerized + anti-CSF1
Tolerized + anti-IgG
Tolerized + anti-CSF1
26
48
19
13
6
75
Ly6C
Ly6G
Cell%
**
LyßChi Ly6G-
LyßClo Ly6G-
LyGChi Ly6G+

C

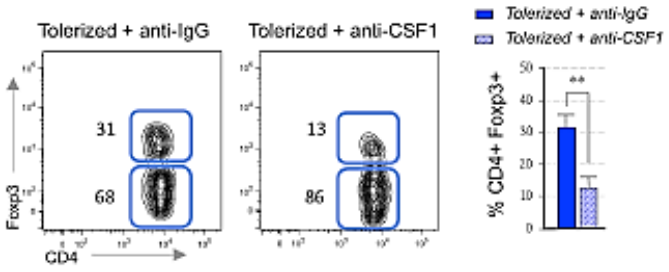
Tolerized + anti-IgG
Tolerized + anti-CSF1
Tolerized + anti-IgG
Tolerized + anti-CSF1
31
68
13
86
Foxp3
CD4
% CD4+ Foxp3+
**

D

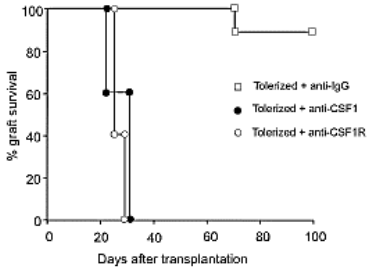
% graft survival
Days after transplantation
Tolerized + anti-IgG
Tolerized + anti-CSF1
Tolerized + anti-CSF1R

E

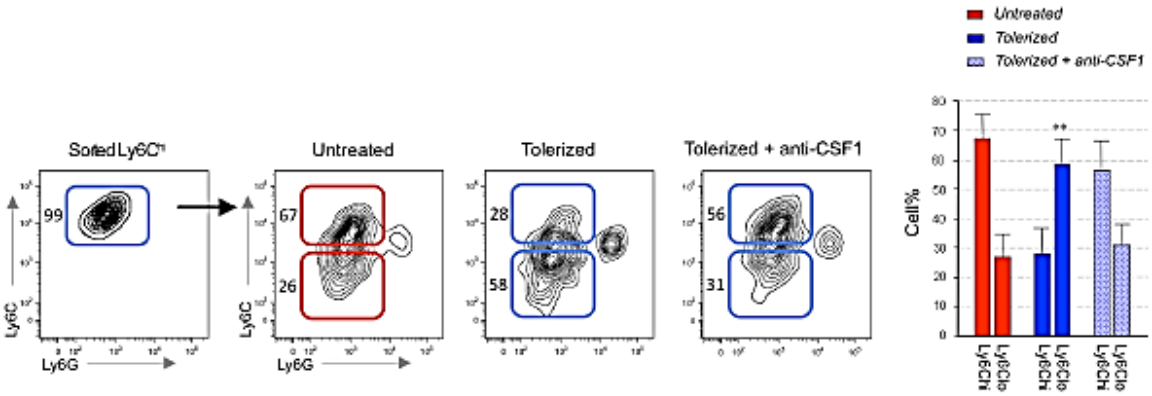
Sorted Ly6C^hi
Untreated
Tolerized
Tolerized + anti-CSF1
99
67
26
28
58
56
31
Ly6C
Ly6G
Untreated
Tolerized
Tolerized + anti-CSF1
Cell%
**
Ly6Chi
Ly6Clo

F

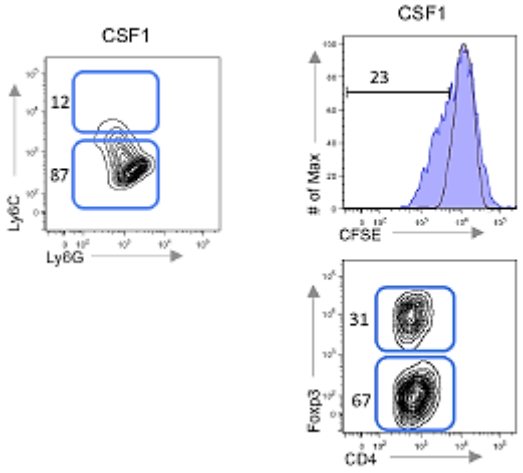

*Figura 4: (A) Expresión del CFS1 en corazones trasplantados de recipientes tolerantes y rechazos recogidos a día 5pt. Las muestras fueron analizadas mediante PCR cuantitativa y representadas en unidades relativas. Las barras graficas representan la media expresados mediante ± SEM de 3 experimentos independientes (**p ≤0.01). (B) Resultados de la citometria de flujo de las poblaciones mieloides en los órganos trasplantados de recipientes WT tolerizados y co-tratados con Ac anti-CFS1. Resultados de la media representados mediante ± SEM (n=4 de 3 experimentos independientes). (C) Expresión de Foxp3 de las células T CD4^{+} infiltradas en órganos de recipientes tolerantes y tratados posteriormente con anti-CFS1. Resultados de la media representados mediante ± SEM (n=4 de 3 experimentos independientes). (D) Efectos del bloqueo de la expresión de CFS1 y CFS1R (CD115) en la supervivencia del órgano trasplantado en recipientes WT tolerantes (n=12). (E) Resultados cito métricos de la transferencia adoptiva de células de medula ósea CFS1R^{+}Ly6C^{hi} a recipientes con o sin tratamiento tolerante y ± tratamiento a día 5 pt con anti-CFS1. Resultados de la media representados mediante ± SEM (n=3 de 3 experimentos independientes). (F) Resultados cito métricos de células Ly6C^{hi} obtenidas de medula ósea y cultivadas in vitro con Ac recombinantes CFS1 o IFNγ durante 96h. Resultados de la media representados mediante ± SEM de 3 experimentos independientes. (G) Función supresora de las células Ly6C^{hi} de medula ósea tras el tratamiento in vitro con CFS1 o IFNγ . Resultados de la media representados mediante ± SEM de 3 experimentos independientes*

Arnold y colegas (85) describen en sus experimentos cómo el daño muscular recluta específicamente monocitos inflamatorios que una vez en el musculo son capaces de cambiar su fenotipo y convertirse en macrofagos supresores con actividad antiinflamatoria. Quisimos comprobar si dicho mecanismo de conversión podría ocurrir también en nuestro modelo experimental de trasplante y demostrar que el CFS1 ejercía un papel fundamental en el proceso. Para ello aislamos monocitos CD11b^{+}CSF1R^{+}Ly6C^{hi}Ly6G^{-} GFP^{+} de medula ósea de ratón MaFIA y las transferimos a recipientes WT tolerizados o no y tratados con o sin anticuerpo bloqueante anti-CFS1 (Fig.4E). Los resultados mostraban que la conversión de monocitos Ly6C^{hi} a macrofagos Ly6C^{lo} se producía de forma normal en los recipientes tolerizados pero los recipientes en

donde se había bloqueado la producción de CSF1 con el anticuerpo neutralizador los monocitos Ly6C^{hi} no eran capaces de convertirse y mantuvieron un número y fenotipo similar al de los recipientes rechazados (sin anti-CD40L). Para confirmar que dichos macrofagos supresores Ly6C^{lo} mediados por CSF1 mantenían su capacidad funcional, realizamos experimentos adicionales de supresión de las células T CD8^{+} y proliferación de las células CD4^{+}Foxp3^{+} (Fig.4F).

DC-SIGN controla la función en los macrofagos supresores

Estudios previos (86) relacionan la expresión de DC-SIGN en macrofagos supresores dependiente de la expresión de CFS1. En concordancia con dichos estudios, nuestros resultados del análisis genético, PCR cuantitativa y de citometria de flujo revelan una sobre expresión de DC-SIGN en los recipientes tolerizados (Fig.5A-C), los cuales, tal y como habíamos comprobado en los experimentos anteriores sobre expresaban también el CFS1. Para valorar la implicación del receptor DC-SIGN durante tolerancia, utilizamos como receptores ratones C57/BL6 WT tolerizados a los que administramos un anticuerpo bloqueante de DC-SIGN. El experimento (Fig.5D) mostraba una disminución significativa en la supervivencia de los trasplantes en recipientes que habían sido tratados con el anti-DC-SIGN bloqueante . Pero al contrario que en los experimentos anteriores, cuando analizamos el órgano trasplantado mediante citometría, no observamos diferencias en cuanto a la disminución en el número de macrofagos Ly6C^{lo} (Fig.5E). Sugiriendo que DC-SIGN no interfería en el proceso de conversión de monocitos Ly6C^{hi} a Ly6C^{lo}. Sin embargo, mientras los macrofagos CD11b^{+}CSF1R^{+}Ly6C^{lo}Ly6G^{-} aislados de los órganos trasplantados tolerizados eran capaces de inhibir la proliferación de las células T CD8^{+} y expandir las CD4^{+}Foxp3^{+} in vitro, la misma población celular aislada de los recipientes tolerizados y tratados con anti-DC-SIGN no mostraban ninguna de las dos funciones supresoras (Fig.5F).

A

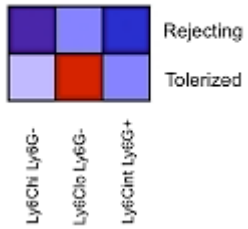
DC-SIGN
Rejecting
Tolerized
Ly6Chi Ly6G-
Ly6Clo Ly6G-
Ly6Cint Ly6G+

B

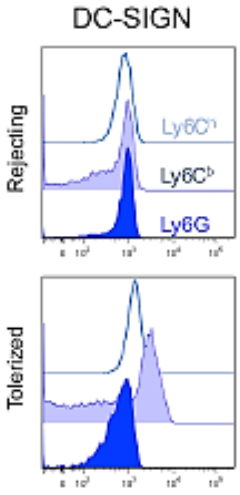
DC-SIGN
Rejecting
Tolerized
Ly6Chi
Ly6Clo
Ly6G

C

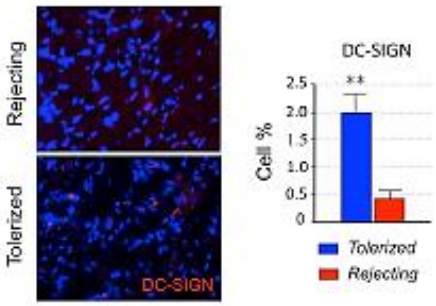
Rejecting
Tolerized
DC-SIGN
DC-SIGN
Cell %
**
Tolerized
Rejecting

D

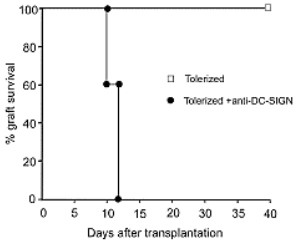
% graft survival
Days after transplantation
Tolerized
Tolerized +anti-DC-SIGN

E

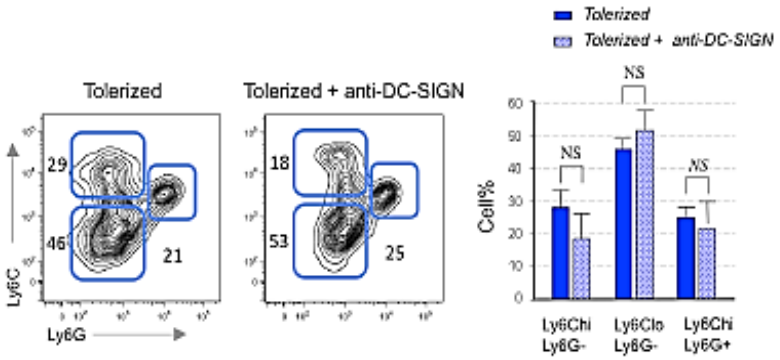
Tolerized
Tolerized + anti-DC-SIGN
Tolerized
Tolerized + anti-DC-SIGN
29
46
21
18
53
25
Ly6C
Ly6G
Cell%
NS
NS
NS
Ly6Chi Ly6G-
Ly6Clo Ly6G-
Ly6Chi Ly6G+

F

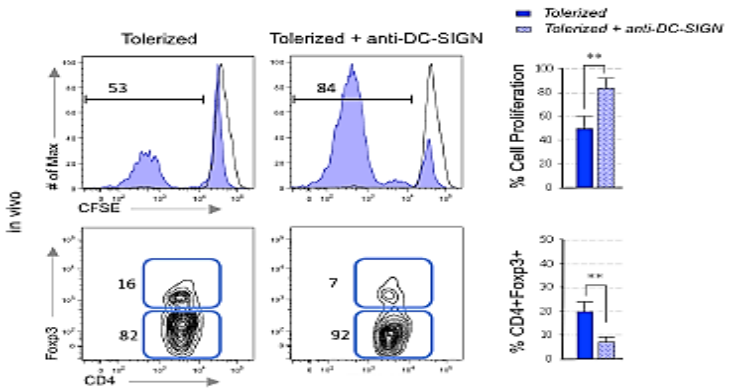
Tolerized
Tolerized + anti-DC-SIGN
In vivo
# of Max
CFSE
53
84
Foxp3
CD4
16
82
7
92
% Cell Proliferation
% CD4+Foxp3+
**
**

G

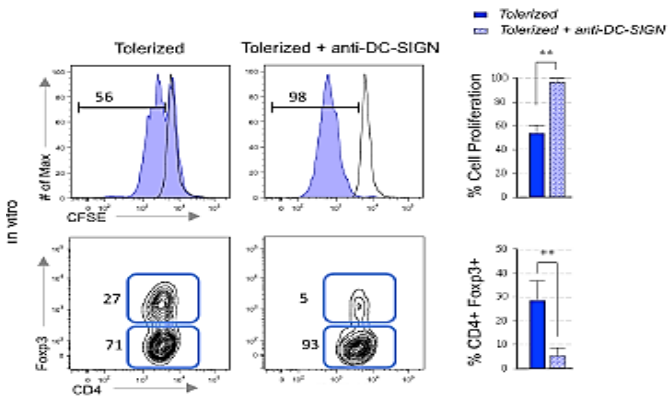

*Figura 5: (A y B) Heatmap del análisis trasncripcional y resultados de citometria de la expresión de DC-SIGN en las distintas poblaciones mieloides obtenidas de órganos de recipientes tolerantes y rechazos a día 5 pt. Los resultados de citometria representan 3 experimentos independientes. (C) Análisis de la fluorescencia de órganos tolerantes y rechazos. Las graficas de barras representan la frecuencia de las células DC-SIGN$^+$ expresadas como porcentaje respecto a un total de 1000 células DAPI$^+$ de los órganos analizados. Resultados de la media de 10 secciones tisulares obtenidos de 4 órganos distintos de cada grupo y representados mediante ± SEM (**p ≤0.01). (D) Efectos del bloqueo y la deficiencia de DC-SIGN en la supervivencia del órgano en recipientes WT tolerantes (n=12 ratones/grupo). (E) Resultados cito métricos de las poblaciones mieloides de los recipientes WT tolerantes tratados con Ac anti-DC-SIGN. Resultados de la media representados mediante ± SEM (n=4 de 3 experimentos independientes). (F) Capacidad de supresión de las células T CD8$^+$ y expansión de las células Treg por macrofagos Ly6C^{lo} obtenidos de recipientes tolerantes co-tratados in vivo con anti-DC-SIGN. Resultados de la media representados mediante ± SEM (n=4 de 3 experimentos independientes). (G) Capacidad de supresión de las células T CD8$^+$ y expansión de las células Treg por macrofagos Ly6C^{lo} obtenidos de recipientes tolerantes tras el co-tratamiento in vitro con anti-DC-SIGN. Resultados de la media representados mediante ± SEM (n=4 de 3 experimentos independientes).*

Para confirmar la capacidad del DC-SIGN en modificar la función inmuno reguladora en nuestra población celular, aislamos macrofagos Ly6C^{lo}de un recipiente WT tolerizado y añadimos in vitro el anticuerpo bloqueador de DC-SIGN. De la misma forma que con el tratamiento in vivo, los macrofagos supresores Ly6C^{lo} no exhibían las capacidades supresoras relacionadas con la proliferación y/o expansión de células T (Fig.5G).

Ligandos fucosilados de DC-SIGN necesarios para inducir tolerancia mediada por macrofagos supresores

Tal y como anteriormente hemos comentado, los ligandos de DC-SIGN son glicolipidos ricos en Man, Fuc y GlcNAc. Estos glicolipidos pueden encontrarse tanto en patógenos como en células y tejidos propios, como es el caso de Le^x. Sabiendo además, que Le^x se acumula en los tejidos durante procesos inflamatorios y/o daño tisular quisimos averiguar la implicación de éste en la inducción de la tolerancia en trasplantes. Para ello en nuestro modelo experimental de trasplante cardiaco en ratón, utilizamos como donantes, ratones doble deficientes (dKO) en fucosiltrasferasas IV y VII (Fuct IV-VII), cuya ausencia imposibilita la expresión de Le^x. Cuando analizamos los órganos trasplantados, los resultados de la inmunoflorescencia muestran una reducción significativa en la expresión de Le^x en los órganos donados por los ratones dKO en comparación con los donantes WT (Fig.6A). Resultados que concuerdan con el rechazo agudo observado en los experimentos de supervivencia de los órganos (Fig.6B).

A B

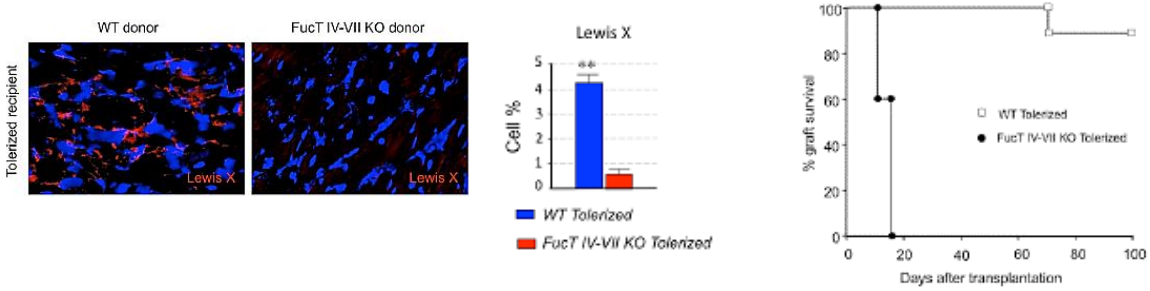

C

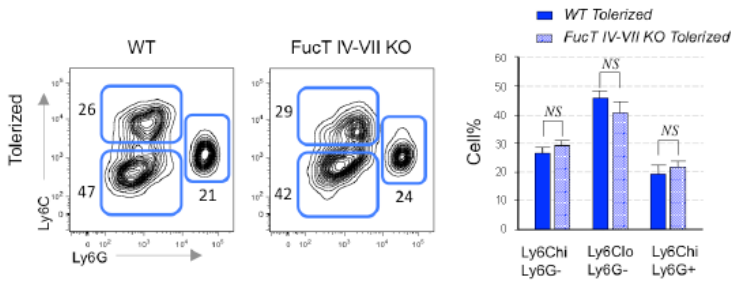

D

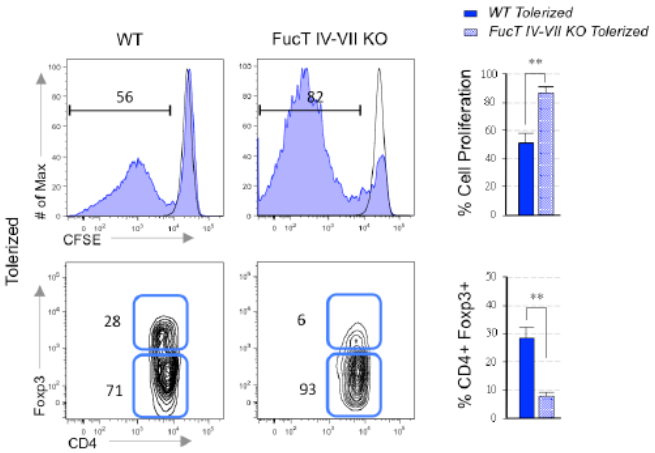

E

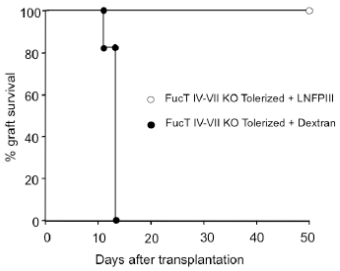

F

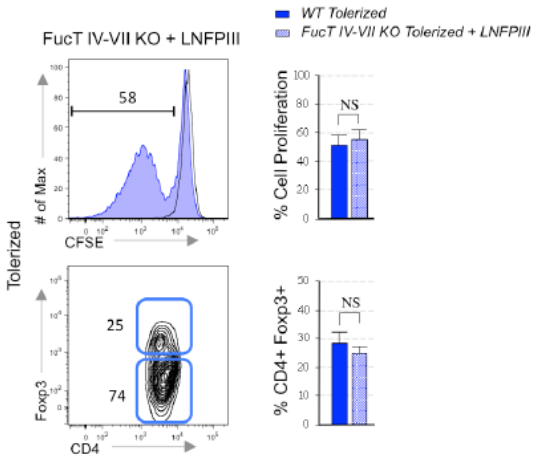

Figura 6: (A) Análisis de la inmuno fluorescencia de los órganos tolerantes y rechazos a día 5 pt. *Las graficas de barras representan la frecuencia de Le^x expresadas como porcentaje respecto a un total de 1000 células DAPI$^+$ analizados de donantes WT y Fuct IV-VII dKO. Resultados de la media de 10 secciones tisulares representados mediante ± SEM (**p ≤0.01). (B) Efectos de la deficiencia de Le*

en la supervivencia del órgano en recipientes WT tolerizados (n=12 ratones/grupo). (C) Resultados cito métricos de las poblaciones mieloides de órganos donados por WT y Fuct IV-VII dKO en recipientes tolerizados. Resultados de la media representados mediante ± SEM (n=4 de 3 experimentos independientes). (D) Capacidad supresora de T CD8+ y expansión de Treg in vitro de macrofagos Ly6C^{lo} obtenidos de los órganos donados por WT y Fuct IV-VII dKO. Resultados de la media representados mediante ± SEM (n=4 de 3 experimentos independientes). (E) Efectos del LNFPIII en la supervivencia del órgano trasplantado en recipientes WT tolerizados. (50µg/ratón administrados a día 0,+1 pt. n=8 ratones/grupo). (F) Capacidad supresora de T CD8+ y expansión de Treg in vitro de macrofagos Ly6C^{lo} obtenidos de l órganos donados por WT y Fuct IV-VII dKO en los recipientes tratados posteriormente con LNFPIII. Resultados de la media representados mediante ± SEM (n=4 de 3 experimentos independientes).

Al igual que en los experimentos anteriores, al analizar los órganos trasplantados mediante citometria, no encontramos diferencias en la frecuencia de macrófagos Ly6C^{lo} entre los donantes dKO y WT (Fig.6C). De la misma forma que ocurría con el receptor DC-SIGN, la ausencia de Le^{x} no implica una disminución en el número de macrofagos supresores Ly6C^{lo} ni en su conversión desde monocitos Ly6C^{hi}. A pesar de ello, mientras que los macrofagos Ly6C^{lo} aislados de los órganos de donantes WT eran capaces de mantener las funciones supresoras en las células T CD8^{+} y favorecer la expansión de las células T reg CD4^{+}Foxp3^{+} , los macrófagos Ly6C^{lo} de los donantes dKO no exhibían ninguna de las dos funciones inmuno reguladoras (Fig.6D). Para finalizar el experimento quisimos comprobar si la administración exogena in vivo de un ligando de DC-SIGN como el pentasacarido lacto-N-fucopentosa III (LNFPIII), era capaz de restaurar las funciones supresoras en los órganos trasplantados de donantes dKO (Fig.6E). Los resultados obtenidos demuestran que los macrofagos Ly6C^{lo} aislados de los órganos dKO tratados posteriormente con LNFPIII eran capaces de suprimir la proliferación de las células T CD8^{+} y expandir la población celular de Tregs (Fig.6F).

IL-10 es esencial en la supresión mediada por DC-SIGN

Descrita en la literatura (87,88) la señalización específica mediante ligandos fucosilados de DC-SIGN provoca una producción de la interleuquina anti-inflamatoria IL-10. Por ello, medimos la expresión de IL-10 en los órganos trasplantados y observamos que existía una sobre regulación de esta en los receptores WT tolerizados con anticuerpo anti-CD40L comparado con los recipientes rechazados sin tolerizar. Al contrario, IL-10 no se

expresaba en los órganos de los recipientes DC-SIGN KO a pesar de haber sido tolerizados (Fig.7A). Analizando minuciosamente las poblaciones celulares de origen mieloide infiltradas en los trasplantes, detectamos que la mayor expresión de IL-10 se producía entre la población de macrófagos Ly6C^{lo} obtenidos de los recipientes tolerizados (Fig.7A y Fig.S4A). En concordancia con los resultados obtenidos con los órganos completos, los macrofagos Ly6C^{lo} de los recipientes DC-SIGN KO exhibían poca expresión de IL-10 a pesar del tratamiento tolerizante. Para comprobar la necesidad especifica de IL-10 por los macrofagos supresores, seleccionamos mediante citometria las células Ly6C^{lo} de los órganos trasplantados en receptores IL-10 deficientes (IL10-/-) tolerizados y comprobamos sus funciones supresoras en cuanto a su capacidad para inhibir la proliferación de células T CD8^{+} y favorecer la expansión de las Treg CD4^{+}Foxp3^{+} (Fig. 7B). Predeciblemente, en ausencia de IL-10 los macrofagos Ly6C^{lo} no fueron capaces de exhibir ninguna de ambas funciones inmunoreguladoras. Para investigar mas a fondo la acción de IL-10 en nuestro modelo de tolerancia, quisimos comprobar si la administración exógena de IL-10 recombinante podía restaurar in vitro la perdida de las funciones supresoras en macrofagos Ly6C^{lo} aislados de recipientes DC-SIGN KO. Los resultados obtenidos mostraban una total recuperación de ambas funciones inmunoreguladoras (Fig.7C).

A

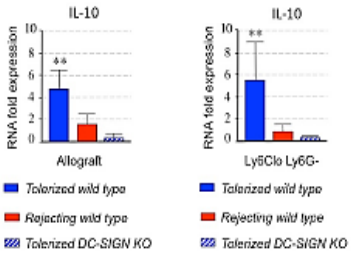

B

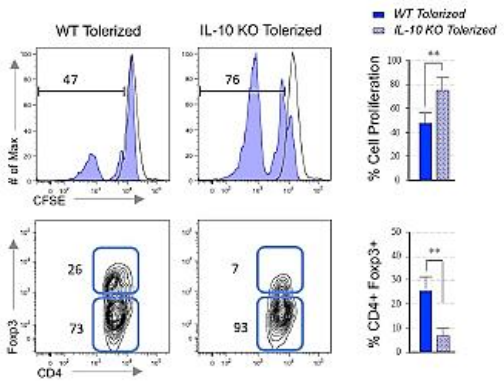

C

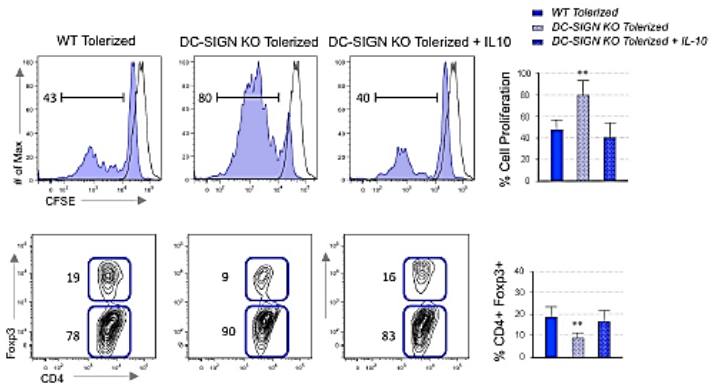

D

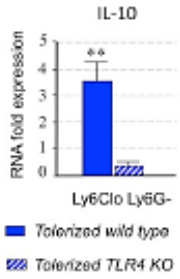

E

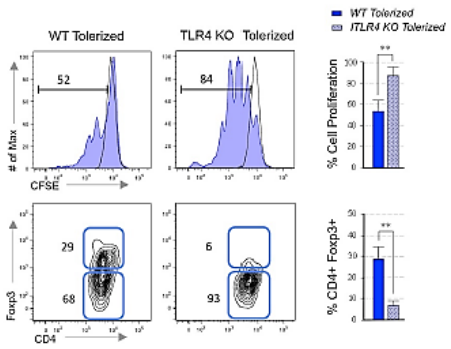

F

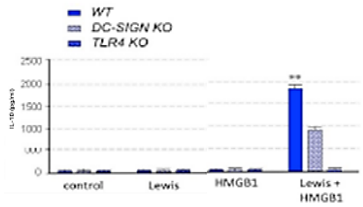

G

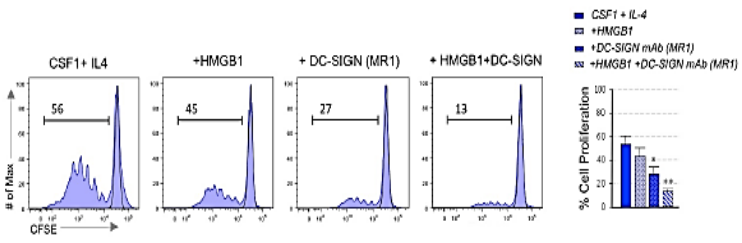

*Figura 7: (A) Expresión de IL-10 corazones trasplantados y en la población de macrofagos lo. Órganos obtenidos de recipientes WT sin tratar, WT tolerizados y DC-SIGN KO tolerizados recogidos a día 5 pt. Las muestras fueron analizadas mediante PCR cuantitativa y representadas en unidades relativas. Las barras graficas representan la media expresados mediante ± SEM de 3 experimentos independientes (**p ≤0.01). (B) Capacidad de supresión de las células T CD8⁺ y expansión de las células Treg por macrofagos Ly6C^{lo} obtenidos de recipientes tolerizados IL-10 deficientes. Resultados de la media representados mediante ± SEM (n=4 de 3 experimentos*

*independientes). (C) Capacidad de supresión de las células T CD8$^+$ y expansión de las células Treg por macrofagos Ly6C^{lo} obtenidos de recipientes DC-SIGN KO tolerizados y estimulados in vitro durante 72h con IL-10 a 10ng/ml. Resultados de la media representados mediante ± SEM (n=4 de 3 experimentos independientes). (D) Expresión de IL-10 en órganos trasplantados a recipientes WT y TLR4 KO tolerizados recogidos a día 5 pt. Las muestras fueron analizadas mediante PCR cuantitativa y representadas en unidades relativas. Las barras graficas representan la media expresados mediante ± SEM de 3 experimentos independientes (**p ≤0.01). (E) Capacidad de supresión de las células T CD8$^+$ y expansión de las células Treg por macrofagos Ly6C^{lo} obtenidos de recipientes WT y TLR4 KO tolerizados. Resultados de la media representados mediante ± SEM (n=4 de 3 experimentos independientes). (F) Expresión de IL-10 en células estimuladas de medula ósea de ratones WT, DC-SIGN KO y TLR4 KO. Las células de medula ósea fueron estimuladas in vitro durante 72h con Le^x (10µg/ml) y HMGB1 recombinante (10µg/ml).Grupo control no estimulado. Los sobrenadantes de los cultivos fueron analizados por ELISA. Resultados de la media representados mediante ± SEM de 3 experimentos independientes (**p ≤0.01). (G) Capacidad de supresión de las células T CD8$^+$ de monocitos aislados de médula ósea diferenciados con CSF1+IL4 y estimulados durante 72h con DC-SIGN (clon MR1; 100µg/ml) y/o HMGB1 recombinante (10µg/ml). Resultados de la media representados mediante ± SEM de 3 experimentos independientes (* p ≤0.05, **p ≤0.01).*

Descrito en la literatura, una producción óptima de IL-10 requiere no solo de la unión específica mediante DC-SIGN y sus ligandos fucosilados, sino que además requiere una señalización simultánea por TLR4 (toll like receptor 4), (88, 89). Para explorar esta hipótesis utilizamos ratones recipientes deficientes en TLR4 (tlr4-/- , TLR4 KO). Los resultados mostraban que efectivamente la ausencia de TLR4 provocaba una disminución en la producción de IL-10 en los macrofagos supresores y que dicha disminución repercutía en sus funciones inmuno reguladoras in vitro (Fig.7D y Fig.7E). Para demostrar la necesidad de la señalización simultanea de DC-SIGN y TLR4 en la producción de IL-10 realizamos un experimento en el que cultivamos células de médula ósea precedente de ratones WT, DC-SIGN KO y TLR4 KO que posteriormente estimulamos con el ligando de DC-SIGN, Le^x y un ligando de TLR4 como es la proteína HMGB1, que biológicamente se excreta durante daño tisular. Tal y como mostramos en la Fig.7F la interferencia en la estimulación en alguno de los dos factores repercute en la disminución significativa de la producción de IL-10. Dado los resultados interesantes obtenidos, quisimos comprobar si dicha estimulación simultanea DC-SIGN / TLR4 también influía en la regulación de la función supresora. Para ello realizamos un ensayo de proliferación con células T CD8$^+$ en co-cultivo con monocitos aislados de médula ósea diferenciados con CSF1+IL4. La adición al medio de ambos estímulos agonistas resultaba en la mayor respuesta in vitro supresora observada en el experimento (Fig.7G).

Los trasplantes cardiacos diana de la nano inmunoterapia mTORi-HDL

Utilizando nuestro modelo experimental de trasplante cardiaco alogeneico descrito previamente quisimos evaluar la especificidad y distribución in vivo de las nano partículas a estudio. 6 días tras la realización del trasplante administramos de forma intravenosa (iv) las nano partículas previamente marcadas con el isotopo zirconio 89 (^{89}Zr-mTORi-HDL). Durante 24h dejamos circular las nano partículas marcadas para permitir una correcta distribución sistémica. Pasadas las 24h determinamos su biodistribución detectando la presencia de ^{89}Zr-mTORi-HDL mediante sistemas de imagen in vivo de tomografía de emisión de positrones combinada con tomografía computerizada (PET-CT) (Fig.8A). Demostrado que las nano partículas se acumulaban en el órgano trasplantado quisimos entonces, evaluar su afinidad celular. En esta ocasión las nano partículas fueron marcadas con una marca fluorescente (DiO) y administradas con el mismo protocolo. Tras 24h, analizamos el corazón trasplantado mediante citometria de flujo. Los datos revelan una marcada afinidad de las nano particulas por las células de origen mieloide acumulándose preferentemente en macrofagos y monocitos y en menor medida en neutrófilos y CD con ausencia total de afinidad por células T (Fig.8B y Fig.S5A).

A B

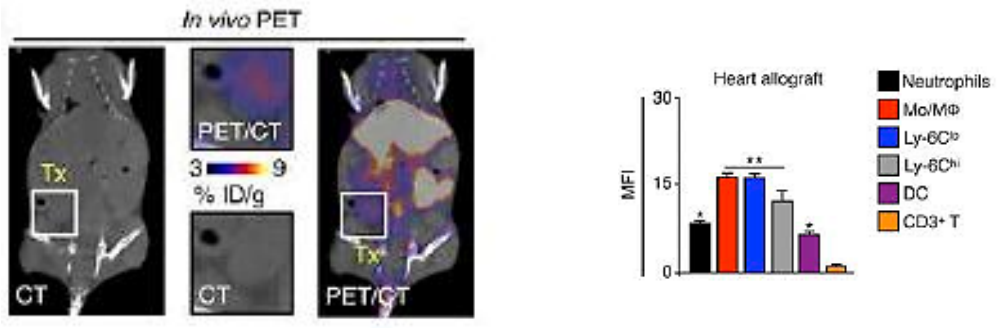

*Figura 8: (A) Representación 3D de la fusión de imágenes obtenidas por PET/CT de un trasplante cardiaco en ratón 24h después de la administración de las nano particulas ^{89}-Zr-mTORi-HDL. La imagen CT fue utilizada como referencia anatómica para localizar el órgano dentro de la cavidad abdominal y el PET permitió monitorizar las nano particulas radio marcadas. (B) Análisis de las intensidades medias de fluorescencia (MFI) de las poblaciones de neutrófilos, monocitos/macrofagos, macrofagos Ly6C^{lo} y Ly6C^{hi}, CD y células T infiltrados en el órgano trasplantado. Las barras graficas representan la media expresados mediante ± SEM de 4 experimentos independientes (**p ≤0.01).*

mTORi-HDL previene los cambios metabólicos y epigenéticos de la inmunidad entrenada

Para estudiar los mecanismos moleculares utilizados por nuestra inmuno nano terapia, aislamos mRNA de macrofagos Ly6C^{lo} obtenidos de recipientes tratados con mTORi-HDL y/o placebo. Los resultados fueron analizados mediante GSEA (Gene Set Enrichment Analysis). Tal y como esperábamos, los datos genéticos obtenidos indican que el tratamiento con la nano terapia mTORi-HDL bloquea las rutas de glicolisis y mTOR asociadas con la inmunidad entrenada (Fig.9 A, B). Para validar dichos resultados, realizamos un experimento en el que los macrofagos Ly6C^{lo} aislados mediante citometria eran cultivados y estimulados con LPS. Trascurridas 24h comprobamos su capacidad de producción de citoquinas inflamatorias y productos derivados de la glicolisis. Observamos que el tratamiento con mTORi-HDL no solo disminuía significativamente la producción de TNFα, IL-6 por parte de los macrofagos sino también se producía una disminución en la producción de lactato. (Fig.9C). Acorde a estos resultados, el análisis in vivo del DNA mostraba una reducción en la metilación H3K4 (H3K4me3) asociado a los cambios epigenéticos que se producen durante la inmunidad entrenada (Fig.9D).

A

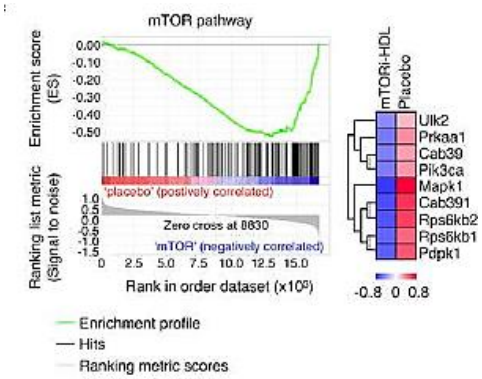

B

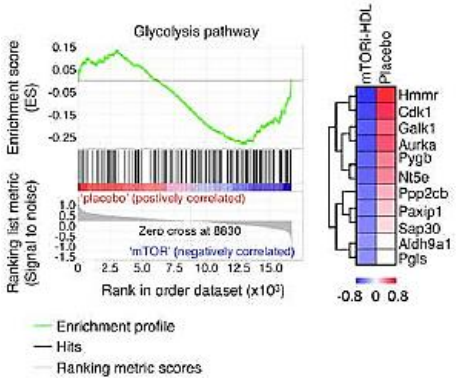

C D

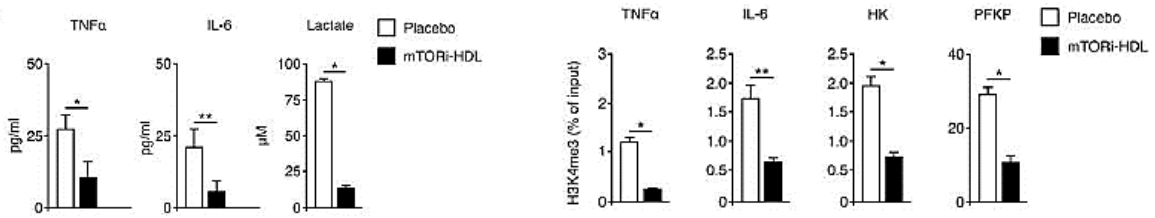

*Figura 9: (A y B) Resultados del GSEA de macrofagos Ly6C^{lo} infiltrados en el órgano trasplantado en recipientes tratados con mTORi-HDL y placebo como grupo control. Heatmap del GSEA de la ruta mTOR y glicolítica con un diferencial de expresión de marcadores de p≤ 0.05 entre las poblaciones de macrofagos Ly6C^{lo} obtenidos a día 6 pt de recipientes tratados con la inmuno terapia y placebo (n=3). (C) Expresión de TNFa, IL-6 y lactato en macrofagos Ly6C^{lo} obtenidos del órgano trasplantado de receptores tratados con placebo y con mTORi-HDL. Los macrofagos fueron re-estimulados con LPS durante 24h y posteriormente los sobrenadantes de los cultivos fueron analizados por ELISA. Resultados de la media representados mediante ± SEM de 3 experimentos independientes (*p≤ 0.05, **p ≤0.01). (D) Resultados de la inmuno precipitación de cromatina realizada para H3K4me3 en los macrofagos Ly6C^{lo} infiltrados en órganos de recipientes tratados con placebo y con mTORi-HDL. 4 de los principales genes relacionados con la inmunidad entrenada fueron analizados mediante PCR cuantitativa (n=3) (*p≤ 0.05, **p ≤0.01).*

mTORi-HDL favorece la acumulación de macrofagos supresores en trasplantes

Para evaluar la efectividad del tratamiento de la nano inmunoterapia en nuestro modelo experimental de trasplante cardiaco, administramos 3 dosis de mTORi-HDL a día 0, 2 y 5 pt. En concordancia con nuestros resultados preliminares observamos que el numero total de macrofagos, neutrófilos y CD fueron predominantemente menores en los recipientes tratados con las nano partículas comparadas con grupo control (placebo) (Fig.10A). Además, al analizar en profundidad los resultados, observamos que los recipientes no tratados con la nano terapia mostraban un mayor número de macrofagos inflamatorios Ly6C^{hi} mientras que los recipientes tratados con mTORi-HDL mostraban un aumento significativo de macrofagos Ly6C^{lo} supresores (Fig.10B).

A

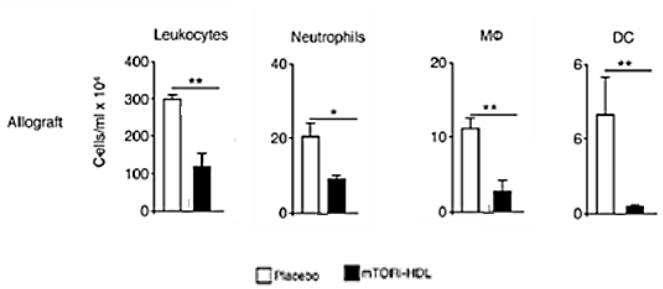
Leukocytes
Neutrophils
MΦ
DC
Allograft
Cells/ml x 10⁴
Placebo
mTORi-HDL

B

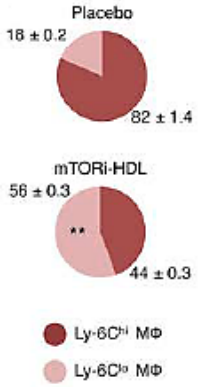
Placebo
18 ± 0.2
82 ± 1.4
mTORi-HDL
56 ± 0.3
44 ± 0.3
Ly-6C^hi MΦ
Ly-6C^lo MΦ

C

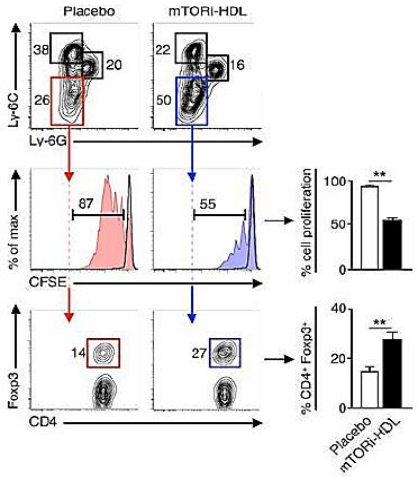
Placebo
mTORi-HDL
Ly-6C
Ly-6G
% of max
CFSE
% cell proliferation
Foxp3
CD4
% CD4+ Foxp3+
Placebo
mTORi-HDL

D

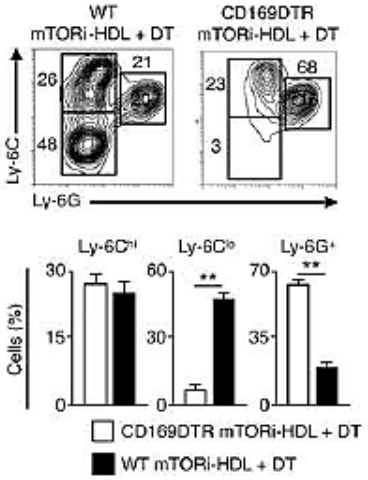
WT
mTORi-HDL + DT
CD169DTR
mTORi-HDL + DT
Ly-6C
Ly-6G
Ly-6C^hi
Ly-6C^lo
Ly-6G+
Cells (%)
CD169DTR mTORi-HDL + DT
WT mTORi-HDL + DT

E

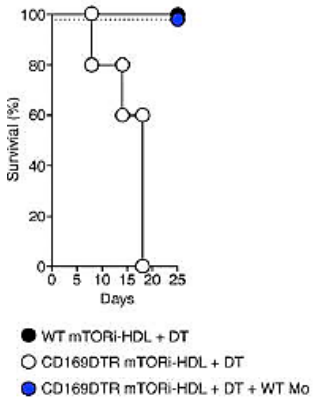
Survival (%)
Days
WT mTORi-HDL + DT
CD169DTR mTORi-HDL + DT
CD169DTR mTORi-HDL + DT + WT Mo

Figura 10: (A) Numero total de leucocitos, neutrófilos, macrofagos y CD obtenidos a día 5pt en recipientes tratados con placebo o *mTORi-HDL. Resultados de la media representados mediante ± SEM (n=4 de 3 experimentos independientes) (* p ≤0.05, **p ≤0.01). (B) Ratio Ly6Chi/Ly6Clo de los macrofagos infiltrados en los órganos trasplantados en recipientes control (placebo) o tratados con mTORi-HDL .Resultados de la media representados mediante ± SEM (n=4 de 3 experimentos independientes) (* p ≤0.05, **p ≤0.01). (C) Resultados de citometría de la expresión de Ly6C y Ly6G en las poblaciones de células mieloides obtenidas a día 5pt en los trasplantes de recipientes tratados con mTORi-HDL y placebo. Capacidad de supresión de las células T CD8$^+$ y expansión de las células Treg por macrofagos Ly6C^{lo} obtenidos de recipientes tratados con mTORi-HDL y placebo. Resultados de la media representados mediante ± SEM (n=4 de 3 experimentos independientes) (**p ≤0.01). (D) Resultados cito métricos de la caracterización fenotípica de las poblaciones mieloides obtenidas a día 6 pt de recipientes WT y CD169DTR tratados con mTORi-HDL y DT. Resultados de la media representados mediante ± SEM (n=4 de 3 experimentos independientes) (**p ≤0.01). (E) Efectos de la depleción in vivo de los macrofagos CD169$^+$Ly6C^{lo}* en la supervivencia del órgano en recipientes *WT y CD169DTR tratados con mTORi-HDL y DT. La transferencia adoptiva de monocitos WT restaura la supervivencia y la tolerancia en los recipientes depleccionados y tratados con mTORi-HDL (n=4ratones/grupo).*

Para determinar las funciones de los macrofagos supresores Ly6C^{lo} aislados de los recipientes tratados con mTORi-HDL, analizamos la capacidad tanto de inhibir la proliferación de las las células T CD8$^+$ como de expandir las células Treg. El ensayo de proliferación nos muestra que los macrofagos Ly6C^{lo} obtenidos de los recipientes tratados con mTORi-HDL no solo previenen la proliferación de células T CD8$^+$ sino que además mantienen la capacidad de expandir la población inmunosupresora de células Treg CD4$^+$Foxp3$^+$ (Fig.10 C). Para comprobar que el tratamiento con la nano inmunoterapia favorecía específicamente el desarrollo de la población de macrofagos supresores necesarios para inducir tolerancia realizamos un ensayo con depleción in vivo. Con la misma metodología que utilizamos en los experimentos del capitulo I, el corazón donante BALB/c se trasplantó en recipientes WT control y/o C57Bl/6 CD169^{DTR} a los cuales se les administró la DT 6 días pt para deplecionar la población de las células *CD169$^+$Ly6C^{lo}* (Fig.10 D). A pesar del tratamiento con las nano partículas mTORi-HDL, la depleción de los macrofagos supresores resultó en un rechazo agudo (12± 2dias) del órgano trasplantado (Fig.10 E). Congruentemente, la trasferencia adoptiva de monocitos procedentes de ratones WT restauraba por completo la supervivencia del órgano (Fig.10 E).

mTORi-HDL/ TRAF6i-HDL induce la tolerancia a trasplantes

Tal y como estudiamos en el capitulo I, la vía co-estimulatoria CD40L-CD40 forma parte de los mecanismos de acción involucrados en la tolerancia en trasplantes. Un análisis exhaustivo de nuestra nano terapia reveló que el tratamiento con mTORi-HDL aumentaba la expresión de CD40 en macrofagos Ly6C^{lo} (Fig.11A) y que ello podría conllevar a un futuro fracaso del órgano trasplantado. Tratando de reducir los efectos de la señalización por CD40, desarrollamos una segunda nano imuno terapia basada en el bloqueo del receptor TRAF6 (TRAF6i-HDL), mediador en la señalización de CD40 en macrofagos (90).

A

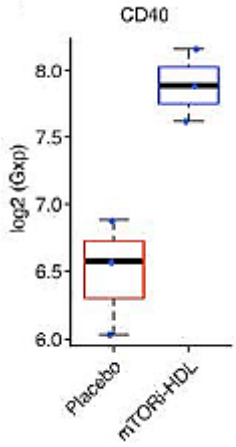

B

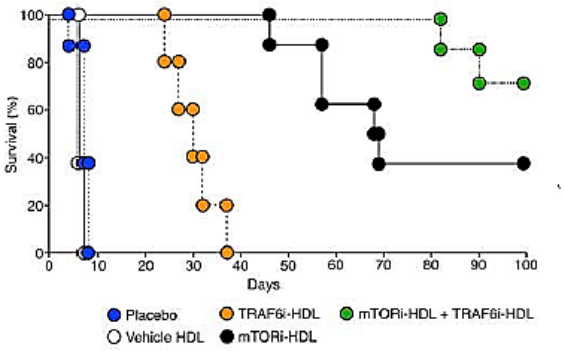

Figura 11: (A) Representación grafica del análisis génico para la expresión de CD40 por macrofagos Ly6C^{lo} obtenidos de los órganos trasplantados en recipientes tratados con mTORi-HDL vs placebo. Resultados de la media representados mediante ± SEM (n=4 de 3 experimentos independientes). (B) Curvas de supervivencia de los órganos trasplantados utilizando distintas terapias. Placebo y vehículo HDL, mTORi-HDL, TRAF6i-HDL y la terapia combinada mTORi-HDL/ TRAF6i-HDL (n= 8 ratones/grupo).

Para evaluar el tratamiento con las nuevas nano partículas utilizamos nuestro modelo experimental de trasplante cardiaco alogeneico con las pautas de dosificación anteriormente descritas. Administramos 3 inyecciones de mTORi-HDL y TRAF6i-HDL solas o en combinación. En el análisis de supervivencia del trasplantes observamos que el tratamiento con mTORi-HDL aumentaba significativamente la supervivencia del

órgano cuando lo comparamos con los controles (placebo y/o vehículo) pero al analizar ambas terapias combinadas obtuvimos el mejor resultado de tolerancia, alcanzando el 70% de supervivencia a los 100 días pt (Fig.11B)

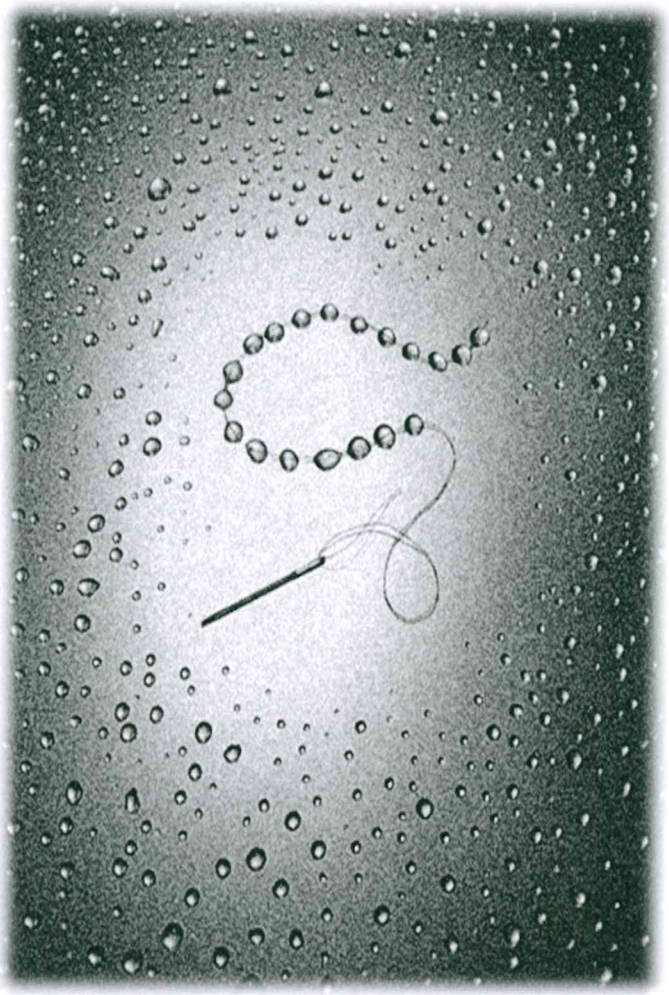

CONCLUSIONES

A pesar del consenso general en la función inmuno reguladora de las células de origen mieloide su acción durante tolerancia en trasplantes es todavía inconcreta. Sabemos que las células mieloides con función supresora están incluidas en la población celular $CD11b^+$ que expresan el el antígeno de diferenciación mieloide Gr-1(91). Dado el amplio rango de células que se pueden abarcar bajo dicha clasificación el propósito de esta tesis ha sido identificar y fenotipar las poblaciones celulares mieloides involucradas en la tolerancia en trasplantes, comprendiendo las bases moleculares implicadas en su desarrollo y los mecanismos de acción implicados en su función inmuno reguladora. Durante el primer capitulo se describen una serie de experimentos realizados para identificar a una población de macrofagos supresores necesarios para inducir tolerancia. Los resultados obtenidos nos permiten delinear específicamente el fenotipo de los macrofagos supresores implicados en la inmuno regulación durante trasplantes. Estos macrofagos expresan la integrina CD11b, el receptor CD115 del CFS1, bajos niveles de la glicoproteína Ly6C, la molécula de adhesión CD169 y la lectina DC-SIGN, cuya función critica en la inducción de la tolerancia ha sido demostrada en los experimentos mediante su ausencia o el bloqueo in vivo. Dada la importancia de esta molécula la proponemos como nuevo marcador para definir las poblaciones de macrofagos inmuno reguladores. Funcionalmente, aportamos nuevos mecanismos de acción tanto in vitro como in vivo, usando técnicas de depleción celular, ratones modificados genéticamente y nuevas estrategias que revelan que los macrofagos $CD11b^+CSF1R^+Ly6C^{lo}Ly6G^-CD169^+DC\text{-}SIGN^+$ inhiben la proliferación de las células T $CD8^+$ y favorecen la expansión de las células Treg $CD4^+Foxp3^+$. En cuanto al desarrollo celular, demostramos que es necesaria una óptima producción de IL-10 solo alcanzable mediante la doble señalización de DC-SIGN y TLR4. En conjunto los datos aportan nuevas ideas para el desarrollo de protocolos terapéuticos basados en el uso del CSF1, que a su vez regula la expresión DC-SIGN, para inducir macrofagos supresores con uso clínico en la prevención del rechazo en trasplantes.

Un innovador descubrimiento en inmunología es el hecho de que las células del sistema inmune innato puedan poseer memoria inmunológica. Este hecho se le conoce por el nombre de “inmunidad entrenada”. En esta tesis proponemos dicha inmunidad

entrenada como responsable en parte de que los macrofagos y células de origen mieloide de los órganos trasplantados mantengan un fenotipo inflamatorio propiciando un ambiente inmunogénico que impida la supervivencia del órgano y favorezca el rechazo inmunológico. El punto de vista general en el que solo la inmunidad adaptativa era capaz de poseer memoria inmunológica ha sido desafiado (61). Se sabía que determinados organismos como plantas y animales invertebrados eran capaces de crear resistencia ante las infecciones, pero estudios recientes han demostrado que incluso en animales vertebrados las células del sistema inmune innato muestran características adaptativas entorno a una memoria no específica (62). Se podría considerar un mecanismo de evolución de la memoria inmune primitiva con el objetivo de proporcionar una protección adicional del hospedador frente a reinfecciones. Mecanismo a su vez con una doble cara. Por un lado con función beneficiosa en situaciones de falta o disminución de acción de la inmunidad adaptativa, como en el caso de recién nacidos o enfermedades del sistema inmune y por otro lado con función nociva en cuanto al mantenimiento de un ambiente inflamatorio con efectos negativos como por ejemplo para la inducción de la tolerancia en trasplantes. Los resultados obtenidos durante el segundo capitulo demuestran que la nano inmuno terapia HDL tiene una fuerte afinidad por los macrofagos en los que previene los cambios epigenéticos asociados con la inmunidad entrenada inhibiendo su fenotipo inflamatorio. Por lo tanto podemos concluir que la nano terapia HDL favorece la acumulación sistémica de macrofagos supresores $Ly6C^{lo}$ durante el trasplante y consecuentemente la inducción de la tolerancia inmunológica.

DISCUSIÓN

CAPITULO I: Fenotipo, desarrollo y mecanismos de acción de macrofagos en tolerancia

Monocitos circulantes y/o macrofagos residentes de tejidos son parte de las células presentadoras de antígeno (CPA) que intervienen en la construcción de la respuesta inmune frente al órgano trasplantado. La acumulación de macrofagos en el órgano trasplantado ha sido siempre un hecho reconocido de rechazo (92). Nahrendorf y colegas apuntaban en su trabajo (93) a los monocitos inflamatorios Ly6C^{hi} como responsables de infiltrar el órgano trasplantado y montar una respuesta inmune contribuyendo al rechazo de este. Durante los últimos años se han investigado distintas estrategias terapéuticas contra los monocitos Ly6C^{hi}, obteniendo resultados prometedores en la reducción de la patogénesis de algunas enfermedades como la ateroesclerosis (94). Sin embargo dada la plasticidad de esta población celular, los monocitos y macrofagos son capaces de adquirir un fenotipo regulatorio con el que inhibir la respuesta inmune. Se ha relacionado la plasticidad de los monocitos y macrofagos con el escenario en el que se encuentren, de forma que monocitos inmunogénicos pueden diferenciarse a macrofagos supresores dependiendo del ambiente (95). De hecho la presencia de los macrofagos supresores en órganos trasplantados de larga duración ha sido anteriormente descrita por algunos autores (96).Consistentes con estos datos y utilizando un modelo experimental de trasplante cardiaco en ratón, en esta tesis hemos demostrado como los monocitos estimulantes Ly6C^{hi} se convierten en macrofagos supresores Ly6C^{lo} durante la tolerancia inducida mediante un bloqueo parcial coestimulatorio (ver grafica hipótesis). Afortunadamente con el tiempo se ha ido asumiendo el rol vital de los macrofagos supresores en cuanto a la prevención del rechazo y en el re-establecimiento de la homeostasis tisular tras el trasplante. Varias estrategias dirigidas a controlar la respuesta de los macrofagos han sido desarrolladas, incluyendo la trasferencia celular adoptiva. La utilización de esta técnica con macrofagos reguladores CD11b^{+}Ly6C^{lo}Ly6G^{-}CD169^{+} generados ex vivo ha demostrado prolongar la supervivencia de un corazón trasplantado en ratón (97). Una población de macrofagos reguladores equivalente en humanos son generados a partir

de monocitos $CD14^{+}CD16^{-}$ circulantes en sangre y cultivados durante 6 días con CSF1 y estimulados posteriormente con IFN-ɣ (98). Durante dicho periodo, se observa una una disminución gradual en la expresión de CD14, semejante a la transición de los monocitos inflamatorios $CD14^{+}CD16^{-}$ hacia macrofagos anti inflamatorios $CD14^{low}$ $CD16^{+}$. Pensamos que el desarrollo endógeno de macrofagos supresores descrito en este trabajo es análogo a la generación in vitro de macrofagos reguladores humanos, ya que la adquisición de funciones supresoras por parte de los macrofagos en ratón va asociada directamente a la perdida de expresión de la glicoproteína Ly6C. Actualmente, macrofagos reguladores humanos han sido desarrollados y aprobados oficialmente para su uso en estudios clínicos junto con el tratamiento inmuno supresor en pacientes trasplantados de riñón de donantes vivos. Hasta la fecha dos pacientes han sido tratados con la novedosa terapia celular sin mostrar signos de rechazo durante 6 años, y además 16 receptores de trasplante renal están previstos para ser tratados con dichos macrofagos reguladores diferenciados con CSF1, como tratamiento complementario a una reducción en la dosis de la droga inmunosupresora.

En los distintos experimento llevados a cabo en el capitulo I observamos que la expresión de DC-SIGN aumentaba en los macrofagos estimulados con CSF1 y que favorecía la supervivencia del órgano trasplantado siendo imprescindible para la inducción de la tolerancia. DC-SIGN es una lectina de trans membrana de tipo II, que se expresa en CD y macrofagos y está involucrada en muchos procesos de la respuesta inmune (99). Inicialmente fue descrita como molécula activadora de la respuesta inmune en CD inmaduras diferenciadas a partir de monocitos en presencia de CSF2+IL4. Los autores observaron que estas CD $DC\text{-}SIGN^{+}$ inducían la proliferación de células T alogeneicas (100). Por otro lado Broxmeyer y colegas demostraron que la diferenciación de macrofagos en presencia de CSF1+IL4 también favorecía la expresión de DC-SIGN y que dichos macrofagos $DC\text{-}SIGN^{+}$ eran menos eficientes en inducir una respuesta a una reacción linfocitaria alogeneica (101). Por ello es admisible mantener la hipótesis de que la respuesta inmune pueda ser en parte determinada por factores de estimulación involucrados en la diferenciación celular de los monocitos bien hacia

CD DC-SIGN$^+$ estimulantes o hacia macrofagos DC-SIGN$^+$ supresores. En la tesis, extendemos este hallazgo para demostrar nuevamente que al contrario que las CD DC-SIGN$^+$ estimuladas con CSF2+IL4, los macrofagos DC-SIGN$^+$ inducidos con CSF1+IL4 inhiben la proliferación de las células T in vitro e in vivo. Usando ratones deficientes en DC-SIGN (CD209a) en nuestro modelo experimental animal demostramos además, que la presencia de dichos macrofagos DC-SIGN$^+$ son totalmente necesarios para inducir la tolerancia, revelando una nueva función de DC-SIGN en ratón, nunca antes descrita. Es importante anotar que muchas de las funciones descritas sobre DC-SIGN están basadas en estudios in vitro con células humanas. Se han descrito ocho tipos de DC-SIGN en ratón homólogos al DC-SIGN humano que difieren en la especificidad del reconocimiento de glicolípidos y en su perfil de expresión (102). El CD209a también denominado mDC-SIGN y/o SIGNR5 es el ortólogo a la molécula humana (103) aunque difiere de ésta en que no está regulado por IL-4, en su habilidad en unirse a residuos manosilados y su actividad endocítica (104,105). Aparte de las diferencias filogenéticas las CD DC-SIGN$^+$ murinas son potentes células estimulatorias por lo que cabe asumir las similitudes funcionales entre el DC-SIGN humano y murino. En concordancia con los datos descritos en la literatura, en la tesis demostramos que el bloqueo de la vía co-estimulatoria CD40/CD40L favorece la producción de CSF-1 fomentando la acumulación de macrofagos supresores DC-SIGN$^+$ que inhiben la proliferación de células T y favorecen la expansión de Treg gracias a IL10. Dado que los macrofagos DC-SIGN$^+$ secretan IL-10 y participan en la generación de células Treg es lógico pensar que DC-SIGN pudiera contribuir al mantenimiento de un ambiente tisular inmuno suprimido que favorezca la aceptación del órgano trasplantado, tal y como propone el laboratorio de van Kooyk (106). La capacidad de los macrofagos DC-SIGN$^+$ en estimular la producción de IL10 requiere de dos señales simultaneas; la señalización vía DC-SIGN mediante la unión a ligandos fucosilados y la señalización vía TLR4 (107). En este trabajo observamos que los macrofagos DC-SIGN$^+$ aislados de recipientes TLR4 deficientes producían menos IL10 y no exhibían funciones supresoras in vitro, y por lo tanto la tolerancia no pudo ser inducida en a pesar del tratamiento con anti-CD40L. Consistente con nuestros resultados otros autores (108) indican también la necesidad

de ambos receptores DC-SIGN-TLR4 para producir suficiente IL-10 capaz de inducir tolerancia periférica. Durante ensayos MLR, observaron una disminución de la proliferación de células T causado posiblemente por un aumento de células Treg, proceso que asociaban con un aumento en la expresión de los glicanos fucosilados en los tejidos (108). Como agonista de la vía de señalización TLR4 utilizamos la proteína HMGB1 recientemente descrita como potenciadora de la función inmuno supresora consecuencia del aumento de la producción de IL10 en macrofagos y células de origen mieloide (109). Esto es de especial interés en nuestra hipótesis ya que HMGB1 está asociada a daño tisular consecuencia de la cirugía del trasplante (110) y de la isquemia (111).

CAPITULO II: Nano inmunoterapia en tolerancia

En el capitulo II validamos con nuestro modelo experimental una novedosa técnica en la manipulación de las células del sistema inmune innato en los trasplantes como es la ingeniería con nano partículas. El objetivo terapéutico de estas nano partículas es el de trasportar antígenos y/o agentes inmuno moduladores a células diana específicas, lo que permite un mejor control de la respuesta inmune a la hora de inducir la tolerancia en trasplantes. El trasporte de un antígeno a una CPA específica puede resultar en la producción de citoquinas reguladoras y en consecuencia la inhibición y/o estimulación de las vías co-estimulatorias participes en la respuesta tolerogénica. Se ha demostrado por ejemplo, que el trasporte de un antígeno a receptores específicos de CD como CD40, CD11c y DEC-205 mediante nano particulas consigue una respuesta citotóxica de las células T asociada a una potente estimulación de las CD (112). Por otro lado, el uso de nano particulas como trasportadoras de drogas inmuno supresoras a bajas dosis previenen la respuesta inmune. El laboratorio de Goldstein (113) llevó a cabo un experimento en trasplante de piel en ratón en el que utilizaron nano partículas PLGA poly(lactic-co-glycolic acid), cargadas con acido micofenólico dirigidas específicamente a células de origen mieloide que les provocaba una sobre regulación del PDL1 (programmed death ligan 1) aumentando consecuentemente la supervivencia del

órgano. Otro estudio llevado a cabo en un modelo experimental similar demuestra la efectividad de las nano micelas cargadas con rapamicina y tacrolimus en abordar distintas poblaciones celulares de los nódulos linfáticos provocando también un aumento de la supervivencia del injerto (114). Recientemente el tratamiento con nano partículas biodegradables cargadas con corticosteroides de lenta liberación ha demostrado prevenir el rechazo en un modelo de trasplante de cornea en rata (114). Todos estos trabajos fueron llevados a cabo utilizando unas nano partículas de gran tamaño (≥100nm de diámetro). El tamaño de dichas nano partículas es importante a la hora de su bio distribución. Mientras que las nano partículas pequeñas (≤25nm) se absorben más fácilmente y se retienen en el organismo por más tiempo, las nano partículas grandes tienden a agregarse y son engullidas por las células fagocíticas de forma no especifica. Las nano particulas utilizadas en nuestros experimentos, son particulas denominadas HDL, realizadas con lipoproteínas de alta densidad, de pequeño tamaño con funciones inmuno reguladoras y con afinidad especifica por los macrofagos. Han sido estudiadas previamente como opción terapéutica en ateroesclerosis (115) y también como herramienta anti macrofagos asociados a tumores en la clínica contra el cáncer (116). Para una translación de nuestros experimentos a la clínica de trasplantes es importante considerar los resultados obtenidos en el capitulo II, que revelan que la terapia combinada mTORi-HDL/TRAF6i-HDL favorece la supervivencia del órgano trasplantado sin necesidad de la administración continuada de inmunosupresores. Por lo tanto la identificación de la inmunidad entrenada como objetivo terapéutico proporciona un punto de partida para el desarrollo de tratamientos específicos enfocados en prevenir los cambios epigenéticos de los macrofagos y promover la inmuno tolerancia en trasplantes.

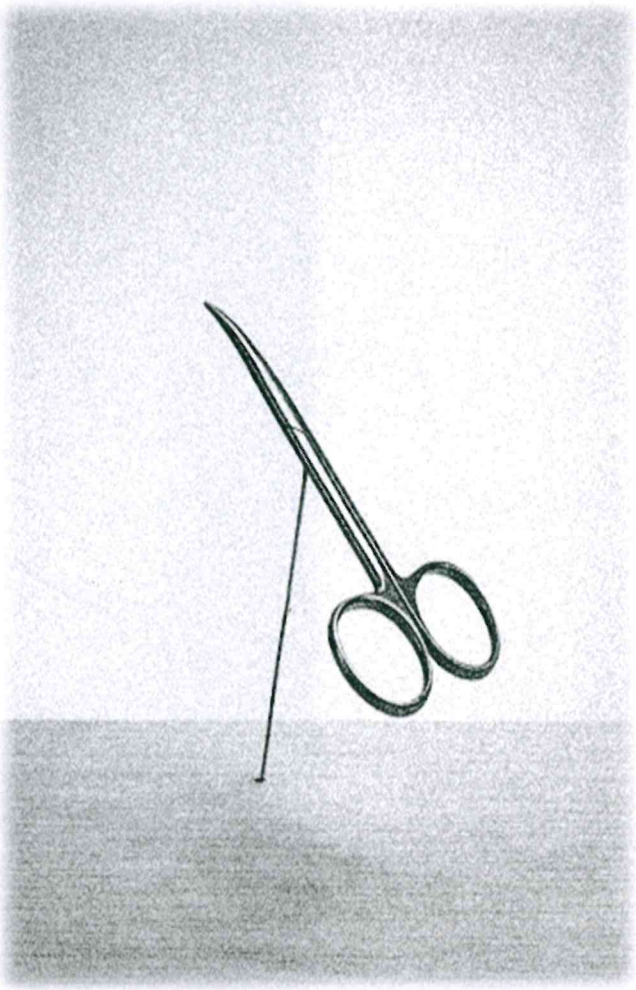

MÉTODOS EXPERIMENTALES

RATONES

Los ratones BALB/c, C57BL/6, C57BL/6-Foxp3tm1Flv/J, B6.129P2-CD40tm1Kik/J y B6.B10ScN-Tlr4lps-del/JthJ fueron obtenidos de los laboratorios Jackson con 8 semanas de edad. Los ratones DC-SIGN defiecientes (DC-SIGN-KO, B6(FVB-Cd209atm1.1Cfg/Mmcd) fueron obtenidos del Mutant Mouse Regional Resource Center del Consorcio de Functional Glycomics (Scripps.Res. Institute). Los ratones alpha(1,3)fucosyltrasferases FucT-IV y FucT-VII dobles deficientes fueron obtenidos de Jonh Lowe de la Universidad de Michigan. Los ratones C57BL/6-Tg (Cfs1r-EGFP-NGFR/FKBP1A/TNFRSF6) 2Bck/J MaFIA fueron obtenidos del D.Cohen de la Universidad de Kentucky (117) y los ratones C57BL/6CD169 ^{DTR} de Masato Tanaka (Kawaguchi, Japón) (118). Todos los experimentos con animales coincidían en sexo y edad y fueron llevados acabo siguiendo los protocolos de experimentación aprobados por el comité de experimentación y bienestar animal del Hospital Monte Sinai, NY.

TRANSPLANTE EXPERIMENTAL DE CORAZÓN

Los corazones de ratones BALB/c fueron trasplantados de forma heterópica totalmente vascularizados a ratones C57BL/6. Esta técnica fue originalmente descrita por Corry et al., (119).Los ratones recipientes fueron tratados para inducir tolerancia a dia 0,2 y 4 pt con 250 µg de anticuerpo anti-CD40L (clon MR1, BioXcell) tal y como se describe en la literatura (120). La función del órgano trasplantado fue monitorizada diariamente mediante palpación abdominal. Los grupos controles, sin tratar recibieron IgG de hámster diluida en PBS. El rechazo del órgano se estableció con el cese total del latido palpable y confirmado mediante visualización directa a posteriori por laparotomía.

DEPLECCION CELULAR IN VIVO

Para la depleción del CD169 expresado por los macrofagos supresores $CD11b^{+}CSF1R^{+}Ly6C^{lo}Ly6G^{-}$ los ratones heterocigotos CD169-DTR se inyectaron

intraperitonealmente (i.p) con 10ng por g de peso vivo de DT (Sigma-Aldrich) a las 24,48 y 72h pt (118). La depleción de Ly6G fue inducida con el anticuerpo anti-Ly6G clon 1A8 (BioXcell) inyectado de forma i.p en dosis de 0.5mg por ratón a día -3, -2 y -1 pt (1).

TRATAMIENTO IN VIVO CON ANTICUERPOS

El anticuerpo agonista anti-CD40 (clon FGK4.5) fue producido por BioXcell. El estimulo del DC40 independientemente del CD40-L fue llevado a cabo mediante la administración i.v de 100µg del anticuerpo agonista CD40 a día 0,+1, pt (121). El anticuerpo bloqueador del IFN-ɣ (clon R4-6A2, BioXcell) fue inyectado i.p a 500µg a día 0 y +1 pt. los anticuerpos bloqueadores del CFS1 (clon 5A1) y CSF1R (clon AFS98) producidos por BioXcell. El anti-CFS1 cuya acción neutralizante del CFS1 es conocida (122, 123), fue administrado i.p a 150µg/ratón en días -1, +1, +2, +3, +4 pt. El anti-CSF1R con acción bloqueadora del receptor, fue inyectado i.p a 2mg/ratón a dia -5 y a 0.5mg/ratón a -4 y -3 dias pt (124, 125). El anticuerpo neutralizador de DC-SIGN (CD209a) fue purificado de sobrenadantes tal y como se describe en la literatura (126). Se inyecto de forma i.p a 250µg/ratón a dia +1, +2,+3 y +4 pt.

AISLAMIENTO DE LEUCOCITOS INFILTRADOS EN EL TRASPLANTE

Los corazones de ratón trasplantados fueron sumergidos in situ con medio HBSS con 1% de heparina. Los corazones se cortaban en pequeños trozos y se digerían con 400 U/ml collagenase IV (Sigma-Aldrich) en HBSS con 0.01% de DNase I (MP Biomedicals) y 10 mM HEPES (Cellgro). La suspensión de tejido digerida se pasaba por un filtro de nylon de 70µm y se centrifugaba. El pellet de células obtenido se re-suspendía en medio RPMI suplementado con 10% FBS (Suero fetal bovino) y 1% de Pen-Strep (Penicilina-Streptomicina). Posteriormente se teñia con los anticuerpos de interés para analizarlos mediante citometria de flujo (BD LSR-II; BD Biosciences).

CITOMETRIA DE FLUJO Y SORTER

Para teñir las células mieloides utilizamos anticuerpos monoclonales, conjugados con distintos fluorocromos, específicos de CD45 (clone 30-F11), CD11b (clone M1/70), F4/80 (clone CI: A3.1), Ly-6C (clone HK1.4) y sus correspondientes isotipos obtenidos de eBioscience. El anticuerpo Ly-6G (clone 1A8) fue obtenido de Biolegend. La citometria se llevo a cabo en un clitómetro LSR II (BD Biosciences) y los resultados fueron analizados con el software de FlowJo (Tree Star, Inc.).Los resultados son expresados como porcentaje de células teñidas o contadas (células por ml) sobre el fondo. Para aumentar la pureza de células mieloides de los órganos trasplantados, las células fueron aisladas con el InFlux cell sorter (BD) obteniendo un 96% de pureza.

ENSAYOS DE SUPRESIÓN

Los bazos de ratones C57BL/6 y C57BL/6-Foxp3tm1Flv/J (H-2^b) fueron disociados hasta obtener suspensiones celulares. Los eritrocitos fueron eliminados con buffer de lisis ACK (Invitrogen). Los esplenocitos fueron teñidos con anti-CD4 y/o CD8 y marcados con CFSE a 5µM (Molecular probes, Invitrogen). Las células T $FoxP3^+CD^+$ y $CFSE^+CD8^+$ fueron sorteadas con el FACS Aria II (BD Bioscience) con una pureza ≥ 98% y estimuladas con anti-CD3 y anti-CD28 dynabeads (Gibco). Las células T $FoxP3^+CD4^+$ y $CFSE^+CD8^+$ activadas se pusieron en co-cultivo con las células mieloides $CD11b^+CSF1R^+Ly6C^{hi}Ly6G^-$, $CD11b^+CSF1R^+Ly6C^{lo}Ly6G^-$ y $CD11b^+CSF1R^+Ly6C^{int}Ly6G^+$ aisladas de los órganos trasplantados durante 72-96h a 37ºC y 5% de CO2. La proliferación celular fue analizada por citometria de flujo midiendo la dilución de la marca de CFSE de las células T $CD8^+$ La expansión de las células Treg fue analizada por citometria de flujo midiendo la señal del FoxP3-RFP de las células T $CD4^+$.

MICROSCOPÍA

Las imagenes de las distintas poblaciones mieloides infiltradas en el trasplante fueron adquiridas de células sorteadas y aisladas por cytospun a 500 r.p.m durante 3 min. con un Cytospin 4 (Thermo Scientific) y teñidas con Hema 3 (Thermo Fisher Scientific). Los órganos trasplantados se seccionaron transversalmente en dos partes iguales y se congelaron a -80ºC directamente en OCT. Utilizando un criomicrotomo (Leica 1900 CM) se obtuvieron secciones de 8µm de tejido que se fijaron con acetona sobre portas cubiertos con polylysine. El anticuerpo anti- DC-SIGN de ratón (CD209a) clon MMD3 se conjugó con el anticuerpo Cy3 obtenido de Jackson Immunoresearch. Todos los portas se montaron utilizando Vectashield (Vector Laboratories) para preservar la fluorescencia. Las imágenes se adquirieron con un microscopio de fluorescencia Leica DMRA2 y con una cámara digitalizada. Se tomaron imágenes separadas en azul, verde y rojo que fueron posteriormente analizadas y editadas con el software Openlab (Improvision).

SINTESIS NANO PARTICULAS HDL

Las nano particulas mTORi-HDL fueron sintetizadas mediante el método de hidratación de capa lipídica (lipid film hydration). Brevemente, el 1,2-dimyristoyl-sn-glycero-3-phosphatidylcholine (DMPC), 1-myristoyl-2-hydroxy-sn-glycero-phosphocholine (MHPC, ambos obtenidos de Avanti Polar Lipids y la Rapamicina (Selleckhem) se disolvieron en cloroformo/metanol (10:1 v/v) haciendo una mezcla con proporciones de 3:1:0,5. Tras la evaporación de los disolventes, el APOA1 disuelto en PBS fue añadido en proporción 5:1 e incubado durante 20 min en hielo. La mezcla total final fue homogenizada durante 15 min usando un sonicador. Las nano particulas mTORi-HDL fueron lavadas y concentradas mediante filtración centrifugal con tubos de filtro 10kDa. Los agregados se eliminaron mediante centrifugación y filtración (0.22µm) posterior. La solución con Rapamicina administrada i.v incluye 4% de etanol y un 5% de TWEEN80 en PBS. En los experimentos de uso terapéutico con las nano particulas, los

ratones recibieron una dosis i.v de 5mg/kg de mTORi-HDL el día del trasplante así como a día 2 y 5 pt. Las nano particulas TRAF6i-HDL se sintetizaron de forma muy similar. La mezcla final en cloroformo/metanol (10:1 v/v) DMPC, MHPC y el inhibidor TRAF6 ((2E)-1-phenyl-3-(2,5-dimethylanilino)-2-propen-1one25) se realizó con un ratio 8.7:1:0.6. La mezcla se seco usando una bomba de vacío y obteniendo como resultado una fina capa lipídica. El APOA1 fue añadido a la capa lipídica en proporción 9.5:1 e incubado a 37ºC durante 4h hasta que la capa se hidrató completamente y la solución se homogenizó. La solución fue sonicada durante 1h hasta obtener las nano particulas TRAF6i-HDL. Posteriormente se lavaron y purificaron mediante centrifugación-filtración. Para los estudios terapéuticos las nano particulas TRAF6i-HDL se administraron a dosis de 5mg/kg el día del trasplante así como a día 2 y 5 pt.

RADIOMARCACIÓN DE LAS NANO PARTICULAS mTORi-HDL

Las mTORi-HDL fueron marcadas con 89Zr de acuerdo al protocolo anteriormente descrito. A las nano particulas HDL sintetizadas se añadió 1mol % del quelante de fosfolípidos DFO. El marcaje con 89Zr se completó mediante la reacción del DFO unido a las nano particulas con oxalato de 89Zr diluido en PBS (pH=7.1) a 37ºC durante 1h. Finalmente las nano particulas 89Zr-mTORi-HDLfueron aisladas mediante filtración centrifugal con tubos de 10kDa (yield 75 ± 2 %).

IMAGEN MICRO-PET/CT Y BIODISTRIBUCIÓN

Los ratones receptores de trasplante cardiaco fueron inyectados con una única dosis de 89Zr-mTORi-HDL (0.17 ± 0.01 mCi, ~0.25 mg APOA1) en 0.2 ml de PBS en la vena lateral de la cola a dia 6 pt. 24h después los animale se anestesiaron con Isoflorano (Baxter Healthcare, Deerfield, IL, USA) con una mezcla de gas/oxigeno (2% para inducción, 1% para mantenimiento) y se realizo el scanner utilizando un sistema Inveon PET/CT (Siemens Healthcare Global, Erlangen, Germany). El scanner del cuerpo completo se realizo durante 15 min almacenando todas las imágenes. La energía y el

tiempo de coincidencia de los eventos fueron de 350−700 keV and 6 ns, respectivamente. Los datos de las imágenes fueron normalizadas para la respuesta no uniforme del PET, perdida de tiempo muerto de contaje, ratio de dispersión de positrones y descomposición física del tiempo de inyección. Se aplicó la corrección de la media de dispersión y/o volumen parcial. La tasa de conteo durante construcción de la imagen fue convertida en animación (porcentaje de dosis inyectada [%ID] por gramo de tejido) usando un sistema de calibración derivado de la imagen fantasma de agua que contenía el 89Zr y equivalente al tamaño de un ratón adulto. Posteriormente las imágenes fueron analizadas con el software ASIPro VMTM (Concorde Microsystems, Knoxville, TN, USA) e Inveon Research Workplace (Siemens Healthcare Global, Erlangen, Germany). Los scanners CT de todo el cuerpo fueron realizados con rayos X con voltajes de 80 kV y corriente de 500µA. Las imágenes fueron adquiridas usando 120 pasos rotatorios con un total de220º a 120s por imagen y 145ms de exposición. Inmediatamente tras el PET/CT los animales fueron sacrificados y los tejidos aislados, pesados y analizados con un contador gamma automático Wizard 2480 (Perkin Elmer, Waltham, MA) para determinar su contenido radioactivo. Los valores fueron corregidos y convertidos a %ID. Para determinar la bio distribución readioactiva en los corazones trasplantados, los órganos naive y trasplantados se mantuvieron en unas placas de iluminación fosfórica (BASMS-2325, Fujifilm, Valhalla, NY) durante 4h a -20ºC. La placa se leyó con una resolución de 25 µm pixeles en un lector de placas Typhoon 7000IP (GE Healthcare, Pittsburgh, PA). Las imágenes finales de analizaron con el software ImageJ.

qPCR e INMUNOPRECIPITACIÓN DE CROMATINA (ChIP)

Las PCR cuantitativas realizadas para IFNγ, IL-10, CSF1, DC-SIGN, CD40L y CD169 se llevaron a cabo mediante la extracción con Trizol (Invitrogen) del RNA de las poblaciones celulares estudiadas. La retro transcripción fue llevada a cabo utilizando el Omniscript reverse-transcription system (Qiagen). La PCR se realizó con LightCycler

system (Roche) y el kit de SYBR Green (Qiagen). Todos los experimentos fueron realizados por triplicado técnico y la expresión génica fue normalizada y expresada en porcentajes relativos al gen constitutivo GAPDH. Las secuencias de los primers utilizados se obtuvieron de PrimerBank (https://pga.mgh.harvard.edu/primerbank/).

Para la realización de la técnica de inmunoprecipitación de cromatina, utilizamos anticuerpos específicos de ratón anti-H3K4me3 (39159; Active Motif), y anti-IgG (ab171870; Abcam). Los ChIP se llevaron a cabo tal y como se describe en la literatura (127). Para fragmentar el DNA utilizamos un sonicador refrigerado Bioruptor (Diagenode) obteniendo fragmentos de aproximadamente 200-1000 pares de bases. Los lisados celulares fueron aclarados durante 2h usando los isotipos apropiados a los anticuerpos utilizados (rabbit IgG; Abcam). Los anticuerpos especificos fueron incubados con bolas magnéticas (Dynabeads® M-280 Sheep Anti-Rabbit IgG; ThermoFisher Scientific) durante la noche a 4ºC, tras lo cual tanto la cromatina como los anticuerpos se inmuno precipitaron. El DNA se aisló tras la digestión con RNasa y proteína K (Roche), utilizando el kit MinElute (Qiagen). Finalmente, la PCR cuantitativa se realizó utilizando iQ SYBR Green Supermix (Bio-Rad) según protocolo del fabricante. Para el diseño de los primers se utilizó la herramienta on line, Primer3 y chequeadas con secuencias murinas en Integrated Genomics Viewer (IGV; Broad). Las secuencias de los primers usados para el ChIP-qPCR fueron las siguientes: Murine. Actb promoter forward, 5'-GTTGGCTGTGCCAGTGTC-3', and Actb promoter reverse, 5'-CAGCTTCTTTGCAGCTCCTT-3'; Tnf-alpha promoter forward, 5'-GCCACAAGCAGGAATGAGA-3', and Tnf-alpha promoter reverse, 5'-CCACATCTCCCTCCAGAA-3'; Il1b promoter forward, 5'-GAGAGAGAGAGAGACTTACTTGCACA-3', and Il1b promoter reverse, 5'-TTTCACAGCTCTTCACTTCTGC-3'; Il-6 promoter forward, 5'-AATGTGGGATTTTCCCATGA-3', and Il-6 promoter reverse, 5'-GCAAGGAACTGCCTTCACTTA-3'; Hk1 promoter forward, 5'-TTCCCCCGAAGACACTTTAC,

and Hk1 promoter reverse, 5'-GAGGCAGAACAGGAACTCCA; Pfkp promoter forward, 5'-GCTGGTCAGGACACCGATAG, and Pfkp promoter reverse, 5'-GCCAGGGCTTCAGTGCTT.

ENZYME-LINKED IMMUNOSORBENT ASSAY (ELISA)

La producción de citoquinas IL-6, TNFα, M-CSF e IFN-γ por los macrofagos aislados del trasplante fue medida en los sobrenadantes utilizando un kit comercial y siguiendo las recomendaciones del fabricante (eBiosciences).

ANALISIS MICROARRAY

Las células mieloides $CD45^{+}CD11b^{+}CSF1R^{GFP}Ly6C^{hi}Ly6G^{-}$, $CD45^{+}CD11b^{+}CSF1R^{GFP}Ly6C^{lo}Ly6G^{-}$, and $CD45^{+}CD11b^{+}CSF1R^{GFP}Ly6C^{int}Ly6G^{+}$ de los recipients tolerizados con anti-CD40L mAb y recipients rechazo sin tartar fueron seleccionadas doblemente con el sorter FACS Aria II (BD Biosciences) alcanzando una pureza >98%. El microarray fue realizado en colaboración con el Immunological Genome Project (ImmGen). Se corrieron un total de 32 Affymetrix Exon GeneChip de ratón. La expresión génica fue corregida con el fondo, normalizada y simplificada con RMA. Las puntuaciones simplificadas de expresión fueron contabilizadas a nivel de meta trascripción- probeset utilizando las indicaciones del fabricante. Debido a que los arrays fueron analizados en diferentes lotes, la expresión génica fue corregida mediante el sva package (129).

Los macrofagos $Ly\text{-}6C^{lo}$ infiltrados en el trasplante procedente de recipientes tratados con la nano terapia mTORi-HDL y/o placebo fueron sortedos con FACS Aria II (BD Biosciences) alcanzando una pureza >98%. El análisis del microarray de las celulas sorteadas se realizo con un total de 6 Affymetrix Exon GeneChip de ratón con el mismo procedimiento que anteriormente. El análisis GSEA (Gene Set Enrichment Analysis) fue realizado utilizando la versión Gene pattern 3.9.6. Los parámetros a analizar fueron los siguientes: Gene sets c2.cp.biocarta.v5.1.symbols.gmt; c2.cp.kegg.v5.1.symbols.gmt; c2.cp.reactome.v5.1.symbols.gmt; c6.all.v5.1.symbols.gmt (Oncogenic Signatures),

c7.all.v5.1.symbols.gmt (Immunologic signatures); y h.all.v5.1.symbols.gmt (Hallmarks). Cada gen fue anlizado por separado. Para seleccionar las rutas significantes en cada set de genes se aplicó el método FDR (The false discovery rate) para comoparaciones multiples y el valor-q de 0.25. Solo los genes con alta significancia fueron considerados en los resultados finales.

ANALISIS ESTADISTICO

La media de los resultados obtenidos fue expresada con ±SEM. Las comparaciones entre dos grupos fueron realizados usando el test Mann-Whitney o Wilcoxon signed-rank para valores pareados. La comparación de 3 o mas grupos fueron realizadas con el test Kruskal-Wallis y Dunn's multiple comparisons. Los resultados del análisis de supervivencia de órganos trasplantados se expresaron gráficamente como curvas de supervivencia estimadas con Kaplan-Meier y las diferencias entre los distintos grupos se compararon con el log-rank test. El programa IBM SPSS statistics 22 fue utilizado para el analisis estadístico. Un valor $p \leq 0.05$ fue considerado como estadisticamente significativo.

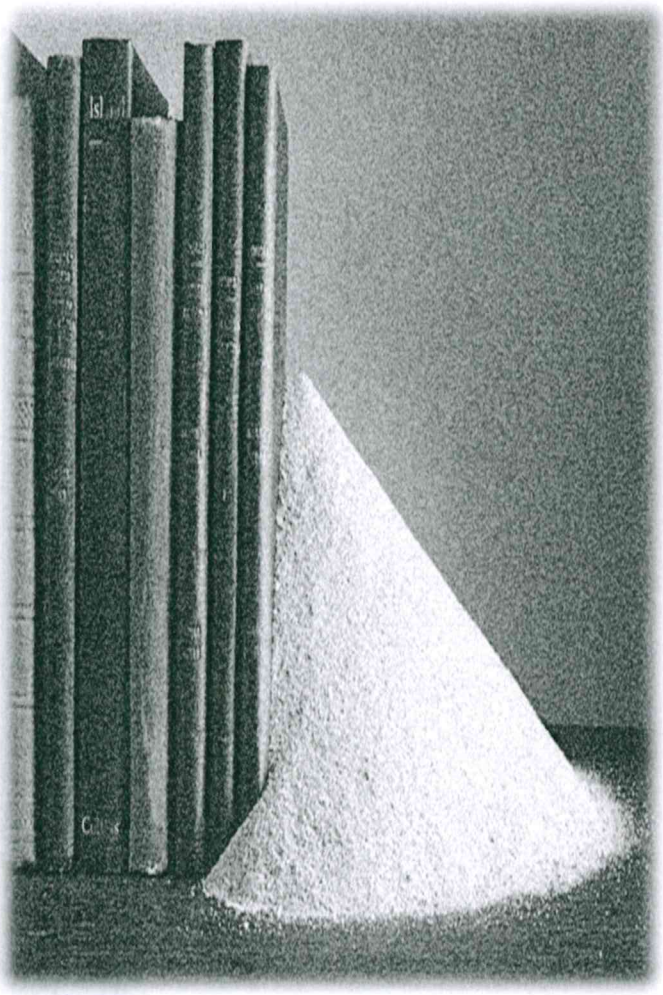

BIBLIOGRAFIA

1. Garcia MR, et al. Monocytic suppressive cells mediate cardiovascular transplantation tolerance in mice. J Clin Invest. 2010; 120(7):2486-96.
2. Fleming TJ, Fleming ML and Malek TR. Selective expression of Ly-6G on myeloid lineage cells in mouse bone marrow. RB6-8C5 mAb to granulocyte-differentiation antigen (Gr-1) detects members of the Ly-6 family. J Immunol. 1993, 1; 151(5):2399-408.
3. Geijtenbeek TB, et al.Identification of DC-SIGN, a novel dendritic cell-specific ICAM-3 receptor that supports primary immune responses Cell. 2000, 3; 100(5):575-85.
4. Van Liempt E, et al. Specificity of DC-SIGN for mannose- and fucose-containing glycans. FEBS Lett. 2006, 13;580(26):6123-31.
5. Lowe JB. Glycosyltransferases and glycan structures contributing to the adhesive activities of L-, E- and P-selectin counter-receptors. Immunol Rev. 2002 ;186:19-36.
6. Van Gisbergen KP, et al. Interactions of DC-SIGN with Mac-1 and CEACAM1 regulate contact between dendritic cells and neutrophils. FEBS Lett. 2005, 7;579(27):6159-68.
7. Gringhuis SI, et al. Carbohydrate-specific signaling through the DC-SIGN signalosome tailors immunity to Mycobacterium tuberculosis, HIV-1 and Helicobacter pylori. Nat Immunol. 2009;10(10):1081-8.
8. Ludwig IS, et al.Hepatitis C virus targets DC-SIGN and L-SIGN to escape lysosomal degradation. J Virol. 2004;78(15):8322-32.
9. Nonaka M, et al. Glycosylation-dependent interactions of C-type lectin DC-SIGN with colorectal tumor-associated Lewis glycans impair the function and differentiation of monocyte-derived dendritic cells. J Immunol. 2008 1;180(5):3347-56.
10. Gringhuis SI, et al. C-type lectin DC-SIGN modulates Toll-like receptor signaling via Raf-1 kinase-dependent acetylation of transcription factor NF-kappaB. Immunity. 2007; 26(5):605-16.
11. Martinez FO, et al.Transcriptional profiling of the human monocyte-to-macrophage differentiation and polarization: new molecules and patterns of gene expression. J Immunol. 2006, 15; 177(10):7303-1.

12. Wing EJ, et al. Peritoneal macrophages exposed to purified macrophage colony-stimulating factor (M-CSF) suppress mitogen- and antigen-stimulated lymphocyte proliferation. J Immunol. 1986, 1; 137(9):2768-73.
13. Netea MG, Quintin J and Van der Meer JW. Trained immunity: a memory for innate host defense. Cell Host Microbe. 2011, 19; 9(5):355-61.
14. Saeed S, et al. Epigenetic programming of monocyte-to-macrophage differentiation and trained innate immunity. Science. 2014, 26; 345(6204):1251086.
15. Van Furth R, et al.The mononuclear phagocyte system: a new classification of macrophages, monocytes, and their precursor cells. Bull World Health Organ. 1972;46(6):845-52.
16. Wake K, Kawai Y and Smedsrød B. Re-evaluation of the reticulo-endothelial system. Ital J Anat Embryol. 2001;106(2 Suppl 1):261-9.
17. Thomas JA. Conception du système réticulohistiocytaire; la régulation de l'état hystiocytaire et la spécificité cellulaire. Rev Hematol. 1949;4(4):639-5.
18. Tedeschi C.In memoriam: Mario VOLTERRA, 1901-1960. J Mt Sinai Hosp N Y. 1961; 28:249-5.
19. Carrel A and Ebeling AH. The fundamental properties of the fibroblast and the macrophages: The macrophage. J Exp Med. 1926 ;44(3):285-305.
20. Ratcliffe NA and Rowley AF. A comparative synopsis of the structure and function of the blood cells of insects and other invertebrates. Dev Comp Immunol. 1979 ;3(2):189-221.
21. Sutton JS and Weiss L. Transformation of monocytes in tissue culture into macrophages, epithelioid cells, and multinucleated giant cells. An electron microscope study. J Cell Biol. 1966;28(2):303-32.
22. Le Borgne de Kaouël C, de Grouchy J and Robineaux R. Microcinematography of a monolayer culture of hematopoietic origin and of a continuous line of the same origin. Study of the dependence relations.C R Acad Sci Hebd Seances Acad Sci D. 1971, 26;273(4):487-90.
23. Van Furth R, Hirsch JG and Fedorko ME. Morphology and peroxidase cytochemistry of mouse promonocytes, monocytes, and macrophages. J Exp Med. 1970, 1;132(4):794-812.

24. Rabinovitch M. Phagocytosis: the engulfment stage. Semin Hematol. 1968 ;5(2):134-55.
25. Rabinovitch M and De Stefano MJ. Particle recognition by cultivated macrophages. J Immunol. 1973 ;110(3):695-701.
26. Ehrenreich BA andCohn ZA. Pinocytosis by macrophages J Reticuloendothel Soc. 1968;5(3):230-42.
27. Volkman A and Gowans JL. The origin of macrophages from bone marrow in the rat. Br J Exp Pathol. 1965;46:62-70.
28. Guilliams M, et al. Dendritic cells, monocytes and macrophages: a unified nomenclature based on ontogeny. Nat Rev Immunol. 2014;14(8):571-8
29. Gomez Perdiguero E, et al.Tissue-resident macrophages originate from yolk-sac-derived erythro-myeloid progenitors. Nature. 2015, 26;518(7540):547-51.
30. Steinman RM and Cohn ZA. Identification of a novel cell type in peripheral lymphoid organs of mice. I. Morphology, quantitation, tissue distribution. J Exp Med. 1973, 1;137(5):1142-62.
31. Naito M, Takahashi K, Nishikawa S. Development, differentiation, and maturation of macrophages in the fetal mouse liver. J Leukoc Biol. 1990; 48(1):27-37.
32. Hoeffel G and Ginhoux F. Ontogeny of Tissue-Resident Macrophages. Front Immunol. 2015 22;6:486
33. Ginhoux F and Guilliams M. Tissue-Resident Macrophage Ontogeny and Homeostasis. Immunity. 2016, 15;44(3):439-449.
34. Hettinger J et al. Origin of monocytes and macrophages in a committed progenitor. Nat Immunol. 2013;14(8):821-30
35. Carlin LM et al. Nr4a1-dependent Ly6C (low) monocytes monitor endothelial cells and orchestrate their disposal. Cell. 2013, 11;153(2):362-75.
36. Auffray C et al. Monitoring of blood vessels and tissues by a population of monocytes with patrolling behavior. Science. 2007, 3;317(5838):666-70.
37. Ensan S et al. Self-renewing resident arterial macrophages arise from embryonic CX3CR1(+) precursors and circulating monocytes immediately after birth. Nat Immunol. 2016 ;17(2):159-68.

38. Jakubzick C et al. Minimal differentiation of classical monocytes as they survey steady-state tissues and transport antigen to lymph nodes. Immunity. 2013 Sep 19;39(3):599-610.
39. Wang Y et al. IL-34 is a tissue-restricted ligand of CSF1R required for the development of Langerhans cells and microglia. Nat Immunol. 2012, 24;13(8):753-60
40. Gautier EL and Yvan-Charvet L. Understanding macrophage diversity at the ontogenic and transcriptomic levels. Immunol Rev. 2014; 262(1):85-95.
41. Palis Jand Yoder MC. Yolk-sac hematopoiesis: the first blood cells of mouse and man. Exp Hematol. 2001 ;29(8):927-36
42. Palis J et al. Development of erythroid and myeloid progenitors in the yolk sac and embryo proper of the mouse. Development. 1999; 126(22):5073-84.
43. Perdiguero EG et al. The Origin of Tissue-Resident Macrophages: When an Erythro-myeloid Progenitor Is an Erythro-myeloid Progenitor. Immunity. 2015, 15; 43(6):1023-4.
44. Organizacion Nacional de Trasplantes (ONT).
45. Ferrara JL. Graft-versus-host disease. Lancet. 2009, 2;373(9674):1550-61.
46. Shlomchik WD. Prevention of Graft Versus Host Disease by Inactivation of Host Antigen-Presenting Cells. Science. 1999,16;285(5426):412-5
47. Irschick EU et al.Studies on the mechanism of tolerance or graft-versus-host disease in allogeneic bone marrow recipients at the level of cytotoxic T-cell precursor frequencies. Blood. 1992, 15;79(6):1622-8.
48. Naesens M, Kuypers DR and Sarwal M. Calcineurin inhibitor nephrotoxicity. Clin J Am Soc Nephrol. 2009; 4(2):481-508.
49. Fishman JA. Infection in solid-organ transplant recipients. N Engl J Med. 2007, 20; 357(25):2601-14.
50. Engels EA et al. Spectrum of cancer risk among US solid organ transplant recipients. JAMA.2011, 2; 306(17):1891-901.
51. Vincenti F. Belatacept and Long-Term Outcomes in Kidney Transplantation. N Engl J Med. 2016, 30; 374(26):2600-1.

52. Xu H et al. Postdepletion Lymphocyte Reconstitution during Belatacept and Rapamycin Treatment in Kidney Transplant Recipients. Am J Transplant.2016; 16(2):550-64.
53. Tilney NL et al. Identification, cytotoxicity, and suppressor activity of infiltrating cells from enhanced organ allografts. Transplant Proc. 1977; 9(1):713-5.
54. Martin WJ. Assay for the immunosuppressive capacity of antilymphocyte serum. I: Evidence for opsonization. III. Opsonizing activity of anti-human lymphocyte serum. J Immunol. 1969;103(5):1000-5
55. Thomas J. Macrophage-related suppressor cells in human renal transplant recipients. Surgery. 1979; 86(2):266-74.
56. Thomas J et al. Suppressor cells in rhesus monkeys treated with antithymocyte globulin. Transplantation. 1982;34(2):83-9.
57. Yoshimura S, Gotoh S and Kamada N.Immunological tolerance induced by liver grafting in the rat: splenic macrophages and T cells mediate distinct phases of immunosuppressive activity. Clin Exp Immunol. 1991;85(1):121-7.
58. Gray CM, Smit JA and Myburgh JA. Identification of non-T suppressor cells with possible contra-interleukin-2 properties in non-human primates tolerant to their renal allograft. Afr J Health Sci. 1995; 2(3):354-358.
59. Dugast AS et al. Myeloid-derived suppressor cells accumulate in kidney allograft tolerance and specifically suppress effector T cell expansion. J Immunol. 2008 15; 180(12):7898-906.
60. Dilek N et al. Control of transplant tolerance and intragraft regulatory T cell localization by myeloid-derived suppressor cells and CCL5. J Immunol. 2012, 1;188(9):4209-16.
61. Kurtz J. Trends Immunol. Specific memory within innate immune systems 2005; 26(4):186-92.
62. Netea MG, Quintin J and Van der Meer JW. Trained immunity: a memory for innate host defense. Cell Host Microbe. 2011, 19;9(5):355-61.
63. Garly ML et al. BCG scar and positive tuberculin reaction associated with reduced child mortality in West Africa. A non-specific beneficial effect of BCG? Vaccine. 2003 20;21(21-22):2782-90.

64. Ota MO et al. Influence of Mycobacterium bovis bacillus Calmette-Guérin on antibody and cytokine responses to human neonatal vaccination. J Immunol. 2002, 15;168(2):919-25
65. Aaby P et al. Early BCG vaccination and reduction in atopy in Guinea-Bissau .Clin Exp Allergy. 2000;30(5):644-50.
66. Jensen H et al. Survival bias in observational studies of the impact of routine immunizations on childhood survival .Trop Med Int Health. 2007;12(1):5-14.
67. Arts RJW et al. Immunometabolic Pathways in BCG-Induced Trained Immunity. Cell Rep. 2016, 6;17(10):2562-2571.
68. Kleinnijenhuis J et al. Bacille Calmette-Guerin induces NOD2-dependent nonspecific protection from reinfection via epigenetic reprogramming of monocytes. Proc Natl Acad Sci U S A. 2012, 23;109(43):17537-42.
69. Novakovic B et al. β-Glucan Reverses the Epigenetic State of LPS-Induced Immunological Tolerance. Cell. 2016, 17;167(5):1354-1368.
70. Azimzadeh AM et al. Humoral immunity to vimentin is associated with cardiac allograft injury in nonhuman primates. Am J Transplant. 2005;5(10):2349-59.
71. Saeed S et al. Epigenetic programming of monocyte-to-macrophage differentiation and trained innate immunity. Science. 2014, 26;345(6204):1251086.
72. Cheng SC et al. mTOR- and HIF-1α-mediated aerobic glycolysis as metabolic basis for trained immunity. Science. 2014, 26;345(6204):1250684.
73. MacIver NJ, Michalek RD and Rathmell JC. Metabolic regulation of T lymphocytes. Annu Rev Immunol. 2013;31:259-83.
74. Pearce EL and Pearce EJ. Metabolic pathways in immune cell activation and quiescence. Immunity. 2013,18;38(4):633-43.
75. Vats D et al. Oxidative metabolism and PGC-1beta attenuate macrophage-mediated inflammation. Cell Metab. 2006;4(1):13-24.
76. McKinnon JG et al. mTOR couples cellular nutrient sensing to organism metabolic homeostasis. Cancer Immunol Immunother. 1990;32(1):38-44.
77. Byles V et al. The TSC-mTOR pathway regulates macrophage polarization. Nat Commun. 2013; 4:2834.

78. Burnett SH et al. Conditional macrophage ablation in transgenic mice expressing a Fas-based suicide gene. J Leukoc Biol. 2004; 75(4):612-23.
79. Jiang X et al. Cardiac allograft acceptance induced by blockade of CD40-CD40L costimulation is dependent on CD4+CD25+ regulatory T cells. Surgery. 2011;149(3):336-46.
80. Gallina G et al. Tumors induce a subset of inflammatory monocytes with immunosuppressive activity on $CD8^+$ T cells. J Clin Invest. 2006;116(10):2777-90.
81. Huang B et al. Gr-1+CD115+ immature myeloid suppressor cells mediate the development of tumor-induced T regulatory cells and T-cell anergy in tumor-bearing host. Cancer Res. 2006 15;66(2):1123-31.
82. Gautier EL et al. Gene-expression profiles and transcriptional regulatory pathways that underlie the identity and diversity of mouse tissue macrophages. Nat Immunol. 2012; 13(11):1118-28.
83. Miyake Y et al. Critical role of macrophages in the marginal zone in the suppression of immune responses to apoptotic cell-associated antigens. J Clin Invest. 2007; 117(8):2268-78.
84. Jutila MA et al. Ly-6C is a monocyte/macrophage and endothelial cell differentiation antigen regulated by interferon-gamma. Eur J Immunol. 1988;18(11):1819-26.
85. Arnold L et al. Inflammatory monocytes recruited after skeletal muscle injury switch into antiinflammatory macrophages to support myogenesis. J Exp Med. 2007, 14;204(5):1057-69.
86. Domínguez-Soto A et al. Dendritic cell-specific ICAM-3-grabbing nonintegrin expression on M2-polarized and tumor-associated macrophages is macrophage-CSF dependent and enhanced by tumor-derived IL-6 and IL-10. J Immunol. 2011 Feb 15;186(4):2192-200.
87. Caparrós E et al. DC-SIGN ligation on dendritic cells results in ERK and PI3K activation and modulates cytokine production. Blood. 200615;107(10):3950-8.
88. Gringhuis S et al. C-Type Lectin DC-SIGN Modulates Toll-like Receptor Signaling via Raf-1 Kinase-Dependent Acetylation of Transcription Factor NF-κB. Immunity. 2007 ;26(5):605-16

89. Gringhuis S et al. Fucose-specific DC-SIGN signalling directs T helper cell type-2 responses via IKKε-and CYLD-dependent Bcl3 activation. Nat Commun. 2014, 28;5:3898.
90. Ishida T et al. Identification of TRAF6, a novel tumor necrosis factor receptor-associated factor protein that mediates signaling from an amino-terminal domain of the CD40 cytoplasmic region. J Biol Chem. 1996,15;271(46):28745-8.
91. Bronte V et al. Identification of a CD11b(+)/Gr-1(+)/CD31(+) myeloid progenitor capable of activating or suppressing CD8(+) T cells. Blood. 2000. 1;96(12):3838-46.
92. Wyburn KR et al. The role of macrophages in allograft rejection. Transplantation. 2005 27;80(12):1641-7.
93. Heidt T et al. Differential contribution of monocytes to heart macrophages in steady-state and after myocardial infarction. Circ Res. 2014 7; 115(2):284-95.
94. Schiopu A et al. Inflammatory Ly-6C(hi) monocytes play an important role in the development of severe transplant arteriosclerosis in hyperlipidemic recipients Atherosclerosis. 2012 Aug; 223(2):291-8.
95. Rivollier A et al. Inflammation switches the diferentiation program of Ly6Chi monocytes from antiinflammatory macrophages to inflammatory dendritic cells in the colon. J Exp Med. 2012, 16;209(1):139-55
96. Guillén FJ et al. Acute cutaneous graft-versus-host disease to minor histocompatibility antigens in a murine model. Evidence that large granular lymphocytes are effector cells in the immune response
97. Riquelme P et al. IFN-γ-induced iNOS expression in mouse regulatory macrophages prolongs allograft survival in fully immunocompetent recipients. Mol Ther. 2013 ;21(2):409-22
98. Hutchinson JA et al. Human regulatory macrophages. Methods Mol Biol. 2011; 677:181-92.
99. Geijtenbeek TB et al. Self- and nonself-recognition by C-type lectins on dendritic cells. Annu Rev Immunol. 2004;22:33-54.
100. Soilleux EJ et al. Constitutive and induced expression of DC-SIGN on dendritic cell and macrophage subpopulations in situ and in vitro. J Leukoc Biol. 2002 Mar;71(3):445-57.

101. Li G, Hangoc G and Broxmeyer HE. Interleukin-10 in combination with M-CSF and IL-4 contributes to development of the rare population of CD14+CD16++ cells derived from human monocytes. Biochem Biophys Res Commun. 2004 ,17;322(2):637-43
102. Garcia-Vallejo JJ & van Kooyk Y. The physiological role of DC-SIGN: a tale of mice and men. Trends Immunol. 2013; 34(10):482-6.
103. Park CG et al. Five mouse homologues of the human dendritic cell C-type lectin, DC-SIGN. Int Immunol. 2001;13(10):1283-90.
104. Caminschi I et al. Functional comparison of mouse CIRE/mouse DC-SIGN and human DC-SIGN. Int Immunol. 2006;18(5):741-53.
105. Powlesland AS et al. Widely divergent biochemical properties of the complete set of mouse DC-SIGN-related proteins. J Biol Chem. 2006, 21;281(29):20440-9.
106. van Gisbergen KP et al. Dendritic cells recognize tumor-specific glycosylation of carcinoembryonic antigen on colorectal cancer cells through dendritic cell-specific intercellular adhesion molecule-3-grabbing nonintegrin. Cancer Res. 2005 1;65(13):5935-44.
107. Gringhuis SI et al. C-type lectin DC-SIGN modulates Toll-like receptor signaling via Raf-1 kinase-dependent acetylation of transcription factor NF-kappaB. Immunity. 2007;26(5):605-16.
108. García-Vallejo JJ et al. CNS myelin induces regulatory functions of DC-SIGN-expressing, antigen-presenting cells via cognate interaction with MOG. J Exp Med. 2014, ;211(7):1465-83.
109. Parker KH et al. HMGB1 enhances immune suppression by facilitating the differentiation and suppressive activity of myeloid-derived suppressor cells. Cancer Res. 2014 Oct 15;74(20):5723-33.
110. Lv Q et al. The role of HMGB1 in heart transplantation. Immunol Lett. 2018;194:1-3.
111. Wu H et al. TLR4 activation mediates kidney ischemia/reperfusion injury. J Clin Invest. 2007 Oct;117(10):2847-59.
112. Cruz LJ et al. Targeting nanoparticles to CD40, DEC-205 or CD11c molecules on dendritic cells for efficient CD8(+) T cell response: a comparative study. J Control Release. 2014,28;192:209-18.

113. Shirali AC et al. Nanoparticle delivery of mycophenolic acid upregulates PD-L1 on dendritic cells to prolong murine allograft survival. Am J Transplant. 2011 ;11(12):2582-92.
114. Pan Q et al. Corticosteroid-loaded biodegradable nanoparticles for prevention of corneal allograft rejection in rats. J Control Release. 2015,10;201:32-40.
115. Tang J et al. Inhibiting macrophage proliferation suppresses atherosclerotic plaque inflammation. Sci Adv. 2015;1(3).
116. Thaxton CS et al. Lipoproteins and lipoprotein mimetics for imaging and drug delivery. Adv Drug Deliv Rev. 2016, 15;106(Pt A):116-131.
117. Burnett SH et al. Conditional macrophage ablation in transgenic mice expressing a Fas-based suicide gene. J Leukoc Biol. 2004;75(4):612-23.
118. Miyake Y et al. Critical role of macrophages in the marginal zone in the suppression of immune responses to apoptotic cell-associated antigens. J Clin Invest. 2007; 117(8):2268-78.
119. Corry RJ, Winn HJ and Russell PS. Primarily vascularized allografts of hearts in mice. The role of H-2D, H-2K, and non-H-2 antigens in rejection. Transplantation. 1973 ;16(4):343-50.
120. Jiang X et al. Cardiac allograft acceptance induced by blockade of CD40-CD40L costimulation is dependent on CD4+CD25+ regulatory T cells. Surgery. 2011;149(3):336-46.
121. Gorbachev AV & Fairchild RL. CD40 engagement enhances antigen-presenting langerhans cell priming of IFN-gamma-producing CD4+ and CD8+ T cells independently of IL-12. J Immunol. 2004 ,15;173(4):2443-52.
122. Lokeshwar BL & Lin HS. Development and characterization of monoclonal antibodies to murine macrophage colony-stimulating factor. J Immunol. 1988, 15;141(2):483-8.
123. Gregory SH et al. Primary listerial infections are exacerbated in mice administered neutralizing antibody to macrophage colony-stimulating factor . J Immunol. 1992 Jul 1;149(1):188-93.
124. Sudo T et al. Oncogene. Functional hierarchy of c-kit and c-fms in intramarrow production of CFU-M. 1995, 21;11(12):2469-76.

125. Hashimoto D et al. Pretransplant CSF-1 therapy expands recipient macrophages and ameliorates GVHD after allogeneic hematopoietic cell transplantation. J Exp Med. 2011, 9;208(5):1069-82.
126. Cheong C et al. New monoclonal anti-mouse DC-SIGN antibodies reactive with acetone-fixed cells. J Immunol Methods. 2010, 31;360(1-2):66-75.
127. Lee TI, Johnstone SE and Young RA. Chromatin immunoprecipitation and microarray-based analysis of protein location.Nat Protoc. 2006;1(2):729-48.
128. Jeffrey T. Leek et al. The sva package for removing batch effects and other unwanted variation in high-throughput experiments. Bioinformatics. 2012, 15;28(6):882-3.

FIGURAS SUPLEMENTARIAS

Figura suplementaria 1: **Genotipo y fenotipo de células mieloides**

(A) Perfil de expresión génica de células mieloides $CD11b^{+}CSF1R^{+}Ly6C^{lo}Ly6G^{-}$ infiltradas en los órganos trasplantados. El heat map representa la expresión relativa de genes específicos de macrofagos (MF) (izquierda); y/o CD (centro) en comparación con células supresoras $CD11b^{+}CSF1R^{+}Ly6C^{lo}Ly6G$ y CD residentes en tejidos (DC1, DC2, DC3) y macrofagos tisulares (MF1, MF2, MF3). La columna derecha representa la expresión relativa de genes específicos de MDSC en comparación con las células supresoras $CD11b^{+}CSF1R^{+}Ly6C^{lo}Ly6G$ y MDSC asociadas a tumores (MDSC1, MDSC2, MDSC3). Resultados expresados en relación a los granulocitos. Los datos han sido obtenidos obtenidos del Immunological Genome Proyect (www.immgen.org) .Resultados de la media expresados mediante ± SEM (n=3). (B)Imágenes representativas de cytospin teñidas con hematoxilina/eosina de las distintas poblaciones mieloides aisladas de órganos trasplantados tolerantes y rechazos.

A

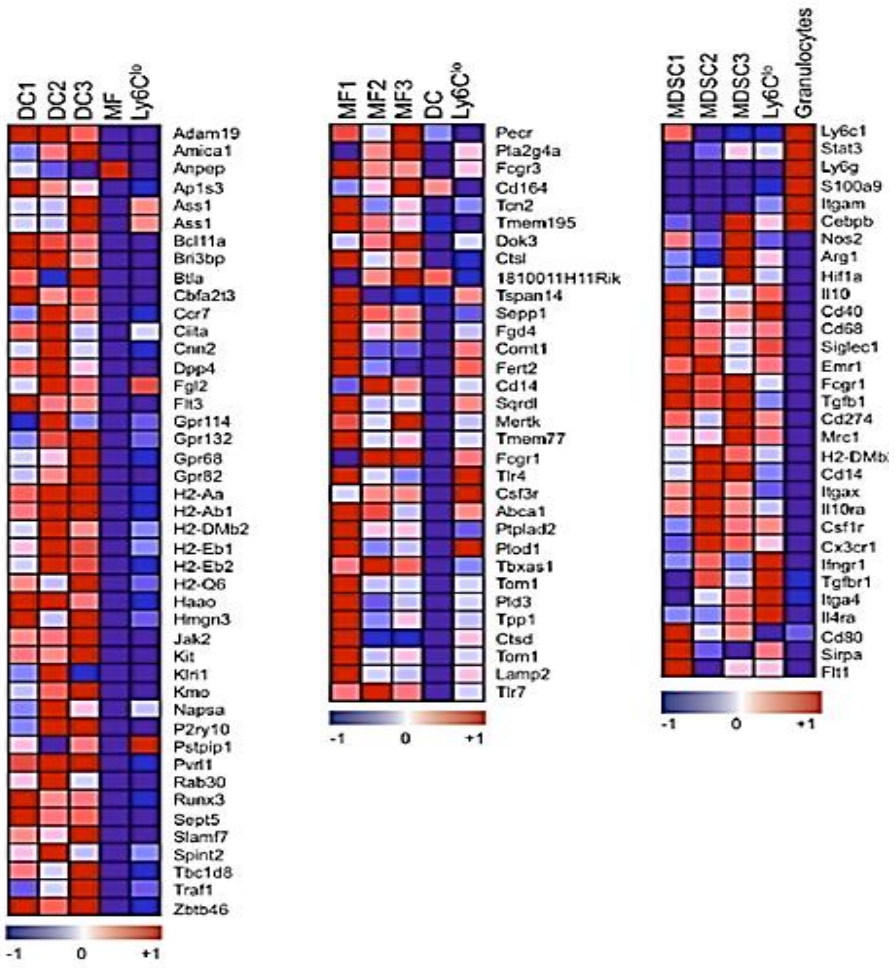

B

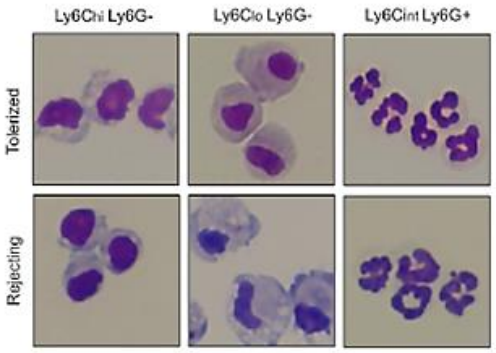

Figura suplementaria 2: Expresión de CD169 en las poblaciones de células mieloides

(A) Heat map derivado del microarray (n=3) y (B) resultados del análisis por PCR cuantitativa expresados en unidades relativas de RNA de las poblaciones mieloides aisladas de organos de recipientes tolerizados. Resultados de la media expresados mediante ± SEM de 3 experimentos independientes (**p ≤0.01).

A

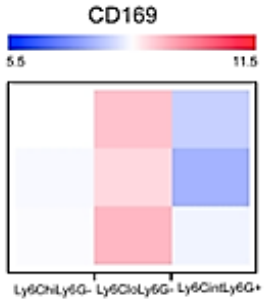

B

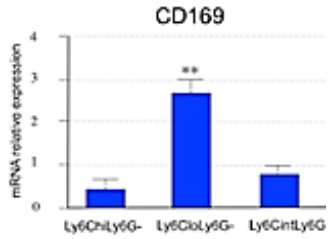

Figura suplementaria 3: Expresión de CD40/CD40L en las poblaciones de células mieloides de recipientes tolerantes

(A) Heat map derivado de los datos del análisis genético (n=3) y (B) resultados del análisis por PCR cuantitativa expresados en unidades relativas de RNA. Resultados de la expresión de CD40L por células T de recipientes control sin tratar. Resultados de la media expresados mediante ± SEM de 3 experimentos independientes (**p ≤0.01).

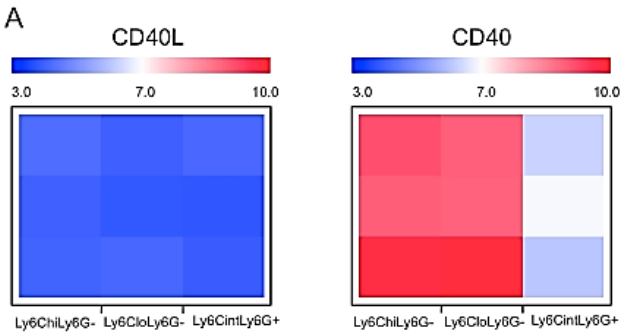

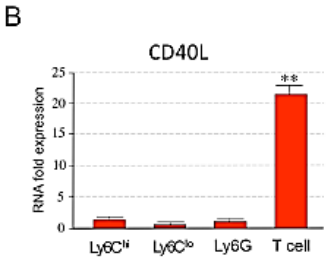

Figura suplementaria 4: Il-10 es necesaria para la inducción de la tolerancia mediada por CD-SIGN

(A) Resultados del análisis por PCR cuantitativa expresados en unidades relativas de RNA de las poblaciones de células mieloides aisladas de órganos de recipientes tolerantes vs rechazo. Resultados de la media expresados mediante ± SEM de 3 experimentos independientes (**p ≤0.01).

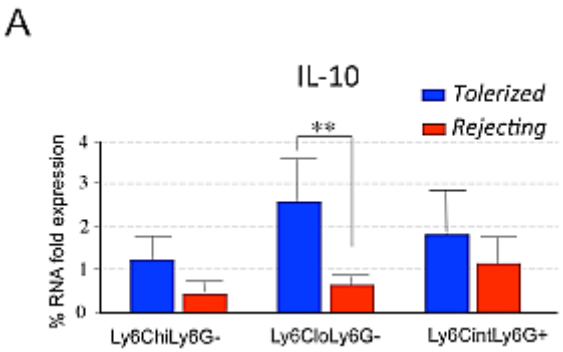

Figura suplementaria 5: Bio distribución de las nano particulas mTORi-HDL

(A) Análisis de las intensidades medias de fluorescencia (MFI) de las poblaciones de monocitos/macrofagos, células T totales $CD3^+$, células T $CD4^+$ y $CD8^+$ infiltradas en el órgano trasplantado, bazo y circulantes en sangre *24h después de la administración de las nano particulas* . Las barras graficas representan la media expresados mediante ± SEM de 4 experimentos independientes (**p ≤0.01).

A

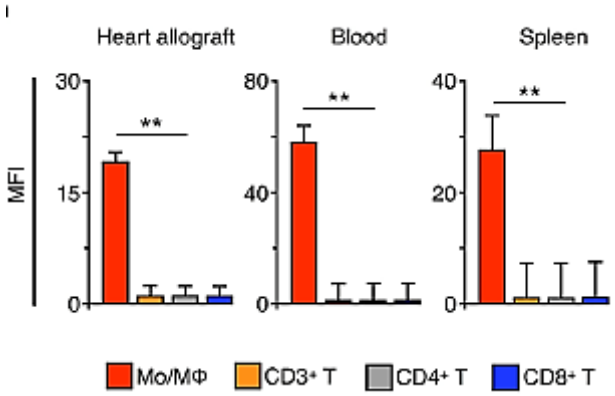

Figura suplementaria 6: CFS1 media el desarrollo de los macrofagos supresores en humanos (A) Capacidad de supresión in vitro y expansión de las Treg de monocitos humanos. Los monocitos CD14+ fueron aislados de sangre de voluntarios sanos y estimulados durante 6 días con CFS1 (25ng/ml) + IL-4(20ng/ml) y/o CFS2 (25ng/ml) + IL4 (20ng/ml). Las células T fueron estimuladas con PHA y puesta en co-cultivo durante 5 días con los monocitos diferenciados con cada condición. Resultados de la media expresados mediante ± SEM de 3 experimentos independientes (**p ≤0.01).

A

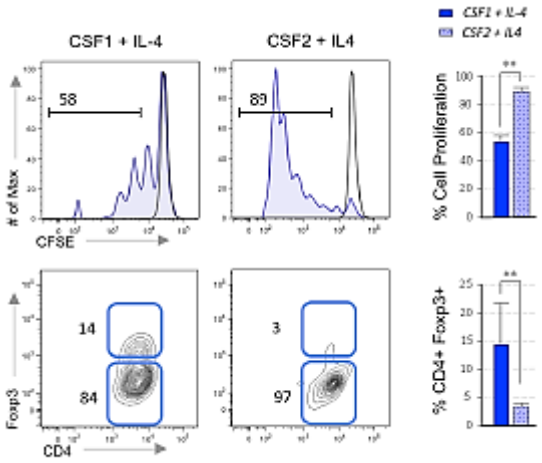

ÍNDICE DE ABREVIATURAS

Ac	Anticuerpo
APC	Células presentadoras de antígeno
APOA-1	Apoliproteína A-I
ATG	Globulina anti- timocitos
BCG	Bacilo Calmette-Guérin
CD	Células dendríticas
CSF1	Factor estimulante de colonias 1
CT	Tomografía computerizada
DAMP	Damage associated patterns
DC-SIGN, CD209	ICAM-3 grabbing non integrin
DTR	Receptor de la toxina de Difteria
Fuc	Fucosa
GlcNAc	N-acetil glucosamina
GVHD	Graft-versus-host desease
HDL	Lipoproteínas de alta densidad
IL	Interleuquina
Lex	Syalil-lewis X
LNFPIII	Pentasacarido lacto-N-fucopentosa III
MaFIA	Macrophage Fas induced apoptosis
Man	Manosa
MDSC	Células mieloides supresoras
MLR	reacción leucocitaria mixta
MHC	Complejo mayor de histocompatibilidad
mTOR	Mammalian target of rapamicyn
PBMC	Células mononucleares de sangre periférica
PCR	Polymerase chain reaction
PDL1	Programmed death ligan 1
PEM	Precursores eritro mieloides
PET	Tomografía de emisión de positrones
PRR	Receptor de la inmunidad innata

PT	Post-trasplante
SAL/ALS	Suero anti-linfocitico
SMF	Sistema mononuclear fagocítico
SRE	Sistema retículo endotelial
SRH	Sistema retículo histiocítico
TLR	Toll like receptor
Treg	Célula T reguladoras

PUBLICACIONES CIENTÍFICAS

Received: 26 July 2017 | Revised: 1 December 2017 | Accepted: 16 December 2017

DOI: 10.1111/ajt.14645

BRIEF COMMUNICATION

AJT

Neutrophil derived CSF1 induces macrophage polarization and promotes transplantation tolerance

Mounia S. Braza[1] | Patricia Conde[1,2] | Mercedes Garcia[2] | Isabel Cortegano[2] | Manisha Brahmachary[1] | Venu Pothula[1] | Francois Fay[3] | Peter Boros[4] | Sherry A. Werner[5] | Florent Ginhoux[6] | Willem J. M. Mulder[3] | Jordi Ochando[1,2,]

[1]Department of Oncological Sciences, Icahn School of Medicine at Mount Sinai, New York, NY, USA

[2]Immunología de Transplantes, Centro Nacional de Microbiología, Instituto de Salud Carlos III, Madrid, Spain

[3]Translational and Molecular Imaging Institute, Icahn School of Medicine at Mount Sinai, New York, NY, USA

[4]Department of Surgery, Icahn School of Medicine at Mount Sinai, New York, NY, USA

[5]Health Science Center, University of Texas, San Antonio, TX, USA

[6]Singapore Immunology Network, Agency for Science, Technology and Research (A*STAR), Singapore, Singapore

Correspondence
Jordi C. Ochando
Email: jordi.ochando@mssm.edu

Funding information
Cancer Center, Grant/Award Number: P30 CA196521; National Institute of Health, Grant/Award Number: R01 HL118440, R01 HL125703 and R01 CA155432; Ministerio de Economia y Competitividad, Grant/Award Number: SAF2016-80031-R; COST

The colony-stimulating factor 1 (CSF1) regulates the differentiation and function of tissue macrophages and determines the outcome of the immune response. The molecular mechanisms behind CSF1-mediated macrophage development remain to be elucidated. Here we demonstrate that neutrophil-derived CSF1 controls macrophage polarization and proliferation, which is necessary for the induction of tolerance. Inhibiting neutrophil production of CSF1 or preventing macrophage proliferation, using targeted nanoparticles loaded with the cell cycle inhibitor simvastatin, abrogates the induction of tolerance. These results provide new mechanistic insights into the developmental requirements of tolerogenic macrophages and identify CSF1 producing neutrophils as critical regulators of the immunological response.

KEYWORDS
basic (laboratory) research/science, immunobiology, macrophage/monocyte biology: differentiation/maturation, tolerance: mechanisms

1 | INTRODUCTION

Macrophage accumulation in the transplanted organ has long been recognized as a feature of allograft rejection.[1] Early after transplantation, macrophage precursors infiltrate the allograft and represent the major cell subset during antibody and T-cell mediated rejection.[2,3] These inflammatory macrophages are characterized phenotypically by their high expression of Ly6C (Ly6C^{hi} or M1).[4] Recent evidence suggests that macrophages are also important during the induction of transplantation tolerance.[5] Presence of graft infiltrating macrophages has been described in long-term surviving transplant recipients and these immunosuppressive macrophages are associated with unresponsiveness to the transplanted organ.[6] These suppressive macrophages are characterized phenotypically by their low expression of Ly6C (Ly6C^{lo} or M2).[5] This suggests that graft-infiltrating monocytes differentiate into either immunogenic (Ly6C^{hi}) or tolerogenic (Ly6C^{lo}) macrophages, which determines the outcome of the immunological response. While the phenotype and function of macrophages that mediate the induction of transplantation tolerance has recently been reported,[5] their developmental requirements remain poorly understood.

Monocytes differentiate into classically (Ly6C^{hi}/M1) or alternatively (Ly6C^{lo}/M2) activated macrophages according to the local

Abbreviations: CSF1, colony-stimulating factor 1; FACS, fluorescence-activated cell sorting; G-MDSC, granulocytic myeloid-derived suppressor cell; HDL, high-density lipoprotein; MDSC, myeloid-derived suppressor cell; M-MDSC, monocytic myeloid-derived suppressor cell; S-HDL, simvastatin high-density lipoprotein.

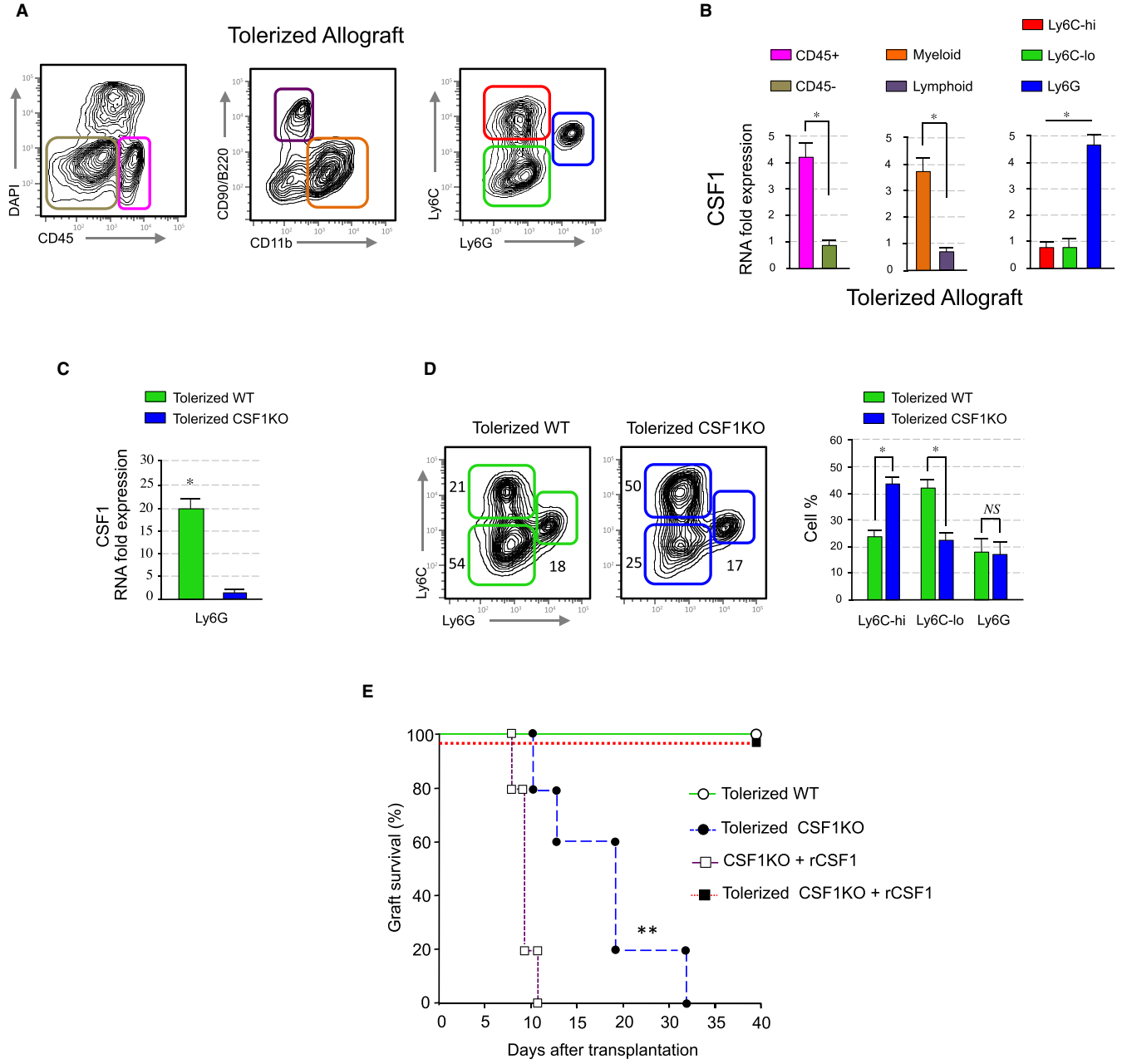

FIGURE 1 Neutrophil derived CSF1 mediates macrophage polarization. (A and B) CSF1 expression in the allografts. Heart allografts of CD40L mAb treated mice were isolated and single cells suspensions were made. CSF1 expression in distinct flow sorted cell subsets was investigated by qPCR. Results represent mean ± SEM of three independent experiments (unpaired Mann-Whitney and Kruskal-Walis with Dunn's multiple comparison test; $*P \leq .5$). (C) CSF1 expression in the allografts of S100A8^{Cre}CSF1 ^{fl} deficient recipient mice. Heart allografts of wt and S100A8^{Cre}CSF1 ^{fl} recipients treated with CD40L mAb were analyzed for CSF1 expression by qPCR. Results represent mean ± SEM of three independent experiments (unpaired Mann-Whitney test; $*P \leq .5$). (D) Representative and quantitative flow cytometry results of graft infiltrating myeloid subsets from anti-CD40L mAb treated wt and S100A8^{Cre}CSF1 ^{fl} recipients at day 5 post-transplantation. Results represent mean ± SEM (n = 4 mice per group of three independent experiments; unpaired Mann-Whitney test; $*P \leq .5$). (E) Graft survival of tolerized wt versus S100A8^{Cre}CSF1 ^{fl} recipients. Tolerized S100A8^{Cre}CSF1 ^{fl} recipient mice rejected their allografts despite anti-CD40L mAb treatment. A third group of tolerized S100A8^{Cre}CSF1 ^{fl} recipients received 2×10^5 U of recombinant CSF1 i.v. on the day of transplantation and on days 1-5 post-transplantation. Non-tolerized S100A8^{Cre}CSF1 ^{fl} recipients treated with 2×10^5 U of recombinant CSF1 were used as controls. Graft survival was assessed with Kaplan-Meier analysis (*MST* 18 ± 8 days; $**P \leq .01$; n = 5 mice per group)

environment.[7,8] Inflammatory Ly6C^{hi} monocytes are rapidly recruited to inflamed tissues and become alternatively activated Ly6C^{lo} macrophages once the inciting inflammatory stimulus has been resolved.[9] In organ transplantation, inflammatory Ly6C^{hi} monocytes infiltrate the allograft early after transplantation and differentiate into suppressive Ly6C^{lo} macrophages following costimulatory blockade.[5] Therefore, the signals that dictate macrophage polarization towards alternatively activated Ly6C^{lo}/M2 control immunological tolerance.[10,11]

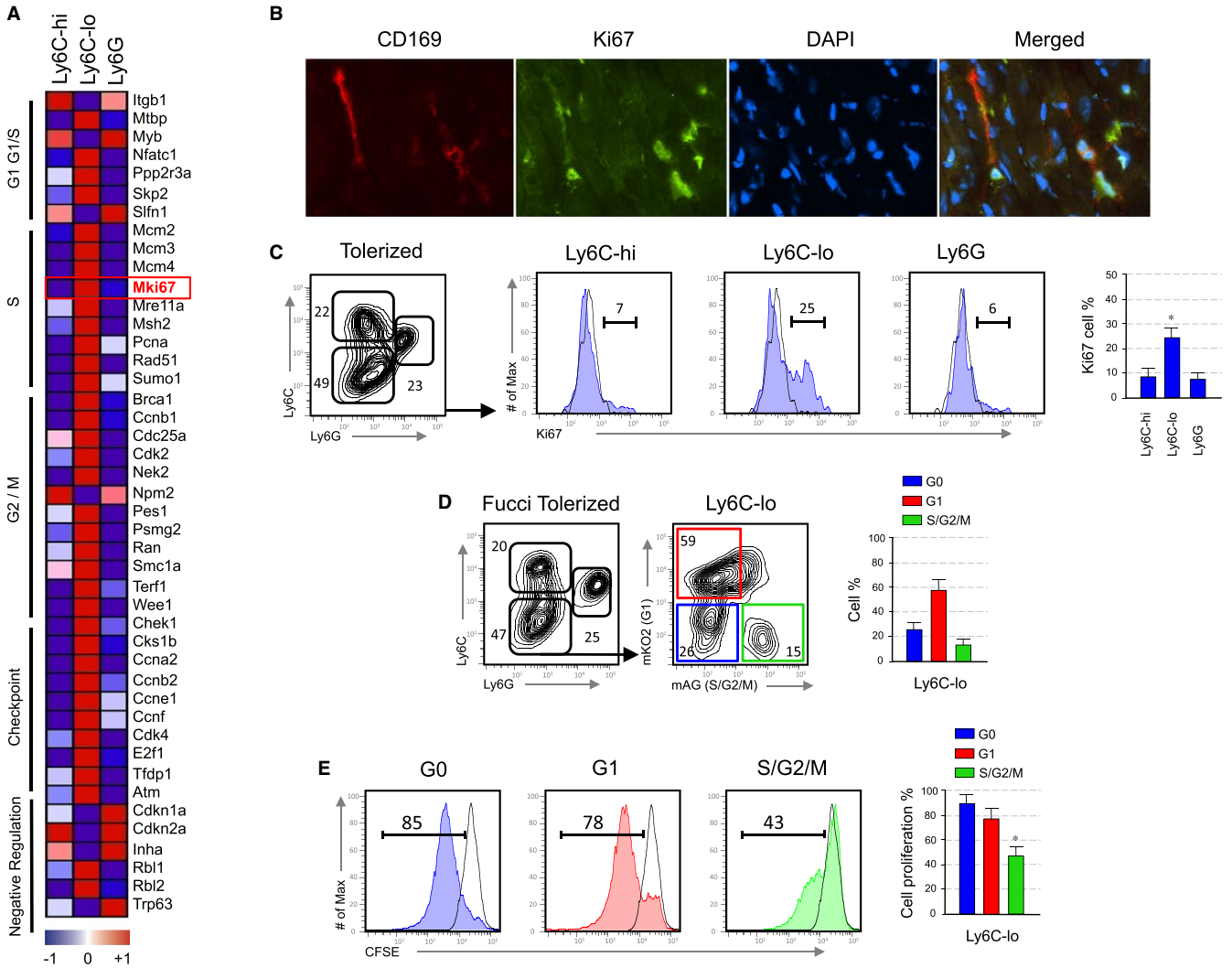

FIGURE 2 Suppressive function of polarized macrophages depends on cell proliferation. (A) Heatmap of cell cycle transcripts derived from microarray data with a *P*-value $P < .05$ in the myeloid subsets obtained from the allografts of anti-CD40L mAb treated recipients at day 5 post-transplantation. Shown is an average of n = 3. (B) Representative immunofluorescent images of allograft tissue stained for CD169, Ki67, DAPI and a merge image depicting overlap obtained from an anti-CD40L mAb treated recipients at day 5 post-transplantation (magnification ×40). (C) Representative and quantitative flow cytometry results for Ki67 expression on myeloid subsets from the allografts of anti-CD40L mAb treated recipients at day 5 post-transplantation. Data are representative of three independent experiments. Results represent mean ± SEM (n = 3 mice per group of three independent experiments; Kruskal-Walis with Dunn's multiple comparison test; $^*P \leq .5$). (D) Representative and quantitative flow cytometry results of myeloid subsets from the allografts of anti-CD40L mAb treated Fucci recipients at day 5 post-transplantation. Further evaluation of cell cycle fluorescent probes indicated that the majority of Ly6C^{lo} macrophages from anti-CD40L mAb-treated Fucci recipients are in G1/S/G2/M phase. Results represent mean ± SEM (n = 3 mice per group of three independent experiments). (E) Suppressive function of Ly6C^{lo} macrophages that are either proliferating (G1S/G2/M) or non-proliferating (G0). Representative and quantitative flow cytometry results of CSFE$^+$CD8$^+$ T proliferation after 72 hours of culture. Results represent mean ± SEM (n = 3 mice per group of three independent experiments; Kruskal-Walis with Dunn's multiple comparison test; $^*P \leq .5$)

Macrophage polarization into suppressive Ly6C^{lo} macrophages is mediated by cytokines and growth factors.[12,13] In this respect, the colony-stimulating factor 1 (CSF1) has been demonstrated to control macrophage polarization.[14] CSF1 also controls the function of macrophages and several reports have documented suppressive function of CSF1 differentiated macrophages in mixed lymphocyte reactions.[15–17] This suggests that the local production of CSF1 controls both the differentiation and immune regulatory function macrophages.

Here, we investigated the mechanistic insights of CSF1 on macrophage differentiation and function and we demonstrate that CSF1 producing neutrophils mediate immunological tolerance by promoting the development of proliferating Ly6C^{lo} macrophages with suppressive function.

2 | EXPERIMENTAL PROCEDURES

2.1 | Mice

BALB/c and C57BL/6 mice eight weeks of age were purchased from The Jackson Laboratory (Bar Harbor, ME). The C57BL/6 mKO2-hCdt1(30/120) and mAG-hGem(1/110) transgenic mice were from D. Atsushi Miyawaki (RIKEN, Brain Science Institute, Hirosawa, Saitama, Japan).[18] The CSF1flox

mice have been previously described.[19] All experiments were performed with age- and sex-matched mice in accordance with Institutional Animal Care and Utilization Committee-approved protocols.

2.2 | Vascularized heart transplantation

BALB/c hearts were transplanted as fully vascularized heterotopic grafts into C57BL/6 mice as previously described.[20] Recipient mice were treated with 250 μg anti-CD40L mAb (clone MR1, BioXcell, West Lebanon, NH) for tolerance induction on days 0, 2, and 4 as previously described.[21] Graft function was monitored every other day by abdominal palpation. Untreated control mice received hamster IgG in PBS. Rejection was defined as complete cessation of a palpable beat and confirmed by direct visualization at laparotomy.

2.3 | Isolation of graft infiltrating leukocytes (GIL)

Mouse hearts were rinsed in situ with HBSS with 1% heparin. Explanted hearts were cut into small pieces and digested for 40 minutes at 37°C with 400 U/ml collagenase IV (Sigma-Aldrich), 10 mM HEPES (Corning Cellgro, Manassas, VA), and 0.01% DNase I (MP Biomedicals) in HBSS (Cellgro). Digested suspensions were passed through a nylon mesh and centrifuged, and the cell pellet was resuspended in 5 ml 45.5% Nycodenz solution (Sigma-Aldrich). Complete DMEM (3 ml) was added to the top of the Nycodenz, and gradient centrifugation was performed (1700 *g* for 15 minutes at 4°C). The cells at the interface were recovered, washed with complete DMEM, stained, and analyzed by flow cytometry (BD LSR-II; BD Biosciences, San Jose, CA).

2.4 | Flow cytometry and cell sorting

Fluorochrome-conjugated mAbs specific to mouse CSF-1R (clone AFS98), CD11b (clone M1/70), CD11c (clone N418), I-A/I-E clone (clone M5/114.15.2), CD45 (clone 30-F11), CD90.2 (clone 53-2.1), CD8 (clone 53-6.7), CD4 (clone GK1.5), Foxp3 (clone JFK 16s), CD44 (clone IM7), CD62L (clone MEL-14), corresponding isotype controls, and secondary reagents (PE-conjugated streptavidin) were purchased from eBioscience. Fluorochrome-conjugated anti-Ly6G (Clone 1A8) mAb was purchased from Biolegend. Cell washes and Ab dilutions were performed in PBS plus 1% BSA at 4°C. Flow cytometric analysis was performed on LSR II (BD Biosciences) and analyzed with FlowJo software (Tree Star, Inc., Ashland, OR). Results are expressed as percentage of cells staining above background, and mAbs were tittered at regular intervals during the course of these studies to ensure that saturating concentrations were used. To purify graft infiltrating myeloid cells, donor heart single cell suspensions were sorted with an FACS Aria cell sorter (BD) to achieve >96% purity at the Flow Cytometry Shared Resource Facility at Icahn School of Medicine at Mount Sinai.

2.5 | Immunofluorescence microscopy

Transplanted hearts were harvested, subdivided, frozen directly in OCT (Fisher, Waltham, MA), and stored at −80°C in preparation for immunological studies. Sections of 8 μm were cut using a Leica 1900CM cryomicrotome, fixed, and mounted with Gel/Mount (Biomeda, Foster City, CA) on polylysine-coated slides. Anti-Ki67 (AbD02531) and CD169 (clone 3D6.112) were purchased from AbD Serotec (Hercules, CA). All slides were mounted with Vectashield (Vector Laboratories, Burlingame, CA) to preserve fluorescence. Images were acquired with a Leica DMRA2 fluorescence microscope (Wetzlar, Buffalo Grove, IL) and a digital Hamamatsu charge-coupled device camera. Separate green, red, and blue images were collected and analyzed with Openlab software (Improvision, Coventry, England).

2.6 | Microarray

Graft infiltrating recipient $CD45^+CD11b^+Ly6C^{hi}Ly6G^-$, $CD45^+CD11b^+$ $Ly6C^{lo}Ly6G^-$, and $CD45^+CD11b^+Ly6C^{int}Ly6G^+$ myeloid cells sorted from anti-CD40L mAb treated and untreated recipients at day 5 after transplantation. Cells were sorted twice with a FACS Aria II sorter (BD Biosciences) to achieve >98% purity. A total of nine Affymetrix Mouse Exon GeneChip arrays were run in triplicate with the samples of interest. Raw CEL file data from Affymetrix Expression Console were background corrected, normalized, and summarized using Robust Multichip Average. The summary expression scores were computed at the transcript meta-probeset level using annotation files supplied by the manufacturer. The data was imported into R. Since these arrays were run in different batches, the gene expression was batch corrected with Combat. Gene expression was filtered based on IQR (0.25) filter using genefilter package. The log2 normalized and filtered data (adjusted $P < .05$) was used for further analysis (GEO accession number GSE68648).

2.7 | Quantitative RT-PCR

Total RNA was extracted from purified cells with RNeasy Plus Micro Kit (Qiagen, Hilden, Germany). Reverse transcription was carried out using the Omniscript reverse-transcription system (Qiagen) and random primers. Quantitative PCR was performed with the LightCycler system (Roche, Basel, Switzerland) and the SYBR Green PCR kit (Qiagen). All experiments were done in triplicate at least three separate times, and expression of specific genes was normalized and expressed as percentage relative to housekeeping genes or RNA fold expression according to the ddCT method.

2.8 | Bone marrow–derived monocyte cultures

Bone marrow $Ly6C^{hi}$ monocytes were FACS sorted from the mice femur and plated in 96-U-botton well plate at 5×10^4 cell/well in RPMI-1640 w/L-Glutamine medium (Corning Cellgro) containing 10% heat-inactivated FCS (Biochrom, Berlin, Germany), 1% penicillin/streptavidin (Corning Cellgro). Bone marrow $Ly6C^{hi}$ monocytes were then cultured for 72 hours in the presence of recombinant murine CSF1 at 10 ng/ml (Peprotech, Rocky Hill, NJ) or simvastatin loaded HDL nanoparticles (S-HDL) at 10 μM.

2.9 | In vitro suppression assay

Spleens of C57BL/6 mice were gently dissociated into single-cell suspensions, and red blood cells were removed using hypotonic ACK lysis buffer. Splenocytes were either stained with anti-CD8 mAb, followed by CFSE at 5 μM concentration (Molecular probes, Invitrogen, Waltham, MA) Responder $CFSE^+CD8^+$ T cells were sorted using FACS Aria II sorter (BD Biosciences) with a purity >98%. Spleens of BALB/c (H-2^d) mice were gently dissociated into single-cell suspensions, and red blood cells were removed using hypotonic ACK lysis buffer. Splenocytes were enriched for $CD11c^+$ cells using the EasySep Mouse CD11c Positive Selection Kit (StemCell, Cambridge, MA). Enriched $CD11c^+$ splenocytes were stained with anti-mouse CD11c mAb for 30 minutes on ice. $CD11c^+$ cells were sorted using FACS Aria II sorter (BD Biosciences) and were used together with anti-CD3/CD28 mAb (1 μg/ml) as stimulators. Responder $CFSE^+CD8^+$ T cells were stimulated allogeneic CD11c plus anti-CD3/CD28 mAb in U-bottom 96-well plates (Corning). Graft infiltrating $CD11b^+$ $Ly6C^{lo}Ly6G^-$ sorted macrophages from anti-CD40L mAb treated recipients at day 5 after transplantation were added to the cultures in a final volume of 250 μl complete medium (RPMI + 10% FCS + l-Glutamine + sodium pyruvate + NEAA + Pen/Strep + β-mercaptoethanol). Cells were cultured for four days at 37°C in a 5% CO_2 incubator. T cell proliferation was measured by flow cytometric analysis of CFSE dilution on $CD8^+$ T cells.

2.10 | In vivo treatment

Human recombinant CSF1 (Peprotech) wan injected i.v. at 2×10^5 U/mice on days 0-5 relative to transplantation.

2.11 | Nanoparticles synthesis

Our targeted approach delivers the drug simvastatin using a synthetic high-density lipoprotein (HDL) nanoparticle. These nanoparticles were synthesized using a lipid film hydration method. Phospholipids and simvastatin were dissolved in methanol/chloroform. After evaporating the solvents, human ApoA1 in PBS was added to hydrate the lipid film. This resulting solution was sonicated to form small simvastatin loaded HDL nanoparticles (S-HDL). The animals received 3 intravenous tail injections of S-HDL at 60 mg/kg on the day of transplantation as well as days 2 and 5 post-transplantation.

2.12 | Statistics

Differences between graft survival rates were assessed by Kaplan-Meier survival analysis with Prism software. Unpaired Mann-Whitney test was used when comparing two groups. Kruskal-Wallis with Dunn's multiple comparison test was used for comparisons among multiple groups. Statistical significance is expressed as follows: $^*P \le .05$, $^{**}P \le .01$, NS not significant.

3 | RESULTS

3.1 | Neutrophil derived CSF1 mediates macrophage polarization

Suppressive $Ly6C^{lo}$ macrophages expressing the macrophage colony-stimulating factor 1 receptor (CSF-1R, MCSFR, or CD115) mediate the induction of indefinite allograft survival.[5,22] Induction of transplantation tolerance is controlled by local expression of CSF1, as in vivo blockade of CSF-1 prevents the conversion of non-suppressive $Ly6C^{hi}$ macrophages into suppressive $Ly6C^{lo}$ Mreg in the allograft and abrogates tolerance.[5] To identify the cells that produce CSF1 BALB/c hearts were transplanted into anti-CD40L mAb-treated C57BL6 recipients for tolerance induction. Allografts were harvested at day 5 post-transplantation, single cells were generated by collagenase treatment and distinct cells subsets were isolated by fluorescence activated cells sorting (FACS), according to the gating strategy in Figure 1A, for CSF1 expression by real-time PCR. Our results indicate that graft-infiltrating neutrophils express the highest levels of CSF1 among the $CD45^+$ hematopoietic (Figure 1B). Within the hematopoietic $CD45^+$ cells, myeloid cells express the highest CSF1 levels, and within the myeloid subsets, we found that neutrophils express the highest levels of CSF1. Further gene array analysis of different myeloid subsets indicated that, while neutrophils from tolerized recipient allografts express high levels of CSF1, neutrophils from untreated rejecting mice express low levels of CSF1 (Figure S1). This suggests a potential role of CSF1 producing neutrophils in the development of $Ly6C^{lo}$ macrophages during the induction of tolerance.

To determine whether CSF1 secreting neutrophils favor the development suppressive $Ly6C^{lo}$ macrophages in vivo, Balb/c (H-2^d) heart grafts were transplanted into fully allogeneic C57/BL6 (H-2^b) transplant recipients that are deficient for CSF1 in neutrophils. To generate these recipients, we crossed CSF1 floxed[19] with the neutrophil specific S100A8-Cre mice.[23] Real-time PCR analysis of the CSF1 expression in graft-infiltrating neutrophils reveals that the expression of CSF1 is significantly decreased in CSF1 $^{fl/fl}$ neutrophils in contrast to wild type controls, despite tolerogenic regimen (Figure 1C).

To test for a mechanistic link between CSF1 and the development of suppressive $Ly6C^{lo}$ macrophages, we transplanted BALB/c hearts into fully allogeneic wild type or neutrophil specific CSF1 $^{fl/fl}$ recipients and treated them with tolerizing anti-CD40L mAb regimen. Our results indicate that interfering with in vivo neutrophil CSF1 production significantly decreases intra-graft accumulation of suppressive $Ly6C^{lo}$ macrophages (Figure 1D). Remarkably, while neutrophil CSF1 deficiency abrogated the induction of transplantation tolerance despite anti-CD40L mAb treatment, peritransplant administration of recombinant CSF1 restored prolonged allograft survival in tolerized CSF1 $^{fl/fl}$ recipients (Figure 1E). This demonstrates that CSF1 producing neutrophils mediate the development of suppressive $Ly6C^{lo}$ macrophages that promote the induction of indefinite allograft survival.

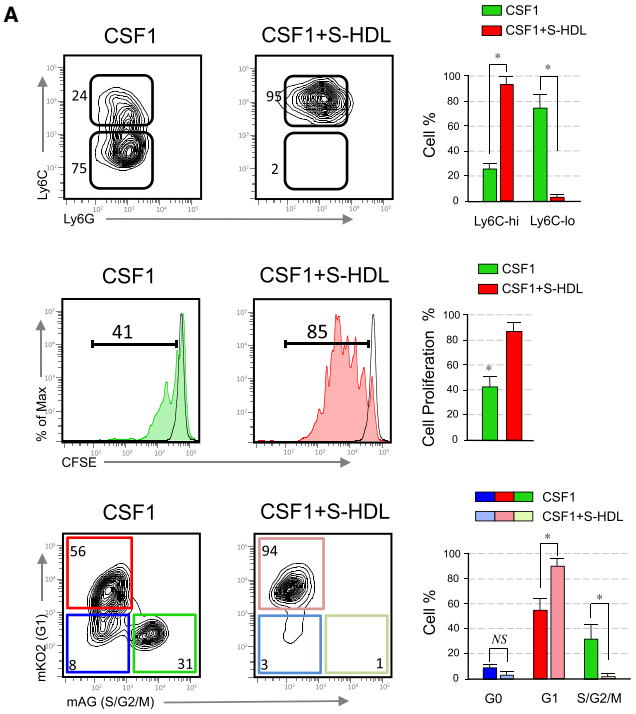
A
CSF1
CSF1+S-HDL
24
75
95
2
Ly6C
Ly6G
Cell %
Ly6C-hi
Ly6C-lo
41
85
% of Max
CFSE
Cell Proliferation %
56
94
8
31
3
1
mKO2 (G1)
mAG (S/G2/M)
NS
G0
G1
S/G2/M

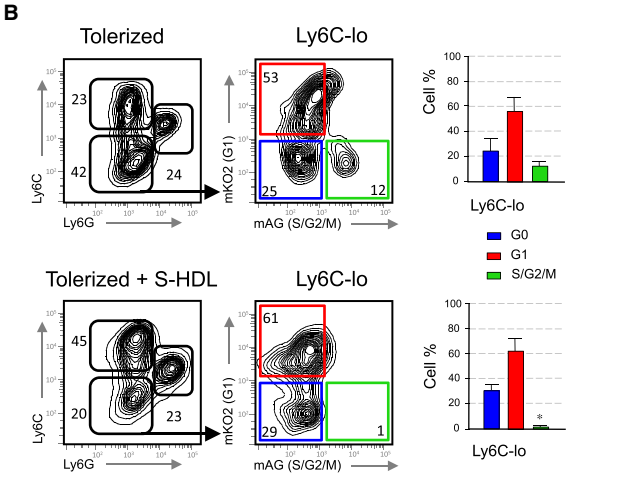
B
Tolerized
Ly6C-lo
Tolerized + S-HDL
23
42
24
53
25
12
45
20
23
61
29
1
Ly6C
Ly6G
mKO2 (G1)
mAG (S/G2/M)
Cell %
G0
G1
S/G2/M

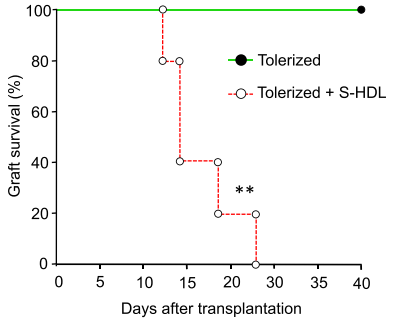
C
Graft survival (%)
Tolerized
Tolerized + S-HDL
**
Days after transplantation

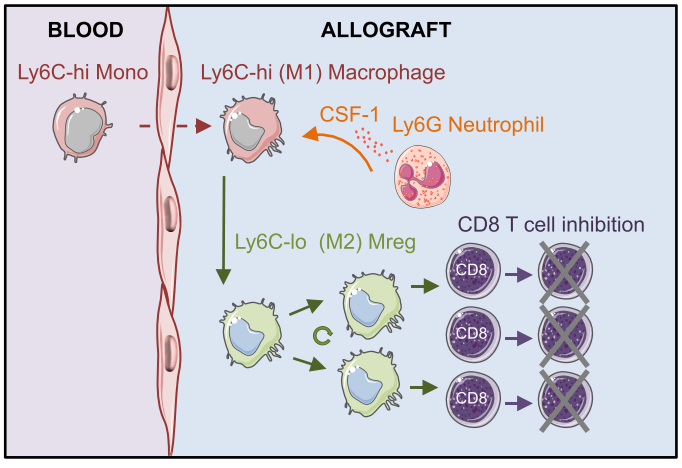
D
BLOOD
ALLOGRAFT
Ly6C-hi Mono
Ly6C-hi (M1) Macrophage
CSF-1
Ly6G Neutrophil
Ly6C-lo (M2) Mreg
CD8 T cell inhibition
CD8

FIGURE 3 Preventing macrophage cell cycle progression abrogates tolerance. (A) Top panel; representative and quantitative flow cytometry results of in vitro cultured bone marrow Ly6C^{hi} monocytes with either CSF1 (10 ng/ml) or CSF1 plus simvastatin loaded HDL nanoparticles (S-HDL) at 10 μM for 72 hours. Middle panel; suppressive function of bone marrow derived Ly6C^{hi} monocytes after treatment with wither CSF1 or CSF1 + S-HDL. Representative and quantitative flow cytometry results of CSFE^{+}CD8^{+} T proliferation after 72 hours of culture. Bottom panel; representative and quantitative flow cytometry results of bone marrow derived Ly6C^{hi} monocytes after treatment with wither CSF1 (10 ng/ml) or CSF1 + S-HDL at 10 μM indicating cell cycle progression after 72 h of culture. Results represent mean ± SEM (n = 3 independent experiments; unpaired Mann-Whitney test; $^{*}P \leq .5$). (B) Representative and quantitative flow cytometry results of myeloid subsets from the allografts of anti-CD40L mAb treated Fucci recipients at day 5 post-transplantation treated with S-HDL (60 mg/kg). Further evaluation of cell cycle fluorescent probes indicated that the majority of Ly6C^{lo} macrophages from anti-CD40L mAb + S-HDL treated Fucci recipients are arrested in G1. Results represent mean ± SEM (n = 3 mice per group of three independent experiments; Kruskal-Walis with Dunn's multiple comparison test; $^{*}P \leq .5$). (C) Graft survival of tolerized recipients treated with or without S-HDL (60 mg/kg) on days 0, 2, and 5 post-transplantation. Tolerized S-HDL recipient mice rejected their allografts despite anti-CD40L mAb treatment. Graft survival was assessed with Kaplan-Meier analysis (*MST* 20 ± 9 days; $^{**}P \leq .01$; n = 5 mice per group). (D) Working hypothesis showing that neutrophil derived CSF1 controls polarization, proliferation, and suppressive function of tolerogenic macrophages that mediate transplantation tolerance

3.2 | Suppressive function of polarized macrophages depends on cell proliferation

Based on the CSF1 requirement for tolerance induction and previous work by others linking CSF1 to cell cycle progression,[24,25] we tested relationship between cell cycle progression of suppressive Ly6C^{lo} macrophages and induction of tolerance. Microarray data analysis of Ly6C^{hi}, Ly6C^{lo}, Ly6G myeloid subsets revealed upregulated expression of genes associated with cell cycle progression in graft infiltrating Ly6C^{lo} macrophages, including the cell proliferation associated gene Mki67 (Figure 2A). Fluorescent immunohistochemistry and flow cytometry analysis confirmed Ki67 protein expression in graft infiltrating Ly6C^{lo} (CD169^{+}) macrophages (Figures 2B and C).

To investigate the relationship between cell cycle progression and suppressive function of Ly6C^{lo} macrophages we employed Fucci transgenic mice. Using Fucci mice as transplant recipients, graft-infiltrating macrophages can be FACS sorted based on their cell cycle stage, as these mice are genetically encoded for fluorescent probes that effectively label the G1 phase nuclei in red (mKO2-hCdt1 30/120) and the S/G2/M phases in green (mAG-hGem 1/110).[18] We transplanted BALB/c hearts into anti-CD40L mAb-treated C57BL6 Fucci transgenic (mKO2/mAG) recipient mice, harvested the allografts at day 5 post-transplantation, and analyzed graft infiltrating myeloid subsets by flow cytometry. We found that >50% of Ly6Clo macrophages from anti-CD40L mAb-treated Fucci recipients are in G1, while >10% are in S/G2/M phase (Figure 2D). We next sorted Ly6Clo macrophages from manti-CD40L mAb-treated Fucci recipients into those in G0, G1, and S/G2/M and tested their immunosuppressive capacity in vitro (Figure 2E). The suppression assay demonstrated that the in vitro inhibitory function of graft infiltrating Ly6Clo macrophages is confined to the proliferating S/G2/M subset. This is consistent with our previous collaborative finding, which demonstrated that suppressive monocytic-derived cells from tumor bearing mice are highly proliferative.[26]

3.3 | Preventing macrophage cell cycle progression abrogates tolerance

To demonstrate that cell proliferation of Ly6C^{lo} macrophages is necessary for the induction of tolerance, we incorporated simvastatin in a high-density lipoprotein (HDL) nanoparticle to generate simvastatin-HDL (S-HDL) nanoparticles, as we recently described.[27] We cultured bone marrow Ly6C^{hi} monocytes with CSF1 to induce their polarization towards suppressive Ly6C^{lo} monocyte-derived cells (Figure 3A). As expected, addition of S-HDL prevented the polarization of Ly6C^{hi} into Ly6C^{lo} monocyte-derived cells in vitro. Next, we tested their ability to suppress T CD8^{+} T cell proliferation and our results indicate that S-HDL treatment prevents the suppressive function of Ly6C^{lo} monocyte-derived cells. This was associated with a S-HDL-mediated cell cycle arrest in G1. This indicates that preventing cell cycle progression interferes with monocyte-derived cell polarization and inhibits their suppressive function. To evaluate the effects of S-HDL in vivo, we next incorporated simvastatin at a concentration of 60 mg/kg in S-HDL nanoparticles to inhibit macrophages proliferation.[28] A conservative S-HDL regimen that included three i.v. injections on days 0, 2, and 5 after transplantation affects the accumulation of Ly6Clo macrophages in the tolerized allografts and promotes graft infiltrating macrophage cell cycle arrest at G1 (Figure 3B). Remarkably, in vivo inhibition of macrophage cell cycle progression abrogated the induction of transplantation tolerance despite tolerogenic regimen (Figure 3C), which demonstrates that proliferation of Ly6C^{lo} macrophages, is required to induce immunological tolerance in the context of organ transplantation.

4 | DISCUSSION

We demonstrate here that graft-infiltrating neutrophils produce CSF1 that mediates polarization of Ly6C^{lo} suppressive macrophages and promotes transplantation tolerance in the context of costimulatory blockade (Figure 3D). This study provides novel understandings about how distinct myeloid cell subsets are interconnected in the tissue and highlights the critical contribution of neutrophils during the induction of indefinite allograft survival.

Neutrophils are the most abundant myeloid cell subset in circulation and rapidly infiltrate the inflamed tissue. As a result, neutrophils have been have been historically viewed as pro-inflammatory cells that protect against intracellular pathogens though the release of extracellular traps.[29] In organ transplantation, the role of neutrophils is commonly associated to antibody mediated and chronic rejection or ischemia

reperfusion injury and resolution of inflammation.[30] However, murine neutrophils also release anti-inflammatory cytokines,[31] and recent evidence suggests that neutrophils are able to negatively regulate T cell mediated immune responses.[32] Here, we show that neutrophils favor tolerance by mediating macrophage polarization in the transplanted organ uncovering a previously unrecognized function of neutrophils in the context of organ transplantation.

Data from tumor models also suggest a close relationship between neutrophilic and monocytic-derived suppressor cells. Myeloid-derived suppressor cells (MDSC) are comprised of two groups of immunosuppressive cells with monocytic (M-MDSC) and granulocytic (G-MDSC) morphology. G-MDSC express high levels of CSF1,[33] which represents a growth factor involved in the generation of M-MDSC that prolongs allograft survival upon adoptive transfer.[34] Therefore, CSF1-dependent macrophage development represents a novel approach for therapeutic intervention either by inhibiting (ie, cancer), or by promoting (ie, transplantation) macrophage polarization. In this respect, the development of monoclonal antibodies that target macrophage polarization through CSF1 receptor signaling has been shown to interfere with macrophage differentiation/proliferation and to prevent tumor progression.[35,36]

We conclude that neutrophils secrete CSF1 that promotes macrophage polarization, progression through the cell cycle, and suppressive function of graft infiltrating macrophages. Future experiments are aimed at elucidating the mechanisms by with anti-CD40L mAb promote "tolerogenic" neutrophils. In this respect, we hypothesize neutrophils scanning for platelets[37] may receive a "tolerogenic" signal following CD40L blockade in activated platelets[38] that may lead to CSF1 production and transplantation tolerance under sterile inflammatory conditions.

ACKNOWLEDGMENTS

We thank the technical contributions of the flow cytometry and microsurgery cores at Mount Sinai. We also acknowledge Marcy Kuenzel and Sridar Chittur at the University of Albany Center for Functional Genomics microarray core facility for their assistance in generating the microarray data. This work was supported by the Cancer Center Grant P30 CA196521; the National Institute of Health grants AG045040 to S.A.W. and R01 HL118440, R01 HL125703, R01 CA155432 to W.J.M.M; and the Ministerio de Economia y Competitividad SAF2016-80031-R to J.O. This work was also supported by the COST Action BM1305: Action to Focus and Accelerate Cell Tolerogenic Therapies (A FACTT), the COST action BM1404: European Network of Investigators Triggering Exploratory Research on Myeloid Regulatory Cells (Mye-EUNITER), and the Mount Sinai Recanati/Miller Transplantation Institute career development funds.

DISCLOSURE

The authors of this manuscript have no conflicts of interest to disclose as described by the *American Journal of Transplantation*.

REFERENCES

1. Poulter LW, Bradley NJ, Turk JL. The role of macrophages in skin allograft rejection. I. Histochemical studies during first-set rejection. *Transplantation*. 1971;12(1):40-44.
2. Bergler T, Jung B, Bourier F, et al. Infiltration of macrophages correlates with severity of allograft rejection and outcome in human kidney transplantation. *PLoS ONE*. 2016;11(6):e0156900.
3. Wyburn KR, Jose MD, Wu H, Atkins RC, Chadban SJ. The role of macrophages in allograft rejection. *Transplantation*. 2005;80(12):1641-1647.
4. Swirski FK, Wildgruber M, Ueno T, et al. Myeloperoxidase-rich Ly-6C+ myeloid cells infiltrate allografts and contribute to an imaging signature of organ rejection in mice. *J Clin Invest*. 2010;120(7):2627-2634.
5. Conde P, Rodriguez M, van der Touw W, et al. DC-SIGN(+) macrophages control the induction of transplantation tolerance. *Immunity*. 2015;42(6):1143-1158.
6. Ochando J, Conde P, Bronte V. Monocyte-derived suppressor cells in transplantation. *Curr Transplant Rep*. 2015;2(2):176-183.
7. Gordon S, Taylor PR. Monocyte and macrophage heterogeneity. *Nat Rev Immunol*. 2005;5(12):953-964.
8. Okabe Y, Medzhitov R. Tissue-specific signals control reversible program of localization and functional polarization of macrophages. *Cell*. 2014;157(4):832-844.
9. Arnold L, Henry A, Poron F, et al. Inflammatory monocytes recruited after skeletal muscle injury switch into antiinflammatory macrophages to support myogenesis. *J Exp Med*. 2007;204(5):1057-1069.
10. Mantovani A, Sozzani S, Locati M, Allavena P, Sica A. Macrophage polarization: tumor-associated macrophages as a paradigm for polarized M2 mononuclear phagocytes. *Trends Immunol*. 2002;23(11):549-555.
11. Porta C, Rimoldi M, Raes G, et al. Tolerance and M2 (alternative) macrophage polarization are related processes orchestrated by p50 nuclear factor kappaB. *Proc Natl Acad Sci USA*. 2009;106(35):14978-14983.
12. Huber S, Hoffmann R, Muskens F, Voehringer D. Alternatively activated macrophages inhibit T-cell proliferation by Stat6-dependent expression of PD-L2. *Blood*. 2010;116(17):3311-3320.
13. Oishi S, Takano R, Tamura S, et al. M2 polarization of murine peritoneal macrophages induces regulatory cytokine production and suppresses T-cell proliferation. *Immunology*. 2016;149(3):320-328.
14. Martinez FO, Gordon S, Locati M, Mantovani A. Transcriptional profiling of the human monocyte-to-macrophage differentiation and polarization: new molecules and patterns of gene expression. *J Immunol*. 2006;177(10):7303-7311.
15. Munn DH, Pressey J, Beall AC, Hudes R, Alderson MR. Selective activation-induced apoptosis of peripheral T cells imposed by macrophages. A potential mechanism of antigen-specific peripheral lymphocyte deletion. *J Immunol*. 1996;156(2):523-532.
16. Sakurai T, Yamada M, Simamura S, Motoyoshi K. Recombinant human macrophage-colony stimulating factor suppresses the mouse mixed lymphocyte reaction. *Cell Immunol*. 1996;171(1):87-94.
17. Wing EJ, Magee DM, Pearson AC, Waheed A, Shadduck RK. Peritoneal macrophages exposed to purified macrophage colony-stimulating factor (M-CSF) suppress mitogen- and antigen-stimulated lymphocyte proliferation. *J Immunol*. 1986;137(9):2768-2773.
18. Sakaue-Sawano A, Kurokawa H, Morimura T, et al. Visualizing spatiotemporal dynamics of multicellular cell-cycle progression. *Cell*. 2008;132(3):487-498.
19. Harris SE, MacDougall M, Horn D, et al. Meox2Cre-mediated disruption of CSF-1 leads to osteopetrosis and osteocyte defects. *Bone*. 2012;50(1):42-53.
20. Corry RJ, Winn HJ, Russell PS. Primarily vascularized allografts of hearts in mice. The role of H-2D, H-2K, and non-H-2 antigens in rejection. *Transplantation*. 1973;16(4):343-350.

21. Jiang X, Sun W, Guo D, et al. Cardiac allograft acceptance induced by blockade of CD40-CD40L costimulation is dependent on CD4 + CD25 + regulatory T cells. *Surgery*. 2011;149(3):336-346.
22. Garcia MR, Ledgerwood L, Yang Y, et al. Monocytic suppressive cells mediate cardiovascular transplantation tolerance in mice. *J Clin Invest*. 2010;120(7):2486-2496.
23. Abram CL, Roberge GL, Pao LI, Neel BG, Lowell CA. Distinct roles for neutrophils and dendritic cells in inflammation and autoimmunity in motheaten mice. *Immunity*. 2013;38(3):489-501.
24. Stanley ER, Guilbert LJ, Tushinski RJ, Bartelmez SH. CSF-1–a mononuclear phagocyte lineage-specific hemopoietic growth factor. *J Cell Biochem*. 1983;21(2):151-159.
25. Roussel MF. Regulation of cell cycle entry and G1 progression by CSF-1. *Mol Reprod Dev*. 1997;46(1):11-18.
26. Ugel S, Peranzoni E, Desantis G, et al. Immune tolerance to tumor antigens occurs in a specialized environment of the spleen. *Cell Rep*. 2012;2(3):628-639.
27. Duivenvoorden R, Tang J, Cormode DP, et al. A statin-loaded reconstituted high-density lipoprotein nanoparticle inhibits atherosclerotic plaque inflammation. *Nat Commun*. 2014;5:3065.
28. Tang J, Lobatto ME, Hassing L, et al. Inhibiting macrophage proliferation suppresses atherosclerotic plaque inflammation. *Sci Adv* 2015;1(3): pii: e1400223
29. Nicolas-Avila JA, Adrover JM, Hidalgo A. Neutrophils in homeostasis, immunity, and cancer. *Immunity*. 2017;46(1):15-28.
30. Scozzi D, Ibrahim M, Menna C, Krupnick AS, Kreisel D, Gelman AE. The role of neutrophils in transplanted organs. *Am J Transplant*. 2017;17(2):328-335.
31. De Santo C, Arscott R, Booth S, et al. Invariant NKT cells modulate the suppressive activity of IL-10-secreting neutrophils differentiated with serum amyloid A. *Nat Immunol*. 2010;11(11):1039-1046.
32. Pillay J, Kamp VM, van Hoffen E, et al. A subset of neutrophils in human systemic inflammation inhibits T cell responses through Mac-1. *J Clin Invest*. 2012;122(1):327-336.
33. Condamine T, Dominguez GA, Youn JI, et al. Lectin-type oxidized LDL receptor-1 distinguishes population of human polymorphonuclear myeloid-derived suppressor cells in cancer patients. *Sci Immunol* 2016;1(2):pii: aaf8943
34. Yang F, Li Y, Wu T, et al. TNFalpha-induced M-MDSCs promote transplant immune tolerance via nitric oxide. *J Mol Med (Berl)*. 2016;94(8):911-920.
35. Pyonteck SM, Akkari L, Schuhmacher AJ, et al. CSF-1R inhibition alters macrophage polarization and blocks glioma progression. *Nat Med*. 2013;19(10):1264-1272.
36. Van Overmeire E, Stijlemans B, Heymann F, et al. M-CSF and GM-CSF receptor signaling differentially regulate monocyte maturation and macrophage polarization in the tumor microenvironment. *Cancer Res*. 2016;76(1):35-42.
37. Sreeramkumar V, Adrover JM, Ballesteros I, et al. Neutrophils scan for activated platelets to initiate inflammation. *Science*. 2014;346(6214):1234-1238.
38. Henn V, Slupsky JR, Grafe M, et al. CD40 ligand on activated platelets triggers an inflammatory reaction of endothelial cells. *Nature*. 1998;391(6667):591-594.

SUPPORTING INFORMATION

Additional Supporting Information may be found online in the supporting information tab for this article.

How to cite this article: Braza MS, Conde P, Garcia M, et al. Neutrophil derived CSF1 induces macrophage polarization and promotes transplantation tolerance. *Am J Transplant*. 2018;00:1-9. https://doi.org/10.1111/ajt.14645

Article

Immunity

The TREM2-APOE Pathway Drives the Transcriptional Phenotype of Dysfunctional Microglia in Neurodegenerative Diseases

Graphical Abstract

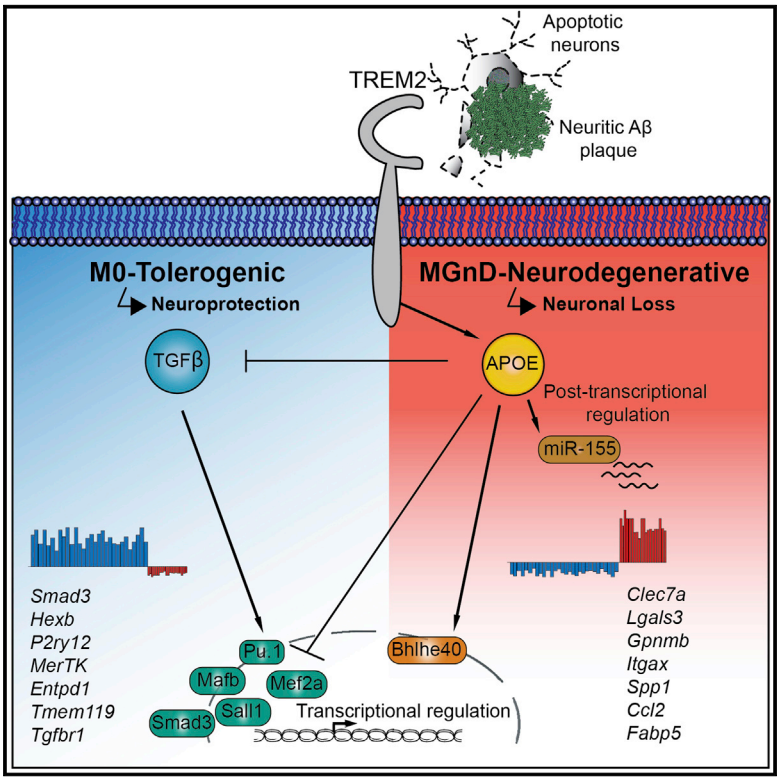

Highlights

- Microglia associated with neuritic Aβ-plaques exhibit a neurodegenerative phenotype
- Phagocytosis of apoptotic neurons suppresses homeostatic microglia
- The TREM2-APOE pathway regulates neurodegenerative microglial phenotypic switch
- Targeting APOE signaling restores homeostatic and tolerogenic microglia

Authors

Susanne Krasemann, Charlotte Madore, Ron Cialic, ..., Jordi Ochando, Christian Haass, Oleg Butovsky

Correspondence

obutovsky@rics.bwh.harvard.edu

In Brief

Microglia change their phenotype and function during aging and neurodegeneration, but the underlying molecular mechanisms for this change remain unknown. Krasemann et al. identify the TREM2-APOE pathway as a major regulator of microglia phenotypic change in neurodegenerative diseases and suggest that targeting this pathway could restore homeostatic microglia.

Krasemann et al., 2017, Immunity *47*, 566–581
September 19, 2017
http://dx.doi.org/10.1016/j.immuni.2017.08.008

CellPress

CellPress

Immunity
Article

The TREM2-APOE Pathway Drives the Transcriptional Phenotype of Dysfunctional Microglia in Neurodegenerative Diseases

Susanne Krasemann,[1,2,17] Charlotte Madore,[1,17] Ron Cialic,[1] Caroline Baufeld,[1] Narghes Calcagno,[1] Rachid El Fatimy,[1] Lien Beckers,[1] Elaine O'Loughlin,[1] Yang Xu,[3] Zain Fanek,[1] David J. Greco,[1] Scott T. Smith,[1] George Tweet,[1] Zachary Humulock,[1] Tobias Zrzavy,[4] Patricia Conde-Sanroman,[5] Mar Gacias,[5] Zhiping Weng,[6] Hao Chen,[6] Emily Tjon,[1] Fargol Mazaheri,[7] Kristin Hartmann,[2] Asaf Madi,[1] Jason D. Ulrich,[8] Markus Glatzel,[2] Anna Worthmann,[9] Joerg Heeren,[9] Bogdan Budnik,[10] Cynthia Lemere,[1] Tsuneya Ikezu,[11] Frank L. Heppner,[12,13] Vladimir Litvak,[3] David M. Holtzman,[8] Hans Lassmann,[4] Howard L. Weiner,[1,14] Jordi Ochando,[5] Christian Haass,[7,15,16] and Oleg Butovsky[1,14,18,*]

[1]Ann Romney Center for Neurologic Diseases, Department of Neurology, Brigham and Women's Hospital, Harvard Medical School, Boston, MA, USA
[2]Institute of Neuropathology, University Medical Center Hamburg-Eppendorf, Hamburg, Germany
[3]Department of Microbiology and Physiological Systems, University of Massachusetts Medical School, Worcester, MA, USA
[4]Center for Brain Research, Medical University of Vienna, Vienna, Austria
[5]Department of Medicine, Icahn School of Medicine at Mount Sinai, NY, USA
[6]Department of Biochemistry and Molecular Pharmacology, University of Massachusetts Medical School, Worcester, MA, USA
[7]German Center for Neurodegenerative Diseases, Munich, Germany
[8]Department of Neurology, Hope Center for Neurological Disorders, Knight Alzheimer's Disease Research Center, Washington University School of Medicine, St. Louis, USA
[9]Department of Biochemistry and Molecular Cell Biology, University Medical Center Hamburg-Eppendorf, Hamburg, Germany
[10]Mass Spectrometry and Proteomics Resource Laboratory, Faculty of Arts and Sciences Division of Science, Harvard University, Cambridge MA, USA
[11]Department of Pharmacology and Experimental Therapeutics and Department of Neurology, Boston University School of Medicine, MA, USA
[12]Department of Neuropathology, Charité-Universitätsmedizin Berlin, Berlin, Germany
[13]Cluster of Excellence, NeuroCure, Charitéplatz 1, 10117 Berlin, Germany
[14]Evergrande Center for Immunologic Diseases, Brigham and Women's Hospital, Harvard Medical School, Boston, MA, USA
[15]Biomedical Center, Biochemistry, Ludwig-Maximilians-Universität Munich, Munich, Germany
[16]Munich Cluster for Systems Neurology, Munich, Germany
[17]These authors contributed equally
[18]Lead Contact
*Correspondence: obutovsky@rics.bwh.harvard.edu
http://dx.doi.org/10.1016/j.immuni.2017.08.008

SUMMARY

Microglia play a pivotal role in the maintenance of brain homeostasis but lose homeostatic function during neurodegenerative disorders. We identified a specific apolipoprotein E (APOE)-dependent molecular signature in microglia from models of amyotrophic lateral sclerosis (ALS), multiple sclerosis (MS), and Alzheimer's disease (AD) and in microglia surrounding neuritic β-amyloid (Aβ)-plaques in the brains of people with AD. The APOE pathway mediated a switch from a homeostatic to a neurodegenerative microglia phenotype after phagocytosis of apoptotic neurons. TREM2 (triggering receptor expressed on myeloid cells 2) induced APOE signaling, and targeting the TREM2-APOE pathway restored the homeostatic signature of microglia in ALS and AD mouse models and prevented neuronal loss in an acute model of neurodegeneration. APOE-mediated neurodegenerative microglia had lost their tolerogenic function. Our work identifies the TREM2-APOE pathway as a major regulator of microglial functional phenotype in neurodegenerative diseases and serves as a novel target that could aid in the restoration of homeostatic microglia.

INTRODUCTION

Neuronal injury and cell death are common hallmarks of neurodegenerative processes (Mattson, 2000). It remains unclear whether neuronal cell death is a cause or result of Alzheimer's disease (AD), especially when one considers that neurodegeneration is not an acute and rapid event but occurs gradually over a long period of time. However, apoptosis, as well as neuritic dystrophy leading to permanent central nervous system (CNS) damage, occurs in neurodegenerative diseases, including AD (Masliah et al., 1998) and amyotrophic lateral sclerosis (ALS) (Kostic et al., 1997), and in inflammatory autoimmune diseases such as multiple sclerosis (MS) (Ofengeim et al., 2015).

Microglia are brain-resident immune cells that maintain CNS homeostasis, constantly survey their environment (Nimmerjahn et al., 2005), and react to homeostasis-perturbing elements by

initiating an inflammatory reaction (Kreutzberg, 1996). In the healthy brain, they have a unique homeostatic molecular and functional signature (M0) (Butovsky et al., 2014; Gautier et al., 2012; Hickman et al., 2013), which is tightly controlled by transforming growth factor β (TGFβ) signaling (Butovsky et al., 2014; Gosselin et al., 2014). However, during the course of disease, microglia lose their homeostatic molecular signature and functions (Butovsky et al., 2015; Holtman et al., 2015) and become chronically inflammatory (Perry and Holmes, 2014). Recent studies identified a common disease-associated microglia signature (Chiu et al., 2013; Hickman et al., 2013; Holtman et al., 2015; Keren-Shaul et al., 2017; Orre et al., 2014). However, the mechanisms that regulate the microglial phenotype in disease have not been identified.

In this study, we identified a role for apolipoprotein E (APOE) in regulating a subset of microglia, which exhibit a common disease-associated phenotype. This neurodegenerative phenotypic switch is triggered by TREM2, leading to activation of APOE signaling and subsequent suppression of homeostatic microglial phenotype. A functional consequence of the activation of TREM2-APOE pathway is that microglia lose the ability to regulate brain homeostasis.

RESULTS

Reciprocal Induction of APOE and Suppression of TGFβ Signaling in Disease-Associated Microglia

To investigate underlying common molecular mechanisms that regulate microglial dysfunction, we isolated microglia and analyzed transcriptomes during aging and disease progression in mouse models of ALS ($SOD1^{G93A}$, expressing human Cu,Zn superoxide dismutase mutation), AD (APP-PS1, overexpressing mutated genes for human amyloid precursor protein and presenilin 1), and MS (experimental autoimmune encephalomyelitis [EAE]) (Table S1). We performed *k*-means clustering and identified two major gene clusters (Figure 1A). Cluster 1 was associated with the loss of 68 homeostatic microglial genes, including *P2ry12*, *Tmem119*, *Gpr34*, *Jun*, *Olfml3*, *Csf1r*, *Hexb*, *Mertk*, *Rhob*, *Cx3Cr1*, *Tgfbr1*, and *Tgfb1* and transcription factors such as *Mef2a*, *Mafb*, *Jun*, *Sall1*, and *Egr1*, which are enriched in adult microglia (Butovsky et al., 2014; Buttgereit et al., 2016; Matcovitch-Natan et al., 2016). Cluster 2 was associated with the upregulation of 28 inflammatory molecules, including *Spp1*, *Itgax*, *Axl*, *Lilrb4*, *Clec7a*, *Ccl2*, *Csf1*, and *Apoe*, of which *Apoe* was one of the most upregulated genes (Figure 1A and Table S1). We termed this microglial neurodegenerative phenotype MGnD, in contrast to M0-homeostatic adult microglia phenotype (Butovsky et al., 2014; Gautier et al., 2012; Hickman et al., 2013). Linear regression analysis showed a negative correlation of *Mef2a*, *Sall1*, and *Tgfbr1* with progression in EAE, SOD1, and APP-PS1 models (Figure 1B). In contrast, induction of *Apoe* was positively correlated with progression (Figure 1B). In EAE, we found suppression of homeostatic genes (e.g., *P2ry12*, *Tmem119*, *Tgfbr1*, *Mafb*, *Mef2a*, *Sall1*, and *Egr1*; Butovsky et al., 2014; Gautier et al., 2012; Hickman et al., 2013; Matcovitch-Natan et al., 2016) during the acute phase and restoration during recovery (Figure 1C; Figures S1A–S1C and Table S1). *Apoe* was reciprocally upregulated (Figure 1C), which we validated by quantitative real-time PCR (qPCR) in two other MOG-induced EAE mouse models: the non-obese diabetic (NOD) (chronic-relapsing) model and the C57BL/6J (acute) model (Figures S1D and S1E). P2ry12 immunoreactivity was lost at onset and disease peak and re-emerged during recovery (Figure S1F). APOE and TGFβ were major upstream regulators of MGnD microglia (Figure 1D and Table S1), as shown by ingenuity pathway analysis (IPA). The top-suppressed TGFβ-dependent homeostatic genes (Butovsky et al., 2014), *Olfml3, P2ry12*, *Tmem119*, *Mef2a*, *Jun*, *Sall1*, and upregulated genes *Apoe* and *Axl* were similarly affected during progression (Figure 1E). These results indicate a common disease-related microglia molecular signature that is associated with the induction of APOE and the suppression of TGFβ signaling.

The MGnD-Microglia Subset Is Associated with Neuritic Aβ Plaques and Diffuse Neuritic Dystrophy in the AD Cortex

The pathology of the AD brain is characterized by widespread neuritic dystrophy (Larner, 1995). These dystrophic axons are enlarged and show intense reactivity for phosphorylated neurofilaments (Sternberger et al., 1985). To address whether a microglial phenotypic switch from M0 homeostatic to MGnD-neurodegenerative is specifically associated with neuritic dystrophy in AD, we analyzed brains from APP-PS1 mice and humans with AD. To distinguish M0 versus MGnD microglia, we used P2ry12 and Clec7a mAbs and found $Clec7a^{+}P2ry12^{-}$ microglia associated with Aβ plaques in APP-PS1 mice (Figure 2A). We identified three microglial subsets: (1) $Clec7a^{-}P2ry12^{+}$ (not associated with Aβ plaques); (2) $Clec7a^{lo}P2ry12^{lo}$ (in close proximity to Aβ plaques); and (3) $Clec7a^{+}P2ry12^{-}$ (associated with neuritic Aβ plaques) (Figure 2A). TMEM119 is stable even when the mRNA is downregulated (Satoh et al., 2016) and co-localized with Aβ-plaque-associated $Clec7a^{+}$ microglia (Figure S2A). $Clec7a^{+}P2ry12^{-}$ microglia were associated with phosphorylated neurofilaments (pNF^{+}) in neuritic plaques in APP-PS1 mice (Figure 2B and Figure S2B). The number of $FCRLS^{+}Clec7a^{+}$ microglia was increased in 24-month-old APP-PS1 mice (Figures S2C–S2G). The phenotype of $Clec7a^{+}$ microglia was similar to that of MGnD microglia identified in SOD1, EAE, and APP-PS1 models and during aging (Figure 2C and Table S2). Suppressed microglial homeostatic genes included *P2ry12*, *Tmem119*, *Olfml3*, *Csf1r*, *Rhob*, *Cx3cr1*, *Tgfb1*, *Mef2a*, *Mafb*, and *Sall1*, and upregulated inflammatory molecules included *Spp1*, *Itgax*, *Axl*, *Lilrb4*, *Clec7a*, *Csf1*, and *Apoe*, the latter of which was among the most upregulated genes (Figures 2C and 2D and Table S2). Transition from $Clec7a^{-}$ to $Clec7a^{int}$ to $Clec7a^{hi}$ correlated with increased expression of *Apoe* and suppression of homeostatic molecules (Figure 2D). Clec7a expression increased during progression in EAE and SOD1 mice (Figures S2H–S2K). RNA sequencing (RNAseq) of the three microglia subsets validated the NanoString analysis and showed that only $FCRLS^{+}Clec7a^{+}$ microglia acquired an MGnD signature (Figures 2E and 2F and Table S2).

To determine whether a microglial phenotype was associated with neuritic plaques, we double stained brains of individuals affected by AD for P2RY12 with Aβ or pNF. $P2RY12^{+}$ microglia were preserved in Aβ diffuse plaques, and P2RY12 signal was lost in pNF^{+} neuritic plaques (Figure 2G). $TMEM119^{+}P2RY12^{-}$ microglia, and not recruited $IBA1^{+}TMEM119^{-}$ peripheral

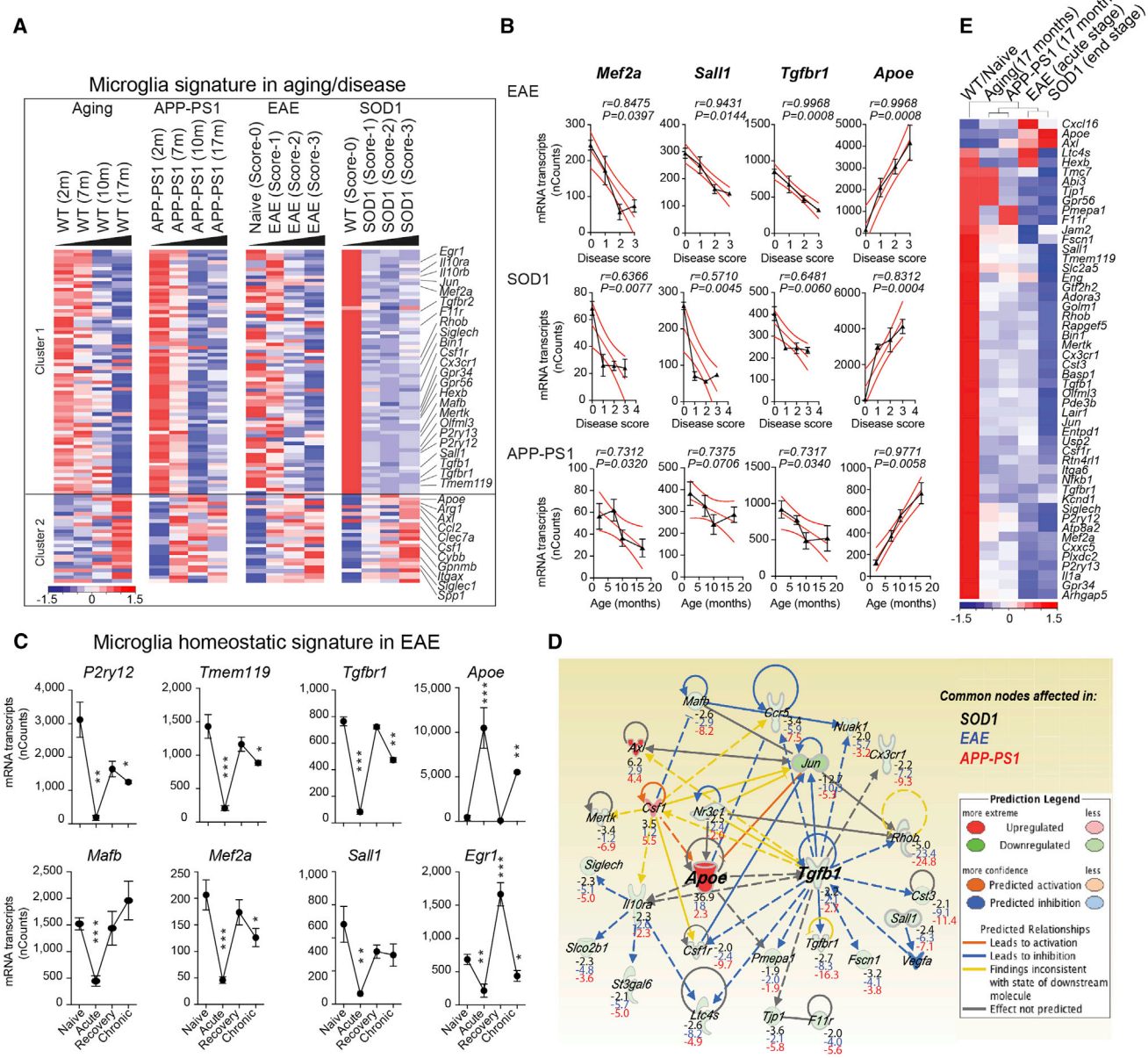

Figure 1. Reciprocal Induction of APOE and Suppression of TGFβ Signaling in Disease-Associated MGnD-Microglia

(A) K-means clustering, via NanoString, of 95 significantly affected common genes in FCRLS$^+$ microglia during aging and disease. Vertical lanes are biological replicates per disease stage or condition in WT aging (n = 12), EAE (n = 18), SOD1 (n = 11) and APP-PS1 (n = 12) mice. Cluster 1: suppressed homeostatic genes. Cluster 2: upregulated genes.

(B) Linear regression curve of *Mef2a*, *Sall1*, *Tgfbr1*, and *Apoe* in EAE (n = 4–6 mice/disease score) and SOD1 (n = 2–4 mice/disease score) spinal-cord microglia and APP-PS1 (n = 3 mice/age) brain microglia. Thick line: 95% confidence interval of the regression line.

(C) Selected homeostatic and disease-associated microglial genes during EAE (n = 3). Data are presented as means ± SEM. *p < 0.05, **p < 0.01, ***p < 0.001 by one-way ANOVA followed by Dunnett's multiple-comparison post-hoc test.

(D) IPA shows common nodes significantly affected in microglia in all three-mouse models in disease. For each molecule, the expression fold change compared to normal, homeostatic microglia is presented.

(E) Heatmap of significantly affected genes dysregulated in all 3 diseases (n = 3–4) determined by NanoString. Vertical lanes: mean of biological replicates per disease stage/condition as indicated in (A).

See also Figure S1 and Table S1.

myeloid cells, were associated with pNF$^+$ neuritic plaques (Figures S2L–S2N). Loss of P2RY12$^+$ microglia correlated with axonal dystrophy, but not with the extent of Aß deposition (Figure 2H). We found increased APOE expression in microglia in close proximity to Aß plaques (Figures S2O and S2P). These data demonstrate that the microglial phenotypic switch from

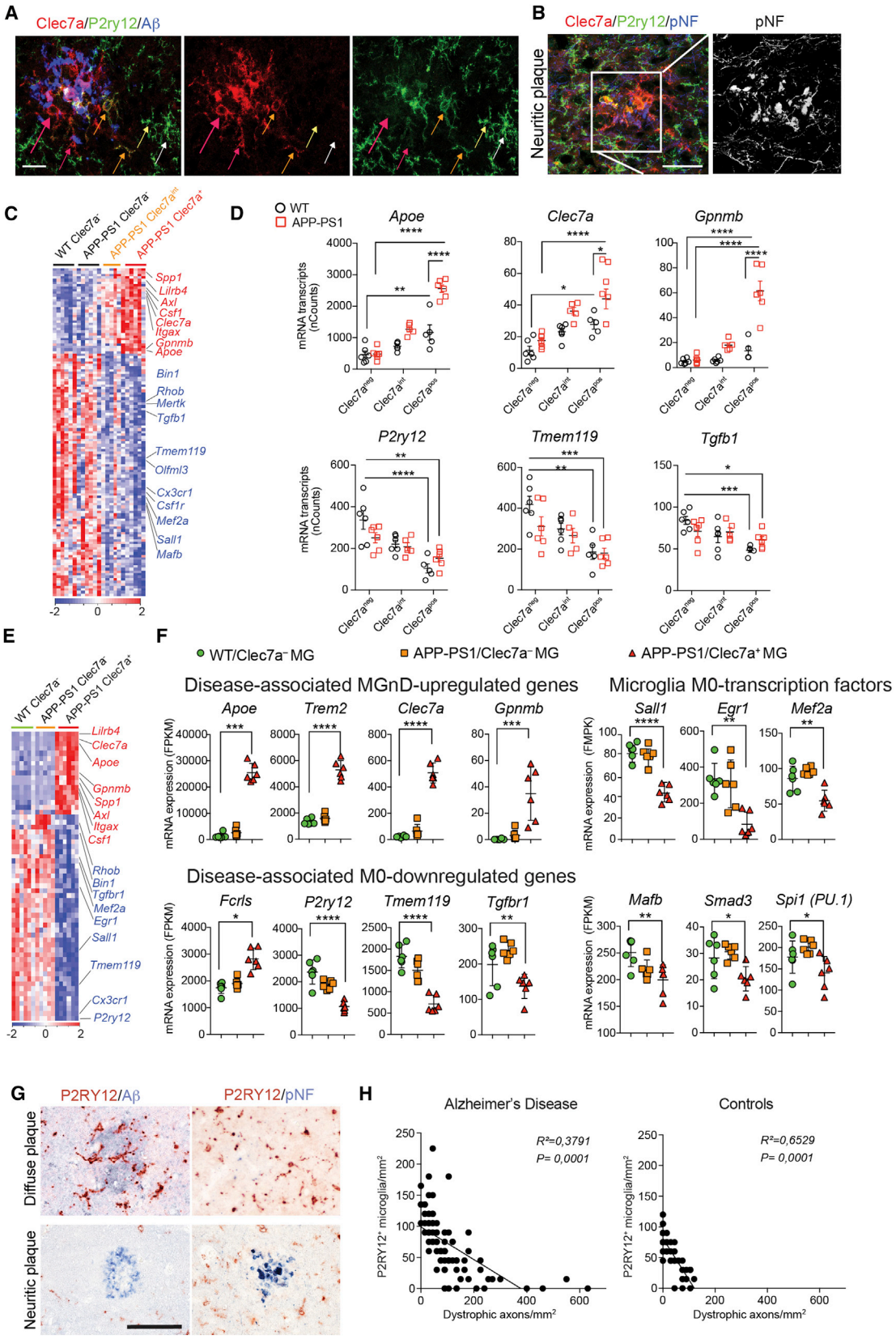

(legend on next page)

M0 to MGnD is associated with neuritic dystrophy in APP-PS1 mice and AD-affected humans.

Phagocytosis of Apoptotic Neurons Suppresses Homeostatic Microglia

To determine the mechanisms by which the MGnD microglia are induced in neurodegeneration, we injected apoptotic neurons (dNs) into the cortex and hippocampus of naive mice. dNs induced the recruitment of P2ry12^{+} microglia toward the site of injection (Figure 3A). P2ry12^{+} microglia changed morphology from an M0 homeostatic non-phagocytic (MG-nΦ) phenotype to an amoeboid-phagocytic (MG-dNΦ) phenotype at the vicinity of the injection site (Figures 3A–3C and Figure S3A). Induction of MGnD microglia was not detected in phosphate-buffered saline (PBS)-injected brains (Figure S3B). Apoptotic neurons were internalized by P2ry12^{+} microglia (Figure 3B). Induction of Apoe was detected in MG-dNΦ microglia (Figure 3C). Increased *Apoe* expression was detected as early as 3 hr after injection and peaked at 16 hr after injection (Figure S3C). Restoration of homeostatic P2ry12^{+}Clec7a^{-} microglia occurred at 14 d post-injection (Figures S2D and S2E). Profiling of MG-dNΦ and MG-nΦ microglia showed that phagocytosis of dNs induced a microglial molecular phenotype similar to the MGnD phenotype (Figures 3D and 3E). M0-microglial homeostatic genes including *Tmem119*, *Egr1*, *Hexb*, *Gpr34*, *P2ry12*, *Olfml3*, and *Tgfbr1* were suppressed in MG-dNΦ microglia, whereas *Apoe* was the major upregulated gene among other inflammatory molecules (Figure 3F and Table S3). This was confirmed by qPCR of microglial genes including upregulation of *Apoe* and microRNA miR-155 (Figure 3G and Figures S3C and S3F). Although injured neurons express elevated *Apoe* (Xu et al., 2006), we observed the upregulation of *Apoe* in MG-dNΦ microglia phagocytosing *Apoe*$^{-/-}$ dNs (Figure S3G). Injection of *E. coli* or zymosan particles did not induce *Apoe* in phagocytic microglia (Figure S3H). In contrast, miR-155 was induced by dNs, *E.coli* and zymosan particles in phagocytic microglia (Figure S3I). Microglia phagocytosed injected dNs, but not live neurons (Figures S3J and S3K). Upregulation of *Apoe* in phagocytic microglia was also induced by apoptotic monocytes (Figure S3L). We validated our paradigm of dN-induced MG-dNΦ phenotype by using kainic acid as a model of acute neuronal cell death (Lévesque and Avoli, 2013). We observed P2ry12^{-}/Clec7a^{+} microglia 48 hr post-injection (Figure S4).

Although in vivo LPS and IFN-γ-stimulated microglia suppressed many of the homeostatic microglial genes including *P2ry12*, *Gpr34*, *Fcrls*, *Tmem119*, *Olfml3*, *Siglech*, *Sall1*, *Hexb*, *Csf1r*, and *Tgfbr1* (Figures S5A–S5C and Table S4), the expression of *Apoe* was suppressed in M1 microglia (Figures S5D–S5E and S5H). In contrast, *Egr1*, which is a key transcription factor in M0 homeostatic microglia (Butovsky et al., 2014; Matcovitch-Natan et al., 2016) and was most suppressed in MG-dNΦ microglia, was induced in M1 microglia (Figures S5F–S5H). Furthermore, arginase 1 (*Arg1*) and chitinase-3-like protein (*Ym1*), the "classical" M2 anti-inflammatory markers, (Martinez and Gordon, 2014) were induced in MG-dNΦ microglia along with inflammatory molecules, including those encoded by *Il1b*, *Ptgs2* (*Cox2*), *Ccl2*, *Ccl5*, *Tspo*, *Msr1*, and *Cebpb* (Figures S5F–S5H). Thus, the MG-dNΦ molecular signature is distinct from that of classical M1induced microglia.

Quantitative mass spectrometry of MG-dNΦ versus MG-nΦ microglia showed increased amounts of Apoe and Lgals3 in MG-dNΦ microglia. In contrast, both Rgs10 and Bin1, two homeostatic microglial proteins (Butovsky et al., 2014), were suppressed (Figure 3H and Table S3). To investigate MG-dNΦ microglia in disease models, we used gene-set enrichment analysis (GSEA). Circos plot network analysis presented an overlap of the phagocytic microglial phenotype with the microglia molecular signature during aging and in a model of brain irradiation. The MG-dNΦ microglia signature was enriched in microglia transcriptomes from models of AD (5XFAD), ALS (SOD1), and *Mfp2* deficiency, which is associated with cerebellar degeneration (Verheijden et al., 2013). In contrast, microglial changes in *Mecp2* deficiency, or changes associated with neuropathic and chronic pain models were not connected with the MG-dNΦ gene signature (Figure 3I and Table S3). Taken together, these data show that MGnD microglia are induced by apoptotic neurons, which are a hallmark of neurodegeneration.

APOE Regulates the Transcriptional and Post-transcriptional Program of the MGnD Phenotype and Function

We previously reported that *Apoe* expression is downregulated in microglia during development, correlates with the induction of M0-homeostatic genes, and is increased in microglia progenitors from CNS *Tgfb1*$^{-/-}$ mice (Butovsky et al., 2014). To assess the role of Apoe in the induction of MGnD microglia during

Figure 2. MGnD-Microglia Are Associated with Neuritic Aβ-Plaques

(A) Staining for P2ry12^{+} and Clec7a^{+} in Aβ-plaque microglia in 24-month-old APP-PS1 mice. MGnD around plaque (red arrows). MGnD transitioning to plaque (yellow arrows). M0 homeostatic microglia (white arrows). Scale bar, 20 μm.

(B) Staining for P2ry12^{+} and Clec7a^{+} in microglia associated with neuritic plaque (pNF) in 24-month-old APP-PS1 mice. Scale bar, 20 μm.

(C) Heatmap of significantly affected genes in Clec7a^{+} versus Clec7a^{int} versus Clec7a^{-} FCRLS^{+} microglia in APP-PS1 versus WT mice (n = 5; 24 month). Selected homeostatic (blue) and inflammatory (red) genes.

(D) Selected genes shown in (C). Dot plots: mRNA transcripts (mean ± SEM). *p < 0.05, **p < 0.01, ***p < 0.001, ****p < 0.0001 by one-way ANOVA followed by Tukey's multiple-comparison post-hoc test.

(E) Heatmap of significantly affected genes determined by RNaseq in Clec7a^{+} versus Clec7a^{-} FCRLS^{+} microglia in APP-PS1 versus WT mice (n = 5; 9 month).

(F) Selected genes shown in (E). Dot plots: FPKM (mean ± s.e.m). *p < 0.05, **p < 0.01, ***p < 0.001, ****p < 0.0001 by one-way ANOVA followed by Tukey's multiple-comparison post hoc test.

(G) Staining for P2RY12 with Aβ or pNF in diffuse versus neuritic plaques in human AD brain. Scale bar, 100 μm.

(H) Linear regression curve of P2RY12^{+} microglia with dystrophic axons in temporal cortex of individuals (n = 14) with AD, as defined by CERAD criteria and Braak stages, and in temporal cortex from age-matched controls (n = 10).

See also Figure S2 and Table S2.

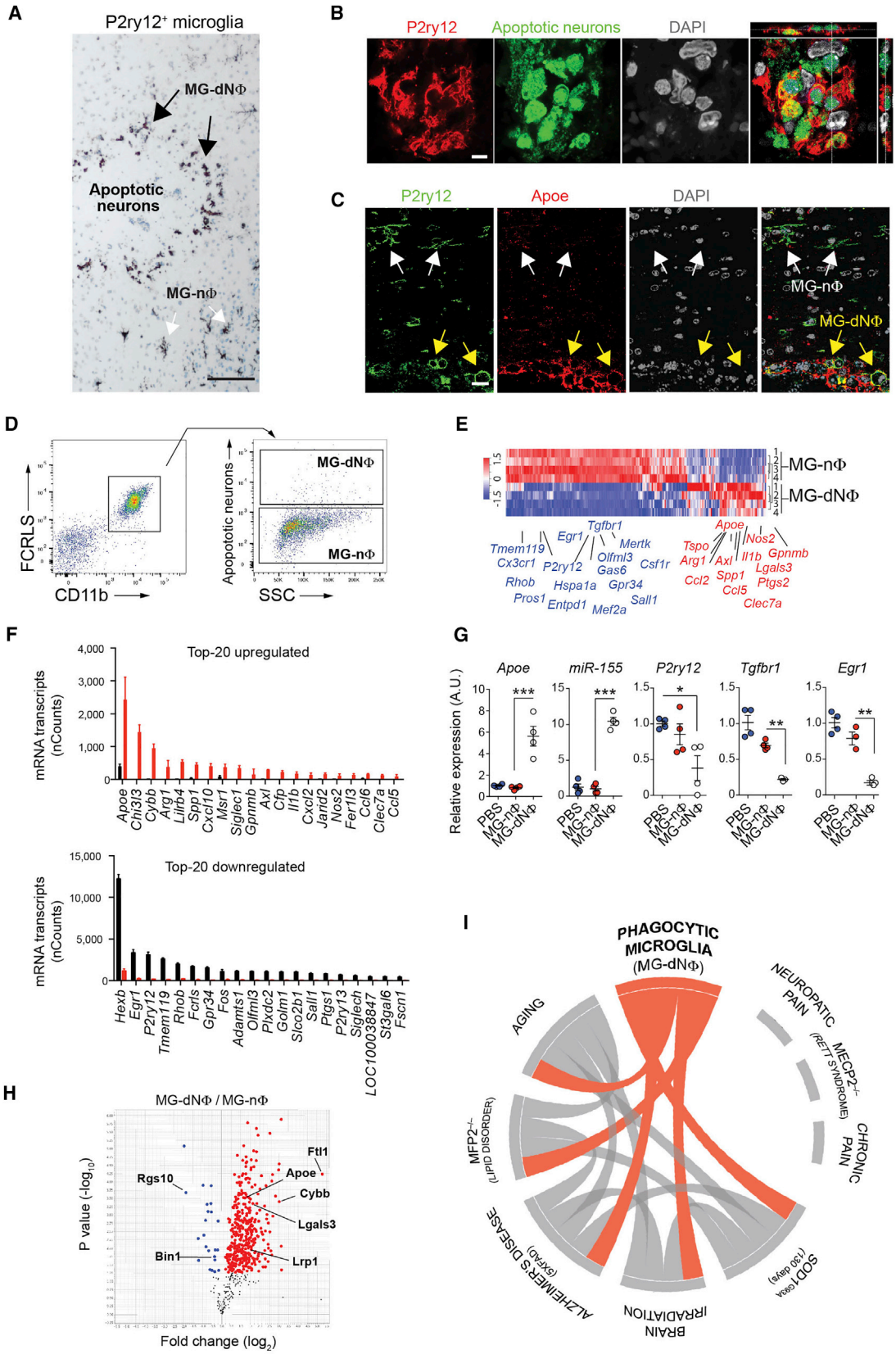

(legend on next page)

phagocytosis of neurons, we analyzed *Apoe*$^{-/-}$ versus WT transcriptomes from MG-nΦ versus MG-dNΦ microglia. We defined clusters on the basis of genes that were differentially expressed in WT non-phagocytic versus phagocytic versus *Apoe*$^{-/-}$ phagocytic microglia (Figure 4A and Table S5). Cluster 1 showed 885 genes that were induced in MG-dNΦ WT microglia but that were repressed in *Apoe*$^{-/-}$ MG-dNΦ microglia. 17 genes among those commonly upregulated in disease (Figure 1A) were suppressed by Apoe (Figure 4A and Table S5); such genes included *Clec7a*, *Gpnmb,* and *Lgals3* (Figure 4B) as well as *Bhlhe40* and others encoding transcription factors (TFs) commonly induced in disease (Figure 4C). Clusters 2 and 3 showed 1,220 genes that were suppressed in WT MG-dNΦ but that were restored in *Apoe*$^{-/-}$ MG-dNΦ microglia. Among 68 genes commonly suppressed in disease, 40 genes, including the major homeostatic genes *Tmem119*, *Tgfbr2*, and *Csf1r* (Figure 4D) and TFs such as *Mef2a*, *Mafb*, and *Sall1* (Figure 4E), were restored in *Apoe*$^{-/-}$ phagocytic microglia. NanoString confirmed de-repression of major homeostatic microglial genes (Figure S6A and Table S5). Disease-associated upregulated genes including *Lgals3* and *Clec7a* were suppressed in *Apoe*$^{-/-}$ microglia (Figure S6B). To assess the possibility of an intrinsic role of APOE regulation in a cell-specific manner, we deleted *Apoe* in microglia from *Cx3cr1*^{CreERT2}*:Apoe*$^{fl/fl}$ mice. qPCR analysis confirmed *Apoe* deletion in *Cx3cr1*^{CreERT2}*:Apoe*$^{fl/fl}$ microglia as compared to *Cx3cr1*^{WT}*:Apoe*$^{fl/fl}$ microglia. Moreover, gene expression of *Clec7a* was repressed, and expression of *Csf1r, Tgfbr1,* and *Tmem119* was restored in MG-dNΦ microglia from *Cx3cr1*^{CreERT2}*:Apoe*$^{fl/fl}$ mice (Figure 4F). Intrinsic deletion of *Apoe* did not affect expression of these genes in MG-nΦ microglia (Figure 4G), demonstrating that *Apoe* deletion had no effect on non-phagocytosing microglia.

A recent report showed induction of *Apoe* among other disease-associated genes in microglia 7 days after facial nerve axotomy (Tay et al., 2017). We assessed the role of Apoe on neuronal survival in WT, *Apoe*$^{-/-}$, *Cx3cr1*^{CreERT2}*:Apoe*$^{fl/fl}$, and control *Cx3cr1*^{WT}*:Apoe*$^{fl/fl}$ mice. Global and conditional deletion of *Apoe* in microglia reduced neuronal loss in *Cx3cr1*^{CreERT2}*:Apoe*$^{fl/fl}$ mice as compared to WT or *Cx3cr1*^{WT}*:Apoe*$^{fl/fl}$ mice in the axotomized facial motor nucleus (Figures 4H–4I and Figure S6C). These data demonstrated the essential role of microglial *Apoe* in the MGnD phenotype.

Genetic ablation of miR-155 reverses the abnormal microglial signature and ameliorates disease in SOD1 mice (Butovsky et al., 2015). In MG-dNΦ microglia from *Apoe*$^{-/-}$ mice, miR-155 expression was suppressed (Figure S6D). In contrast, expression of *Apoe* was unaffected in miR-155$^{-/-}$ MG-dNΦ microglia (Figure S6E). Thus, miR-155 expression was regulated downstream of the APOE pathway. IPA upstream-regulator analysis identified TGFβ1 as the most significantly de-repressed molecule in *Apoe*$^{-/-}$ phagocytic microglia (Figure S6F). The top upstream regulator in miR-155$^{-/-}$ phagocytic microglia was IL-6 (Figure S6F), suggesting that its role in regulation of MGnD microglia was different from that of other proteins involved in inflammatory signaling. The *Egr1* transcription factor was the most de-repressed gene in the TGFβ pathway in *Apoe*$^{-/-}$ phagocytic microglia (Figure S6F). We determined the Apoe-dependent transcriptional effect in microglia by injecting recombinant Apoe intra-hippocampally in *Apoe*$^{-/-}$ mice. MGnD disease-associated genes such as *Msr1*, *Lilrb4,* and *Tlr2* were induced, and homeostatic transcriptional factors including *Smad3*, *Mef2a*, *Mafb*, and *Egr1* were suppressed (Figures S6G and S6H and Table S5). Thus, APOE signaling has a twofold effect on microglia regulation in neurodegeneration: (1) suppression of the microglial homeostatic transcriptional factors, including *Mef2a*, *Mafb*, and *Smad3,* and (2) induction of an inflammatory program involving transcription factors *Bhlhe40*, *Tfec*, and *Atf3*, and a transcriptional and translational regulator, miR-155.

Genetic Targeting of *Trem2* Suppresses the APOE Pathway and Restores the Homeostatic Microglia in APP-PS1 and SOD1 Mice

TREM2 is a sensor of membrane-associated lipids, including phosphatidylserine (PS), which is focally exposed on apoptotic cells and processes or synapses of damaged neurons (Wang et al., 2015). We found that blocking phosphatidylserine on dNs with Annexin V (Koopman et al., 1994) reduced microglial phagocytosis by 88% (Figure S7A). Because dNs suppressed homeostatic microglia genes, we asked whether they activated the APOE pathway in a TREM2-dependent manner. We found that expression of homeostatic genes, including *P2ry12*, *Gpr34*, *Tmem119*, *Tgfbr1*, and *Csf1r* was restored to WT levels in *Trem2*$^{-/-}$ MG-dNΦ microglia (Figure 5A), whereas *Apoe* and

Figure 3. Phagocytosis of Apoptotic Neurons Suppresses Homeostatic Microglia

For a Figure360 author presentation of Figure 3, see http//dx.doi.org/10.1016/j.immuni.2017.08.008#mmc8.

(A) Staining for P2ry12^{+} microglia at the site of apoptotic-neuron injection 16 hr after injection in WT mice (n = 6). Phagocytic (MG-dNΦ) and non-phagocytic (MG-nΦ) microglia. Scale bar, 80 μm.

(B) Orthogonal projections of confocal z stacks show intracellular Alexa488^{+} dNs co-stained with DAPI in P2ry12^{+} microglia (n = 6). Scale bar, 5 μm. One of two individual experiments.

(C) Staining for Apoe in P2ry12^{+} MG-dNΦ. White arrows: Apoe^{-} MG-nΦ; yellow arrows: Apoe^{+} MG-dNΦ (n = 3). Scale bar, 15 μm.

(D) FACS-sorted CD11b^{+}FCRLS^{+} MG-dNΦ containing Alexa488^{+} dNs and MG-nΦ from the same injection site 16 hr later.

(E) Heatmap of affected genes in MG-dNΦ (n = 4) versus MG-nΦ (n = 4) 16 hr after injection with dNs. One of two individual experiments.

(F) Top 20 affected genes shown in (E). Bars: mRNA NanoString (nCounts) (mean ± s.e.m) detected in 100 μg total RNA. *p < 0.05 bytwo-tailed Student's t test.

(G) qPCR validation of selected genes. Gene expression level normalized against *Gapdh* via ΔCt (n = 3–4/group). Results: mean normalized expression ± SEM. *p < 0.05, **p < 0.01, ***p < 0.001 by one-way ANOVA followed by Tukey's multiple-comparison post-hoc test.

(H) Volcano plot of 552 TMT-mass spectrometry-identified proteins highlighting changes in MG-dNΦ versus MG-nΦ. p < 0.05 by two-tailed Student's t test.

(I) Circos plot: connectivity map derived from the pairwise comparison of transcriptome data from mouse AD models, ALS and *Mfp2*$^{-/-}$; aging and irradiation are shown in orange. Each line represents a pairwise dataset overlap, determined by GSEA analysis and filtered by p < 0.001.

See also Figures S3, S4, and S5 and Tables S3 and S4.

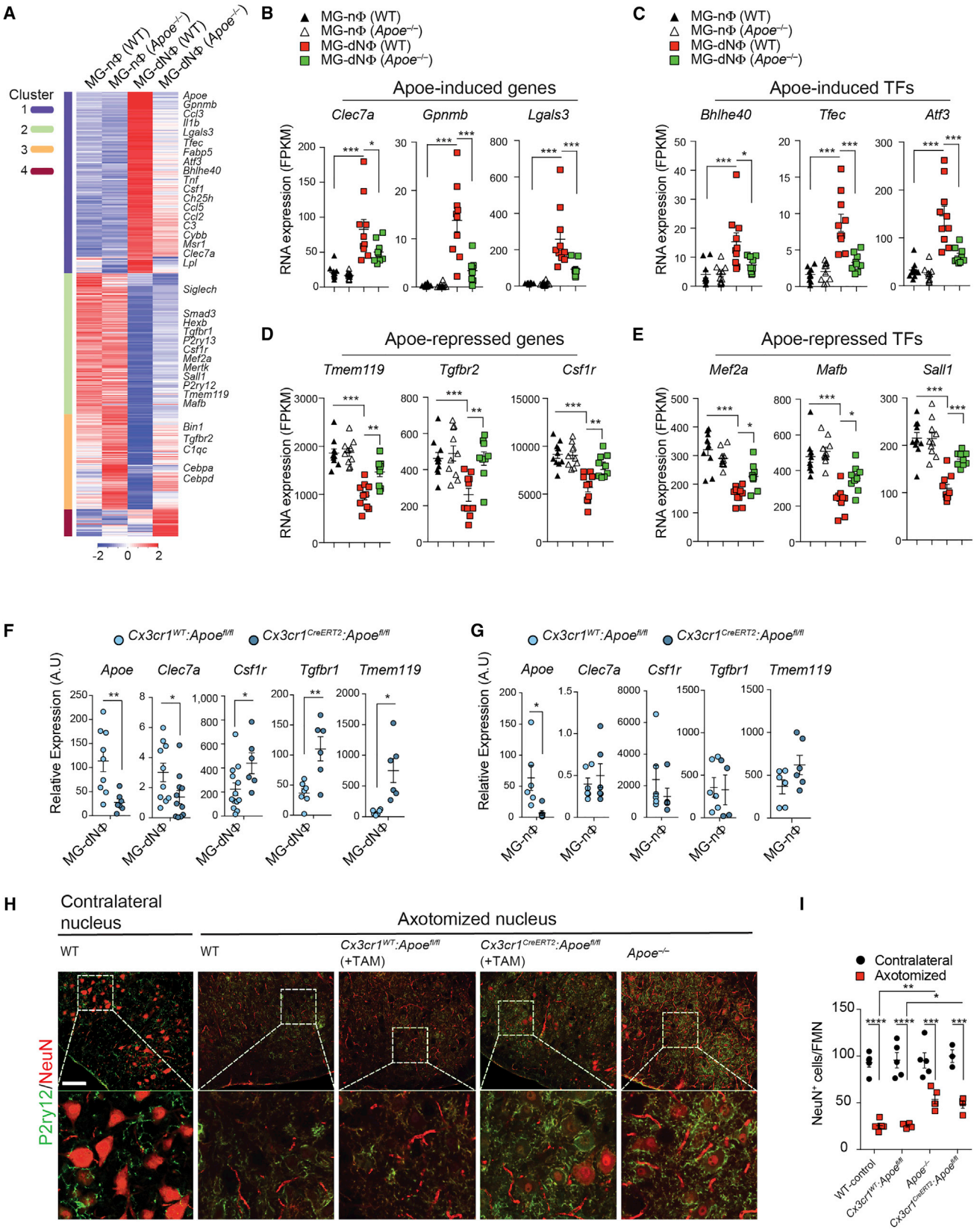

(legend on next page)

miR-155 were suppressed in *Trem2*$^{-/-}$ MG-dNΦ microglia (Figures 5B and Figure S7B). Targeting TREM2 signaling in the facial nerve axotomy (FNA) model also ameliorated neuronal loss in *Trem2*$^{-/-}$ mice (Figure 5C). To determine whether TREM2 induced the MGnD phenotype in disease, we genetically ablated *Trem2* in APP-PS1 and SOD1 mice. NanoString profiling of brain microglia from APP-PS1:*Trem2*$^{-/-}$ mice showed suppression of seven inflammatory molecules (*Trem2*, *Axl*, *Clec7a*, *Csf1*, *Itgax*, *Cd34*, and *Apoe*), which were among the most upregulated genes in the common disease-associated signature (Figure 5D). Among 108 restored genes in APP-PS1:*Trem2*$^{-/-}$ mice, 54 were commonly suppressed homeostatic microglial genes in disease; these included *P2ry12, Tmem119*, *Gpr34*, *Olfml3*, *Csf1r*, *Mertk*, *Rhob*, *Cx3Cr1*, *Tgfbr1*, and *Tgfb1* and transcriptional-factor-encoding genes such as *Mef2a*, *Mafb*, and *Sall1* (Figure 5D). Moreover, we confirmed the protein-level restoration of P2ry12 and suppression of Clec7a in microglia associated with Aβ plaques in APP-PS1:*Trem2*$^{-/-}$ mice as compared to APP-PS1 mice (Figures 5E–5G). Consistent with previous findings (Jay et al., 2015), the Aβ-plaque load was decreased in APP-PS1:*Trem2*$^{-/-}$ mice (Figure 5H). In SOD1:*Trem2*$^{-/-}$ microglia, among 36 downregulated inflammatory genes, 11 genes were common to the disease-associated signature. Among 240 restored genes in SOD1:*Trem2*$^{-/-}$ mice, 66 were commonly suppressed homeostatic genes (Figure 5I). Transcription factors such as those encoding *Mef2a*, *Mafb*, and *Sall1* and molecules involved in TGFβ signaling such as *Tgfb* and *Tgfbr1*, which were restored in *Trem2*$^{-/-}$ microglia in disease, were restored in *Apoe*$^{-/-}$ MG-dNΦ microglia. Clec7a^{+}P2ry12^{-} microglia were detected in spinal cords of SOD1:*Trem2*$^{+/-}$ but not SOD1:*Trem2*$^{-/-}$ mice at 115 days of age (Figure 5J). Clec7a^{-}P2ry12^{+} homeostatic microglia were preserved in SOD1:*Trem2*$^{-/-}$ mice (Figures 5J–5L). Expression of miR-155 was not induced in SOD1:*Trem2*$^{-/-}$ mice (Figure 5M). We had previously found early induction of Apoe in SOD1 males before clinical onset (Butovsky et al., 2015). To determine the TREM2 gender-dependent regulation of microglia in SOD1 mice, we performed unbiased RNaseq of the same samples shown in Figure 5I. We found 279 commonly affected genes (cluster 2) and 3,214 gender-specific genes (575 genes in females [cluster 1] and 2,639 genes in males [cluster 3]) (Figure 5N and Table S6). In commonly affected genes, SOD1:*Trem2*$^{+/-}$ males show induction of *Apoe* as compared to female littermates (Figures 5O and 5P), which is in line with our previous report (Butovsky et al., 2015). Genetic deletion of *Trem2* in males as compared to SOD1:*Trem2*$^{-/-}$ female littermates resulted in marked suppression of *Apoe* and restoration of master regulators of homeostatic microglia; such regulators included those encoded by *Spi1* (*PU.1*), *Smad3*, *Tgfbr1*, and *Sall1* (Figure 5P).

To validate TREM2 in regulating the microglial phenotypic switch in disease, we used GSEA to determine that transcripts from 5XFAD:*Trem2*$^{-/-}$ mice were enriched for the TREM2 responsive gene signature (Figures S7C–S7F and Table S6). Among the four disease models, TREM2-induced genes, including *Clec7a*, *Gpnmb*, *Fabp5*, *Lgals3*, *Csf1*, and *Ch25*, were also induced by Apoe (Table S5).

To investigate whether findings in APP-PS1:*Trem2*$^{-/-}$ mice were found in AD subjects carrying AD-associated *TREM2* variants (AD-TREM2), we compared heterozygous carriers of R47H (AD-TREM2^{R47H}) and R62H (AD-TREM2^{R62H}) to common-variant AD-patients (AD-TREM2^{WT}). In line with experimental data in mice (Wang et al., 2015), we found that microglia were more evenly distributed within the cortex in AD-TREM2 in both types of mutations and did not cluster around Aβ plaques as in AD-TREM2^{WT} (Figures 6A–6C). Moreover, TMEM119 intensity was significantly higher in both TREM2 mutation carriers (Figures 6D and 6E). Taken together, these results demonstrate that activation of APOE signaling by dNs is TREM2 mediates and regulates the microglial phenotypic switch in APP-PS1 and SOD1 mice.

Activation of the APOE Pathway Suppresses the Tolerogenic Function of Microglia

Genetic targeting of *Apoe* reduces neuroinflammation and disease in EAE (Shin et al., 2014). We tested the ability of microglia to inhibit T cell proliferation ex vivo because this has previously been reported as a tolerogenic function (Bai et al., 2009). CSFE-labeled T cells were stimulated in vitro with anti-CD3 and anti-CD28 mAbs (Figure 7A). M0 homeostatic microglia from the spinal cord of naive mice suppressed T cell proliferation. Stimulation of microglia with recombinant Apoe (rApoe) abrogated tolerogenic function of microglia. rApoe did not affect T cell proliferation in the absence of microglia (Figures 7A and 7B). Nonetheless, MGnD microglia from peak EAE was associated with the highest expression of *Apoe* (Figures 1B and 1C) and were unable to suppress T cell proliferation (Figures 7C and 7D). We then induced EAE in WT and *Apoe*$^{-/-}$ mice and

Figure 4. APOE Regulates Transcriptional and Post-transcriptional Program of MGnD Phenotype

(A) K-means clustering (k = 4) of 2,234 affected genes in bulk microglia (1,000 cells per animal) from WT and *Apoe*$^{-/-}$ mice. Vertical lane: mean of biological replicates of 1,000 MG-nΦ versus MG-dNΦ cells from WT (n = 10) versus *Apoe*$^{-/-}$ mice for MG-nΦ (n = 10) and MG-dNΦ (n = 9). Microglia isolated 16 hr after injection of dNs.

(B–E) Selected Apoe-induced genes (B), Apoe-induced Transcription Factors (TFs) (C), Apoe-repressed genes (D) and Apoe-repressed TFs (E) from WT and *Apoe*$^{-/-}$ mice 16 hr after injection of dNs. Means ± SEM are shown. *p < 0.05, **p < 0.01, ***p < 0.001 by one-way ANOVA followed by Tukey's multiple-comparison post-hoc test.

(F) qPCR validation of selected genes in MG-dNΦ from *Cx3cr1*^{CreERT2}:*Apoe*$^{fl/fl}$ versus *Cx3cr1*^{wt}:*Apoe*$^{fl/fl}$ controls. Expression levels normalized against *Gapdh* via ΔCt (n = 6-10/group). Mean normalized expression ± SEM is shown. *p < 0.05, **p < 0.01, by two-tailed Student's t test.

(G) qPCR validation of genes in MG-nΦ from *Cx3cr1*^{CreERT2}:*Apoe*$^{fl/fl}$ versus *Cx3cr1*^{wt}:*Apoe*$^{fl/fl}$ controls. Expression level normalized against *Gapdh* via ΔCt (n = 6-10/group). Mean normalized expression ± SEM is shown. *p < 0.05, **p < 0.01, by two-tailed Student's t test.

(H) Staining for NeuN^{+} and P2ry12^{+} in contralateral versus axotomized facial motor nucleus 7 days after surgery in WT (n = 5) versus *Apoe*$^{-/-}$ (n = 5) versus *Cx3cr1*^{CreERT2}:*Apoe*$^{fl/fl}$ (n = 4) versus *Cx3cr1*^{wt}:*Apoe*$^{fl/fl}$ (n = 4) control mice. Scale bar, 80 μm.

(I) Quantification of NeuN^{+} per facial motor nucleus in contralateral versus axotomized nucleus 7 days after surgery (n = 5). Means ± SEM are shown. *p < 0.05, **p < 0.01, ****p < 0.0001 by one-way ANOVA followed by Tukey's multiple-comparison post-hoc test.

See also Figure S6 and Table S5.

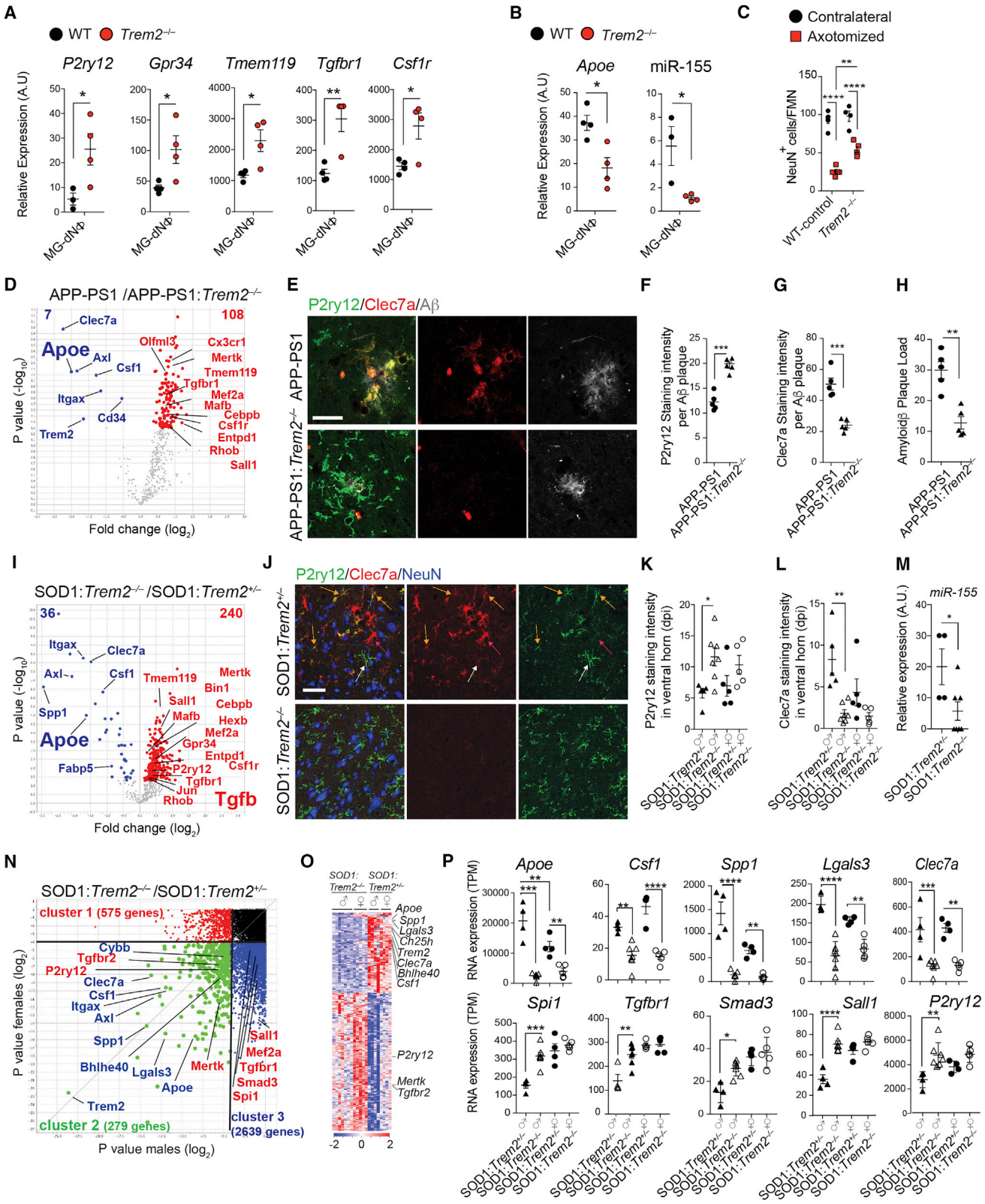

Figure 5. Genetic Targeting of *Trem2* Suppresses APOE Pathway and Restores the Homeostatic Microglia in APP-PS1 and SOD1 Mice

(A) qPCR analysis of homeostatic genes in MG-dNΦ from *Trem2*$^{-/-}$ versus WT mice (n = 4). Means ± SEM are shown. *p < 0.05, **p < 0.01 by one-way ANOVA.

(legend continued on next page)

found that, unlike WT-EAE microglia, *Apoe*$^{-/-}$ microglia from the spinal cord at disease peak suppressed T cell proliferation (Figures 7E and 7F), demonstrating the maintenance of the tolerogenic function. De novo stimulation of *Apoe*$^{-/-}$ microglia from EAE mice with rApoe inhibited their tolerogenic function (Figures 7G and 7H). Moreover, microglia isolated from SOD1 mice at disease peak, which show the highest expression of *Apoe* (Figure 1B), were also unable to suppress T cell proliferation (Figures 7I and 7J). In summary, we observed a loss of the tolerogenic function of microglia at peak EAE and in SOD1 mice. This loss was regulated by Apoe-dependent transcriptional effects in microglia.

DISCUSSION

We identified a molecular signature of disease-associated microglia (MGnD) and found that this signature is dependent on the TREM2-APOE pathway. The MGnD phenotype was seen in several neurodegenerative models and was induced by phagocytosis of apoptotic neurons. In a mouse model and in human AD, neuritic Aβ-plaque-associated microglia showed a MGnD phenotype consistent with reports of senescent microglia in aging and AD (Streit et al., 2009). These microglia lose sensome function including TGFβ signaling (Hickman et al., 2013). Apoptotic cells are efficiently phagocytosed during nervous system development (Jacobson et al., 1997). We reported that during early stages of development microglia induce *Apoe* expression, which is inversely correlated with the suppression of homeostatic genes (Butovsky et al., 2014). Thus, microglia during development and in neurodegenerative processes might share common modulatory mechanisms induced by apoptotic neurons. Neuronal apoptosis is a rare event in human AD (Stadelmann et al., 1999). However, focal apoptosis (synaptosis and necroptosis) associated with phosphatidylserine exposure commonly occurs on neuronal processes, dendrites, or synapses (Mattson et al., 1998; Ofengeim et al., 2015). We found that dNs triggered the TREM2-APOE pathway to induce MG-dNΦ and suppress the homeostatic signature, which is tightly regulated by the TGFβ pathway (Butovsky et al., 2014; Gosselin et al., 2014).

We report a role for APOE in regulating the MGnD microglial subset in a cell-autonomous manner. Senile plaques contain dystrophic neurites (Grutzendler et al., 2007), and microglia engulf amyloid fibers (Dickson et al., 1988). We suggest that MGnD microglia, amyloid plaques, and dystrophic neurites form a microenvironment highly enriched in APOE, which could play a major role in AD progression. APOE both accumulates in amyloid plaques and facilitates Aβ aggregation (Kim et al., 2012). Along with APOE induction, we found increased expression of APP in EAE microglia. Chiu et al. reported increased APOE and APP expression in SOD1 microglia (Chiu et al., 2013), and Huang et al. showed that APOE stimulates APP and increases amyloid-β load in AD (Huang et al., 2017). Similarly, we found that Aβ-plaque-associated microglia express a high level of APP in APP-PS1 mice. Our results are consistent with a report that increased APOE in CSF is associated with cognitive decline (Toledo et al., 2014). Thus, microglial APOE might play a detrimental role in AD.

Transcriptome profiling of disease-associated and homeostatic genes in microglia during aging and disease progression in SOD1, APP-PS1, and EAE identified APOE and TGFβ as the major upstream regulators of MGnD microglia. This phenotype was associated with neuritic plaques in APP-PS1 mice. Microglia acquire an MGnD phenotype after phagocytosis of dNs. Interestingly, the LPS- and IFN-γ-induced (previously named M1) phenotype overlaps to some extent the MGnD microglia phenotype. However, microglia activated with LPS and IFN-γ suppressed *Apoe* and induced *Egr1*, both of which are

(B) qPCR analysis of *Apoe* and miR-155 expression in MG-dNΦ from *Trem2*$^{-/-}$ versus WT mice (n = 3–4/group). Means ± SEM are shown. Data are normalized against *Gapdh* and U6 expression via ΔCt. *p < 0.05 by two-tailed Student;s t test.
(C) Quantification of NeuN^{+} per facial motor nucleus in contralateral versus axotomized nucleus in WT versus *Trem2*$^{-/-}$ (n = 4–5/group), 7 days after surgery. Means ± SEM are shown. *p < 0.05, **p < 0.01, ****p < 0.0001 by one-way ANOVA followed by Tukey's multiple-comparison post-hoc test.
(D) Volcano plot based on differentially expressed genes in microglia from APP-PS1 (n = 4) versus APP-PS1:*Trem2*$^{-/-}$ (n = 5) mice at 120 days. p < 0.05 by two-tailed Student's t test. Selected restored homeostatic (red) and suppressed inflammatory (blue) genes.
(E) Staining for P2ry12, Clec7a, and Aβ plaques in APP-PS1 versus APP-PS1:*Trem2*$^{-/-}$ mice (120 days). Scale bar, 20 μm.
(F and G) Quantification of P2ry12 and Clec7a intensity per Aβ plaque in APP-PS1 versus APP-PS1:*Trem2*$^{-/-}$ mice (n = 5; 120 days). ***p < 0.001, by two-tailed Student's t test.
(H) Quantification of Aβ-plaque load per animal in APP-PS1 versus APP-PS1:*Trem2*$^{-/-}$ mice (n = 5; 120 days). **p < 0.01, by two-tailed Student's t test.
(I) Volcano plot based on differentially expressed genes in microglia from SOD1:*Trem2*$^{+/-}$ (n = 9) versus SOD1:*Trem2*$^{-/-}$ (n = 13) mice at 115 days (neurological score: 1). p < 0.05 by two-tailed Student's t test.
(J) Staining for P2ry12, Clec7a, and NeuN in SOD1:*Trem2*$^{+/-}$ versus SOD1:*Trem2*$^{-/-}$ mice (lumbar section, 115 days). M0 homeostatic microglia (white arrows). M0 microglia transitioning to MGnD (yellow arrows). MGnD at the epicenter of the ventral horn (red arrows). Scale bar, 50 μm.
(K and L) Quantification of P2ry12 and Clec7a intensity in ventral horn of SOD1:*Trem2*$^{+/-}$ (n = 4, n = 5 females) versus SOD1:*Trem2*$^{-/-}$ (n = 7 males, 5 females) mice (lumbar section, 115 days). **p < 0.001, ***p < 0.001 by two-tailed Student's t test.
(M) qPCR analysis of miR-155 expression in microglia isolated from the ventral horn of SOD1:*Trem2*$^{+/-}$ (n = 4) versus SOD1:*Trem2*$^{-/-}$ (n = 5) mice (lumbar section, 115 days). Means ± SEM are shown. Data are normalized against U6 expression via ΔCt. *p < 0.05 by two-tailed Student's t test.
(N) Volcano plot: differentially expressed genes in spinal-cord microglia from male and female SOD1:*Trem2*$^{+-}$ (n = 4 males, 4 females) versus SOD1:*Trem2*$^{-/-}$ (n = 7 males, 5 females) mice at 115 days (neurological score: 1). p < 0.05 by two-tailed Student's t test. Cluster 1: female-specific differentially expressed genes. Cluster 2: differentially expressed genes in both genders. Cluster 3: male-specific differentially expressed genes.
(O) Heatmap of affected genes in male and female SOD1:*Trem2*$^{+/-}$ (n = 4 males, 4 females) versus SOD1:*Trem2*$^{-/-}$ mice (n = 7 males, 5 females) at 115 days (cluster 2). Vertical lanes: biological replicates per genotype and gender.
(P) Gender comparison of homeostatic (lower panel) and MGnD genes (upper panel) from SOD1:*Trem2*$^{+/-}$ and SOD1:*Trem2*$^{-/-}$ mice (n = 4–7/group). Data represent means ± SEM. *p < 0.05, **p < 0.01, ***p < 0.001, ****p < 0.0001 by one-way ANOVA followed by Tukey's multiple-comparison post-hoc test.
See also Table S6.

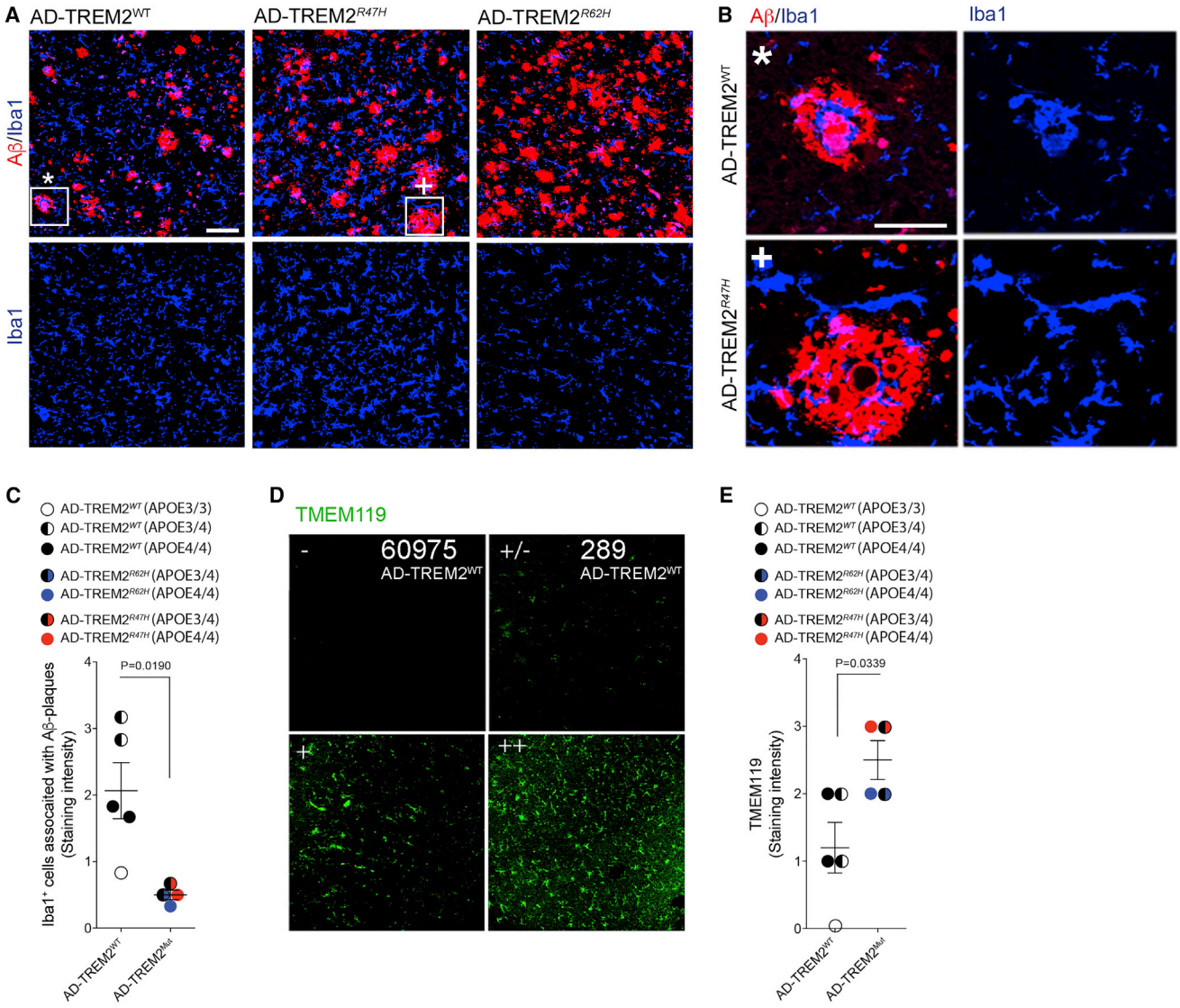

Figure 6. *TREM2* Haplodeficiency in Human AD Leads to Preservation of Microglia Morphology and TMEM119 Immunoreactivity

(A) Staining for Aβ (red) and IBA1 (blue) in AD control subjects (AD-TREM2^{WT}, n = 6) and TREM2 variant carriers (AD-TREM2^{R47H}, n = 2 and AD-TREM2^{R62H}, n = 2). Lower panels: single distribution of IBA1^{+} microglia in the same section areas. Scale bar, 100 μm.

(B) Higher magnification of the plaques indicated by * and + in (A). Scale bar, 50 μm.

(C) Quantification of IBA1^{+} microglia associated with Aβ plaques in AD-TREM2^{WT} and AD-TREM2^{Mut} cortical tissue. Two-tailed Student's t test.

(D) Cortical tissue from AD-TREM2^{WT} and AD-TREM2^{R62H} cases stained with TMEM119. Panels show basis for scoring microglia staining, described in (E). Scores: − no cells stained; +/− single cells stained; + moderate number of microglia with TMEM119 reactivity; and ++ most microglia are TMEM119 positive.

(E) Quantification of TMEM119 in AD-TREM2^{WT} and AD-TREM2^{Mut} cortical tissue. TMEM119 expression in microglia rated as in (D); the ratings are shown in numbers: − (0), +/− (1), + (2), ++ (3). Two-tailed Student's t test.

See also Table S7.

reciprocally induced and suppressed in MGnD and MG-dNΦ microglia. Macrophage-lineage-determining factor PU.1 (Heinz et al., 2010) cooperates with microglia-specific enhancer regions of the Mef2 family (Butovsky et al., 2014; Matcovitch-Natan et al., 2016). Mef2a might partner with PU.1 to establish a microglia-specific signature (Lavin et al., 2014). Motif analysis of PU.1 binding revealed enrichment for Smad3, Mef2, and Mafb consensus sequences, which cooperate with PU.1 to establish microglia-specific enhancer profiles, including TGFβ signaling (Butovsky et al., 2014; Gosselin et al., 2014; Matcovitch-Natan et al., 2016). We found that APOE signaling suppresses PU.1, MEF2a, SMAD3, and TGFβ signaling. Deletion of *Apoe* in phagocytic microglia showed cell-autonomous regulation of the phenotypic switch. miR-155 is a major pro-inflammatory miRNA in ALS and the SOD1 model (Butovsky et al., 2012). Targeting miR-155 restored homeostatic microglia and attenuated disease in SOD1 mice (Butovsky et al., 2015). Here, we show that APOE signaling induces miR-155 in MGnD microglia. Targeting

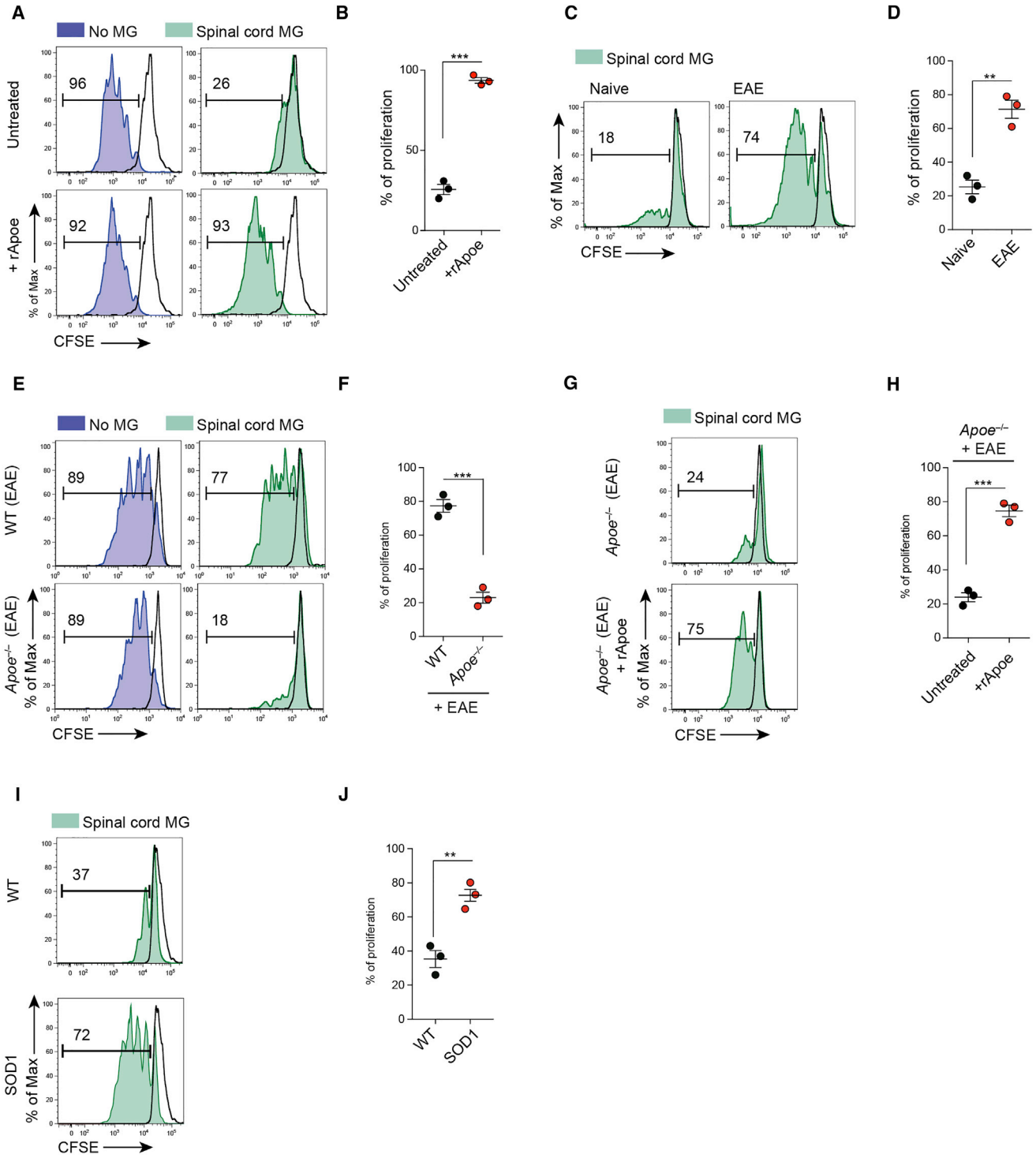

Figure 7. Activation of APOE Pathway Suppresses Tolerogenic Function in Microglia

(A) $CFSE^{+}$ $CD3^{+}$ T cells cultured with spinal cord microglia of WT-naive mice. Cultures treated with soluble rApoe (100 ng/ml) for 72 hr.

(B) T cell proliferation: means ± SEM are shown ***$p < 0.001$, two-tailed Student's t test ($n = 3$).

(C) $CFSE^{+}CD3^{+}$ T cells cultured for 72 hr with spinal-cord microglia from naive or EAE mice at disease peak.

(D) T cell proliferation: means ± SEM are shown **$p < 0.01$, two-tailed Student's t test ($n = 3$).

(E) $CFSE^{+}$ $CD3^{+}$ T cells cultured for 72 hr with spinal-cord microglia from EAE WT versus *Apoe*$^{-/-}$ mice at disease peak.

(F) T cell proliferation: means ± SEM are shown. ***$p < 0.001$, two-tailed Student's t test ($n = 3$).

(legend continued on next page)

TREM2-APOE signaling in phagocytic microglia and in SOD1 mice suppressed miR-155 expression. Studies have shown that miR-155 directly targets Mef2a (Seok et al., 2011) and PU.1 (Lu et al., 2014). Together, these data suggest that TREM2-APOE signaling via miR-155 regulates microglia enhancers, and this regulation governs the core microglia-specific molecular signature.

Although TREM2 polymorphisms are associated with a risk of late-onset AD (Guerreiro et al., 2013), their role in neurodegenerative diseases is controversial. Wang et al. showed that deletion of TREM2 in 5XFAD mice, another model of AD, reduced Aβ accumulation as a result of a dysfunctional response of microglia to cluster around Aβ plaques (Wang et al., 2015). However, Jay et al. showed that TREM2 deficiency resulted in reduced infiltration of inflammatory myeloid cells and thereby ameliorated AD pathology (Jay et al., 2015) at early stages and exacerbated it at later stages (Jay et al., 2017). Subsequently, Wang et al. showed that amyloid-associated myeloid cells are derived from brain-resident microglia rather than from recruited peripheral monocytes (Wang et al., 2016). We found that genetic targeting of *Trem2* in APP-PS1 mice at early stages restored homeostatic microglia associated with the reduction of Aβ plaques. In line with previous reports in mice and humans (Wang et al., 2015; Yuan et al., 2016), we found that microglia did not cluster around Aβ plaques in TREM2-haplodeficient AD subjects. However, TMEM119 homeostatic microglia were more preserved in AD-TREM2 variants than in common-variant AD subjects, a result similar to the findings in APP-PS1:*Trem2*$^{-/-}$ mice. Consistent with our report, increased *TREM2* expression is associated with the *CD33* AD risk allele (Chan et al., 2015), and recent data showed that soluble TREM2 in the CSF is increased in the early symptomatic phase of AD in association with neuronal injury markers (Suárez -Calvet et al., 2016). This might reflect a dysregulation of homeostatic microglia in response to neuronal injury.

Keren-Shaul et al. reported that APOE induction is TREM2-independent in 5XFAD mice (Keren-Shaul et al., 2017), although a previous study (Wang et al., 2016) found that *Apoe* expression in 5XFAD mice was moderately lower than in WT mice. We found that genetic targeting of *Trem2* suppresses the APOE pathway and restores homeostatic microglia in APP-PS1 and SOD1 mice. As a ligand for TREM2 in microglia, APOE binds to dNs and increases Trem2-mediated phagocytosis (Atagi et al., 2015). We found that APOE ligand suppresses major transcription factors of homeostatic microglia. Future studies will determine whether the effect is TREM2 dependent. We identified TREM2 gender-dependent regulation of microglia in SOD1 mice; such regulation was not addressed by Wang et al. or Keren-Shaul et al.

We propose that the consequence of activating the TREM2-APOE pathway is the loss of the ability of MGnD microglia to prevent neuronal loss and provide tolerogenic signals to T cells. In the context of MS, this would amplify the pro-inflammatory properties of T cells. MGnD microglia might also be protective and constitute an initial response to neuronal injury. As we showed recently, TREM2 deficiency might lock microglia in a homeostatic state (Mazaheri et al., 2017) and block essential defense functions of microglia during disease progression. In summary, we demonstrate that the TREM2-APOE pathway induces a microglia phenotypic switch from a homeostatic to neurodegenerative phenotype. The modulation of the microglial neurodegenerative phenotype through targeting of the TREM2-APOE pathway might serve as a way to restore homeostatic microglia and treat neurodegenerative disorders.

STAR★METHODS

Detailed methods are provided in the online version of this paper and include the following:

- KEY RESOURCES TABLE
- CONTACT FOR REAGENT AND RESOURCE SHARING
- EXPERIMENTAL MODEL AND SUBJECT DETAILS
  - Mice
  - Human Specimens
- METHOD DETAILS
  - Scoring of SOD1 Mice
  - Conditional Genetic Deletion of *Apoe* in Microglia
  - Generation of Chimeric Mice
  - Immunohistochemistry
  - Analysis of P2RY12 and Dystrophic Axons in AD Brains
  - Induction of EAE
  - Isolation of Primary Neurons
  - Induction of Apoptosis and Labeling of Neurons
  - Induction of Necrosis in Neurons
  - Stereotactic Injections
  - Intrahippocampal Injection of Kainic Acid
  - Facial Nerve Axotomy
  - Mouse Microglia Isolation and Sorting
  - Isolation of Spleenic CD11b^{+}Ly6C^{+} Monocytes
  - Mass Spectrometry Analysis
  - RNA Isolation and NanoString RNA Counting
  - Quantitative Real-Time PCR
  - Mouse MG550 Chip Design
  - NanoString Data Analysis
  - RNA Sequencing
  - In Vitro Suppression Assay
  - Heatmaps
  - Circos Plot
  - Ingenuity Pathway Analysis
- QUANTIFICATION AND STATISTICAL ANALYSIS
- DATA AND SOFTWARE AVAILABILITY

(G) CFSE^{+}CD3^{+} T cells cultured for 72 hr with spinal-cord microglia from EAE *Apoe*$^{-/-}$ mice at disease peak. Cultures treated with soluble rApoe (100 ng/) for 72 hr.

(H) T cell proliferation: means ± SEM are shown ***$p < 0.001$, two-tailed Student's t test ($n = 3$).

(I) CFSE^{+}CD3^{+} T cells cultured for 72 hr with spinal-cord microglia from WT versus SOD1 mice at disease peak (neurologic score: 4).

(J) T cell proliferation: means ± SEM are shown **$p < 0.01$, two-tailed Student's t test ($n = 3$). Black line: isotype control. Numbers on FACS plots: representative T cell proliferation (%).

Data are representative of three independent experiments (A–J).

SUPPLEMENTAL INFORMATION

Supplemental Information includes seven figures and seven tables and can be found with this article online at http://dx.doi.org/10.1016/j.immuni.2017.08.008.

AUTHOR CONTRIBUTIONS

O.B., S.K., C.M.: conceived study. S.K., C.M.: performed experiments, analyzed data, experimental design, writing. R.C.: NanoString analysis, LPS-injection. C.B.: isolated AD microglia for RNASeq, histology, imaging. N.C.: SOD1:*Trem2*$^{-/-}$ mice. L.B.: nerve axotomy, imaging, analysis. E.O., Z.F., D.J.G., G.T., K.H., Z.H., S.T.S.: performed experiments. REIF: neuronal culture. P.C.S., M.G., J.O.: T cell assays. D.H., J.U.: human AD-TREM2 variants. H.L., T.Z.: histology. C.L.: APP-PS1 experiments. A.W., J.H.: *Apoe*^{floxed} mice. F.H., F.M., C.H.: APP-PS1:*Trem2*$^{-/-}$ mice. T.I.: analysis. B.B.: mass spec. V.L., Y.X.: network analysis. Z.W., H.C.: circos plot. E.T., A.M., C.M.: RNaseq analyses, k-means clustering. H.L.W.: design, editing. O.B.: design, analysis, wrote manuscript with input from all authors.

ACKNOWLEDGMENTS

This work was supported by grants from the following organizations to the indicated authors. O.B.: NIH National Institute of Neurological Disorders and Stroke (1R01NS088137), NIH National Institute on Aging (NIH-NIA) (R01AG051812 and R01AG054672), National Multiple Sclerosis Society (5092A1), Amyotrophic Lateral Sclerosis Association (2087), Nancy Davis Foundation Faculty Award, Cure Alzheimer's Fund (2017APOE:Butovsky). H.L.W.: Department of Defense (AL120029), Thome Foundation (2011D002865), NIH-NIA (R01AG043975 and R01AG040092). C.H.: European Research Council (321366-Amyloid), Deutsche Forschungsgemeinschaft (DFG) (EXC 1010 SyNergy), Cure Alzheimer's Fund, MetLife Foundation Award. J.H.: DFG (SFB841). D.M.H.: P50AG05681, P01-AG0399. C.L.: NIH-NIA (R01AG040092). T.I.: NIH-NIA (RF1AG054199-01). M.G.: DFG (GRK1459, SFB877). H.L.: Austrian Science Foundation Project (P27744-B27). C.M.: National Multiple Sclerosis Society (postdoctoral fellowship). We thank Prize4Life, a nonprofit organization dedicated to the discovery of treatments and a cure for ALS; Marco Colonna for *Trem2*$^{-/-}$ mice; Microscopy Core Facility/Universitätsklinikum Hamburg-Eppendorf; Deneen Kozoriz for FACS sorting. C.H. is a Roche advisor and collaborator.

Received: March 2, 2017
Revised: July 6, 2017
Accepted: August 17, 2017
Published: September 19, 2017

REFERENCES

Atagi, Y., Liu, C.C., Painter, M.M., Chen, X.F., Verbeeck, C., Zheng, H., Li, X., Rademakers, R., Kang, S.S., Xu, H., et al. (2015). Apolipoprotein E Is a Ligand for Triggering Receptor Expressed on Myeloid Cells 2 (TREM2). J. Biol. Chem. *290*, 26043–26050.

Bai, B., Song, W., Ji, Y., Liu, X., Tian, L., Wang, C., Chen, D., Zhang, X., and Zhang, M. (2009). Microglia and microglia-like cell differentiated from DC inhibit CD4 T cell proliferation. PLoS ONE *4*, e7869.

Boillée, S., Yamanaka, K., Lobsiger, C.S., Copeland, N.G., Jenkins, N.A., Kassiotis, G., Kollias, G., and Cleveland, D.W. (2006). Onset and progression in inherited ALS determined by motor neurons and microglia. Science *312*, 1389–1392.

Butovsky, O., Siddiqui, S., Gabriely, G., Lanser, A.J., Dake, B., Murugaiyan, G., Doykan, C.E., Wu, P.M., Gali, R.R., Iyer, L.K., et al. (2012). Modulating inflammatory monocytes with a unique microRNA gene signature ameliorates murine ALS. J. Clin. Invest. *122*, 3063–3087.

Butovsky, O., Jedrychowski, M.P., Moore, C.S., Cialic, R., Lanser, A.J., Gabriely, G., Koeglsperger, T., Dake, B., Wu, P.M., Doykan, C.E., et al. (2014). Identification of a unique TGF-β-dependent molecular and functional signature in microglia. Nat. Neurosci. *17*, 131–143.

Butovsky, O., Jedrychowski, M.P., Cialic, R., Krasemann, S., Murugaiyan, G., Fanek, Z., Greco, D.J., Wu, P.M., Doykan, C.E., Kiner, O., et al. (2015). Targeting miR-155 restores abnormal microglia and attenuates disease in SOD1 mice. Ann. Neurol. *77*, 75–99.

Buttgereit, A., Lelios, I., Yu, X., Vrohlings, M., Krakoski, N.R., Gautier, E.L., Nishinakamura, R., Becher, B., and Greter, M. (2016). Sall1 is a transcriptional regulator defining microglia identity and function. Nat. Immunol. *17*, 1397–1406.

Chan, G., White, C.C., Winn, P.A., Cimpean, M., Replogle, J.M., Glick, L.R., Cuerdon, N.E., Ryan, K.J., Johnson, K.A., Schneider, J.A., et al. (2015). CD33 modulates TREM2: convergence of Alzheimer loci. Nat. Neurosci. *18*, 1556–1558.

Chiu, I.M., Morimoto, E.T., Goodarzi, H., Liao, J.T., O'Keeffe, S., Phatnani, H.P., Muratet, M., Carroll, M.C., Levy, S., Tavazoie, S., et al. (2013). A neurodegeneration-specific gene-expression signature of acutely isolated microglia from an amyotrophic lateral sclerosis mouse model. Cell Rep. *4*, 385–401.

Dickson, D.W., Farlo, J., Davies, P., Crystal, H., Fuld, P., and Yen, S.H. (1988). Alzheimer's disease. A double-labeling immunohistochemical study of senile plaques. Am. J. Pathol. *132*, 86–101.

Gautier, E.L., Shay, T., Miller, J., Greter, M., Jakubzick, C., Ivanov, S., Helft, J., Chow, A., Elpek, K.G., Gordonov, S., et al.; Immunological Genome Consortium (2012). Gene-expression profiles and transcriptional regulatory pathways that underlie the identity and diversity of mouse tissue macrophages. Nat. Immunol. *13*, 1118–1128.

Gosselin, D., Link, V.M., Romanoski, C.E., Fonseca, G.J., Eichenfield, D.Z., Spann, N.J., Stender, J.D., Chun, H.B., Garner, H., Geissmann, F., and Glass, C.K. (2014). Environment drives selection and function of enhancers controlling tissue-specific macrophage identities. Cell *159*, 1327–1340.

Grutzendler, J., Helmin, K., Tsai, J., and Gan, W.B. (2007). Various dendritic abnormalities are associated with fibrillar amyloid deposits in Alzheimer's disease. Ann. N Y Acad. Sci. *1097*, 30–39.

Guerreiro, R., Wojtas, A., Bras, J., Carrasquillo, M., Rogaeva, E., Majounie, E., Cruchaga, C., Sassi, C., Kauwe, J.S., Younkin, S., et al.; Alzheimer Genetic Analysis Group (2013). TREM2 variants in Alzheimer's disease. N. Engl. J. Med. *368*, 117–127.

Heinz, S., Benner, C., Spann, N., Bertolino, E., Lin, Y.C., Laslo, P., Cheng, J.X., Murre, C., Singh, H., and Glass, C.K. (2010). Simple combinations of lineage-determining transcription factors prime cis-regulatory elements required for macrophage and B cell identities. Mol. Cell *38*, 576–589.

Hickman, S.E., Kingery, N.D., Ohsumi, T.K., Borowsky, M.L., Wang, L.C., Means, T.K., and El Khoury, J. (2013). The microglial sensome revealed by direct RNA sequencing. Nat. Neurosci. *16*, 1896–1905.

Holtman, I.R., Raj, D.D., Miller, J.A., Schaafsma, W., Yin, Z., Brouwer, N., Wes, P.D., Möller, T., Orre, M., Kamphuis, W., et al. (2015). Induction of a common microglia gene expression signature by aging and neurodegenerative conditions: a co-expression meta-analysis. Acta Neuropathol. Commun. *3*, 31.

Huang, Y.A., Zhou, B., Wernig, M., and Sudhof, T.C. (2017). ApoE2, ApoE3, and ApoE4 Differentially Stimulate APP Transcription and Abeta Secretion. Cell *168*, 427–441, e421.

Jacobson, M.D., Weil, M., and Raff, M.C. (1997). Programmed cell death in animal development. Cell *88*, 347–354.

Jay, T.R., Miller, C.M., Cheng, P.J., Graham, L.C., Bemiller, S., Broihier, M.L., Xu, G., Margevicius, D., Karlo, J.C., Sousa, G.L., et al. (2015). TREM2 deficiency eliminates TREM2+ inflammatory macrophages and ameliorates pathology in Alzheimer's disease mouse models. J. Exp. Med. *212*, 287–295.

Jay, T.R., Hirsch, A.M., Broihier, M.L., Miller, C.M., Neilson, L.E., Ransohoff, R.M., Lamb, B.T., and Landreth, G.E. (2017). Disease Progression-Dependent Effects of TREM2 Deficiency in a Mouse Model of Alzheimer's Disease. J. Neurosci. *37*, 637–647.

Keren-Shaul, H., Spinrad, A., Weiner, A., Matcovitch-Natan, O., Dvir-Szternfeld, R., Ulland, T.K., David, E., Baruch, K., Lara-Astaiso, D., Toth, B., et al. (2017). A Unique Microglia Type Associated with Restricting Development of Alzheimer's Disease. Cell *169*, 1276–1290, e1217.

Kim, J., Eltorai, A.E., Jiang, H., Liao, F., Verghese, P.B., Kim, J., Stewart, F.R., Basak, J.M., and Holtzman, D.M. (2012). Anti-apoE immunotherapy inhibits amyloid accumulation in a transgenic mouse model of Aβ amyloidosis. J. Exp. Med. *209*, 2149–2156.

Koopman, G., Reutelingsperger, C.P., Kuijten, G.A., Keehnen, R.M., Pals, S.T., and van Oers, M.H. (1994). Annexin V for flow cytometric detection of phosphatidylserine expression on B cells undergoing apoptosis. Blood *84*, 1415–1420.

Kostic, V., Jackson-Lewis, V., de Bilbao, F., Dubois-Dauphin, M., and Przedborski, S. (1997). Bcl-2: prolonging life in a transgenic mouse model of familial amyotrophic lateral sclerosis. Science *277*, 559–562.

Kreutzberg, G.W. (1996). Microglia: a sensor for pathological events in the CNS. Trends Neurosci. *19*, 312–318.

Larner, A.J. (1995). The cortical neuritic dystrophy of Alzheimer's disease: nature, significance, and possible pathogenesis. Dementia *6*, 218–224.

Lavin, Y., Winter, D., Blecher-Gonen, R., David, E., Keren-Shaul, H., Merad, M., Jung, S., and Amit, I. (2014). Tissue-resident macrophage enhancer landscapes are shaped by the local microenvironment. Cell *159*, 1312–1326.

Lévesque, M., and Avoli, M. (2013). The kainic acid model of temporal lobe epilepsy. Neurosci. Biobehav. Rev. *37*, 2887–2899.

Lu, D., Nakagawa, R., Lazzaro, S., Staudacher, P., Abreu-Goodger, C., Henley, T., Boiani, S., Leyland, R., Galloway, A., Andrews, S., et al. (2014). The miR-155-PU.1 axis acts on Pax5 to enable efficient terminal B cell differentiation. J. Exp. Med. *211*, 2183–2198.

Martinez, F.O., and Gordon, S. (2014). The M1 and M2 paradigm of macrophage activation: time for reassessment. F1000Prime Rep. *6*, 13.

Masliah, E., Mallory, M., Alford, M., Tanaka, S., and Hansen, L.A. (1998). Caspase dependent DNA fragmentation might be associated with excitotoxicity in Alzheimer disease. J. Neuropathol. Exp. Neurol. *57*, 1041–1052.

Matcovitch-Natan, O., Winter, D.R., Giladi, A., Vargas Aguilar, S., Spinrad, A., Sarrazin, S., Ben-Yehuda, H., David, E., Zelada González, F., Perrin, P., et al. (2016). Microglia development follows a stepwise program to regulate brain homeostasis. Science *353*, aad8670.

Mattson, M.P. (2000). Apoptosis in neurodegenerative disorders. Nat. Rev. Mol. Cell Biol. *1*, 120–129.

Mattson, M.P., Keller, J.N., and Begley, J.G. (1998). Evidence for synaptic apoptosis. Exp. Neurol. *153*, 35–48.

Mazaheri, F., Snaidero, N., Kleinberger, G., Madore, C., Daria, A., Werner, G., Krasemann, S., Capell, A., Trümbach, D., Wurst, W., et al. (2017). TREM2 deficiency impairs chemotaxis and microglial responses to neuronal injury. EMBO Rep. *18*, 1186–1198.

Nimmerjahn, A., Kirchhoff, F., and Helmchen, F. (2005). Resting microglial cells are highly dynamic surveillants of brain parenchyma in vivo. Science *308*, 1314–1318.

Ofengeim, D., Ito, Y., Najafov, A., Zhang, Y., Shan, B., DeWitt, J.P., Ye, J., Zhang, X., Chang, A., Vakifahmetoglu-Norberg, H., et al. (2015). Activation of necroptosis in multiple sclerosis. Cell Rep. *10*, 1836–1849.

Orre, M., Kamphuis, W., Osborn, L.M., Melief, J., Kooijman, L., Huitinga, I., Klooster, J., Bossers, K., and Hol, E.M. (2014). Acute isolation and transcriptome characterization of cortical astrocytes and microglia from young and aged mice. Neurobiol. Aging *35*, 1–14.

Perry, V.H., and Holmes, C. (2014). Microglial priming in neurodegenerative disease. Nat. Rev. Neurol. *10*, 217–224.

Picelli, S., Björklund, A.K., Faridani, O.R., Sagasser, S., Winberg, G., and Sandberg, R. (2013). Smart-seq2 for sensitive full-length transcriptome profiling in single cells. Nat. Methods *10*, 1096–1098.

Radde, R., Bolmont, T., Kaeser, S.A., Coomaraswamy, J., Lindau, D., Stoltze, L., Calhoun, M.E., Jäggi, F., Wolburg, H., Gengler, S., et al. (2006). Abeta42-driven cerebral amyloidosis in transgenic mice reveals early and robust pathology. EMBO Rep. *7*, 940–946.

Satoh, J., Kino, Y., Asahina, N., Takitani, M., Miyoshi, J., Ishida, T., and Saito, Y. (2016). TMEM119 marks a subset of microglia in the human brain. Neuropathology *36*, 39–49.

Seok, H.Y., Tatsuguchi, M., Callis, T.E., He, A., Pu, W.T., and Wang, D.Z. (2011). miR-155 inhibits expression of the MEF2A protein to repress skeletal muscle differentiation. J. Biol. Chem. *286*, 35339–35346.

Shin, S., Walz, K.A., Archambault, A.S., Sim, J., Bollman, B.P., Koenigsknecht-Talboo, J., Cross, A.H., Holtzman, D.M., and Wu, G.F. (2014). Apolipoprotein E mediation of neuro-inflammation in a murine model of multiple sclerosis. J. Neuroimmunol. *271*, 8–17.

Stadelmann, C., Deckwerth, T.L., Srinivasan, A., Bancher, C., Brück, W., Jellinger, K., and Lassmann, H. (1999). Activation of caspase-3 in single neurons and autophagic granules of granulovacuolar degeneration in Alzheimer's disease. Evidence for apoptotic cell death. Am. J. Pathol. *155*, 1459–1466.

Sternberger, N.H., Sternberger, L.A., and Ulrich, J. (1985). Aberrant neurofilament phosphorylation in Alzheimer disease. Proc. Natl. Acad. Sci. USA *82*, 4274–4276.

Streit, W.J., Braak, H., Xue, Q.S., and Bechmann, I. (2009). Dystrophic (senescent) rather than activated microglial cells are associated with tau pathology and likely precede neurodegeneration in Alzheimer's disease. Acta Neuropathol. *118*, 475–485.

Suárez-Calvet, M., Araque Caballero, M.A., Kleinberger, G., Bateman, R.J., Fagan, A.M., Morris, J.C., Levin, J., Danek, A., Ewers, M., and Haass, C.; Dominantly Inherited Alzheimer Network (2016). Early changes in CSF sTREM2 in dominantly inherited Alzheimer's disease occur after amyloid deposition and neuronal injury. Sci. Transl. Med. *8*, 369ra178.

Tay, T.L., Mai, D., Dautzenberg, J., Fernández-Klett, F., Lin, G., Sagar, Datta, M., Drougard, A., Stempfl, T., Ardura-Fabregat, A., et al. (2017). A new fate mapping system reveals context-dependent random or clonal expansion of microglia. Nat. Neurosci. *20*, 793–803.

Toledo, J.B., Da, X., Weiner, M.W., Wolk, D.A., Xie, S.X., Arnold, S.E., Davatzikos, C., Shaw, L.M., and Trojanowski, J.Q.; Alzheimer's Disease Neuroimaging Initiative (2014). CSF Apo-E levels associate with cognitive decline and MRI changes. Acta Neuropathol. *127*, 621–632.

Trapnell, C., Roberts, A., Goff, L., Pertea, G., Kim, D., Kelley, D.R., Pimentel, H., Salzberg, S.L., Rinn, J.L., and Pachter, L. (2012). Differential gene and transcript expression analysis of RNA-seq experiments with TopHat and Cufflinks. Nat. Protoc. *7*, 562–578.

Turnbull, I.R., Gilfillan, S., Cella, M., Aoshi, T., Miller, M., Piccio, L., Hernandez, M., and Colonna, M. (2006). Cutting edge: TREM-2 attenuates macrophage activation. J. Immunol. *177*, 3520–3524.

Verheijden, S., Bottelbergs, A., Krysko, O., Krysko, D.V., Beckers, L., De Munter, S., Van Veldhoven, P.P., Wyns, S., Kulik, W., Nave, K.A., et al. (2013). Peroxisomal multifunctional protein-2 deficiency causes neuroinflammation and degeneration of Purkinje cells independent of very long chain fatty acid accumulation. Neurobiol. Dis. *58*, 258–269.

Wagner, T., Bartelt, A., Schlein, C., and Heeren, J. (2015). Genetic Dissection of Tissue-Specific Apolipoprotein E Function for Hypercholesterolemia and Diet-Induced Obesity. PLoS ONE *10*, e0145102.

Wang, Y., Cella, M., Mallinson, K., Ulrich, J.D., Young, K.L., Robinette, M.L., Gilfillan, S., Krishnan, G.M., Sudhakar, S., Zinselmeyer, B.H., et al. (2015). TREM2 lipid sensing sustains the microglial response in an Alzheimer's disease model. Cell *160*, 1061–1071.

Wang, Y., Ulland, T.K., Ulrich, J.D., Song, W., Tzaferis, J.A., Hole, J.T., Yuan, P., Mahan, T.E., Shi, Y., Gilfillan, S., et al. (2016). TREM2-mediated early microglial response limits diffusion and toxicity of amyloid plaques. J. Exp. Med. *213*, 667–675.

Xu, Q., Bernardo, A., Walker, D., Kanegawa, T., Mahley, R.W., and Huang, Y. (2006). Profile and regulation of apolipoprotein E (ApoE) expression in the CNS in mice with targeting of green fluorescent protein gene to the ApoE locus. J. Neurosci. *26*, 4985–4994.

Yuan, P., Condello, C., Keene, C.D., Wang, Y., Bird, T.D., Paul, S.M., Luo, W., Colonna, M., Baddeley, D., and Grutzendler, J. (2016). TREM2 Haplodeficiency in Mice and Humans Impairs the Microglia Barrier Function Leading to Decreased Amyloid Compaction and Severe Axonal Dystrophy. Neuron *92*, 252–264.

STAR★METHODS

KEY RESOURCES TABLE

REAGENT or RESOURCE	SOURCE	IDENTIFIER
Antibodies		
Mouse monoclonal anti-NeuN (clone A60)	Millipore	Cat#MAB377
Rabbit polyclonal anti-Iba1	WAKO Chemicals	Cat#019-19741
Rabbit polyclonal anti-P2RY12	Butovsky et al., 2014	N/A
Rat-monoclonal microglia-specific 4D4	Butovsky et al., 2012	N/A
Rat monoclonal anti-P2RY12	This paper	N/A
Goat polyclonal anti-APOE	Millipore	Cat# AB947
Mouse monoclonal anti-phosphorylated neurofilament (clone SMI31)	BioLegend	Cat#801601
Rabbit polyclonal anti-human TMEM119	Sigma	Cat# HPA051870
Rabbit monoclonal [28-3] anti-mouse TMEM119	Abcam	Cat#ab209064
Rat monoclonal anti-Clec7a (clone R1-8g7)	Invivogene	Cat#mabg-mdect
Ly6C-FITC	BD Biosciences	Cat#553104
Rat-monoclonal anti-FCRLS (clone 4G11)	Butovsky et al., 2014	N/A
Mouse monoclonal anti-Amyloidβ (clone 6E10)	Covance	Cat#SIG-39320
Mouse monoclonal anti-Amyloidβ (clone BAM-10)	Zytomed	Cat#Mob 410-05
Mouse monoclonal anti-Amyloidβ (Clone W02)	Millipore	Cat#MABN10
Rat monoclonal anti-CD11b-PeCy7 (clone M1/70)	BD Biosciences	Cat#552850
Armenian Hamster monoclonal anti-CD3 (clone 145-2C11)	BioLegend	Cat#100302
Super Clonal anti-goat Alexa Fluor555	Thermo Fisher Scientific	Cat#A27017
Biological Samples		
Human cortical specimens	Massachusetts General Hospital	Massachusetts Alzheimer Disease Research Center (MADRC; NIA P50 AG005134)
Human Brain Autopsies (AD and Controls)	Center for Brain Research, Medical University of Vienna	Archival Collection; EK #: 535/2004/2017
Human Brain specimens (AD controls and AD Trem2-polymorphisms)	Washington University	Knight Alzheimer's Disease Research Center (NIA P50 AG0568)
Chemicals, Peptides, and Recombinant Proteins		
Annexin V	Biolegend	Cat#640901
7-AAD	Biolegend	Cat#420403
Tamoxifen	Sigma-Aldrich	Cat#T5648
TritonX-100	Roche	Cat#11332481001
Pierce Protein-Free T20 blocking buffer	Thermo Fisher Scientific	Cat#37571
DAPI-Fluoromount-G	Southern Biotech	Cat#0100-20
Fluoromount-G	Southern Biotech	Cat#0100-01
Antibody diluent	DAKO	Cat#S2022
Avidin peroxidase	Jackson	Cat#016-030-084
Tyramine	Sigma	Cat#T-7255
Gallate Geltol: Glycerol Moviol Gallate	Invitrogen Calbiochem Sigma	Cat#15514-011 Cat#475904 Cat#P-3130
Pertussis toxin	List Biological Laboratories	Cat#180
CFA Complete Freund Adjuvant	Difco	Cat#231131
myelin oligodendrocyte glycoprotein (MOG)35–55 peptide	Genemed Synthesis	Cat# MOG3555-P-5

(*Continued on next page*)

Continued

REAGENT or RESOURCE	SOURCE	IDENTIFIER
5(6)-Carboxyfluorescein N-hydroxysuccinimidyl ester	Thermo Fisher Scientific	Cat#C34554
LPS Lipopolysaccharide from Escherichia coli 0127:B8	Thermo Fisher Scientific	Cat#L3129
Mouse recombinant APOE (host: yeast)	My Biosource	Cat#MBS955382
pHrodo® Green Zymosan Bioparticles® Conjugate for Phagocytosis	Life Technologies	Cat#P35365
pHrodo® Green E. coli BioParticles® Conjugate for Phagocytosis	Life Technologies	Cat#P35366
Kainic Acid	Sigma-Aldrich	K0250-10MG
Fluoro-Jade C	Histo-chem	#1FJC
Alexa Fluor488 5-SDP Ester	Thermo Fisher Scientific (Molecular Probes)	Cat#A30052
Alexa Flour405 5-NHS Ester	Thermo Fisher Scientific (Molecular Probes)	Cat#A30000
Anhydrous DMSO	Thermo Fisher Scientific	Cat#D12345
Critical Commercial Assays		
mirVanaTM miRNA isolation kit	Ambion	Cat#AM1561
high-capacity cDNA Reverse Transcription Kit	Applied Biosystems	Cat#4368814
anti-CD11b magnetic beads	Miltenyi Biotec	Cat#130-049-601
T cell-activator CD3/CD28 magnetic beads	Thermo Fisher Scientific	Cat#11456D
Fc Receptor blocking anti-CD16/32 antibodies	BD Biosciences	Cat#553141
Deposited Data		
Gene expression data	GSE101689	N/A
Protein data	PeptideAtlas: PASS01081	N/A
Experimental Models: Organisms/Strains		
Mouse: C57Bl/6J	The Jackson Laboratory	JAX: 00664
Mouse: *Apoe*$^{-/-}$	The Jackson Laboratory	JAX: 002052
Mouse: *miR-155*$^{-/-}$	The Jackson Laboratory	JAX: 007745
Mouse: *Apoe*$^{fl/fl}$	Wagner et al., 2015	N/A
Mouse: APP-PS1	Radde et al., 2006	N/A
Mouse: *Trem2*$^{-/-}$	Turnbull et al., 2006	N/A
Mouse: Cx3cr1^{CreERT2}	The Jackson Laboratory	JAX: 021160
Mouse: SOD1^{G93A}	The Jackson Laboratory	JAX: 004435
Oligonucleotides		
Apoe (Mm01307193_g1)	Thermo Fisher Scientific	Cat#4331182
Clec7a (Mm01307193_g1)	Thermo Fisher Scientific	Cat#4331182
Csf1r (Mm01266652_m1)	Thermo Fisher Scientific	Cat#4331182
Egr1 (Mm00656724_m1)	Thermo Fisher Scientific	Cat#4331182
Gapdh (Mm99999915_g1)	Thermo Fisher Scientific	Cat#4331182
Gpr34 (Mm02620221_s1)	Thermo Fisher Scientific	Cat#4331182
P2ry12 (Mm01950543_s1)	Thermo Fisher Scientific	Cat#4331182
Tgfb1 (Mm01178820_m1)	Thermo Fisher Scientific	Cat#4331182
Tgfbr1 (Mm00436964_m1)	Thermo Fisher Scientific	Cat#4331182
Tmem119 (Mm00525305_m1)	Thermo Fisher Scientific	Cat#4331182
miR-155 (RT002571)	Thermo Fisher Scientific	Cat#4427975
U6 (RT001973)	Thermo Fisher Scientific	Cat#4427975
Software and Algorithms		
Leica application suite software (LAS-AF-lite)	Leica	http://www.leica-microsystems.com
Ingenuity software	Ingenuity Systems	http://www.ingenuity.com
Multiplot studio 1.5.20	GParc	http://gparc.org/

(*Continued on next page*)

Continued		
REAGENT or RESOURCE	SOURCE	IDENTIFIER
GraphPad Prism 7	GraphPad Software	http://www.graphpad.com
FlowJo (version 10.0.8R1)	FlowJo	http://www.flowjo.com
Proteome Discoverer 2.1.0.81 software	Thermo Fisher Scientific	https://portal.thermo-brims.com/
Sequest HT algorithm	Thermo Fisher Scientific	https://portal.thermo-brims.com/
GSEA algorithm	N/A	http://software.broadinstitute.org/gsea/index.jsp
oPOSSUM	oPOSSUM	http://opossum.cisreg.ca/oPOSSUM3/
Circos package 0.68.12	N/A	http://circos.ca/software/download/circos/
R software (version 3.4.0)	N/A	https://cran.r-project.org/
MeV software (version 10.2)	N/A	http://mev.tm4.org
Other		
NanoString nCounter MG400 chip	Butovsky et al., 2014	http://www.nanostring.com/
NanoString nCounter MG468 chip	Butovsky et al., 2015	http://www.nanostring.com/
NanoString nCounter MG550 chip	This paper	http://www.nanostring.com/
LTQ Orbitrap Velos	Thermo Fisher Scientific	http://planetorbitrap.com/
C18 Reprosil resin (5 μm, 100 Å)	Dr. Maisch GmbH	http://www.dr-maisch.com/xedin.php
C18 Reprosil resin (1.8 μm, 200 Å)	Dr. Maisch GmbH	http://www.dr-maisch.com/xedin.php

CONTACT FOR REAGENT AND RESOURCE SHARING

Further information and requests for resources and reagents should be directed to and will be fulfilled by the Lead Contact, Oleg Butovsky (obutovsky@rics.bwh.harvard.edu).

EXPERIMENTAL MODEL AND SUBJECT DETAILS

Mice

C57BL/6J, B6.Cg-Tg(SOD1*G93A)1Gur/J (SOD1^{G39A}), B6.129P2-*Apoe*^{tm1Unc}/J (*Apoe*$^{-/-}$), B6.Cg-Mir155tm1.1Rsky/J (miR-155$^{-/-}$), and *B6.129P2(Cg)-Cx3cr1tm2.1(cre/ERT)Litt/WganJ (Cx3cr1*^{CreERT2}) mice were purchased from Jaxmice. *Trem2*$^{-/-}$ mice (Turnbull et al., 2006) were generously provided by Dr. Marco Colonna (Washington Univ.). APP-PS1 mice were kindly provided by Dr. Mathias Jucker (University of Tübingen). These mice develop amyloid plaque deposition approximately at six weeks of age in the neocortex. Deposits appear in the hippocampus at about three to four months, and in the striatum, thalamus, and brainstem at four to five months (Radde et al., 2006). These mice were analyzed at 9 and 24 months, respectively. APP-PS1:*Trem2*$^{-/-}$, were generated by crossing APP-PS1 mice with *Trem2*$^{-/-}$ mice. These mice were analyzed at 4 months of age. Generation of *Apoe*$^{fl/fl}$ mice has been described recently (Wagner et al., 2015) and these mice were used for microglia specific deletion of *Apoe*. If not otherwise stated, mice were female and 6-8 weeks of age at the beginning of the experiments. Mice were housed under specific pathogen free conditions. Mice from different genotypes were cohoused. Mice did not undergo any procedures prior to their stated use. All mice were housed with food and water ad libitum. Mice were euthanized by CO_2 inhalation. The Institutional Animal Care and Use Committee at Harvard Medical School approved all experimental procedures involving animals.

Human Specimens

Cortex samples from AD patients and respective controls from Center for Brain Research, Medical University of Vienna were examined and chosen with identical settings and were investigated to determine the degree of P2ry12 abundance associated with either diffuse or neuritic plaques. Brain tissues from AD patients with and without mutations in TREM2 were sampled and characterized at the University of Washington by David Holtzman and his team (St. Louis). Beside age, gender and disease severity (Braak stage, estimated CDR), the APOE genotype was determined for each patient. The cases examined in this study are summarized in Table S7. Tissues were embedded in paraffin and paraffin sections were cut at a thickness of 8μm. After deparaffination, tissue sections were stained as described in the immunohistochemistry section. All stains and subsequent analyses were performed blinded to the investigator. Use of post-mortem human brain tissue was approved by the Knight Alzheimer's Disease Research Center Biospecimens Committee. The approved use of post-mortem human brain tissue obtained through the Knight ADRC was exempt from the university human studies committee review (exemption numbers 89-055, 89-056). Written informed consent was obtained from participants in studies at the Knight Alzheimer's Disease Research center (P50 AG05681) and their collateral sources.

METHOD DETAILS

Scoring of SOD1 Mice

SOD1^{G39A} mice were assessed clinically by monitoring body weight (3 times/week) and neurological score (daily) starting at day 60. Disease progression was documented according to established methodology provided by Prize4Life and The Jackson Laboratory. Symptomatic analysis was conducted by monitoring neurological score and weight starting at day 60, and symptomatic onset was defined as the age at which animals began to decline in weight (Boillée et al., 2006). The neurological score used a scale of 0 to 4 developed by ALSTDI. Criteria used to assign each score level were: 0 = Full extension of hind legs away from the lateral midline when the mouse is suspended by its tail, and mouse can hold this position for 2 s, suspended 2–3 times; 1 = Collapse or partial collapse of leg extension toward lateral midline (weakness) or trembling of hind legs during tail suspension; 2 = Curling of the toes and dragging of at least one limb during walking; 3 = Rigid paralysis or minimal joint movement, foot not being used for forward motion; 4 = Mouse cannot right itself within 30 s from either side. A score of 4 also corresponded with the humane endpoint of the study.

Conditional Genetic Deletion of *Apoe* in Microglia

To induce Cre-recombinase expression, a dose of tamoxifen (75 mg/kg of body weight) in corn oil (Sigma) was injected i.p. for 5 consecutive days. For genetic depletion of APOE in microglia cells, *Apoe*$^{fl/fl}$ were crossed with tamoxifen-inducible *Cx3cr1*^{CreERT2} transgenic mice. Recombination was induced in *Cx3cr1*^{CreERT2}*:Apoe*$^{fl/fl}$ adult mice and *Cx3cr1*^{wt}*:Apoe*$^{fl/fl}$ littermates were used as controls.

Generation of Chimeric Mice

Cx3cr1:GFP$^{+/-}$ chimera mice were generated as previously described (Butovsky et al., 2014). In brief, 30-day-old C57BL/6J recipient mice protected by lead head shielding were lethally irradiated (950 Rad) and transplanted with bone marrow (BM) from *Cx3cr1*:GFP$^{+/-}$ donor mice. 8 weeks post-BM transplantation, EAE was induced in these chimera mice as described below.

Immunohistochemistry

Following immersion fixation in 4% PFA, brains were dehydrated and embedded in paraffin. H&E staining was performed according to standard procedures. For immunohistochemical staining, frontal sections (2-5 μm) were collected on superfrost slides, deparaffinized in xylol and rehydrated. After heat induced antigen retrieval, the following primary antibodies were used for detection: Neurons, anti-NeuN (clone A60, Millipore, 2 μg ml^{-1}), microglia/macrophages/monocytes, anti-Iba1 (polyclonal, #019-19741; WAKO Chemicals, 1 μg ml^{-1}), resident microglia, anti-P2ry12 [polyclonal, 0.4 μg ml^{-1}, validated in ref. (Butovsky et al., 2015; Butovsky et al., 2014)], anti-P2ry12 (monoclonal, 0.4 μg ml^{-1}, validated in this study), microglia specific 4D4 (monoclonal, validated in ref. (Butovsky et al., 2012), anti-Apoe (polyclonal, AB947; Millipore, 5 μg ml^{-1}) phosphorylated neurofilament (pNF; (clone SMI31 Biolegend; 1:2,000), and anti-human TMEM119 antibody (Sigma, HPA051870; 1:300). Detection was performed with the respective secondary antibodies and diaminobenzidine.

For immunofluorescence staining, antigen retrieval was performed for 30 min at 96°C in 10 mM citrate buffer pH 6.0. Subsequently, sections were permeabilized with 0.2% Triton X-100 (Roche) in TBS for 5 min. Tissues were blocked in Pierce Protein-Free T20 blocking buffer (Thermo Scientific) and treated with 1% Sudan Black to reduce autofluorescence. Sections were incubated with the first antibody at 4°C overnight, washed with TBS Tween (TBS-T) and incubated with secondary donkey anti-rabbit Alexa555 antibody (Life Technologies, 6 μg ml^{-1}) or chicken anti-rabbit Alexa488, anti-mouse Alexa647 (Life Technologies, 6 μg ml^{-1}) during 90 min. Apoe was stained with goat anti-Apoe (polyclonal, Millipore, 5 μg ml^{-1}) and detected with the superclonal rabbit anti-goat Alexa555 (Thermo Scientific, 1 μg ml^{-1}). Sections were washed again and slides were mounted with DAPI-Fluoromount-G (SouthernBiotech, Birmingham, USA). Staining and analyses of tissues from APP-PS1:*Trem2*$^{-/-}$, APP-PS1, *WT, Cx3cr1*^{wt}*:Apoe*$^{fl/fl}$*, Apoe*$^{-/-}$*, Trem2*$^{-/-}$*, and Cx3cr1*^{CreERT2}*:Apoe*$^{fl/fl}$ mice were performed on cryo or floating sections and the following additional antibodies were used: anti-mouse Clec7a (clone R1-8g7, Invivogene, 1:30); anti-mouse TMEM119 (clone 28-3, Abcam, 1:100); anti-Aβ (clone 6E10, Covance, 1:100 or Mob 410-05, Zytomed, 1:100); goat anti-mouse Alexa405; chicken anti-rat Alexa488 or Alexa647. Anti-Aβ antibody (clone 6E10, Covance) was applied on cryo sections (30 μm) for staining in Figure 2a, only. Sections were permeabilized with 0.2% Triton X-100 as mentioned above with subsequent antibody incubations. Data acquisition and quantification was performed using a Leica TCS SP5 confocal microscope and Leica application suite software (LAS-AF-lite). Quantification of positive staining within microglia or amyloid β (Aβ)-plaque region was performed using the LAS-AF quantification tool. Briefly, the region of interest was carefully selected and the sum of the values of the pixels in the selection was calculated. For quantification of Apoe-signal in human microglia (paraffin sections 5 μm), only cells with fully visible cell bodies, away from plaques (stained with anti-Aβ antibody Mob 410-05, Zytomed) or astrocytes were used. Selected area was 300 μm^2 and 30 cells were measured each (n = 3 AD subjects versus n = 3 controls). To investigate selected protein expression profiles in APP-PS1 versus APP-PS1:*Trem2*$^{-/-}$ mouse brains, we used floating sections (30 μm). For quantification of Clec7a signal within single plaque (stained with anti-Aβ antibody Mob 410-05, Zytomed) associated microglia in mouse brains, we measured an area of 250μm^2 from 10-14 plaques each in APP-PS1 (n = 5) and APP-PS1:*Trem2*$^{-/-}$ (n = 5) mice. P2ry12 protein expression in microglia associated with Aβ plaque area was measured in 3,000 μm^2 from 15 plaques per each animal in APP-PS1 (n = 5) and APP-PS1:*Trem2*$^{-/-}$ (n = 5) mice. For quantification of plaque burden, we stained for Aβ (anti-Aβ antibody Mob 410-05, Zytomed) and quantified the Aβ positive signal in the cortex of each mouse within an area of 600,000 μm^2. For quantification of Clec7a and P2ry12 signal intensity in the ventral horn of SOD1: *Trem2*$^{-/-}$ (n = 13)

and SOD1:*Trem2*$^{+/-}$ (n = 9) mice, 5 areas of 3,600 μm^2 were measured in 3 sections per spinal cord (cryo-sections 30 μm). For quantitative evaluation of P2RY12 and dystrophic axons in human AD brains (paraffin sections 5 μm), double staining for P2RY12 with Aβ or phosphorylated neurofilament was performed on paraffin sections as described previously. After deparaffinization heat induced epitope retrieval was performed in EDTA buffer (pH: 8.5). The primary antibodies (rabbit polyclonal anti- P2RY12; mouse monoclonal anti-Aβ, Clone W02, Millipore and mouse monoclonal anti-phosporylated neurofilament, SMI31; Sternberger Monoclonals, Affiniti Res Prod.) were applied together overnight. Antibody binding was visualized with either alkaline phosphatase-conjugated anti-mouse antibodies or with biotinylated anti-rabbit secondary antibodies and peroxidase-conjugated streptavidin. Alkaline phosphatase or peroxidase reaction products were visualized by development with fast blue BB salt (blue) or amino ethyl carbazole (AEC; red), respectively.

Serial tissue sections from AD patients with and without mutations in TREM2 were stained by immunofluorescence double labeling with antibodies against IBA1, TMEM119, APOE (see above), and Aβ (Clone W02, Millipore) in the following combinations: IBA1/Aβ and TMEM119/APOE as described above. All quantifications were performed blinded to the researchers. For quantification of positive staining signal, six images through the cortical layers I-IV were taken with a 20x objective. Microglia clusters in Aβ plaques were determined in sections double stained for Aβ and Iba-1 and manually counted within 6 standardized images/case of (0.6 mm^2). Images were saved as tiff-format, converted into 8-bit greyscale in ImageJ and inverted. In the resulting images, the area fraction with positive signal was calculated and plotted as percentage of cortical area covered by amyloid deposits, APOE deposits or IBA1-signal in the respective graph. The association of Iba1 positive cells associated with Aβ plaques was quantified manually by counting the number of Aβ plaques with clustered microglia. As positive plaque with microglia clusters we defined the abundance of 2–5 microglia cells surrounded by a small halo of tissue with low or without presence of microglia processes. In classical AD, such clusters or nodules are associated with neuritic or core plaques, but rarely seen in diffuse plaques.

In fluorescence staining where two primary antibodies came from the same species (rabbit), a triple staining was performed using extensive heat-induced epitope retrieval. The paraffin-embedded tissue was deparaffinized, and slices were steamed for 45 min in EDTA pH 9.0. Non-specific protein binding was blocked by incubation with diluent. The first primary Antibody (P2ry12 or Tmem119) was applied over night at 4°C and on the following day reapplied at room temperature for 1 hr. Consequently, we incubated sections with biotinylated anti-rabbit antibody and then with avidin-coupled peroxidase, which catalyzed signal amplification with tyramine. Antigen retrieval was repeated by steaming with EDTA pH 9,0 for 30 min, which abolishes antibody reactivity from the previous round but leaves the amplified avidin binding intact, thus preserving the localized binding of Cy2 labeled streptavidin. In a next step two additional primary antibodies were simultaneously applied overnight at 4°C (Iba-1+SMI31 or Aβ; Tmem119+SMI31 or Aβ) and reapplied the next day for one hour at room temperature. Secondary antibodies anti-rabbit Cy5 (Iba-1/Tmem119) and anti-mouse Cy3 (Smi31/ Amyloid β) used for visualizing the immunohistochemical reaction. Covering with slips was done by mounting with Gallate Geltol for 5 min.

For Fluoro-Jade C staining, frozen cut tissue sections were first immersed in a basic alcohol solution consisting of 1% sodium hydroxide in 80% ethanol for 5 min, then rinsed for 2 min in 70% ethanol, for 2 min in distilled water and finally, incubated in 0.06% potassium permanganate solution for 2 min. Slides were then transferred for 10 min to a 0.0001% solution of Fluoro-Jade C (Histo-Chem Inc; Jefferson, AR) dissolved in 0.1% acetic acid vehicle. Slides were then rinsed three times in distilled water for 1 min, cleared in xylene and coverslipped with DPX (Sigma).

Analysis of P2RY12 and Dystrophic Axons in AD Brains

Independent patient cohort Quantitative evaluation for P2RY12 and dystrophic axons was performed by manual counting. Plaques were identified using the anti-Amyloidβ antibody, Clone W02 (Millipore). Following immunohistochemistry on respective serial sections the previously defined regions of interest (ROI) were manually outlined. In the individual cases three different ROIs were quantified by overlaying a morphometric grid (0.27 mm^2) placed within the ocular lens: two fields in areas with the highest density of P2RY12 reactive microglia, two fields in areas of intermediate density and two fields in areas of the lowest density within the respective case and lesion.

Induction of EAE

For the PLP-induced EAE, SJL/J female mice (6-8 weeks old) were immunized subcutaneously (s.c.) with 200 μg of PLP139-151 peptide in a 0.2 mL emulsion comprised of equal volumes of phosphate-buffered saline (PBS) solution. For the MOG-induced EAE, female mice (6-8 weeks) were injected s.c. in both flanks with 100 μg myelin oligodendrocyte glycoprotein (MOG) 35–55 peptide dissolved in PBS. For both models, the solutions were emulsified in an equal volume of CFA (Difco) containing killed *Mycobacterium tuberculosis* strain H37RA at a final concentration of 5 mg ml^{-1} *Mycobacterium tuberculosis* H37Ra and injected twice i.p. with 200 ng pertussis toxin (List Biological Laboratories, Campbell, CA) administered on the day of immunization and 48 hr later. Clinical assessment of EAE was performed daily after disease induction according to the following criteria: 0, no signs of disease; 1, loss of tone in the tail; 2, hind limb paresis; 3, hind limb paralysis; 4, tetraplegia; 5, moribund, during the duration of the acute phase (15 d), or only during the progressive or chronic phase (days 30–50). Microglia from these mice were sorted at the scores (i.e., 0, 1, 2, 3) indicated in Figures 1A and 1B and Table S1.

Isolation of Primary Neurons

Primary neurons were prepared from embryos at age E18.5. Cerebral hemispheres were isolated and freed from meninges. Tissues were digested with 0.25% trypsin in HBSS for 15 min at 37°C, and triturated with fire-polished glass pipettes to obtain single cell preparation. Cell suspension was filtered through a 70 and a 40 μm cell strainer, and cells were collected at 1,000 *g* for 5 min. Cell density was then determined using a hemocytometer, and cells were seeded at different densities according to the experimental design and need. We used DMEM supplemented with 10% FBS for the initial plating, and the medium was changed to Neurobasal supplemented with 1 × B27 (Invitrogen) 3 h later. Half medium was changed every 3 days.

Induction of Apoptosis and Labeling of Neurons

To induce apoptosis, neurons were carefully detached from the plate surface by repeated washes with PBS. Neurons were irradiated with UV light (302 nm) with an intensity of 6 × 15 W for 15 min. From now on, neurons were kept on ice. Cells were harvested by centrifugation and the pellet processed for downstream applications. The labeling dye (1mg) was resuspended in 100 μL special anhydrous DMSO (Thermo Fisher Scientific) and immediately used. Alternatively, dissolved dye was quickly aliquoted at 5 μL and stored at −80°C until use. Neurons were carefully resuspended in 1 mL of PBS and incubated in darkness for 15 min at 37°C with 2 μL of the dissolved labeling dye (Alexa488 5-SDP Ester or Alexa405 NHS Ester, Life Technologies/Thermo Fisher Scientific). To block and capture residual dye, cells were diluted with PBS, harvested by centrifugation, resuspended in 1 mL FBS and washed twice with PBS. Total apoptotic cell number was determined using Trypan Blue staining. Neurons were resuspended at a density of approximately 100,000 cells per 4 μL for stereotactic injection.

Induction of Necrosis in Neurons

To induce necrosis, plated neurons were irradiated with UV light for 15 min and then placed back in the incubator for 24 hr. Neurons were labeled with Alexa488 5-SDP Ester (Life Technologies). To distinguish between apoptotic and necrotic cells, dying neurons were incubated with Annexin V (Biolegend) and 7-AAD (Biolegend, 5 μg ml^{-1}) for 5 min before flow cytometry analysis.

Stereotactic Injections

Mice were anesthetized by i.p injection of a mixture of Ketamine (100 mg kg^{-1}), Xylazine (10 mg kg^{-1}) and Acepromazine (3 mg kg^{-1}). 2 μL of compound (which could be labeled as dNs, recombinant mouse APOE [0.5 mg mL^{-1} My Biosource], bacterial LPS [Sigma], Zymosan [Life Technologies], or *E. coli* [Life Technologies]) or saline solution were each distributed into the hippocampus and cortex bilaterally (Y: ± 1.5mm; X: −2mm; Z: −2mm and −1mm) using stereotaxic equipment (Harvard Apparatus). After recovery from surgery, animals were returned to their home cages. Post-surgery (16 hr or 3 days), mice were euthanized by CO_2 inhalation and perfused for subsequent experiments.

Intrahippocampal Injection of Kainic Acid

Mice were injected into the dorsal hippocampus of both hemispheres with Kainic acid dissolved in saline (0.2 μg in 50 nl) using a microsyringe (Hamilton, Reno, Nevada) with a 26-gauge needle and the stereotaxic coordinates from bregma: anteroposterior (AP), - 1.8 mm; mediolateral (ML), 1.6 mm; dorsoventral (DV), - 1.8 mm. Control animals received 0.9% NaCl under the same surgical conditions. After 48 hr, mice were euthanized by CO_2 inhalation and perfused for subsequent experiments.

Facial Nerve Axotomy

Unilateral facial nerve transection at the stylomastoid foramen was performed in *WT, ApoE*$^{-/-}$*, Trem2*$^{-/-}$, and *Cx3cr1*^{CreERT2}*:ApoE*$^{fl/fl}$ and *Cx3cr1*^{wt}*:ApoE*$^{fl/fl}$ (control) mice (n = 4-5/group). Successful nerve injury indicated by ipsilateral whisker paresis was assessed upon recovery from mild anesthesia by isoflurane. All mice were sacrificed at 7 days post-facial nerve axotomy. Immunohistochemical staining for NeuN (clone A60, Millipore, 2 μg ml^{-1}) and P2ry12 (polyclonal, 0.4 μg ml^{-1}) and analyses were performed on 30 μm floating sections as described in previous section. For quantification of $NeuN^+$ neurons, only cells within the facial motor nucleus with fully visible cell bodies and visible cytoplasm were included.

Mouse Microglia Isolation and Sorting

Microglia isolation was performed according to our previously described protocol (Butovsky et al., 2014). Briefly, mice were transcardially perfused with ice-cold Hanks' Balanced Salt Solution (HBSS), spinal cords and brains separately dissected. For sample post-stereotaxic injection, tissue around the site of injection was collected corresponding to the following measurements 3x4x4 mm/hemisphere and a mass in average of ∼90 mg. From this tissue, ∼1,000 phagocytic cells and 20,000 non-phagocytic cells were sorted in average from the same site of injection for Nanostring, RNaseq and qPCR analyses. Single cell suspensions were prepared and centrifuged over a 37%/70% discontinuous Percoll gradient (GE Healthcare), mononuclear cells were isolated from the interface. In order to distinguish resident microglia from recruited myeloid cells, we used a monoclonal antibody that recognizes FCRLS, which is expressed on microglia, but not on infiltrating myeloid cells (Butovsky et al., 2014). Isolated cells were stained with anti-FCRLS [clone 4G11, 3 μg ml^{-1}, validated in ref.], followed by secondary detection with goat anti-rat IgG conjugated to APC [clone Poly4054, Biolegend, 0.7 μg ml^{-1}, validated in reference (Butovsky et al., 2014)] and then CD11b-PeCy7 [clone M1/70, BD Biosciences, 2 μg ml^{-1}, validated in reference (Butovsky et al., 2014)] antibody to specifically sort resident microglia. Phagocytic versus non-phagocytic microglia were further sorted from the $FCRLS^+CD11b^+$-population by detection of Alexa488

fluorescence. FCRLS^{+}Clec7a^{+}, FCRLS^{+}Clec7a^{Int} and FCRLS^{+}Clec7a^{-} cells were sorted using mClec7a (clone R1-8g7, Invivogene, 1:10) and FITC goat-anti-rat (BioLegend #405404, 1:100).

Isolation of Spleenic CD11b^{+}Ly6C^{+} Monocytes

Spleen was dissected and homogenized using a cell strainer (70 μm). After centrifugation, the cell pellet was resuspended in ACK lysing buffer to remove red blood cells. Splenocytes were incubated with anti-CD11b magnetic beads (1:10, Miltenyi Biotec) for 15 min on ice. CD11b^{+} cells were collected after magnetic separation. Unspecific antigen binding sites were blocked using Fc Receptor blocking anti-CD16/32 antibodies (BD Biosciences, 5 μg ml^{-1}) and cells were stained using anti-Ly6C-FITC and anti-CD11b-PeCy7 (BD Biosciences, 5 μg ml^{-1}) and sorted accordingly.

Mass Spectrometry Analysis

Single LC-MS/MS experiment was performed on a LTQ Orbitrap Velos (Thermo Fischer) equipped with Waters (Milford, MA) NanoAcquity HPLC pump. Peptides were separated onto a 100 μm inner diameter microcapillary trapping column packed first with approximately 5 cm of C18 Reprosil resin (5 μm, 100 Å, Dr. Maisch GmbH, Germany) followed by ~20 cm of Reprosil resin (1.8 μm, 200 Å, Dr. Maisch GmbH, Germany). Separation was achieved through applying a gradient from 5%–27% ACN in 0.1% formic acid over 180 or 600 min at 100 nL min^{-1}. Electrospray ionization was enabled through applying a voltage of 1.8 kV using a homemade electrode junction at the end of the microcapillary column and sprayed from fused silica pico tips (New Objective, MA). The LTQ Orbitrap Velos was operated in data-dependent mode for the mass spectrometry methods. The mass spectrometry survey scan was performed in the Orbitrap in the range of 395 –1,800 m/z at a resolution of 6 × 10^{4}, followed by the selection of the twenty most intense ions (TOP20) for CID-MS2 fragmentation in the Ion trap using a precursor isolation width window of 2 m/z, AGC setting of 1,000, and a maximum ion accumulation of 200 ms. Singly charged ion species were not subjected to CID fragmentation. Normalized collision energy was set to 35 V and an activation time of 10 ms. Ions in a 10 ppm m/z window around ions selected for MS2 were excluded from further selection for fragmentation for 60 s. The same TOP20 ions were subjected to HCD MS2 event in Orbitrap part of the instrument. The fragment ion isolation width was set to 0.7 m/z, AGC was set to 10,000, the maximum ion time was 200 ms, normalized collision energy was set to 27V and an activation time of 1 ms for each HCD MS2 scan. Raw data were submitted for analysis in Proteome Discoverer 2.2.0.386 (Thermo Scientific) software. Assignment of MS/MS spectra was performed using the Sequest HT algorithm by searching the data against a protein sequence database including all entries from the Mouse Uniprot database (SwissProt 16,768 2016) and other known contaminants such as human keratins and common lab contaminants. Sequest HT searches were performed using a 20 ppm precursor ion tolerance and requiring each peptides N-/C termini to adhere with Trypsin protease specificity, while allowing up to two missed cleavages. 6-plex TMT tags on peptide N termini and lysine residues (+229.162932 Da) was set as static modifications while methionine oxidation (+15.99492 Da) was set as variable modification. A MS2 spectra assignment false discovery rate (FDR) of 1% on protein level was achieved by applying the target-decoy database search. Filtering was performed using a Percolator (64bit version). For quantification, a 0.02 m/z window centered on the theoretical m/z value of each the six reporter ions and the intensity of the signal closest to the theoretical m/z value was recorded. Reporter ion intensities were exported in result file of Proteome Discoverer 2.2 search engine as an excel tables. The total signal intensity across all peptides quantified was summed for each TMT channel, and all intensity values were normalized to account for potentially uneven TMT labeling and/or sample-handling variance for each labeled channel.

RNA Isolation and NanoString RNA Counting

Total RNA was extracted using mirVana miRNA isolation kit (Ambion) according to the manufacturer's protocol. NanoString nCounter technology (http://www.nanostring.com/) allows expression analysis of multiple genes from a single sample (Butovsky et al., 2014). We performed nCounter multiplexed target profiling of 400 to 542 microglial transcripts (MG400 and MG550, see MG custom-chip design). 100 ng of total RNA per sample were used in all described nCounter analyses according to the manufacturer's suggested protocol (Butovsky et al., 2014).

Quantitative Real-Time PCR

For conventional quantitative reverse transcription polymerase chain reaction (qRT-PCR), total RNA (30 ng) with specific mRNA probes and 3 ng of RNA with specific miRNA probes (Applied Biosystems) were used after reverse transcription reaction according to the manufacturer (high-capacity cDNA Reverse Transcription Kit; Applied Biosystems). All mRNA/miRNA amplifications were performed with commercially available FAM-labeled Taqman probes (Applied Biosystems/Thermo Fisher Scientific). mRNA or miRNAs levels were normalized relative to GAPDH or U6, respectively. Real-time PCR reaction was performed using Vii7 (Applied Biosystems). All qRT-PCRs were performed in duplicate, and the data are presented as relative expression compared to GAPDH or U6 as mean ± s.e.m.

Mouse MG550 Chip Design

The MG550 NanoString chip was designed using the quantitative NanoString nCounter platform. Selection of genes is based on analyses that identified genes and proteins which are specifically or highly expressed in adult mouse microglia (Butovsky et al., 2014) plus 40 inflammation-related genes which were significantly affected in EAE, APP-PS1 and SOD1 mice. Two other versions were done after MG400 (Butovsky et al., 2014). MG468 contains additional 48 inflammation- and phagocytosis-related genes (Butovsky

et al., 2015). Using this signature, we generated a new version of NanoString-based microglia chip termed MG550 that encompasses 400 unique and enriched microglial genes we have identified previously (Butovsky et al., 2014) and additional 150 inflammation-, inflammasome- and phagocytosis-related genes.

NanoString Data Analysis

NanoString data were normalized and analyzed using nSolver software. RNA ncounts were normalized using the geometric mean of 6 housekeeping genes (HKGs): *Cltc*, *Gapdh*, *Gusb*, *Hprt*, *Pgk1,* and *Tubb5*. A cutoff was introduced at the value of the highest negative control present on the chip. Fold changes were calculated using the average of each group. For each experiment, the fold changes were calculated comparing the experimental group to their appropriate controls.

RNA Sequencing

1,000 FACS-sorted FCRLS^{+} microglia cells were lysed in TCL buffer. Smart-Seq2 libraries were prepared by the Broad Technology Labs and sequenced by the Broad Genomics Platform. cDNA libraries were generated from sorted cells using the Smart-seq2 protocol (Picelli et al., 2013). RNA sequencing was performed using Illumina NextSeq500 using a High Output v2 kit to generate 2 × 25 bp reads. RNA-Sequencing data was pooled from 3 separate experiments. Transcripts were quantified by the BTL computational pipeline using Cuffquant version 2.2.1(Trapnell et al., 2012). Raw counts were normalized using TMM normalization and then log2-transformed. Batch effects were corrected using removeBatchEffect from the R package limma (v. 3.28.21).

In Vitro Suppression Assay

Spleens of C57BL/6J mice were gently dissociated into single-cell suspensions, and red blood cells were removed using Ammonium-Chloride-Potassium (ACK) lysis buffer (GIBCO). Splenocytes were labeled with 5(6)-Carboxyfluorescein N-hydroxysuccinimidyl ester (CFSE, Molecular probes – Invitrogen, 5 μmol l^{-1}) at 37°C followed by staining with anti-CD3 mAb (clone 145-2C11, Biolegend, 2 μg ml^{-1}) for 30 min on ice. Responder CFSE^{+} CD3^{+} T cells were sorted using FACS Aria II (BD Biosciences) with a purity > 98%. T cells were stimulated with mouse T cell-activator CD3 and CD28 magnetic beads (Dynabeads-GIBCO). Stimulated CFSE^{+} CD3^{+} T cells were co-cultured in round bottom 96-well plates with FCRLS^{+} spinal cord microglia for 72 hr at 37°C in a 5% CO2 incubator. T cell-to-microglia ratio was 4:1 in a final volume of 200 μL per well in DMEM media supplemented with 10% Fetal Bovine Serum (FBS), 1% Penicillin-Streptomycin (PS, 10,000 U ml^{-1}), L-Glutamine 2 mmol l^{-1}, sodium pyruvate 1 mmol l^{-1}, non-essential amino acids 0.1 mmol l^{-1}, HEPES 5 mmol l^{-1} and 2-Mercaptoethanol 0.05 mmol l^{-1}. T cell proliferation was measured by flow cytometric analysis by CFSE dilution on CD3^{+} T cells. Soluble recombinant ApoE (rApoe) was added into the media at 100 ng ml^{-1}.

Heatmaps

Heatmaps and clustering were generated in R (version 3.2.0) using heatmap.2 from the gplots package and the prcomp from the stats package. For clustering, the z-scores were calculated using the mean expression of biological replicates per disease stage/condition and then subsequently clustered using K-means. A scree plot was used to assess the number of clusters.

Circos Plot

The custom-made microglia transcriptional signatures (Figure 3I) were generated by retrieving genes upregulated at least 1.5 fold and p value less than 0.01 (Student t test) in disease conditions from previously identified microglia transcriptomes from mouse models of neuropathic pain (GSE60670), chronic pain (GSE71133), Rett syndrome (*Mecp2*$^{-/-}$) (GSE66211), lipid disorder (*Mfp2*$^{-/-}$) (GSE66420), ALS (SOD1) (GSE43366), AD (5xFAD) (GSE65067), brain irradiation (GSE55968), and aging (GSE62420). All custom signatures were derived from publicly available transcriptomes downloaded from Gene Expression Omnibus (GEO). A GSEA algorithm was applied to identify the enrichment of phagocytic microglia signaling pathways in the microglia transcriptomes in various diseases conditions. This includes Aging, Mfp2-deficiency, Alzheimer's disease, ALS, neuropathic pain, chronic pain, and Mecp2-deficiency. GSEA assesses whether the expression of a previously defined group of related genes is enriched in one biological state. Statistical significance of GSEA results was assessed using 1,000 sample permutations. A nominal P value less than 0.001 was used to determined pairwise transcriptome connectivity. A Circos graph was generated using Circos package 0.68.12.

TREM2 pathway analysis in MGnD microglia. A GSEA algorithm was used to identify genes that are differentially expressed in microglia transcriptomes from lipid disorder (*Mfp2*$^{-/-}$) (GSE66420), ALS (SOD1) (GSE43366), AD (5XFAD) (GSE465067), and aging (GSE62420), as compared with their control counterparts. High-scoring differentially expressed 'leading-edge' genes were selected on the basis of their presence in the TREM2-responsive gene signature 5xFAD:*Trem2*$^{-/-}$ and SOD1:*Trem2*$^{-/-}$ mice. The statistics were determined using Euclidean distance.

Ingenuity Pathway Analysis

Data were analyzed using Ingenuity software (Ingenuity Systems, http://www.ingenuity.com). Differentially expressed genes (with corresponding n-fold changes and p values) were incorporated in canonical pathways and bio-functions and were used for generating biological networks as described previously (Butovsky et al., 2014). Briefly, uploaded dataset for analysis was filtered using the following cutoff definitions: fivefold change, $p < 0.01$.

QUANTIFICATION AND STATISTICAL ANALYSIS

Statistical analysis was done using GraphPad Prism 7 software. Data distribution was assumed to be normal, but this was not formally tested. Data are presented as mean ± s.e.m and 2-tailed Student's t tests (unpaired) or ANOVA multiple comparison tests were used to assess statistical significance. Data collection and analysis were blindly performed. Data for each experiment were collected and processed randomly and animals were assigned to various experimental groups randomly as well. All n and P values and statistical tests are indicated in figure legends. Volcano plots were generated using Multiplot studio software. Heatmaps were generated using MEV and R-software.

DATA AND SOFTWARE AVAILABILITY

The accession number for the RNAseq and Nanostring gene sequence data reported in this paper is Gene Expression Omnibus (GEO): GSE101689. The accession number for the protein data reported in this paper is PeptideAtlas: PASS01081.

Video Article

Functional Characterization of Regulatory Macrophages That Inhibit Graft-reactive Immunity

Jordi Ochando[1,2], Patricia Conde[1,2]

[1]Department of Medicine, Icahn School of Medicine at Mount Sinai

[2]Immunología de Trasplantes, Centro Nacional de Microbiología, Instituto de Salud Carlos III

Correspondence to: Patricia Conde at p.conde@isciii.es

URL: https://www.jove.com/video/54242
DOI: doi:10.3791/54242

Keywords: Immunology, Issue 124, Regulatory macrophages, allograft, immune tolerance, transplantation, costimulatory blockade, suppression assay.

Date Published: 6/7/2017

Citation: Ochando, J., Conde, P. Functional Characterization of Regulatory Macrophages That Inhibit Graft-reactive Immunity. *J. Vis. Exp.* (124), e54242, doi:10.3791/54242 (2017).

Abstract

Macrophage accumulation in transplanted organs has long been recognized as a feature of allograft rejection[1]. Immunogenic monocytes infiltrate the allograft early after transplantation, mount a graft reactive response against the transplanted organ, and initiate organ rejection[2]. Recent data suggest that suppressive macrophages facilitate successful long-term transplantation[3] and are required for the induction of transplantation tolerance[4]. This suggests a multidimensional concept of macrophage ontogeny, activation, and function, which demands a new roadmap for the isolation and analysis of macrophage function[5]. Due to the plasticity of macrophages, it is necessary to provide a methodology to isolate and characterize macrophages, depending on the tissue environment, and to define their functions according to different scenarios. Here, we describe a protocol for immune characterization of graft-infiltrating macrophages and the methods we used to functionally evaluate their capacity to inhibit $CD8^+$ T proliferation and to promote $CD4^+Foxp3^+$ Treg expansion *in vitro*.

Video Link

The video component of this article can be found at https://www.jove.com/video/54242/

Introduction

This protocol describes *in vitro* techniques to study the function of tissue-infiltrating macrophages isolated from cardiac allografts, according to their ability to modulate T-cell responses. Widely described in the literature, fluorescent cell-tracking dyes in combination with flow cytometry, are powerful tools to study the suppressive function of specific cell types *in vitro* and *in vivo*. Our protocol follows the carboxyfluorescein succinimidyl ester (CFSE) method for monitoring lymphocyte proliferation *in vitro*.

When a CFSE-labeled cell divides, its progeny acquires half the number of carboxyfluorescein-tagged molecules[6]. The corresponding decrease in cell fluorescence by flow cytometry can be used to assess cell division, monitoring the capacity of suppressive macrophages to modulate T-cell immune responses. Since CFSE is a fluorescein-based dye, it is compatible with a broad range of other fluorochromes, making it applicable to multi-color flow cytometry. The appropriate choice of fluorochromes for phenotyping is also important to avoid excessive spectral overlap and the inability to recognize antibody-positive cells, particularly with visible protein dyes such as CFSE[7].

There are many advantages of using fluorescent dyes over alternative techniques that measure cell proliferation, such as the thymidine incorporation assay, which uses radiolabeled thymidine (TdR)[8]. This assay utilizes tritiated thymidine (^{3}H-TdR) that is incorporated into new strands of chromosomal DNA during mitotic cell division. A safety concern associated with this assay is the use of radioisotopes, since a scintillation beta-counter is used to measure the radioactivity in DNA recovered from the cells in order to determine the extent of cell division. Methodologically, the tritiated thymidine assay is not flexible enough to fit important clinical laboratory constraints such as low number of cells and delayed analysis after staining. On the contrary, CFSE staining has been shown to prevent cell proliferation and to interfere with critical activation markers, such as CD69, HLA-DR and CD25[9]. Therefore, understanding advantages and limitations of each methodology, particularly in multicolor studies where multiple dyes are used to track different cell types, is critical for obtaining accurate and reproducible results.

Protocol

In this study, mice are housed in accordance with the United States Department of Agriculture guidelines and the recommendations of the Public Health Service Guide for the Care and Use of Laboratory Animals. All experimental techniques involving animal use were performed in accordance with Institutional Animal Care and Utilization Committee (IACUC)-approved protocols of the Mount Sinai School of Medicine.

1. Media Preparation

1. Prepare complete RPMI 1640 medium with 10% FBS and 1% penicillin-streptomycin (10,000 U/mL) by using 2 mM L-glutamine, 1 mM sodium pyruvate, 0.1 mM non-essential amino acids, 5 mM HEPES, and 0.05 mM 2-mercaptoethanol.

2. Allograft Isolation and single-cell Suspension

NOTE: The transplantation and anastomosis technique of the pulmonary artery and inferior cava vein was initially described by Corry and collaborators and can be visualized in Liu & Kang[10,11] (**Figure 1A**).

1. Anesthetize a transplanted mouse with 4-5% isoflurane in an induction chamber. Sacrifice it by cervical dislocation.
2. Make a midline abdominal incision with standard scissors and remove the abdominal contents to localize the aorta.
   NOTE: The transplanted heart will be on the right side of the recipient abdominal aorta (**Figure 1B**).
3. Pull out the graft gently using fine sharp-teeth forceps and place it immediately into ice-cold RPMI medium.
   NOTE: Using a surgery scissor to separate the graft from the aorta can damage the graft and cause some tissue to remain adhered to the recipient.
4. After all grafts have been collected, move them into a sterile culture hood for tissue processing. Place the graft in a petri dish and dice the tissue into small pieces (1 mm) using sterile, blunt, microsurgery scissors.
5. With sharp-teeth forceps, transfer the pieces to a 50 mL tube with 5 mL of collagenase A (0.1 mg/mL collagenase in sterile 1x PBS). Incubate it for 1 h in a 37 °C bath.
6. Add 5 mL of RPMI medium to neutralize the collagenase and transfer the sample through a 100 µm strainer with the help of the plunger of a 1 mL syringe.
7. Spin the sample down at 400 x g for 5 min at 4 °C.
8. Resuspend the pellet in 1 mL of ACK lysis buffer. Mix well and incubate for 5 min at 4 °C.
9. Add 1 mL of RPMI medium to neutralize the lysis buffer and spin the sample down at 400 x g for 5 m at 4 °C.
10. Resuspend the cell pellet in 200 µL of RPMI medium and transfer it to a 5 mL polypropylene round-bottom tube.
    NOTE: Polypropylene tubes support less adherence. Also, maintaining the cells at low temperature, such as 4 °C, reduces adhesion.

3. Isolation of Graft-infiltrating Macrophages Using Fluorescence-activated Cell Sorting

1. Block unwanted specific binding on myeloid cells by using Fc receptor blocking mAb (rat anti-mouse CD16/32). Add 1-2 µL per sample, 15 min prior to surface staining.
2. Stain with anti-mouse CD11b Percp/Cy5.5 (0.6 µg/µL final concentration in the RPMI medium), anti-mouse CD45 APC/eFluor780 (0.6 µg/µL), anti-mouse Ly6C APC (2 µg/µL), and anti-mouse Ly6G Pe/Cy7 (2 µg/µL). Cover the tubes with aluminum foil to protect the fluorescent antibodies from light and incubate the tubes in the refrigerator at 4 °C for 45 min.
   NOTE: For single-stain compensations, prepare a negative control tube (no stain) and tubes with cells labeled singly with each of the fluorochromes. To help set up the gate, isotype controls can be used especially for Ly6C (IgG2a) and Ly6G (IgG2b).
3. Wash the cells twice with RPMI medium and spin them at 400 x g for 5 min at 4 °C. Count the cells using trypan blue and a hemocytometer and dilute them in 1 mL of RPMI medium per 1 x 10^6 cells. Before sorting, transfer the samples through a 5 mL, 70 µm cell strainer tube cap. Add DAPI (1 µg/mL) as a cell viability marker and proceed to sort.
4. Because macrophages are sensitive and fragile cells, set the sort conditions to 20 psi and use a 100 µm nozzle size to isolate macrophages using a 4-way purity mode.
5. Prepare collection tubes with 1 mL of RPMI medium in a 5 mL polypropylene tube.
6. Using the sorter software open new experiment and select blank experiment with a blank panel to define settings.
7. **Set up a dot plot that displays the forward (FSC) versus (*vs.*) side scatter (SSC) and gate on all leukocytes, excluding debris and clumps with the lowest forward and side scatter. From this parent gate, create a new dot plot that displays SSC *vs.* DAPI and gate on DAPI cells.**
   1. On this newly-gated population, create a dot plot that displays CD11b *vs.* CD45 and gate on double-positive ($CD11b^+$ $CD45^+$) macrophages and neutrophils.
   2. From here, create a final dot plot displaying Ly6C *vs.* Ly6G and gate the desirable populations: $Ly6C^{hi}$ $Ly6G^-$, $Ly6C^{lo}Ly6G^-$, and $Ly6C^{int}Ly6G^+$ (**Figure 2**).
8. After sorting, check for purity and cell viability (>90%) and spin the collection tubes at 400 x g for 5 min at 4 °C. Count the cells using trypan blue and a hemocytometer and resuspend them at the desired concentration (*e.g.,* 1 x 10^6 macrophages/mL) in complete RPMI medium.
9. Plate 50 x 10^3 macrophages per well in a 96-well round-bottom plate with a final volume of 100 µL of complete RPMI medium. Leave the cells undisturbed for at least 24 h at 37 °C and 5% CO_2.

4. Isolation of T Cells Using Fluorescence-activated Cell Sorting

NOTE: C57BL/6-Foxp3tm1Flv/Jn is an X-linked targeted knock-in mouse strain that co-marks cells expressing the Foxp3 (forkhead box P3) gene with monomeric red fluorescent protein (mRFP).

1. Anesthetize and sacrifice C57BL/6 and C57BL/6-Foxp3tm1Flv/J (H-2b) mice as previously described in step 2.1. Isolate the spleen and lymph nodes (LN: inguinal, lumbar, axillar, brachial, and cervical) and rapidly place them in ice-cold RPMI medium.
2. In order to isolate the LN, place the mouse in a supine position, make a midline skin incision from bottom to top, carefully cutting the peritoneum and gently spreading the skin apart. Once all inguinal, lumbar, axillary, brachial, and cervical LN are collected (**Figure 1C**, colored in red), cut the peritoneum and isolate the spleen at the upper left side of the gut.

3. Disaggregate the spleen and LN using a 100 µm filter placed on top of a 50 mL tube. Using the plunger of a 1-mL syringe, gently press the tissue. Rinse the filter with RPMI medium as many times as necessary until it is clean.
   NOTE: LN and spleen from each mouse can be pooled together in the same tube.
4. Spin down at 400 x g for 5 min at 4 °C.
5. Resuspend the pellet in 2 mL of ACK lysis buffer. Mix well and incubate for 5 min at 4 °C.
6. Add 2 mL of RPMI medium to neutralize the lysis buffer. Spin down at 400 x g for 5 min at 4 °C.
7. Resuspend the cell pellet in 200 µL of RPMI medium and transfer it to a 5 mL polystyrene round-bottom tube.
8. Stain for anti-mouse CD4 APC (0.6 µg/µL) and/or anti-mouse CD8 PeCy7 (2 µg/µL). Cover the tubes with aluminum foil to protect the fluorescent antibodies from light, and incubate the tubes in the refrigerator at 4 °C for 45 min.
   NOTE: For single-stain compensations, prepare a negative control tube (no stain) and tubes with cells labeled singly with each of the fluorochromes.
9. Wash the cells twice with RPMI medium and spin them at 400 x g for 5 min at 4 °C. Count the cells using trypan blue and a hemocytometer.
   NOTE: CFSE dye is provided as carboxyfluorescein diacetate succinimidyl ester powder usually at 50 µg. Add 18 µL DMSO to a vial of CFSE for a final stock solution of 5 mM and store at -20 °C for several months.
10. For CFSE labeling, resuspend CD8 stained cells at a concentration of up to 10^6 cells per mL in PBS at a final working concentration of 5 µM CFSE from the stock solution. Incubate them in a bath at 20 °C for 5 min as previously described[6].
    NOTE: (CRITICAL STEP) For cells at a low concentration (≤10^6 per mL), it is essential that the cells be labeled in the presence of added protein to buffer the toxic effects of CFSE. Therefore, PBS can contain 5% FBS. Note that if medium is used, free amino acids may lower the labeling efficiency by competing for CFSE.
11. Neutralize the CFSE with 2 mL of RPMI medium. Spin at 400 x g for 5 min at 4 °C. Add 1 mL of RPMI medium per 1 x 10^6 CD8 T cells.
12. Before sorting, transfer the sample through a 70 µm cell strainer on a 5 mL tube cap. Add 50 µL of 1x DAPI (1 µg/mL) as a cell viability marker and proceed to sorting.
    NOTE: 1x means 1:1 ratio of the reagent with respect other constituent.
13. Set the sort conditions at 20 psi and 100 µm nozzle size to isolate double-positive $CD8^+CFSE^+$ T cells (**Figure 3A**).
14. Prepare collection tubes with 1 mL of RPMI medium in a 5 mL polypropylene tube and proceed to sort.
15. Using the sorter software open new experiment and select blank experiment with a blank panel to define settings.
16. **For $CD4^+$ T cell isolation, set up a dot plot that displays the FSC vs. SSC and gate on lymphocytes, excluding debris as well as large granular cells, such as dendritic cells.**
    1. From this parent gate, create a new dot plot that displays SSC vs. DAPI and gate on DAPI cells.
    2. On this newly-gated population, create a dot plot that displays SSC vs. CD4 to isolate all $CD4^+$ cells (**Figure 3B**). Alternatively, an anti-CD3 mAb can be used to ensure isolation of pure T cell populations.
       NOTE: A small fraction of all $CD4^+$ T cells (5-10%) should be $Foxp3^+mRFP^+$.
17. After sorting, check for purity and cell viability (>90%) and spin the collection tubes at 400 x g for 5 min at 4 °C. Count the cells using trypan blue and a hemocytometer. Resuspend using 1 mL of complete RPMI medium per 2x10^6 T cells.
18. Set up suppression assay by culturing T cells with previously-sorted macrophages. Plate 10 x 10^4 $CD4^+$ T and 10 x 10^4 $CD8^+CFSE^+$ T cells in the same well in a final volume of 100 µL of complete RPMI medium. Incubate at 37 °C and 5% CO_2 for 96 h.
    NOTE: Macrophages and T cells were used in a 1:4 ratio.
19. Stimulate T cell division by washing T cell-activator CD3/CD28 magnetic beads in 2 mL of PBS before using them in order to clear the azide-containing buffer. Add 5 µL of mouse T cell-activator CD3/CD28 beads per well.
    NOTE: Magnetics beads are similar in size to antigen-presenting cells and are coupled to anti-CD3 and anti-CD28 mAb, offering a simple method for the activation and expansion of T cells.

Representative Results

The representative results show the gating strategy described in the above protocol. Results also display the analysis of the T-cell proliferation activity after the co-culture with graft-infiltrating macrophages. The *in vitro* suppressive capacity of macrophage subsets was analyzed in **Figure 4**. The results indicate that the $Ly6C^{lo}Ly6G^-$ macrophages obtained from tolerized recipients are suppressive. The results also indicate that $Ly6C^{int}Ly6G^+$ cells display a modest suppressive capacity. Only $Ly6C^{lo}Ly6G^-$ cells promoted the expansion of $CD4^+Foxp3^+$ Treg *in vitro*. Together, the data support the conclusion that graft-infiltrating $CD11b^+Ly6C^{lo}Ly6G^-$ macrophages possess many of the properties reported to be associated with monocyte-derived suppressor cells[12], including their ability to inhibit CD8 T-cell proliferation[13] and to promote $CD4^+Foxp3^+$ Treg expansion[14].

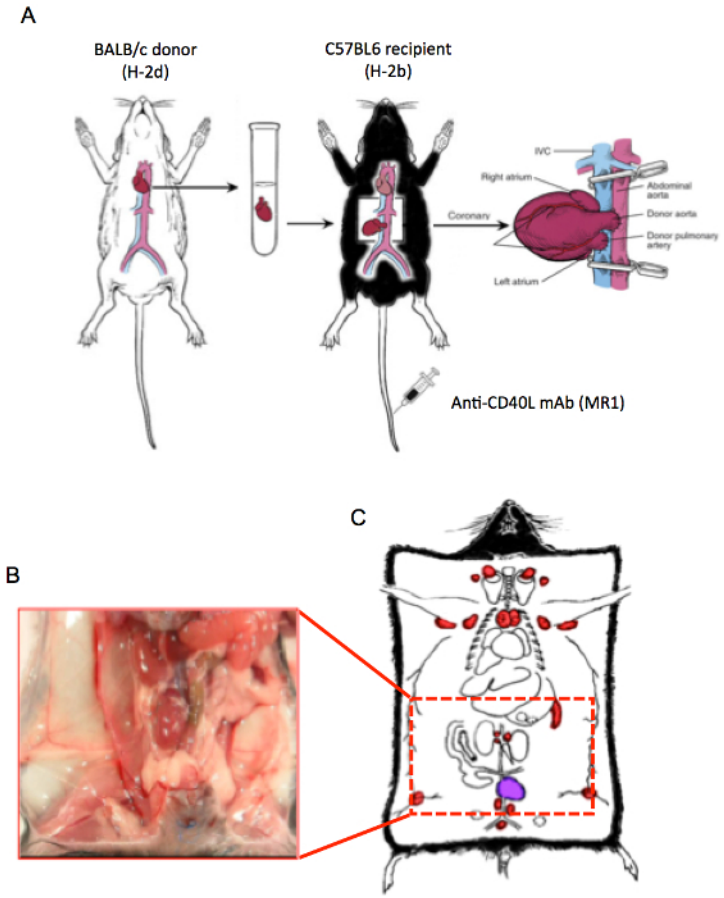

Figure 1: Animal model. (**A**) Balb/c hearts (H2-d) were transplanted into fully allogeneic C57BL/6 (H2-b) as as previously described[10]. Anastomosis, of the recipient's cava vein and abdominal aorta with the donor's pulmonary artery and ascending aorta respectively, is shown. Recipient mice were treated with 250 µg of anti-CD40L mAb (clone MR1) for tolerance induction on days 0, 2, and 4, as we recently reported[4]. Graft function was monitored every other day by abdominal palpation. Rejection was defined as complete cessation of a palpable heartbeat and was confirmed by direct visualization at laparotomy. (**B**) Representative Image and (**C**) illustration of anatomical location of LN and spleen (colored in red) and the allograft (colored in purple) Please click here to view a larger version of this figure.

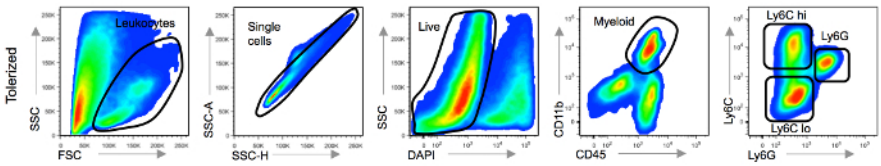

Figure 2: Macrophage sorting strategy. Starting from the upper left, leukocytes are first gated by size, and then singlet cells are discriminated from debris and clumps. From singlets, dead cells are excluded gating on the DAPI negative fraction. From live cells, $CD45^{+}CD11b^{+}$ is used to identify myeloid cells. Three myeloid cells populations are further identified based on Ly6C and Ly6G expression. Please click here to view a larger version of this figure.

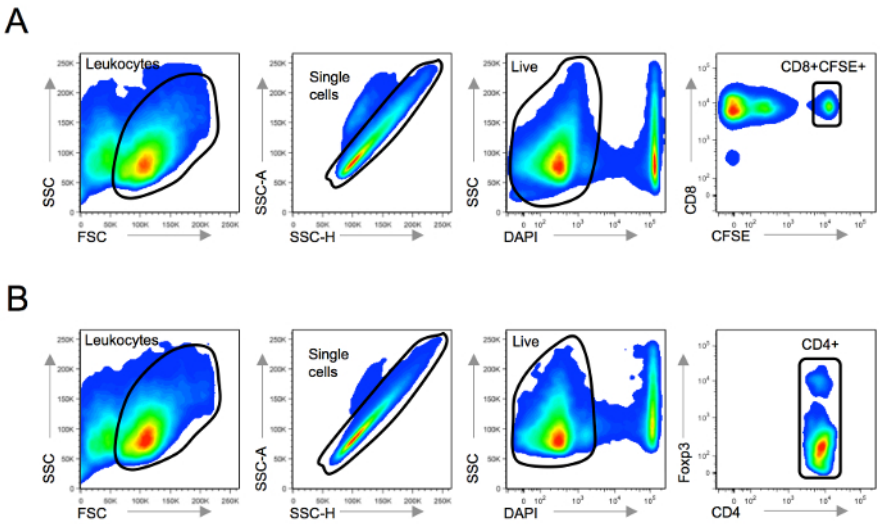

Figure 3: Lymphocyte sorting strategy. Representative flow cytometry results for the lymphocyte sorting strategy. From the upper left, gate on the lymphocyte population according to forward and side scatter. Exclude debris and clumps. From singlets, dead cells are excluded by gating on the DAPI negative fraction. From live cells, (**A**) $CD8^+$ $CFSE^+$ double-positive cells and (**B**) all $CD4^+$ T cells, which contain a fraction of $Foxp3^+$ positive cells, are gated. Please click here to view a larger version of this figure.

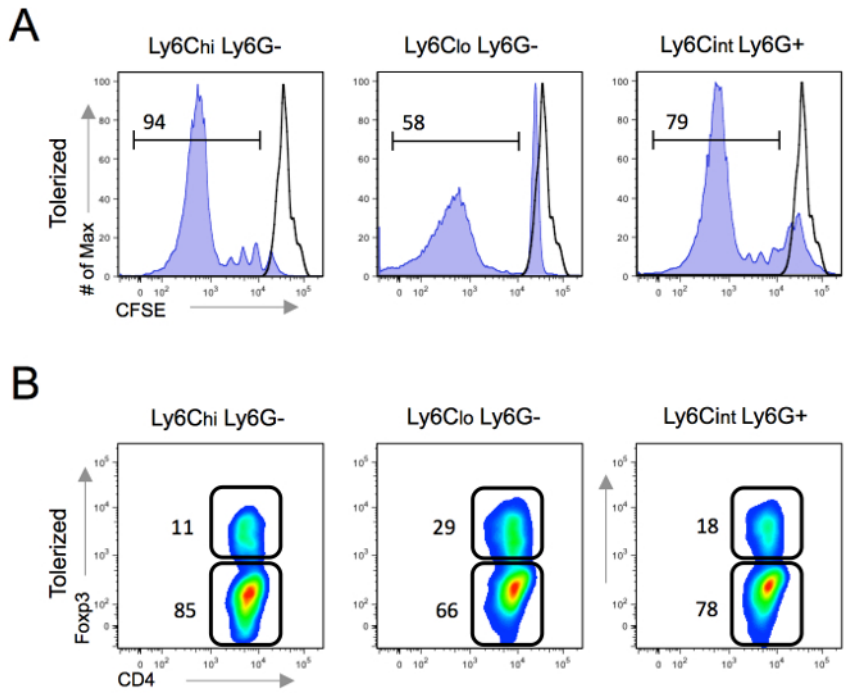

Figure 4: Suppression assay. (**A**) *In vitro* suppressive capacity of each myeloid subset. $CD8^+$ T-cell proliferation was monitored by CFSE dilution after 96 h of co-culture with myeloid subsets. (**B**) *In vitro* Treg expansion of each myeloid subset. Flow cytometry analysis of Foxp3 expression on $CD4^+$ T cells after 96 h of co-culture with myeloid subsets. Please click here to view a larger version of this figure.

Discussion

This protocol describes the methods we used to immunocharacterize graft-infiltrating myeloid cell subsets in an experimental murine model of heart transplantation, which is also applicable to other tissues in different murine experimental models. Low-pressure cell sorting at 20 psi was the preferred method to isolate a good yield of pure cell subsets. Maintaining the purity of each myeloid subset is critical to establish conclusive results of the suppressive capacity between the different myeloid populations. However, other methods can be used for the isolation of various leukocyte populations, such as commercial enrichment kits. Regardless of the cell population of interest, obtaining viable single-cell suspensions from the transplanted tissue is required for optimal surface staining and flow cytometry results. Incorrect tissue manipulation may cause cell loss and therefore a low yield of myeloid subsets. To increase the yield, make sure to process the sample using cold buffers and to maintain the cells in containers with low cell adherence (polypropylene tubes). In this protocol, we used Collagenase A from *C. histolyticum*, which is widely used for the disaggregation of many types of tissues (*e.g.*, lung, heart, muscle, bone, adipose, liver, kidney, cartilage, mammary gland, placenta, blood

vessel, brain, and tumor). To prevent the loss of cells while sorting, optimizing the antibodies and generating an efficient gating strategy is highly recommended. In this protocol, we characterized murine macrophages using CD11b-Percp/Cy5.5, CD45-APC/eFluor780, Ly6C/APC, and Ly6G Pe/Cy7 fluorescent-conjugated antibodies and flow cytometry. Since the epitopes Ly6C/G do not exist in human, the use of CD14/CD15/CD16 is required for sorting human myeloid cells[15].

In multicolor flow cytometry analysis, possible spectral overlaps of the chosen fluorochromes may occur. Therefore, as noted before, single-stain compensations are very helpful to avoid overlapping issues. In addition, antibody titration is highly recommended in order to reduce the background fluorescence and to get optimal results. Another important consideration to reduce non-specific binding is the use of viability dyes. In this protocol, DAPI is used as viability dye. DAPI (4', 6-diamidino-2-phenylindole) is a blue fluorescent stain that binds strongly to AT-rich regions in DNA. The excitation maximum for DAPI bound to DNA is 358 nm, and the emission maximum is 461 nm. When used according to protocol, DAPI stains nuclei specifically, with little or no cytoplasmic labeling, excluding dead cells in the flow analysis. However, depending on the panel of antibodies chosen, other viability dyes, such as 7-Aminoactinomycin D (7-AAD) and propidium iodide (PI), may be used. Accurate dead-cell exclusion and live-cell identification is a prerequisite to successfully monitor *in vitro* T cells, as it is important to have procedures that can follow lymphocyte proliferation with minimal disruption to cell viability and function.

As mentioned above, there are critical steps for cell labeling and proliferation analyses with cell tracking dyes such as CFSE. As an example described in the literature, careful attention must be paid to the exclusion of dead/dying cells in order to obtain uniform distributions and distinguishable daughter peaks when using CFSE[16]. There are many commercially available cell tracking dyes to choose from, depending on the staining panels. As an alternative to cell tracking dyes, thymidine titriated assay are performed to evaluate the proliferation of lymphocytes and other cells in cancer studies[13,14]. Thymidine incorporation protocols assess the replication of DNA during cell division by the measure of radiolabeled 3H- or 14C- thymidine. Although this method is quite sensitive and well established, the major disadvantages for thymidine titrated technique is that it involves radioactivity and does not provide information at the single cell level. In the other hand, CFSE flow cytometry analysis provides clear information about responding lymphocyte subsets and has less inter and intralaboratory variability.

Disclosures

The authors have nothing to disclose.

Acknowledgements

We acknowledge the technical contributions of the Flow Cytometry, Microsurgery, and Bio- repository/Pathology Centers of Research Excellence at Mount Sinai. This work was supported by the COST Action BM1305: Action to Focus and Accelerate Cell Tolerogenic Therapies (A FACTT), the Mount Sinai Recanati/Miller Transplantation Institute developmental funds, Ministerio de Ciencia e Innovacion SAF2013-48834-R and SAF2016-80031-R J.O.

References

1. Jose, M. D., Ikezumi, Y., van Rooijen, N., Atkins, R. C., & Chadban, S. J. Macrophages act as effectors of tissue damage in acute renal allograft rejection. *Transplantation.* **76** (7), 1015-1022 (2003).
2. Oberbarnscheidt, M. H. *et al.* Non-self recognition by monocytes initiates allograft rejection. *J Clin Invest.* **124** (8), 3579-3589 (2014).
3. Garcia, M. R. *et al.* Monocytic suppressive cells mediate cardiovascular transplantation tolerance in mice. *J Clin Invest.* **120** (7), 2486-2496 (2010).
4. Conde, P. *et al.* DC-SIGN(+) Macrophages Control the Induction of Transplantation Tolerance. *Immunity.* **42** (6), 1143-1158 (2015).
5. Ginhoux, F., Schultze, J. L., Murray, P. J., Ochando, J., & Biswas, S. K. New insights into the multidimensional concept of macrophage ontogeny, activation and function. *Nat Immunol.* **17** (1), 34-40 (2016).
6. Quah, B. J., Wijesundara, D. K., Ranasinghe, C., & Parish, C. R. The use of fluorescent target arrays for assessment of T cell responses in vivo. *J Vis Exp.* (88), e51627 (2014).
7. Tario, J. D., Jr. *et al.* Optimized staining and proliferation modeling methods for cell division monitoring using cell tracking dyes. *J Vis Exp.* (70), e4287 (2012).
8. Poujol, F. *et al.* Flow cytometric evaluation of lymphocyte transformation test based on 5-ethynyl-2'deoxyuridine incorporation as a clinical alternative to tritiated thymidine uptake measurement. *J Immunol Methods.* **415** 71-79 (2014).
9. Last'ovicka, J., Budinsky, V., Spisek, R., & Bartunkova, J. Assessment of lymphocyte proliferation: CFSE kills dividing cells and modulates expression of activation markers. *Cell Immunol.* **256** (1-2), 79-85 (2009).
10. Corry, R. J., Winn, H. J., & Russell, P. S. Primarily vascularized allografts of hearts in mice. The role of H-2D, H-2K, and non-H-2 antigens in rejection. *Transplantation.* **16** (4), 343-350 (1973).
11. Liu, F., & Kang, S. M. Heterotopic heart transplantation in mice. *J Vis Exp.* (6), 238 (2007).
12. Ochando, J., Conde, P., & Bronte, V. Monocyte-Derived Suppressor Cells in Transplantation. *Curr Transplant Rep.* **2** (2), 176-183 (2015).
13. Gallina, G. *et al.* Tumors induce a subset of inflammatory monocytes with immunosuppressive activity on CD8+ T cells. *J Clin Invest.* **116** (10), 2777-2790 (2006).
14. Huang, B. *et al.* Gr-1+CD115+ immature myeloid suppressor cells mediate the development of tumor-induced T regulatory cells and T-cell anergy in tumor-bearing host. *Cancer Res.* **66** (2), 1123-1131 (2006).
15. Luan, Y. *et al.* Monocytic myeloid-derived suppressor cells accumulate in renal transplant patients and mediate CD4(+) Foxp3(+) Treg expansion. *Am J Transplant.* **13** (12), 3123-3131 (2013).
16. Tario, J. D., Jr., Muirhead, K. A., Pan, D., Munson, M. E., & Wallace, P. K. Tracking immune cell proliferation and cytotoxic potential using flow cytometry. *Methods Mol Biol.* **699** 119-164 (2011).

Article

Immunity

DC-SIGN+ Macrophages Control the Induction of Transplantation Tolerance

Graphical Abstract

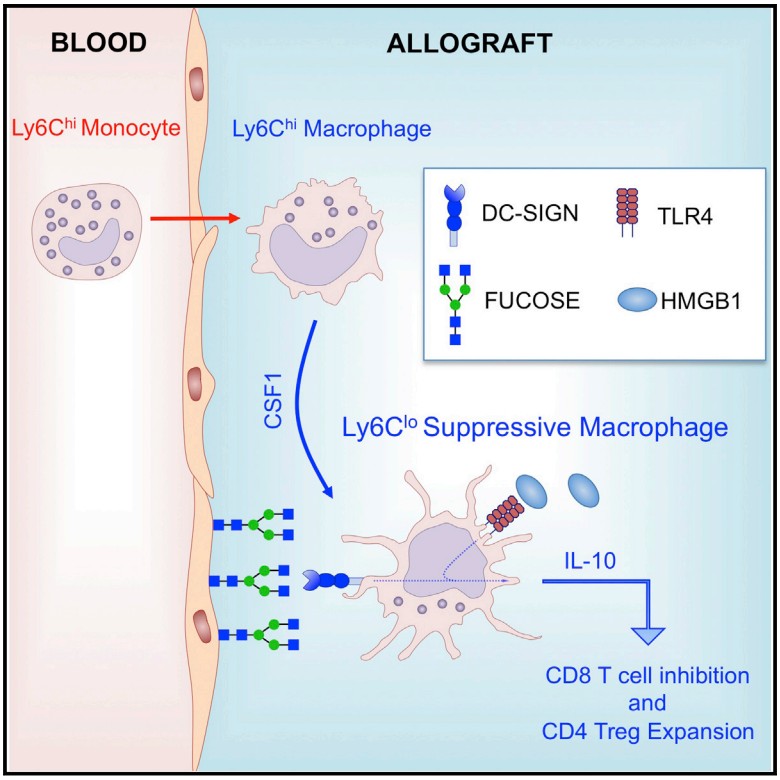

Authors

Patricia Conde, Mercedes Rodriguez, William van der Touw, ..., James Hutchinson, Shu-Hsia Chen, Jordi Ochando

Correspondence

jordi.ochando@mssm.edu

In Brief

Ochando and colleagues identify and characterize a subset of monocyte-derived macrophages that develop in the allografts of transplanted organs under costimulatory blockade. These DC-SIGN-expressing recipient macrophages are required for the induction of tolerance.

Highlights

- DC-SIGN+ macrophages inhibit CD8+ T cell proliferation and expand CD4+Foxp3+ Treg
- In vivo development of DC-SIGN+ macrophages is regulated by IFN-γ and CSF1
- IL-10 is essential for DC-SIGN+ macrophage-mediated suppression
- Simultaneous Fucose-DC-SIGN and HMGB1-TLR4 signaling is required for IL-10 production

Accession Number

GSE68648

Conde et al., 2015, Immunity *42*, 1–16
June 16, 2015
http://dx.doi.org/10.1016/j.immuni.2015.05.009

CellPress

Please cite this article in press as: Conde et al., DC-SIGN+ Macrophages Control the Induction of Transplantation Tolerance, Immunity (2015), http://dx.doi.org/10.1016/j.immuni.2015.05.009

DC-SIGN+ Macrophages Control the Induction of Transplantation Tolerance

Patricia Conde,[1] Mercedes Rodriguez,[2] William van der Touw,[3] Ana Jimenez,[3] Matthew Burns,[1] Jennifer Miller,[3] Manisha Brahmachary,[4] Hui-ming Chen,[3] Peter Boros,[5] Francisco Rausell-Palamos,[6] Tae Jin Yun,[7] Paloma Riquelme,[8] Alberto Rastrojo,[9] Begoña Aguado,[9] Joan Stein-Streilein,[10] Masato Tanaka,[11] Lan Zhou,[12] Junfeng Zhang,[13] Todd L. Lowary,[13] Florent Ginhoux,[14] Chae Gyu Park,[15] Cheolho Cheong,[7] Joshua Brody,[3] Shannon J. Turley,[16] Sergio A. Lira,[17] Vincenzo Bronte,[18] Siamon Gordon,[19] Peter S. Heeger,[1] Miriam Merad,[3] James Hutchinson,[8] Shu-Hsia Chen,[3] and Jordi Ochando[1,2,*]

[1]Department of Medicine, Icahn School of Medicine at Mount Sinai, New York, NY 10129, USA
[2]Immunología de Trasplantes, Centro Nacional de Microbiología, Instituto de Salud Carlos III, Madrid 28220, Spain
[3]Department of Oncological Sciences Icahn School of Medicine at Mount Sinai, New York, NY 10129, USA
[4]Department of Genetics and Genomic Sciences, Icahn School of Medicine at Mount Sinai, New York, NY 10129, USA
[5]Department of Surgery, Icahn School of Medicine at Mount Sinai, New York, NY 10129, USA
[6]Diabetes Obesity and Metabolism Institute, Icahn School of Medicine at Mount Sinai, New York, NY 10129, USA
[7]Institut de Researches Cliniques de Montréal, Montréal, Québec H2W1R7, Canada
[8]Department of Surgery, University Hospital Regensburg, Regensburg 93053, Germany
[9]Centro de Biología Molecular Severo Ochoa, Consejo Superior de Investigaciones Científicas-Universidad Autónoma de Madrid, Madrid 28049, Spain
[10]Schepens Eye Research Institute, Department of Ophthalmology, Harvard Medical School, Boston, MA 02114, USA
[11]Laboratory of Immune Regulation, Tokyo University of Pharmacy and Life Sciences, Tokyo 192-0392, Japan
[12]Department of Pathology, Case Western Reserve University, Cleveland, OH 44106, USA
[13]Alberta Glycomics Centre and Department of Chemistry, University of Alberta, Edmonton T6G 2G2, Canada
[14]Singapore Immunology Network, Agency for Science Technology and Research, Singapore 138648, Singapore
[15]Laboratory of Immunology, Yonsei University College of Medicine, Seoul 120-752, Korea
[16]Department of Cancer Immunology and AIDS, Dana-Farber Cancer Institute, Boston, MA 02284, USA
[17]Immunology Institute, Icahn School of Medicine at Mount Sinai, New York, NY 10129, USA
[18]Verona University Hospital, Verona 37129, Italy
[19]Sir William Dunn School of Pathology, University of Oxford, Oxford OX1 2JD, England
*Correspondence: jordi.ochando@mssm.edu
http://dx.doi.org/10.1016/j.immuni.2015.05.009

SUMMARY

Tissue effector cells of the monocyte lineage can differentiate into different cell types with specific cell function depending on their environment. The phenotype, developmental requirements, and functional mechanisms of immune protective macrophages that mediate the induction of transplantation tolerance remain elusive. Here, we demonstrate that costimulatory blockade favored accumulation of DC-SIGN-expressing macrophages that inhibited CD8+ T cell immunity and promoted CD4+Foxp3+ Treg cell expansion in numbers. Mechanistically, that simultaneous DC-SIGN engagement by fucosylated ligands and TLR4 signaling was required for production of immunoregulatory IL-10 associated with prolonged allograft survival. Deletion of DC-SIGN-expressing macrophages in vivo, interfering with their CSF1-dependent development, or preventing the DC-SIGN signaling pathway abrogated tolerance. Together, the results provide new insights into the tolerogenic effects of costimulatory blockade and identify DC-SIGN+ suppressive macrophages as crucial mediators of immunological tolerance with the concomitant therapeutic implications in the clinic.

INTRODUCTION

Myeloid cells with suppressive activity inhibit graft-reactive T cell immunity and facilitate induction of regulatory T (Treg) cells, together enabling the induction of transplantation tolerance (Dugast et al., 2008; Garcia et al., 2010; Zhang et al., 2008). An emerging consensus is that myeloid cells with immune regulatory function are contained within a population of CD11b+ mononuclear cells that express the myeloid differentiation antigen Gr-1 (Bronte et al., 2000; Bronte et al., 1998). Given the wide range of myeloid cells that might be included in this category, identifying specific myeloid subsets capable of mediating suppression, understanding the molecular basis of their developmental requirements, and deciphering the mechanisms that control their immune regulatory function represents a difficult task.

In previously published work, we demonstrated that monocytic cells that co-express CD11b, Gr-1, and the macrophage colony-stimulating factor 1 receptor (CSF1R) accumulate in cardiac allografts during tolerance induction, mediate T cell suppression in vitro, and are required for long-term graft survival induced by donor-specific transfusion plus anti-CD40L mAb

(Garcia et al., 2010). Building upon these published observations, and the recognition that Gr-1 comprises the distinct and independently regulated surface-expressed glycoproteins Ly6C and Ly6G (Fleming et al., 1993), we demonstrate that myeloid suppressive cells expressing $CD11b^+CSF1R^+Ly6C^{lo}Ly6G^-CD169^+$ are responsible for transplantation tolerance. Transcriptome analysis revealed that graft infiltrating immune regulatory $CD11b^+CSF1R^+Ly6C^{lo}Ly6G^-CD169^+$ monocyte-derived cells correspond to suppressive macrophages.

Blockade of the CD40L-CD40 costimulatory pathway promotes the conversion of immunogenic $CD11b^+CSF1R^+Ly6C^{hi}Ly6G^-CD169^-$ into suppressive $CD11b^+CSF1R^+Ly6C^{lo}Ly6G^-CD169^+$ macrophages through partial inhibition of interferon-γ (IFN-γ) production in the transplanted allograft. The conversion process requires CSF1, and interfering with this cytokine or its receptor (CSF1R) abrogates the induction of indefinite allograft survival. Mechanistically, we demonstrate that the dendritic cell-specific ICAM-grabbing non-integrin (DC-SIGN, CD209a) is upregulated in $CD11b^+CSF1R^+Ly6C^{lo}Ly6G^-CD169^+$-suppressive macrophages and that simultaneous DC-SIGN engagement by fucosylated ligands and TLR4 signaling is required for production of immunoregulatory interleukin-10 (IL-10) associated with immune regulation and prolonged allograft survival. In addition to delineating a unique set of phenotypic markers and offering new mechanistic insights into suppressive macrophage development and function during transplant tolerance, the data provide a foundation for developing robust protocols potentially capable of inducing immune regulatory macrophages for clinical use.

RESULTS

Suppressive Macrophages Accumulate during Tolerance Induction

To characterize myeloid cells that accumulate in allografts during tolerance induction, we transplanted BALB/c hearts ($H\text{-}2^d$) into fully mismatched C57BL6/MaFIA ($H\text{-}2^b$) recipient mice. These recipient animals constitutively express green fluorescent protein (GFP) under the CSF1R promoter, permitting us to identify recipient-derived graft-infiltrating myeloid cells that include monocytes, dendritic cells (DCs), macrophages, and neutrophils (Burnett et al., 2004). We treated groups of allograft recipients with anti-CD40L mAb (clone MR1) or with control anti-immunoglobulin G (IgG) mAb (Figure 1A), confirming previous work, which demonstrated that anti-CD40L mAb induced indefinite allograft survival, whereas rejection occurred by day 10 in the IgG-treated controls (Jiang et al., 2011). We harvested donor heart allografts on day 5 post-transplantation and analyzed graft-infiltrating leukocytes by flow cytometry. When we gated on live $CD45^+CD11b^+CSF1R^{GFP+}$ recipient graft-infiltrating myeloid cells, we discerned three major populations based on differential expression patterns of Ly6C and Ly6G (Figure 1B). Quantitative analysis revealed a higher frequency of $CD11b^+CSF1R^+Ly6C^{lo}Ly6G^-$ cells and a lower frequency of $CD11b^+CSF1R^+Ly6C^{hi}Ly6G^-$ cells in the allografts of anti-CD40L mAb-treated recipients compared to rejecting animals ($p < 0.01$). No differences in the frequencies of Ly6G cells were observed between groups.

We tested the ability of each myeloid cell subset to inhibit anti-CD3 and anti-CD28 stimulated $CD8^+$ naive T cell proliferation (Figure 1C). The $CD11b^+CSF1R^+Ly6C^{lo}Ly6G^-$ cell subset, but not the $CD11b^+CSF1R^+Ly6C^{hi}Ly6G^-$ cell subset obtained from anti-CD40L mAb treated recipients, was potently suppressive. The $CD11b^+CSF1R^+Ly6C^{int}Ly6G^+$ cell subset obtained from the anti-CD40L mAb-treated recipients also exhibited a modest suppressive activity. None of the myeloid cell subsets obtained from control IgG treated rejecting allografts exhibited in vitro suppression. We next tested the ability of each myeloid cell subset to induce expansion of $CD4^+Foxp3^+$ Treg cell in vitro (Figure 1D). Consistent with suppression assay results, only the $CD11b^+CSF1R^+Ly6C^{lo}Ly6G^-$ cells obtained from anti-CD40L mAb-treated recipients, promoted the expansion of $CD4^+Foxp3$ expressing Treg cell numbers. Thus, the graft-infiltrating $CD11b^+CSF1R^+Ly6C^{lo}Ly6G^-$ cell subset that accumulates in anti-CD40L mAb-treated recipients possess many of the properties reported to be associated with monocytic myeloid suppressor cells, including their ability of inhibit CD8 T cell proliferation (Gallina et al., 2006) and to promote $CD4^+Foxp3^+$ Treg cell number expansion (Huang et al., 2006).

Further gene array characterization of graft-infiltrating myeloid $CD11b^+CSF1R^+Ly6C^{lo}Ly6G^-$ cells that accumulate in tolerized recipients revealed that suppressive $CD11b^+CSF1R^+Ly6C^{lo}Ly6G$ correspond to macrophages (Gautier et al., 2012), but not dendritic cells (Miller et al., 2012) (Figure S1A). Morphological examination of flow-sorted graft-infiltrating myeloid subsets (Figure S1B) confirmed that myeloid $CD11b^+CSF1R^+Ly6C^{lo}Ly6G^-$ cells are of monocytic origin.

Suppressive Macrophages Are Required for Tolerance Induction

The transcriptional analyses of myeloid cell subsets revealed significantly higher transcript expression of CX3CR1, F4/80, CD206 (mannose macrophage receptor), CD68, CD172 (Sirp-α), CD169, and MHC-II in $Ly6C^{lo}$ suppressive macrophages from anti-CD40L mAb treated mice (Figure 2A). Flow cytometry confirmed higher expression of these proteins on suppressive macrophages, and we exploited their differential CD169 expression (Figure 2A and Figures S2A and S2B) along with the availability of CD169 diphtheria toxin receptor (DTR) mice (Miyake et al., 2007) to evaluate the suppressive function of $Ly6C^{lo}CD169^+$ macrophages in vivo. We transplanted BALB/c hearts into anti-CD40L mAb-treated WT or $CSF1R^{GFP+}/CD169^{DTR}$ C57BL6 recipients and treated them with DT on the day of transplantation to deplete recipient $CD169^+$ cells. Graft-infiltrating leukocytes by flow cytometry examined 5 days later (Figure 2B) showed specific depletion of recipient suppressive macrophages only in DT-treated animals. Depletion of $Ly6C^{lo}CD169^+$ macrophages in the anti-CD40L mAb-treated recipients was associated with accumulation of memory or activated $CD44^{hi}CD62L^{lo}$ $CD8^+$ T cells on day 5 (Figures 2C and 2D) and a reduced percentage of graft infiltrating $CD4^+Foxp3^+$ Treg on day 21 posttransplant (Figure 2E). To verify that in vitro suppressive $Ly6C^{lo}CD169^+$ macrophages also exhibit inhibitory function in vivo, we adoptively transferred CFSE-labeled CD8 T cells into anti-CD40L mAb-treated $CD169^{DTR}$ recipients and evaluated their ability to proliferate measured by CFSE dilution 5 days after DT treatment (Figure 2F). Whereas CD8 T cells transferred into tolerized recipients did not proliferate in vivo, CD8 T cells underwent proliferation in the allografts of tolerized

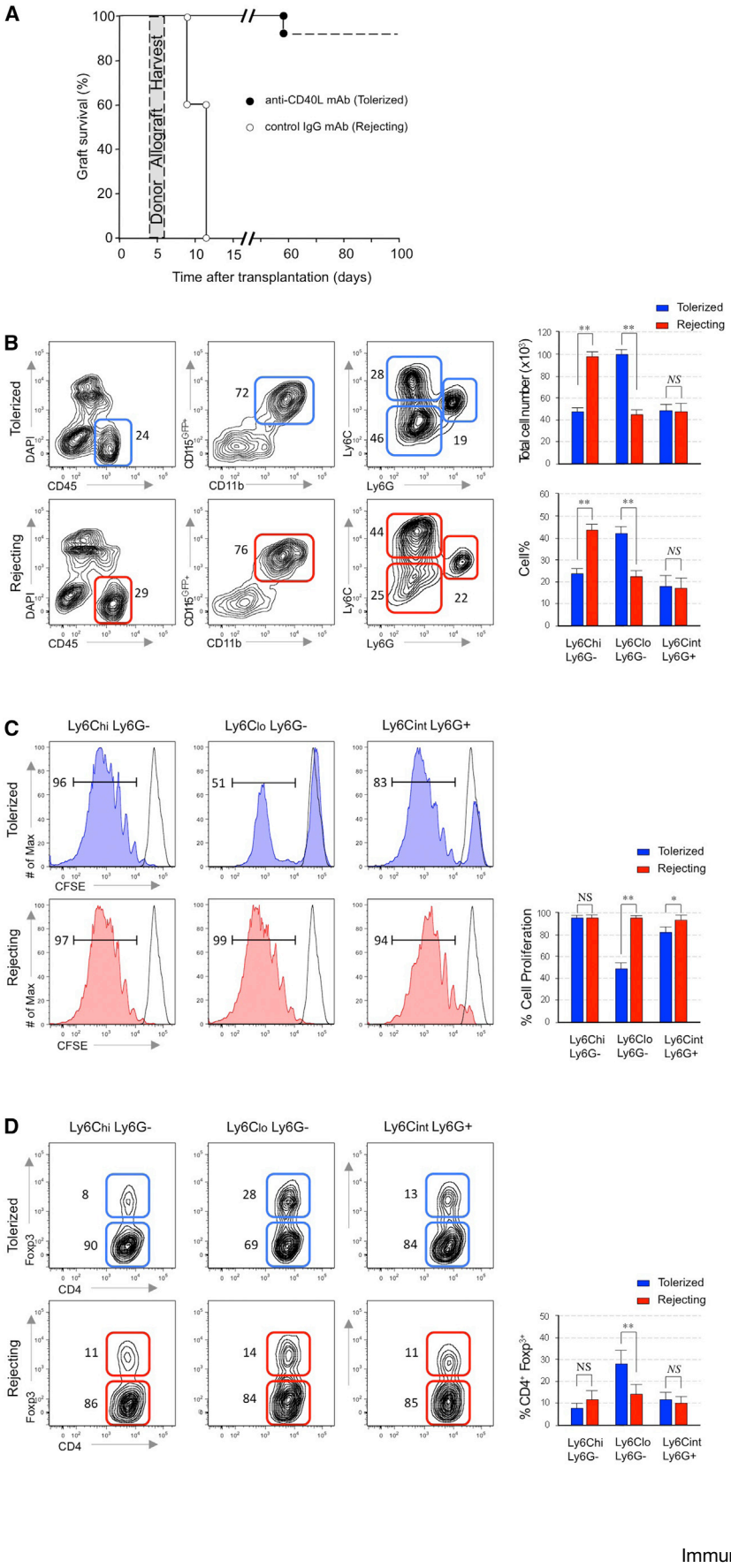

Figure 1. Suppressive Macrophages Accumulate during Tolerance Induction

(A) Graft survival of control IgG mAb (rejecting) and anti-CD40L mAb (tolerized) recipients of heterotopic cardiac allografts (n = 20 mice/group). The shaded area depicts heart allografts that were harvested at day 5 post-transplantation for subsequent analyses.

(B) Representative and quantitative flow cytometry results for Ly6C and Ly6G expression in $CD45^+CD11b^+CSF1R^{GFP}$ myeloid cell subsets from the allografts of tolerized and rejecting recipients at day 5 post-transplantation. Results represent mean ± SEM (n = 8 mice per group).

(C) In vitro suppressive capacity of each myeloid subset for $CD8^+$ T cells. Proliferation was measured by CSFE dilution after 96 hr by flow cytometry. Percentage of cell proliferation is presented as mean ± SEM of five independent experiments.

(D) In vitro Treg expansion of each myeloid subset. Flow cytometric analysis indicates Foxp3 expression on CD4 T cells after co-culture for 96 hr with myeloid subsets. Percentage of Treg expansion is presented as mean ± SEM of five independent experiments.

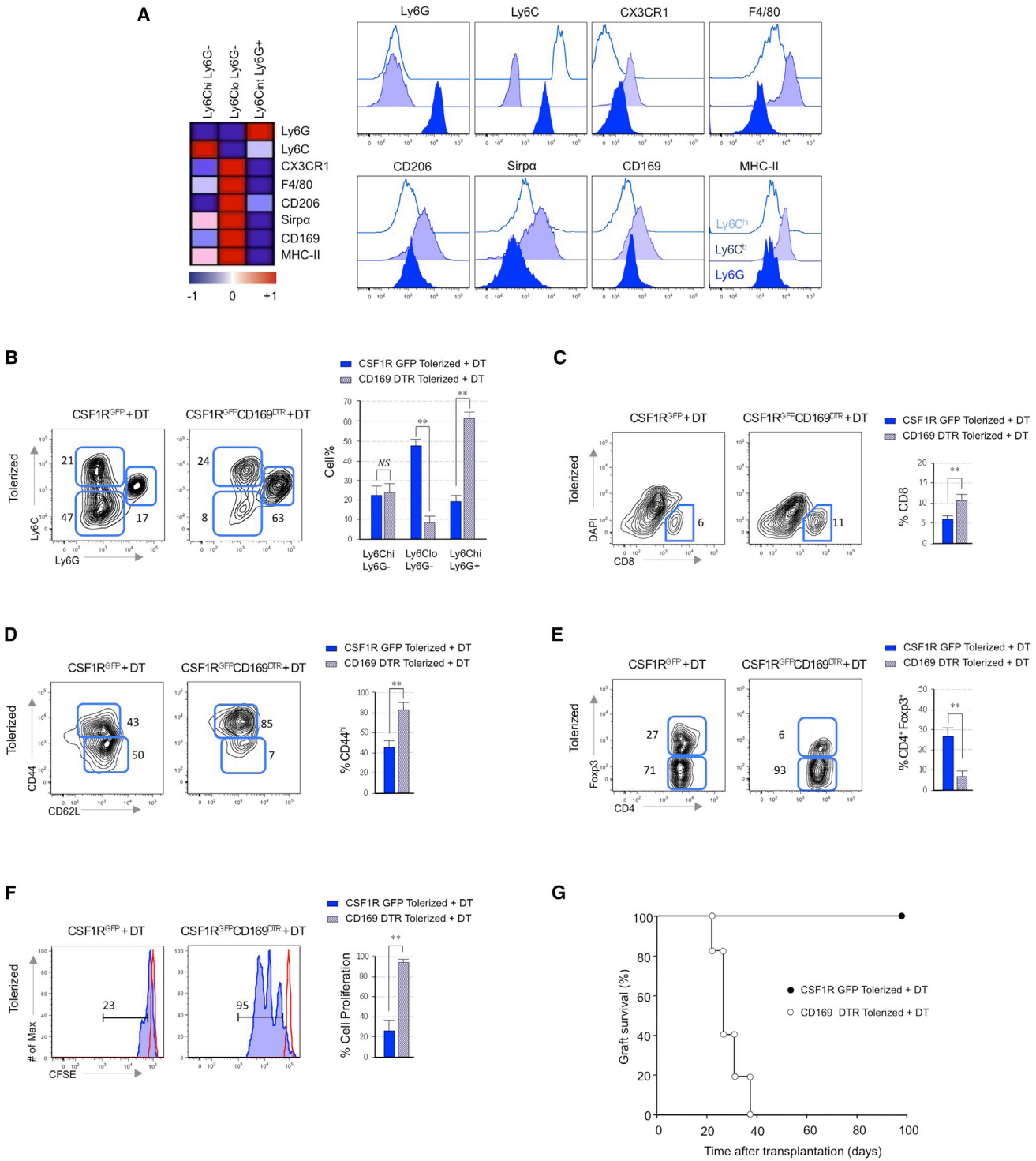

Figure 2. Suppressive Macrophages Are Required for Tolerance Induction

(A) Heatmap derived from microarray data of selected myeloid markers that achieve $p < 0.05$ in myeloid subsets from the allografts of tolerized recipients at day 5 post-transplantation (means of n = 3 per group). Representative flow cytometry plots of the above myeloid markers on each myeloid subset. Data is representative of three independent experiments.

(B) Representative and quantitative flow cytometry results of recipient myeloid cell subsets in the allografts of tolerized CSF1R^{GFP} (wild-type) and CSF1R^{GFP} CD169^{DTR} recipients at day 5 post-transplantation. Results represent mean ± SEM (n = 12 mice per group of 3 independent experiments).

(C and D) Representative and quantitative flow cytometry results depicting percentages (C) and surface memory/naive CD44/CD62L phenotypes (D) of graft infiltrating CD8 T cells after CD169^{+} macrophage depletion. Results represent mean ± SEM (n = 12 mice per group of 3 independent experiments).

(legend continued on next page)

recipients following depletion of CD169$^+$ suppressive macrophages. Moreover, graft survival experiments showed that DT induced in vivo depletion of CD169$^+$-suppressive macrophages resulted in graft rejection by day 30 despite tolerogenic treatment with anti-CD40L mAb ($p < 0.01$) (Figure 2G). Thus, Ly6C^{lo}CD169$^+$-suppressive macrophages that accumulate in the allografts of anti-CD40L mAb-treated recipients inhibit T cell immune responses in vivo and are required for the induction of transplantation tolerance.

CD40L Blockade Inhibits Accumulation of Immunogenic Macrophages

Graft-infiltrating myeloid subsets express CD40, but not CD40L (Figures S3A and S3B), suggesting that tolerogenic properties of the anti-CD40L mAb treatment are not due to a direct effect on monocyte-derived cells because they do not express CD40L. To test whether anti-CD40L mAb therapy induces suppressive macrophages via inhibiting transmission of a CD40-dependent signal on the myeloid cells, we attempted to circumvent the effects of the anti-CD40L mAb blockade by co-administering an agonistic anti-CD40 antibody FGK45.5, an antibody that has been shown to transmit CD40-dependent signals to APC in the absence of CD40L (Bennett et al., 1998; Rolink et al., 1996; Schoenberger et al., 1998). Administration of the agonistic anti-CD40 mAb promoted the accumulation of immunogenic Ly6C^{hi} macrophages in the allograft (Figure 3A). CD40-mediated accumulation of Ly6C^{hi} macrophages might be mediated by increased IFN-γ expression in the allografts of tolerized recipients (Jutila et al., 1988). To test for a link between CD40L-CD40 ligation and IFN-γ-mediated Ly6C^{hi} macrophage activation in our transplant model, we measured IFN-γ in the allografts of untreated recipients, tolerized recipients, and tolerized recipients co-treated with agonistic anti-CD40 mAb (Figure 3B). These assays showed reduction of intra-graft IFN-γ in the tolerized allografts compared to the untreated controls as previously reported (Hancock et al., 1996) but restoration of intra-graft IFN-γ observed in the anti-CD40 mAb co-treated recipient. On the contrary, agonistic CD40 ligation-mediated accumulation of immunogenic Ly6C^{hi} macrophages and increased intra-graft IFN-γ expression was not observed in tolerized CD40-deficient (*Cd40*$^{-/-}$) recipients (Figures 3C). Agonistic CD40 mAb abrogated the induction of tolerance despite CD40L blockade in wild-type (WT), but not in *Cd40*$^{-/-}$ recipients (Figure 3D). The data suggest that anti-CD40L mAb-induced tolerance can be abrogated by CD40 ligation, which favors the accumulation of Ly6C^{hi} immunogenic macrophages in the allograft through IFN-γ. To confirm this hypothesis, we treated tolerized recipients with recombinant IFN-γ and observed reduced intra-graft accumulation of Ly6C^{lo} macrophages on day 5 (Figure 3E) associated with allograft rejection (Figure 3F). Conversely, partial IFN-γ blockade restored accumulation of Ly6C^{lo} macrophages in the allografts (Figure 3G) and reestablished indefinite allograft survival (Figure 3H) in tolerized recipients despite agonistic anti-CD40 mAb treatment. Thus, costimulation blockade with anti-CD40L mAb prevents IFN-γ production and accumulation of immunogenic Ly6C^{hi} macrophages in the transplanted allografts.

CSF1 Mediates the Development of Suppressive Macrophages

The expression of CSF1R in CD11b$^+$CSF1R$^+$Ly6C^{lo}Ly6G$^-$ CD169$^+$-suppressive macrophages suggests an involvement of CSF1 in the development of these cells. We quantified CSF1 transcripts in transplanted mice by RT-PCR (Figure 4A) and observed significant upregulation of CSF1 in the allografts of anti-CD40L mAb-treated recipients. To test for a mechanistic link between CSF1 and development of Ly6C^{lo}-suppressive macrophages in anti-CD40L mAb-treated recipient mice, we transplanted BALB/c hearts into anti-CD40L mAb-treated tolerized C57BL6 recipients with or without neutralizing anti-CSF1 mAb (clone 5A1) at doses shown by others to inhibit their function in vivo (Gregory et al., 1992). Our results indicate that in vivo CSF1 blockade abrogated intra-graft accumulation of Ly6C^{lo} suppressive macrophages (Figure 4B). CSF1 blockade also prevented the in vivo expansion of CD4$^+$ Foxp3$^+$ Treg cell and abrogated the induction of transplantation tolerance (Figures 4C and 4D). In vivo blockade of CSF1R receptor (clone AFS98), at doses shown by others to inhibit their function in vivo (Hashimoto et al., 2011), also abrogated tolerance, which suggests that CSF1-CSF1R signaling is necessary for the development of suppressive macrophages. Ly6C^{hi} monocytes convert into Ly6C^{lo} macrophages (Arnold et al., 2007), the latter being able to function as suppressive cells in tumor models (Corzo et al., 2010). To test whether analogous mechanisms apply in transplant tolerance, we isolated CD11b$^+$CSF1R$^+$ Ly6C^{hi}Ly6G$^-$GFP$^+$ bone marrow monocytes from C57BL6/MaFIA mice and transferred them into C57BL6/WT recipients with or without anti-CD40L mAb and anti-CSF1 blocking mAb (Figure 4E). Whereas the Ly6C^{hi} monocytic precursors converted into Ly6C^{lo} macrophages in the allografts of anti-CD40L mAb-treated mice, Ly6C^{hi} monocytic precursors from anti-CSF1 mAb-treated recipient mice failed to convert and maintained a Ly6C^{hi} phenotype, similar to the untreated rejecting controls. Additional in vitro experiments confirmed that CSF1 mediates the conversion of Ly6C^{hi} monocytic precursors into Ly6C^{lo} myeloid cells that were functionally able to inhibit CD8$^+$ T cell proliferation and promote Treg expansion (Figures 4F and 4G). Our in vitro human data is consistent with this hypothesis and suggests that CSF1, but not CSF2, promotes the development of CD14 monocytes into suppressive monocyte-derived cells that inhibit CD8 T cell proliferation and expand Foxp3-expressing Treg in vitro (Figure S4A) Thus, anti-CD40L mAb-induced tolerance requires prevention of IFN-γ production and upregulation of CSF1, the latter driving conversion of monocytic precursors into suppressive macrophages.

(E) Representative flow cytometry results depicting percentages of Foxp3 expressing graft infiltrating CD4$^+$ T cells on day 21 post-transplantation in tolerized recipients with or without CD169$^+$ macrophage depletion. Results represent mean ± SEM (n = 4 mice per group of 3 independent experiments).

(F) Effects of CD169$^+$ macrophage depletion on in vivo T cell proliferation. CFSE-labeled CD8$^+$ T cells (5×10^6) were injected into tolerized CSF1R^{GFP} and CSF1R^{GFP} CD169^{DTR} recipients. Proliferation was measured in the allograft by CSFE dilution after 120 hr by flow cytometry. Results represent mean ± SEM (n = 4 mice per group of 3 independent experiments).

(G) Effects of CD169$^+$ macrophage depletion on graft survival in tolerized CSF1R^{GFP} and CSF1R^{GFP} CD169^{DTR} recipients (n = 12 mice/group).

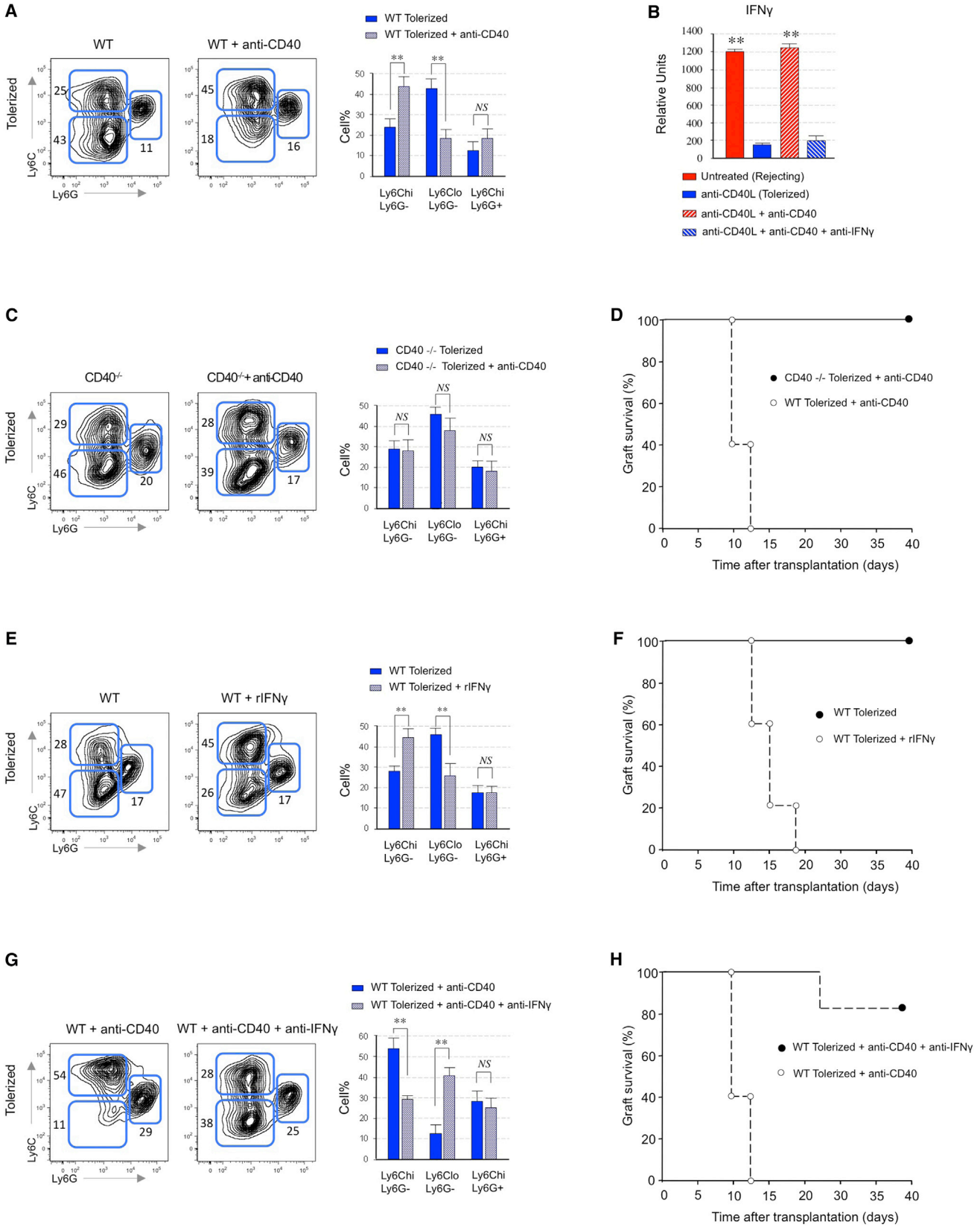

(legend on next page)

DC-SIGN Controls the Function of Suppressive Macrophages

CSF1 upregulates the expression of the dendritic-cell-specific intercellular adhesion molecule-3-grabbing non-integrin (DC-SIGN, CD209a) (Choi et al., 2011; Domínguez-Soto et al., 2011). Our gene array, real-time PCR, flow cytometry, and immunofluorescence studies revealed higher expression of DC-SIGN in macrophages obtained from the allografts of anti-CD40L mAb-treated mice, non-rejecting human renal transplant recipients, or in vitro derived CSF1-dependent human macrophages (Figures 5A–5C, Figures S5A–S5D). To test whether DC-SIGN is required for anti-CD40L mAb-induced allograft survival, we transplanted BALB/c hearts into WT C57BL6 recipients under the cover of anti-CD40L mAb, together with either a blocking anti-DC-SIGN mAb or an isotype IgG control. DC-SIGN blockade abrogated the induction of indefinite allograft survival in anti-CD40L mAb-treated mice (Figure 5D). When we isolated and compared graft-infiltrating leukocytes from anti-DC-SIGN mAb-treated recipients with control mice (all treated with anti-CD40L mAb), we observed similar frequencies of graft-infiltrating Ly6C^{lo}Ly6G$^-$ macrophages, suggesting that anti-DC-SIGN mAb treatment does not prevent intra-graft accumulation of Ly6C^{lo}Ly6G$^-$ macrophages (Figure 5E). However, whereas flow-sorted graft-infiltrating CD11b$^+$CSF1R$^+$Ly6C^{lo}Ly6G$^-$ macrophages from tolerized recipients suppressed CD8$^+$ T cell proliferation and expanded CD4$^+$Foxp3$^+$ Treg in vitro, flow-sorted CD11b$^+$CSF1R$^+$Ly6C^{lo}Ly6G$^-$ macrophages obtained from tolerized recipients treated with anti-DC-SIGN mAb did not exhibit either of these immune regulatory functions (Figure 5F). Finally, we flow-sorted CD11b$^+$CSF1R$^+$Ly6C^{lo}Ly6G$^-$-suppressive macrophages from anti-CD40L mAb-treated recipients and assessed their ability to suppress CD8$^+$ T cell proliferation and expanded CD4$^+$Foxp3$^+$ Treg following in vitro blockade of DC-SIGN by adding anti-DC-SIGN mAb to the cell cultures (Figure 5G). Thus, DC-SIGN expression is required for the immune regulatory function of suppressive macrophages that mediate indefinite allograft survival. Using DC-SIGN deficient (*CD209a*$^{-/-}$) and CD169^{DTR} tumor bearing mice our data revealed that depletion of CD169$^+$ macrophages or absence of DC-SIGN significantly reduces in vivo tumor growth (Figure S6A). Together with data from renal cell carcinoma patients showing increased DC-SIGN expression at the tumor site (Figure S6B), this suggests that DC-SIGN$^+$ macrophages also participate in the immune regulatory function that controls tumor progression.

Fucosylated DC-SIGN Ligands Are Required for Macrophage-Mediated Suppression and Tolerance

DC-SIGN binds to carbohydrates containing mannose or fucose residues, such as Lewis^X (van Liempt et al., 2006). We next investigated the role of fucosylated Lewis^X in the induction of transplantation tolerance using the α1,3/4-fucosyltransferases (FucTs) IV-VII double-deficient (dKO) donor mice, which display impaired Lewis^X expression (Lowe, 2002). We next used FucT-IV and FucT-VII mice as donors to evaluate the effects of Lewis^X inhibition on suppressive Ly6C^{lo} macrophages and tolerance. Figure 6A indicates that the Lewis^X expression was significantly reduced in tolerized dKO donor allografts, which was associated with acute rejection despite tolerogenic treatment with anti-CD40L mAb (Figure 6B). We next compared recipient graft-infiltrating leukocytes from donor dKO and WT allografts treated with anti-CD40L mAb, and we observed similar frequencies of graft-infiltrating Ly6C^{lo}Ly6G$^-$ macrophages (Figure 6C). These results suggest that Lewis^X deficiency does not prevent intragraft accumulation of Ly6C^{lo} macrophages. However, whereas flow-sorted graft-infiltrating Ly6C^{lo} macrophages from WT donors suppressed CD8$^+$ T cell proliferation and expanded CD4$^+$Foxp3$^+$ Treg cell in vitro, the flow-sorted Ly6C^{lo} macrophages obtained from dKO donor allografts did not exhibit neither of these immune regulatory functions (Figure 6D). We next investigated whether lacto-N-fucopentaose III (LNFPIII), a Lewis^X containing pentasaccharide that binds to DC-SIGN (Meyer et al., 2005), could overcome the fucosylated Lewis^X deficiency in dKO donor allograft recipients (Figure 6E). Our results indicate that unlike dextran (which does not bind to CD209a-mDC-SIGN [Takahara et al., 2004]), LNFPIII is able to restore tolerance in transplant recipients containing dKO donor allografts. Flow-sorted graft-infiltrating Ly6C^{lo} macrophages from LNFPIII-treated dKO donor allograft tolerized recipients were able to suppress CD8$^+$ T cell proliferation and expanded CD4$^+$Foxp3$^+$ (Figure 6F). Our results indicate that in vivo LNFPIII treatment restores the suppressive activity of Ly6C^{lo} macrophages. Thus, Lewis^X-mediated DC-SIGN ligation is necessary for the immune regulatory function of suppressive macrophages and for the induction of indefinite allograft survival.

Figure 3. CD40L Blockade Inhibits Accumulation of Immunogenic Macrophages

(A) Representative and quantitative flow cytometry results of recipient myeloid cell subsets in the allografts of tolerized WT recipients with or without co-treatment with agonistic CD40 mAb. Results represent mean ± SEM (n = 4 mice per group of 3 independent experiments).

(B) IFN-γ expression in cardiac allografts. Cardiac allografts were harvested 5 days after transplantation from each group. Agonistic anti-CD40 mAb was injected at 100 μg/mouse on days 0 and +1 relative to transplantation. Recombinant mouse IFN-γ was injected at 4 × 10^5 units/day for 10 days (n = 4 mice/group). Supernatants of single cell suspensions were analyzed for IFN-γ measured by ELISA. Bar graphs represent mean ± SEM of three independent experiments (**$p < 0.01$).

(C) Representative and quantitative flow cytometry results of recipient myeloid cell subsets in the allografts of tolerized CD40 deficient recipients with or without agonistic CD40 mAb treatment. Results represent mean ± SEM (n = 4 mice per group of 3 independent experiments).

(D) Effects of CD40 ligation on graft survival in tolerized WT and CD40 deficient recipients (n = 8 mice/group).

(E) Representative and quantitative flow cytometry results of recipient myeloid cell subsets in the allografts of tolerized WT recipients with or without recombinant IFN-γ treatment (4 × 10^5 units/day for 5 days). Results represent mean ± SEM (n = 4 mice per group of 3 independent experiments).

(F) Effects of recombinant IFN-γ on graft survival in tolerized WT recipients (n = 8 mice/group).

(G) Representative and quantitative flow cytometry results of recipient myeloid cell subsets in the allografts of tolerized WT recipients co-treated with agonistic CD40 mAb with or without anti-IFN-γ mAb treatment. Results represent mean ± SEM (n = 4 mice per group of 3 independent experiments).

(H) Effects of partial IFN-γ blockade on graft survival in tolerized wild-type recipients co treated with agonistic CD40 mAb (n = 8 mice/group).

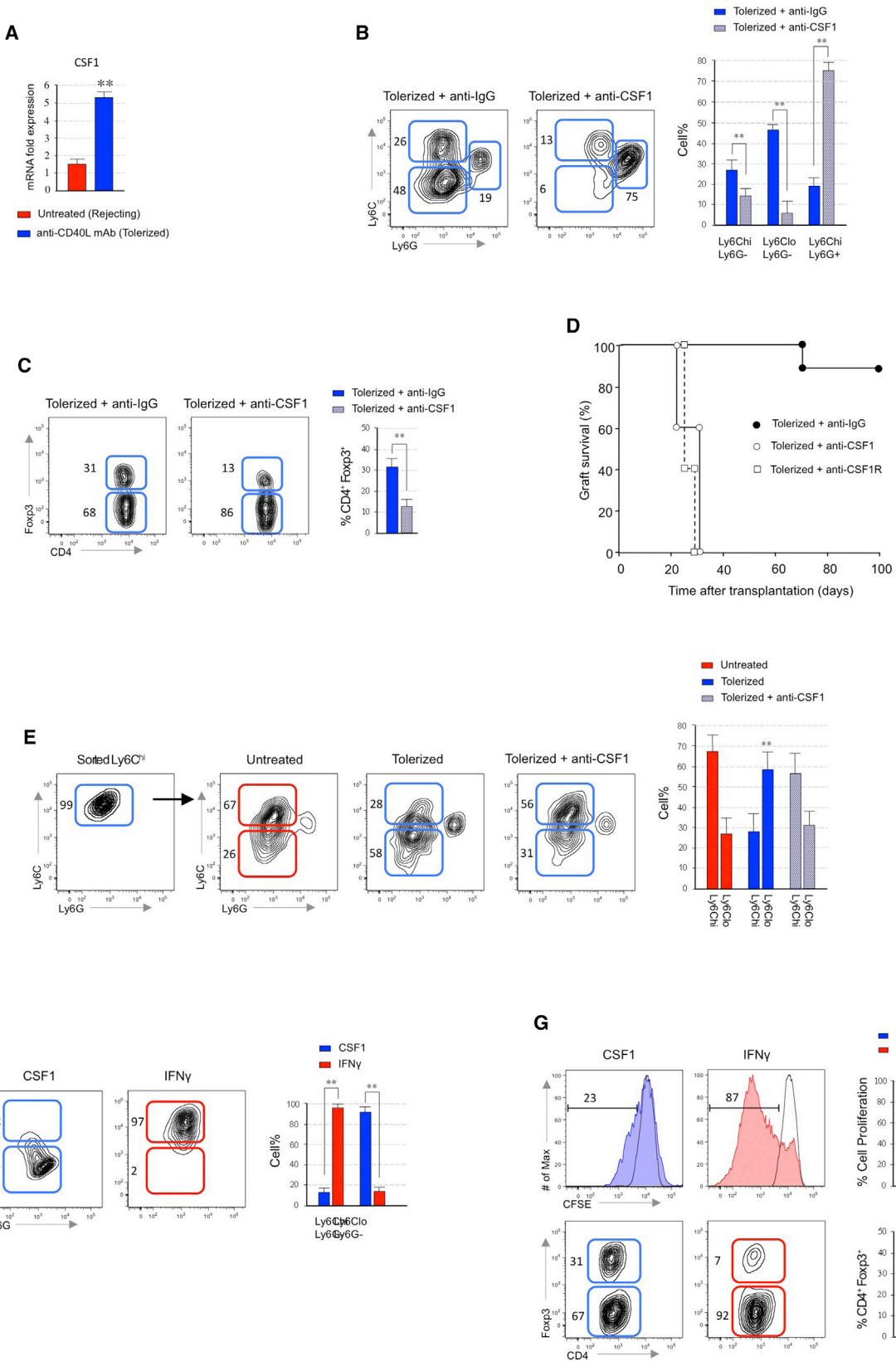

(legend on next page)

IL-10 Is Essential for DC-SIGN-Mediated Suppression

Fucose-specific DC-SIGN signaling results in production of IL-10 (Caparrós et al., 2006; Gringhuis et al., 2014). We observed a significant IL-10 upregulation in the allografts of anti-CD40L mAb-treated WT recipients compared to untreated rejecting controls (Figure 7A). In contrast, IL-10 was essentially absent in anti-CD40L mAb-treated DC-SIGN-deficient (*CD209a*$^{-/-}$) recipient mice. Among graft-infiltrating leukocytes, we detected the highest IL-10 expression in Ly6C^{lo} macrophages obtained from anti-CD40L mAb treated recipients, but the same Ly6C^{lo} macrophages obtained from the allografts of *CD209a*$^{-/-}$ recipients exhibited significant less IL-10 expression despite anti-CD40L mAb treatment (Figure 7A; Figure S7A). To specifically test whether IL-10 is required for regulatory macrophage function, we sorted intra-graft Ly6C^{lo} macrophages from anti-CD40L mAb treated IL-10-deficient (*Il10*$^{-/-}$) recipient mice and tested their ability to suppress CD8^{+} T cell proliferation and to expand CD4^{+}Foxp3^{+} Treg cell in vitro (Figure 7B). In the absence of IL-10, Ly6C^{lo} macrophages did not exhibit either of these immune regulatory functions despite tolerogenic treatment with anti-CD40L mAb. Using *CD209a*$^{-/-}$recipient mice, we next investigated whether recombinant IL-10 could restore the suppressive function of Ly6C^{lo} graft-infiltrating macrophages (Figure 7C). Although intra-graft *CD209a*$^{-/-}$Ly6C^{lo} macrophages were unable to suppress CD8^{+} T cell proliferation and to expand CD4^{+}Foxp3^{+} Treg in vitro, IL-10 addition rescued the immune regulatory function of *CD209a*$^{-/-}$ Ly6C^{lo} macrophages. Thus, graft-infiltrating DC-SIGN^{+}Ly6C^{lo} macrophages exert their immune regulatory function in part through an IL-10-dependent mechanism. Because crosstalk between DC-SIGN and TLR4 signaling is required for fucose binding-meditated production of IL-10 (Gringhuis et al., 2007; Gringhuis et al., 2014), we explored the effects of TLR4 deficiency in suppressive macrophages using tolerized TRL4 recipients, and showed that in the absence of TLR4 stimulation, IL-10 production was reduced in Ly6C^{lo} macrophages (Figure 7D), and their in vitro suppressive function was defective (Figure 7E). To demonstrate that synergistic DC-SIGN and TRL4 signaling was necessary for IL-10 production, we cultured bone marrow cells from WT, *CD209a*$^{-/-}$, and TRL4-deficient (*Tlr4*$^{-/-}$) mice and stimulated them with the DC-SIGN ligand Lewis^{X} and the TLR4 ligand high mobility group box 1(HMGB1) (Figure 7F). Simultaneous DC-SIGN and TRL4 signaling was necessary for optimal IL-10 production, and interfering with one of the signals resulted in impaired IL-10 production. We investigated whether ligation of DC-SIGN and/or TLR4 resulted in an increased inhibitory function (Figure 7G). Addition of both DC-SIGN and TLR4 agonists resulted in the highest suppressive function observed in monocyte-derived human cells in comparison with each of the ligands alone. Thus, DC-SIGN^{+} macrophages stimulated though DC-SIGN and TLR4 are negative regulators of the immune response and that their manipulation will open new avenues for therapeutic intervention either by inhibiting their function (i.e., in cancer patients) or by enhancing their suppressive effects and promoting their expansion (i.e., in transplant recipients).

DISCUSSION

We demonstrate here that DC-SIGN-expressing macrophages are required for the induction of transplantation tolerance. DC-SIGN is a type II transmembrane C-type lectin with a carbohydrate recognition domain, which is expressed in human DCs and macrophages (Geijtenbeek et al., 2000; Soilleux et al., 2002), and is involved in multiple aspects of the immunological response (van Kooyk and Geijtenbeek, 2003). Broxmeyer and colleagues reported that in vitro differentiation of monocytes in the presence of M-CSF and IL-4, which induces DC-SIGN expression (Martinez et al., 2006), are less efficient inductors of allogeneic mixed lymphocyte reactions (Li et al., 2004; Li et al., 2005). Here, we extend these findings to newly demonstrate that DC-SIGN^{+} macrophages inhibit T cell proliferation in vitro and in vivo in an experimental mouse model of solid organ transplantation. Additionally, we demonstrate that human DC-SIGN expressing macrophages stimulated with M-CSF and IL-4 (Figure S5D) induced the expansion of Foxp3-expressing Treg from allogeneic naive CD4^{+} T cell precursors in vitro, whereas macrophages treated with GM-CSF and IL-4 did not drive Treg expansion (Figure S4A).

The ability of murine DC-SIGN^{+} macrophages to promote IL-10-mediated transplantation tolerance requires two synergistic signals: DC-SIGN engagement by fucosylated ligands and TLR4 signaling. The CDR domain of human DC-SIGN recognizes fucosylated Lewis glycans (van Liempt et al., 2006) expressed by self and non-self antigens (Geijtenbeek et al., 2004). In humans, DC-SIGN ligation potentiates the secretion of IL-10 (Geijtenbeek et al., 2003). Because DC-SIGN macrophages secrete IL-10 upon fucose ligand engagement (Gringhuis et al., 2014) and participate in the generation of regulatory T cells (Cai et al., 2013; Smits et al., 2005), DC-SIGN could actively contribute to the maintenance of an immunosuppressive tissue environment, as proposed by Yvette van Kooyk's laboratory (van Gisbergen et al., 2005). Indeed, DC-SIGN ligation by non-immune cells,

Figure 4. CSF1 Mediates the Development of Suppressive Macrophages

(A) CSF1 expression in cardiac allografts. Cardiac allografts were harvested 5 days after transplantation from tolerized and rejecting recipients. Total single cell suspensions were analyzed for CSF1 measured by real-time PCR. Bar graphs represent mean ± SEM of three independent experiments (**p < 0.01).

(B) Representative and quantitative flow cytometry results of recipient myeloid cell subsets in the allografts of tolerized WT recipients co-treated with anti-CSF1 mAb. Results represent mean ± SEM (n = 4 mice per group of 3 independent experiments).

(C) Representative and quantitative flow cytometry results of Foxp3 expression on CD4 T cells in the allografts of tolerized recipients on day 21 post-transplantation following anti-CSF1 mAb treatment. Results represent mean ± SEM (n = 4 mice per group of 3 independent experiments).

(D) Effects of CSF1 and CSF1R blockade on graft survival in tolerized WT recipients (n = 12 mice/group).

(E) Representative and quantitative flow cytometry results of adoptively transferred CSF1R^{+}Ly6C^{hi} bone marrow cells into recipient mice treated with anti-CD40L mAb ± anti-CSF1 mAb 5 days after transplantation. Results represent mean ± SEM (n = 3 mice per group of 3 independent experiments).

(F) Representative and quantitative flow cytometry results of in vitro cultured Ly6C^{hi} bone marrow cells with either recombinant CSF1 or IFNγ for 96 hr. Results represent mean ± SEM of three independent experiments.

(G) Suppressive function of Ly6C^{hi} bone marrow cells after CSF1 or IFN-γ in vitro treatment. Results represent mean ± SEM of three independent experiments.

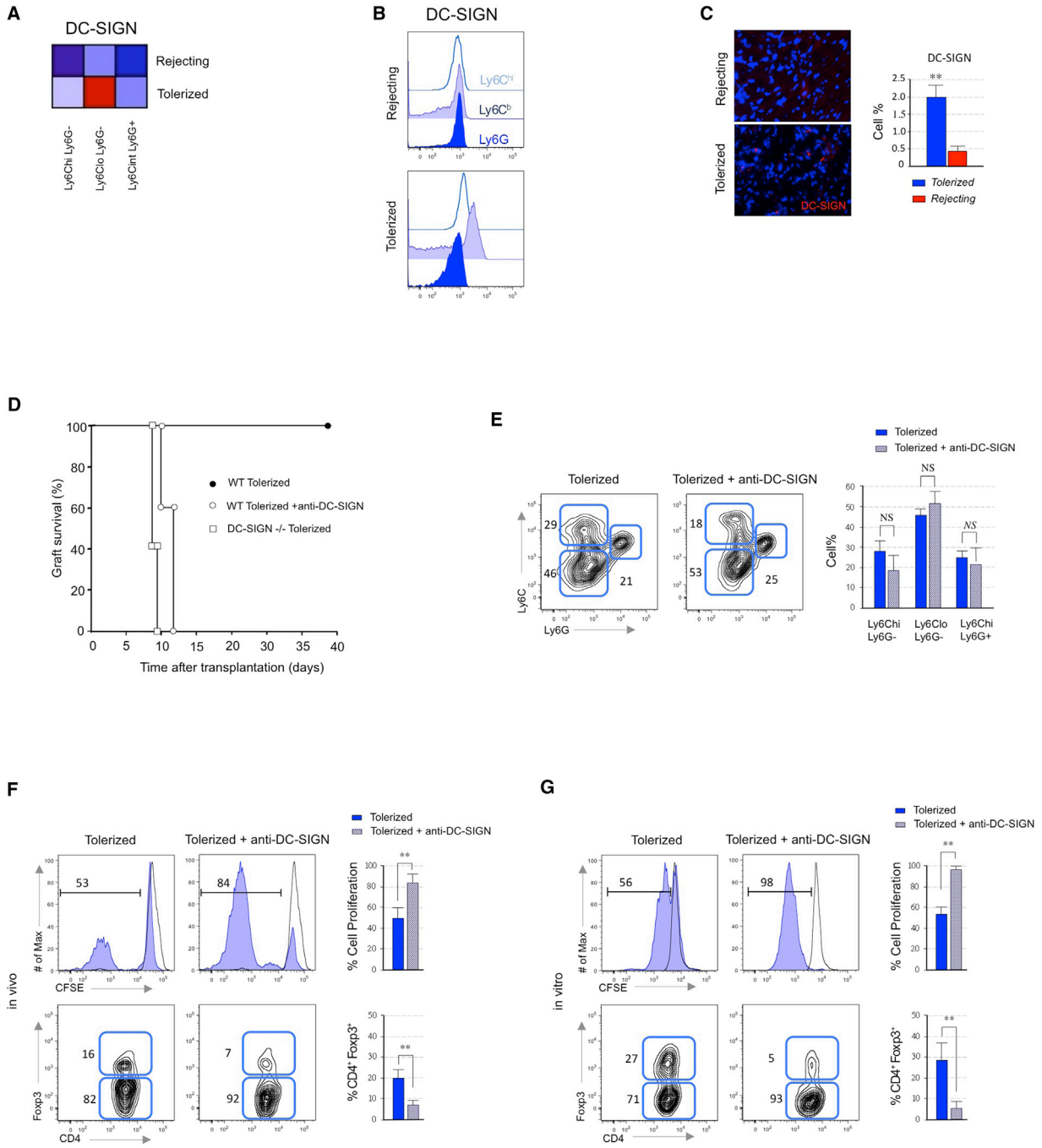

Figure 5. DC-SIGN Controls the Function of Suppressive Macrophages

(A and B) Heatmap derived from microarray data (A) and flow cytometry expression (B) of DC-SIGN in myeloid subsets from the allografts of tolerized and rejecting recipients at day 5 post-transplantation (means of n = 3 per group). Flow cytometry plots are representative of three independent experiments.

(C) Quantitative immunofluorescent analysis of tolerized and rejecting allografts at day 5 post-transplantation. Bar graphs represent frequency of DCSIGN+ cells expressed as percentage of a total of 1,000 DAPI nucleated cells from the allografts of tolerized and rejecting mice. Results represent mean ± SEM of 10 tissue sections from 4 cardiac allografts per group (**$p < 0.01$).

(D) Effects of DC-SIGN blockade and DC-SIGN deficiency on graft survival in tolerized WT recipients (n = 12 mice/group).

(E) Representative and quantitative flow cytometry results of recipient myeloid cell subsets in the allografts of tolerized WT recipients co-treated with anti-DC-SIGN mAb. Results represent mean ± SEM (n = 4 mice per group of 3 independent experiments).

(F) Representative and quantitative flow cytometry results of in vitro suppressive capacity and Treg expansion of Ly6C^{lo} macrophages from tolerized recipients co-treated with anti-DC-SIGN. Results represent mean ± SEM (n = 4 mice per group of 3 independent experiments).

(G) Suppressive function of Ly6C^{lo} macrophages from tolerized recipients after in vitro treatment with anti-DC-SIGN mAb. Results represent mean ± SEM of three independent experiments.

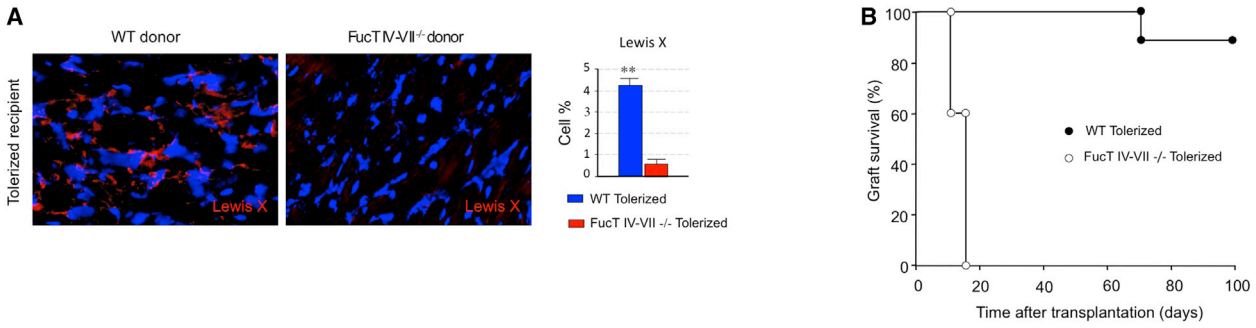

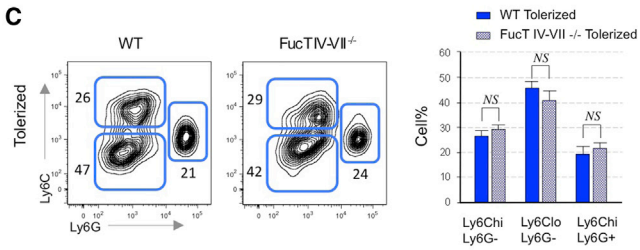

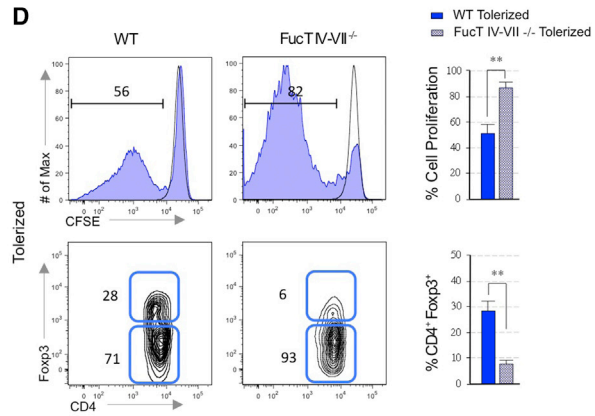

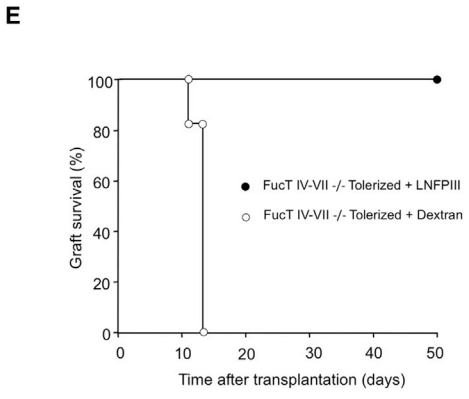

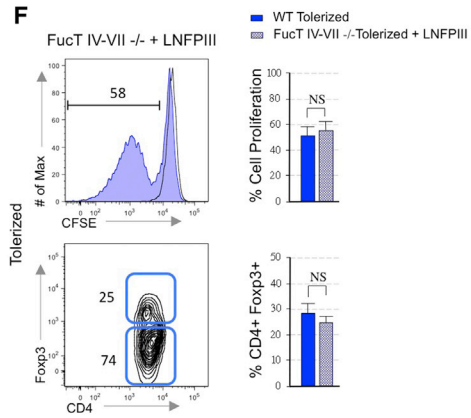

(legend on next page)

such as pathogens and tumor tissue results in immune escape (Geijtenbeek and Gringhuis, 2009), suggesting that both tumor and pathogens have ways to escape immune activation by targeting DC-SIGN. Consistent with this hypothesis our data reveals that depletion of CD169$^+$ macrophages or absence of DC-SIGN significantly reduces in vivo tumor growth (Figure S6A), suggesting that DC-SIGN$^+$ macrophages might participate in the immune regulatory function that controls tumor progression (Figure S6B). Our transplant results indicate that fucosylated glycans are present in the donor allografts of tolerized recipients that serve as ligands of DC-SIGN expressing macrophages. Using fucosyltransferase-deficient donor heart allografts inhibits the expression of Lewis^X glycoproteins and prevents the induction of indefinite allograft survival despite tolerogenic treatment with anti-CD40L mAb treatment. This suggests common mechanisms of immune regulation following engagement of DC-SIGN by tumor and transplant microenvironment via Lewis^X recognition that lead to the production of IL-10 producing macrophages (Domínguez-Soto et al., 2011; Nonaka et al., 2008; van Gisbergen et al., 2005).

Induction of transplantation mediated by DC-SIGN$^+$-suppressive macrophages depends on simultaneous TLR4 signaling. DC-SIGN signaling crosstalk with TLR4 has been demonstrated to mediate IL-10 production (Geijtenbeek et al., 2003; Gringhuis et al., 2007; Gringhuis et al., 2014). Here we report that DC-SIGN$^+$ macrophages from TLR4-deficient heart recipients produce significantly less IL-10 and do not exhibit suppressive function. Consistent with these results, a recent study indicates that during peripheral tolerance, DC-SIGN and TLR4 are required for IL-10 secretion and decreased T cell proliferation in mixed leukocyte reactions possibly caused by an increased frequency of Treg cell, which is associated with a high fucosyltransferase expression (García-Vallejo et al., 2014). In transplantation, while absence of absence of innate MyD88 signaling prevents acute allograft rejection and promotes inducible allograft acceptance (Goldstein et al., 2003; Walker et al., 2006), it is possible that specific signaling molecules of the MyD88 pathway, such as TRL4, might have a critical role in the induction of tolerance mediated by suppressive myeloid cells. In this respect, the TLR4 agonist HMGB1, which is upregulated during tissue damage associated with ischemia reperfusion (Wu et al., 2007) and surgical transplantation (Huang et al., 2007), has been recently demonstrated to enhance the immune-suppressive capacity of myeloid-derived suppressor cells through the production of IL-10 (Parker et al., 2014).

In conclusion, we demonstrate that graft-infiltrating DC-SIGN$^+$-suppressive macrophages mediate the induction of transplantation tolerance, revealing a previously unknown function of mouse DC-SIGN. Our delineation of a specific cell-surface phenotype for immunoregulatory, graft-protective suppressive macrophages in transplantation, as well as the mechanistic insights underlying the requirements for their differentiation in vivo, have important implications for understanding and potentially manipulating pathogenic immune responses. The C-type lectin DC-SIGN (CD209a) has a critical function in the induction of transplantation tolerance as demonstrated by its absence or in vivo blockade and might be used as phenotypic marker to define immune regulatory macrophages. The data provide a framework for developing CSF1-based in vitro protocols to induce therapeutic macrophages for clinical use to prevent transplant rejection and suggest that depleting or blocking suppressive macrophage development by targeting CSF1, which upregulates the expression of DC-SIGN, could be exploited to enhance anti-tumor immunity.

EXPERIMENTAL PROCEDURES

Mice

BALB/c, C57BL/6, C57BL/6-Foxp3tm1Flv/J, B6.129P2-Cd40tm1Kik/J, and B6.B10ScN-Tlr4lps-del/JthJ mice 8 weeks of age were purchased from The Jackson Laboratory. DC-SIGN-deficient mice (DC-Sign-KO, B6 [FVB]-Cd209atm1.1Cfg/Mmcd) were from the Mutant Mouse Regional Resource Centers, Consortium for Functional Glycomics (Scripps Res. Institute). The alpha(1,3)fucosyltransferases FucT-IV and FucT-VII double-deficient mice were from John Lowe (University of Michigan). The C57BL/6-Tg (Csf1r-EGFP-NGFR/FKBP1A/TNFRSF6) 2Bck/J MaFIA mice from D. Cohen (University of Kentucky) (Burnett et al., 2004). The C57BL/6 CD169^{DTR} mice have been previously described (Miyake et al., 2007). All experiments were performed with age- and sex-matched mice in accordance with Institutional Animal Care and Utilization Committee-approved protocols.

Vascularized Heart Transplantation

BALB/c hearts were transplanted as fully vascularized heterotopic grafts into C57BL/6 mice as previously described (Corry et al., 1973). Recipient mice were treated with 250 μg anti-CD40L mAb (clone MR1, BioXcell) for tolerance induction on days 0, 2, and 4 as previously described (Jiang et al., 2011). Graft function was monitored every other day by abdominal palpation. Untreated control mice received hamster IgG in PBS. Rejection was defined as complete cessation of a palpable beat and confirmed by direct visualization at laparotomy.

In Vivo Cell Depletion

For depletion of CD169 expressing CD11b$^+$CSF1R$^+$Ly6C^{lo}Ly6G$^-$ regulatory macrophages heterozygous CD169-DTR recipients were injected intraperitoneally (i.p.) with 10 ng/g body weight of DT (Sigma-Aldrich) 24, 48, and

Figure 6. Fucosylated DC-SIGN Ligands Are Required for Macrophage Mediated Suppression

(A) Quantitative immunofluorescent analysis of tolerized and rejecting allografts at day 5 post-transplantation. Bar graphs represent frequency of Lewis X$^+$ cells expressed as percentage of a total of 1,000 DAPI nucleated cells from tolerized mice receiving WT and fucosyltranferase (Fut) IV and VII double-deficient donor allografts. Results represent mean ± SEM of ten tissue sections from four cardiac allografts per group (**p < 0.01).

(B) Effects of Lewis^X deficiency on graft survival in tolerized WT recipients (n = 12 mice/group).

(C) Representative and quantitative flow cytometry results of recipient myeloid cell subsets in tolerized mice type receiving WT and FucT IV-VII dKO donor allografts. Results represent mean ± SEM (n = 4 mice per group of 3 independent experiments).

(D) Representative and quantitative flow cytometry results of in vitro suppressive capacity and Treg expansion of Ly6C^{lo} macrophages from the allografts of tolerized mice receiving WT and FucT IV-VII dKO donor allografts. Results represent mean ± SEM (n = 4 mice per group of 3 independent experiments).

(E) Effects of Lacto-N-fucopentaose III (LNFPIII) on graft survival in tolerized wild-type recipients (n = 8 mice/group).

(F) Representative and quantitative flow cytometry results of in vitro suppressive capacity and Treg expansion of Ly6C^{lo} macrophages from the allografts of tolerized mice receiving WT and FucT IV-VII dKO donor allografts following administration of LNFPIII. Results represent mean ± SEM (n = 4 mice per group of 3 independent experiments).

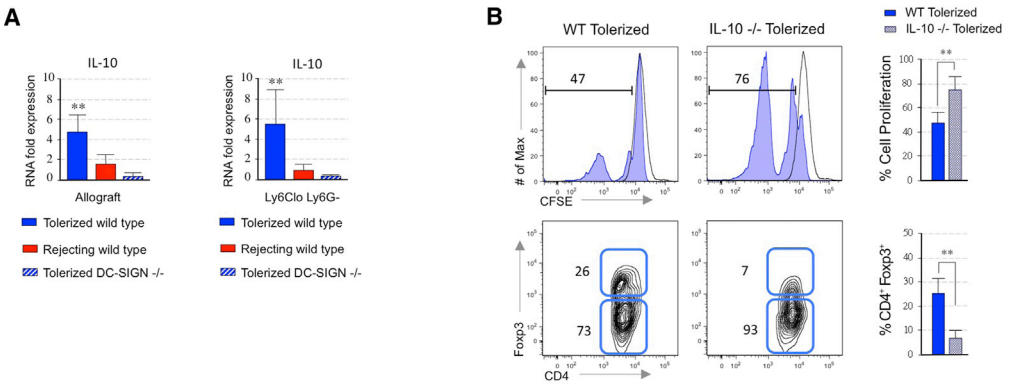

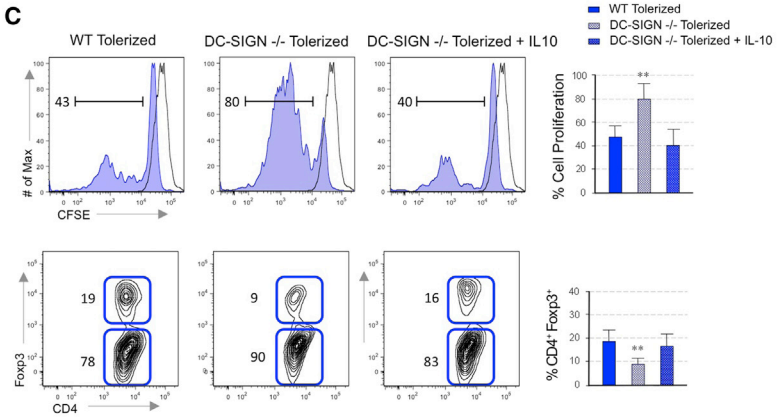

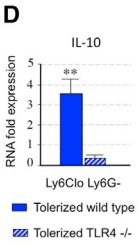

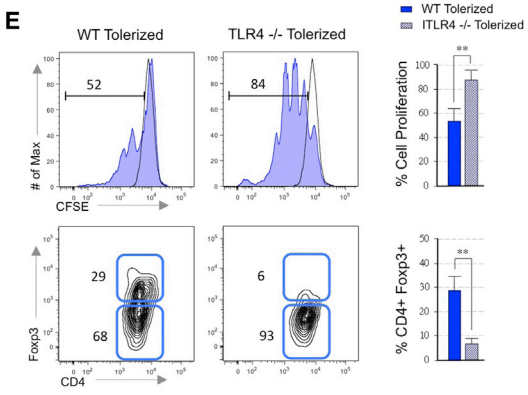

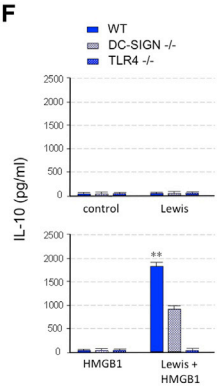

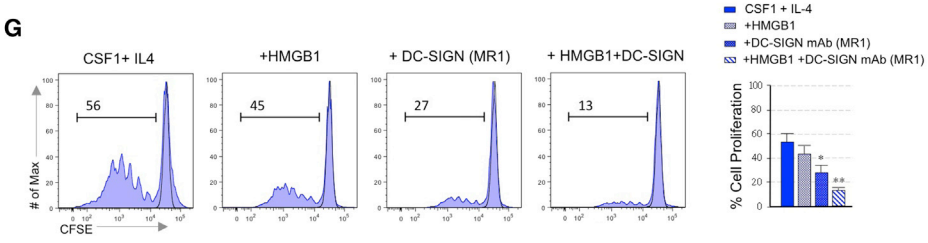

(legend on next page)

72 hr after transplantation (Miyake et al., 2007). Ly6G$^+$ cell depletion was induced with anti-Ly6G mAb clone 1A8 (BioXcell) injected at 0.5 mg i.p. on days –3, –2, and –1 relative to transplantation as previously described (Daley et al., 2008; Garcia et al., 2010).

Antibody-Mediated In Vivo Treatment

Agonistic anti-CD40 mAb (clone FGK4.5 mAb) was produced by BioXcell. CD40-mediated priming independent of CD40L was achieved by intravenous (i.v.) injection of 100 μg of agonistic anti-CD40 mAb on days 0 and +1 relative to transplantation (Gorbachev and Fairchild, 2004). Blocking antibody to IFN-γ (Clone R4-6A2) was produced by BioXcell. Anti-IFN-γ mAb was injected at 500 μg on days 0 and +1 relative to transplantation. Blocking antibody to CSF1 (clone 5A1) (Lokeshwar and Lin, 1988) and CSF1R (clone AFS98) (Sudo et al., 1995) were produced by BioXcell. Anti-CSF1 mAb was injected at 150 μg i.p. on days −1, +1, +2, +3, and +4 relative to transplantation, which is known to neutralize the biological functions of CSF1 in vivo (Gregory et al., 1992). Anti-CSF1R mAb was injected at 2 mg/mouse on day −5 and 0.5 mg/mouse on days −4 and −3, which is known to neutralize the biological functions of CSF1R in vivo (Hashimoto et al., 2011). Blocking antibody to DC-SIGN (CD209a) (Cheong et al., 2010) was mAb was purified from culture supernatant, grown in a CELLine Flask (BD) in serum-free medium (PFHM-II; Invitrogen) and injected at 250 μg i.p. on days +1, +2, +3, and +4 relative to transplantation.

Mouse Suppression Assay

Spleens of C57BL/6 or C57BL/6-Foxp3tm1Flv/J (H-2^b) mice were gently dissociated into single-cell suspensions, and red blood cells were removed using hypotonic ACK lysis buffer. Splenocytes were either stained with anti-CD4 mAb, or labeled with CFSE at 5 μM concentration (Molecular probes - Invitrogen) followed by staining with anti-CD8 mAb for 30 min on ice. Responder FoxP3$^+$CD4$^+$ and CFSE$^+$CD8$^+$ T cells were sorted using FACS Aria II (BD Biosciences) with a purity > 98%. Spleens of BALB/c (H-2^d) mice were gently dissociated into single-cell suspensions and were enriched for CD11c$^+$ cells using the EasySep Mouse CD11c Positive Selection Kit (StemCell). Enriched CD11c$^+$ splenocytes were stained with anti-mouse CD11c mAb and sorted using FACS Aria II (BD Biosciences) and were used together with anti-CD3 plus CD28 mAb (1 μg/ml) as stimulators. Stimulated FoxP3$^+$CD4$^+$ or CFSE$^+$CD8$^+$ T cells were cultures with graft infiltrating CD11b$^+$CSF1R$^+$Ly6C^{hi}Ly6G$^-$, CD11b$^+$CSF1R$^+$Ly6C^{lo}Ly6G$^-$, and CD11b$^+$CSF1R$^+$Ly6C^{int}Ly6G$^+$ myeloid cells for 4 days at 37°C in a 5% CO_2 incubator. T cell proliferation was measured by flow cytometric analysis of CFSE dilution on CD8$^+$ T cells. Treg expansion was measured by flow cytometric analysis of Foxp3-RFP on CD4$^+$ T cells.

ACCESSION NUMBER

The GEO accession number for the microarray data reported in this paper is GSE68648.

SUPPLEMENTAL INFORMATION

Supplemental Information includes seven figures and Supplemental Experimental Procedures and can be found with this article online at http://dx.doi.org/10.1016/j.immuni.2015.05.009.

ACKNOWLEDGMENTS

We thank Andres Hidalgo (Centro Nacional de Investigaciones Cardiovasculares, ISCIII) and Emmanuel Gautier (Department of Pathology & Immunology, Washington University) for critical review of the manuscript. We acknowledge the technical contributions of the Flow Cytometry, Microsurgery, and the Biorepository/Pathology Centers of Research Excellence at Mount Sinai, and the Alberta Glycomics Centre for their help on the LNFPIII synthesis. Acknowledgments to Marcy Kuentzel and Sridar Chittur at the University of Albany Center for Functional Genomics Microarray Core facility for their assistance in generating the microarray data. This work was supported by the COST Action BM1305: Action to Focus and Accelerate Cell Tolerogenic Therapies (A FACTT), the Mount Sinai Recanati/Miller Transplantation Institute developmental funds, AST/Pfizer Basic Science Faculty Development Grant, Ministerio de Educación y Ciencia SAF2010-15062, SAF2013-48834-R, and Fundación Mutua Madrileña grants to J.O. A portion of this work appears as part of the doctoral thesis of P.C.

Received: May 12, 2014
Revised: February 6, 2015
Accepted: April 6, 2015
Published: June 9, 2015

REFERENCES

Arnold, L., Henry, A., Poron, F., Baba-Amer, Y., van Rooijen, N., Plonquet, A., Gherardi, R.K., and Chazaud, B. (2007). Inflammatory monocytes recruited after skeletal muscle injury switch into antiinflammatory macrophages to support myogenesis. J. Exp. Med. *204*, 1057–1069.

Bennett, S.R., Carbone, F.R., Karamalis, F., Flavell, R.A., Miller, J.F., and Heath, W.R. (1998). Help for cytotoxic-T-cell responses is mediated by CD40 signalling. Nature *393*, 478–480.

Bronte, V., Wang, M., Overwijk, W.W., Surman, D.R., Pericle, F., Rosenberg, S.A., and Restifo, N.P. (1998). Apoptotic death of CD8+ T lymphocytes after immunization: induction of a suppressive population of Mac-1+/Gr-1+ cells. J. Immunol. *161*, 5313–5320.

Bronte, V., Apolloni, E., Cabrelle, A., Ronca, R., Serafini, P., Zamboni, P., Restifo, N.P., and Zanovello, P. (2000). Identification of a CD11b(+)/Gr-1(+)/CD31(+) myeloid progenitor capable of activating or suppressing CD8(+) T cells. Blood *96*, 3838–3846.

Figure 7. IL-10 Is Essential for DC-SIGN Mediated Suppression

(A) IL-10 expression in cardiac allografts and Ly6C^{lo} macrophages. Cardiac allografts from WT untreated, WT tolerized, and DC-SIGN KO tolerized recipients were harvested 5 days after transplantation. Total single cell suspensions and Ly6C^{lo} cells were analyzed for IL-10 measured by real-time PCR. Bar graphs represent mean ± SEM of three independent experiments (**p < 0.01).

(B) Representative and quantitative flow cytometry results of in vitro suppressive capacity and Treg expansion of Ly6C^{lo} macrophages from the allografts of tolerized IL-10 deficient recipient mice. Results represent mean ± SEM (n = 4 mice per group of 3 independent experiments).

(C) Representative and quantitative flow cytometry results of in vitro suppressive capacity and Treg expansion of Ly6C^{lo} macrophages from the allografts of tolerized DC-SIGN deficient recipient mice receiving in vitro IL-10 stimulation for 72 hr at 10 ng/ml. Results represent mean ± SEM (n = 4 mice per group of 3 independent experiments).

(D) IL-10 expression in cardiac allografts. Cardiac allografts from tolerized WT and TLR4 KO recipients were harvested 5 days after transplantation. Total single cell suspensions were analyzed for IL-10 measured by real-time PCR. Bar graphs represent mean ± SEM of three independent experiments (**p < 0.01).

(E) Representative and quantitative flow cytometry results of in vitro suppressive capacity and Treg expansion of Ly6C^{lo} macrophages from the allografts of tolerized TLR4 deficient recipient mice. Results represent mean ± SEM (n = 4 mice per group of 3 independent experiments).

(F) IL-10 expression in stimulated bone marrow cells from WT, DC-SIGN-deficient, and TLR4-deficient mice. Bone marrow cells were stimulated with Lewis^X (10 μg/ml) and recombinant HMGB1 (10 μg/ml) for 72 hr in vitro stimulation (control group non-stimulated). Supernatants of single cell suspensions were analyzed for IL-10 measured by ELISA. Results represent mean ± SEM of three independent experiments (**p < 0.01).

(G) Representative and quantitative flow cytometry results for in vitro suppressive capacity of human monocytes cultured with CSF1 plus IL-4. Results represent mean ± SEM of three independent experiments (*p < 0.05, **p < 0.01).

Burnett, S.H., Kershen, E.J., Zhang, J., Zeng, L., Straley, S.C., Kaplan, A.M., and Cohen, D.A. (2004). Conditional macrophage ablation in transgenic mice expressing a Fas-based suicide gene. J. Leukoc. Biol. *75*, 612–623.

Cai, M., Wu, J., Mao, C., Ren, J., Li, P., Li, X., Zhong, J., Xu, C., and Zhou, T. (2013). A Lectin-EGF antibody promotes regulatory T cells and attenuates nephrotoxic nephritis via DC-SIGN on dendritic cells. J. Transl. Med. *11*, 103.

Caparrós, E., Munoz, P., Sierra-Filardi, E., Serrano-Gómez, D., Puig-Kröger, A., Rodríguez-Fernández, J.L., Mellado, M., Sancho, J., Zubiaur, M., and Corbí, A.L. (2006). DC-SIGN ligation on dendritic cells results in ERK and PI3K activation and modulates cytokine production. Blood *107*, 3950–3958.

Cheong, C., Matos, I., Choi, J.H., Schauer, J.D., Dandamudi, D.B., Shrestha, E., Makeyeva, J.A., Li, X., Li, P., Steinman, R.M., and Park, C.G. (2010). New monoclonal anti-mouse DC-SIGN antibodies reactive with acetone-fixed cells. J. Immunol. Methods *360*, 66–75.

Choi, J.H., Cheong, C., Dandamudi, D.B., Park, C.G., Rodriguez, A., Mehandru, S., Velinzon, K., Jung, I.H., Yoo, J.Y., Oh, G.T., and Steinman, R.M. (2011). Flt3 signaling-dependent dendritic cells protect against atherosclerosis. Immunity *35*, 819–831.

Corry, R.J., Winn, H.J., and Russell, P.S. (1973). Primarily vascularized allografts of hearts in mice. The role of H-2D, H-2K, and non-H-2 antigens in rejection. Transplantation *16*, 343–350.

Corzo, C.A., Condamine, T., Lu, L., Cotter, M.J., Youn, J.I., Cheng, P., Cho, H.I., Celis, E., Quiceno, D.G., Padhya, T., et al. (2010). HIF-1α regulates function and differentiation of myeloid-derived suppressor cells in the tumor microenvironment. J. Exp. Med. *207*, 2439–2453.

Daley, J.M., Thomay, A.A., Connolly, M.D., Reichner, J.S., and Albina, J.E. (2008). Use of Ly6G-specific monoclonal antibody to deplete neutrophils in mice. J. Leukoc. Biol. *83*, 64–70.

Domínguez-Soto, A., Sierra-Filardi, E., Puig-Kröger, A., Pérez-Maceda, B., Gómez-Aguado, F., Corcuera, M.T., Sánchez-Mateos, P., and Corbí, A.L. (2011). Dendritic cell-specific ICAM-3-grabbing nonintegrin expression on M2-polarized and tumor-associated macrophages is macrophage-CSF dependent and enhanced by tumor-derived IL-6 and IL-10. J. Immunol. *186*, 2192–2200.

Dugast, A.S., Haudebourg, T., Coulon, F., Heslan, M., Haspot, F., Poirier, N., Vuillefroy de Silly, R., Usal, C., Smit, H., Martinet, B., et al. (2008). Myeloid-derived suppressor cells accumulate in kidney allograft tolerance and specifically suppress effector T cell expansion. J. Immunol. *180*, 7898–7906.

Fleming, T.J., Fleming, M.L., and Malek, T.R. (1993). Selective expression of Ly-6G on myeloid lineage cells in mouse bone marrow. RB6-8C5 mAb to granulocyte-differentiation antigen (Gr-1) detects members of the Ly-6 family. J. Immunol. *151*, 2399–2408.

Gallina, G., Dolcetti, L., Serafini, P., De Santo, C., Marigo, I., Colombo, M.P., Basso, G., Brombacher, F., Borrello, I., Zanovello, P., et al. (2006). Tumors induce a subset of inflammatory monocytes with immunosuppressive activity on CD8+ T cells. J. Clin. Invest. *116*, 2777–2790.

Garcia, M.R., Ledgerwood, L., Yang, Y., Xu, J., Lal, G., Burrell, B., Ma, G., Hashimoto, D., Li, Y., Boros, P., et al. (2010). Monocytic suppressive cells mediate cardiovascular transplantation tolerance in mice. J. Clin. Invest. *120*, 2486–2496.

García-Vallejo, J.J., Ilarregui, J.M., Kalay, H., Chamorro, S., Koning, N., Unger, W.W., Ambrosini, M., Montserrat, V., Fernandes, R.J., Bruijns, S.C., et al. (2014). CNS myelin induces regulatory functions of DC-SIGN-expressing, antigen-presenting cells via cognate interaction with MOG. J. Exp. Med. *211*, 1465–1483.

Gautier, E.L., Shay, T., Miller, J., Greter, M., Jakubzick, C., Ivanov, S., Helft, J., Chow, A., Elpek, K.G., Gordonov, S., et al.; Immunological Genome Consortium (2012). Gene-expression profiles and transcriptional regulatory pathways that underlie the identity and diversity of mouse tissue macrophages. Nat. Immunol. *13*, 1118–1128.

Geijtenbeek, T.B., and Gringhuis, S.I. (2009). Signalling through C-type lectin receptors: shaping immune responses. Nat. Rev. Immunol. *9*, 465–479.

Geijtenbeek, T.B., Torensma, R., van Vliet, S.J., van Duijnhoven, G.C., Adema, G.J., van Kooyk, Y., and Figdor, C.G. (2000). Identification of DC-SIGN, a novel dendritic cell-specific ICAM-3 receptor that supports primary immune responses. Cell *100*, 575–585.

Geijtenbeek, T.B., Van Vliet, S.J., Koppel, E.A., Sanchez-Hernandez, M., Vandenbroucke-Grauls, C.M., Appelmelk, B., and Van Kooyk, Y. (2003). Mycobacteria target DC-SIGN to suppress dendritic cell function. J. Exp. Med. *197*, 7–17.

Geijtenbeek, T.B., van Vliet, S.J., Engering, A., 't Hart, B.A., and van Kooyk, Y. (2004). Self- and nonself-recognition by C-type lectins on dendritic cells. Annu. Rev. Immunol. *22*, 33–54.

Goldstein, D.R., Tesar, B.M., Akira, S., and Lakkis, F.G. (2003). Critical role of the Toll-like receptor signal adaptor protein MyD88 in acute allograft rejection. J. Clin. Invest. *111*, 1571–1578.

Gorbachev, A.V., and Fairchild, R.L. (2004). CD40 engagement enhances antigen-presenting langerhans cell priming of IFN-gamma-producing CD4+ and CD8+ T cells independently of IL-12. J. Immunol. *173*, 2443–2452.

Gregory, S.H., Wing, E.J., Tweardy, D.J., Shadduck, R.K., and Lin, H.S. (1992). Primary listerial infections are exacerbated in mice administered neutralizing antibody to macrophage colony-stimulating factor. J. Immunol. *149*, 188–193.

Gringhuis, S.I., den Dunnen, J., Litjens, M., van Het Hof, B., van Kooyk, Y., and Geijtenbeek, T.B. (2007). C-type lectin DC-SIGN modulates Toll-like receptor signaling via Raf-1 kinase-dependent acetylation of transcription factor NF-kappaB. Immunity *26*, 605–616.

Gringhuis, S.I., Kaptein, T.M., Wevers, B.A., Mesman, A.W., and Geijtenbeek, T.B. (2014). Fucose-specific DC-SIGN signalling directs T helper cell type-2 responses via IKKε- and CYLD-dependent Bcl3 activation. Nat. Commun. *5*, 3898.

Hancock, W.W., Sayegh, M.H., Zheng, X.G., Peach, R., Linsley, P.S., and Turka, L.A. (1996). Costimulatory function and expression of CD40 ligand, CD80, and CD86 in vascularized murine cardiac allograft rejection. Proc. Natl. Acad. Sci. USA *93*, 13967–13972.

Hashimoto, D., Chow, A., Greter, M., Saenger, Y., Kwan, W.H., Leboeuf, M., Ginhoux, F., Ochando, J.C., Kunisaki, Y., van Rooijen, N., et al. (2011). Pretransplant CSF-1 therapy expands recipient macrophages and ameliorates GVHD after allogeneic hematopoietic cell transplantation. J. Exp. Med. *208*, 1069–1082.

Huang, B., Pan, P.Y., Li, Q., Sato, A.I., Levy, D.E., Bromberg, J., Divino, C.M., and Chen, S.H. (2006). Gr-1+CD115+ immature myeloid suppressor cells mediate the development of tumor-induced T regulatory cells and T-cell anergy in tumor-bearing host. Cancer Res. *66*, 1123–1131.

Huang, Y., Yin, H., Han, J., Huang, B., Xu, J., Zheng, F., Tan, Z., Fang, M., Rui, L., Chen, D., et al. (2007). Extracellular hmgb1 functions as an innate immune-mediator implicated in murine cardiac allograft acute rejection. American journal of transplantation: official journal of the American Society of Transplantation and the American Society of Transplant Surgeons *7*, 799–808.

Jiang, X., Sun, W., Guo, D., Cui, Z., Zhu, L., Lin, L., Tang, Y., Wang, X., and Liang, J. (2011). Cardiac allograft acceptance induced by blockade of CD40-CD40L costimulation is dependent on CD4+CD25+ regulatory T cells. Surgery *149*, 336–346.

Jutila, M.A., Kroese, F.G., Jutila, K.L., Stall, A.M., Fiering, S., Herzenberg, L.A., Berg, E.L., and Butcher, E.C. (1988). Ly-6C is a monocyte/macrophage and endothelial cell differentiation antigen regulated by interferon-gamma. Eur. J. Immunol. *18*, 1819–1826.

Li, G., Hangoc, G., and Broxmeyer, H.E. (2004). Interleukin-10 in combination with M-CSF and IL-4 contributes to development of the rare population of CD14+CD16++ cells derived from human monocytes. Biochem. Biophys. Res. Commun. *322*, 637–643.

Li, G., Kim, Y.J., and Broxmeyer, H.E. (2005). Macrophage colony-stimulating factor drives cord blood monocyte differentiation into IL-10(high)IL-12absent dendritic cells with tolerogenic potential. J. Immunol. *174*, 4706–4717.

Lokeshwar, B.L., and Lin, H.S. (1988). Development and characterization of monoclonal antibodies to murine macrophage colony-stimulating factor. J. Immunol. *141*, 483–488.

Lowe, J.B. (2002). Glycosylation in the control of selectin counter-receptor structure and function. Immunol. Rev. *186*, 19–36.

Martinez, F.O., Gordon, S., Locati, M., and Mantovani, A. (2006). Transcriptional profiling of the human monocyte-to-macrophage differentiation and polarization: new molecules and patterns of gene expression. J. Immunol. *177*, 7303–7311.

Meyer, S., van Liempt, E., Imberty, A., van Kooyk, Y., Geyer, H., Geyer, R., and van Die, I. (2005). DC-SIGN mediates binding of dendritic cells to authentic pseudo-LewisY glycolipids of Schistosoma mansoni cercariae, the first parasite-specific ligand of DC-SIGN. J. Biol. Chem. *280*, 37349–37359.

Miller, J.C., Brown, B.D., Shay, T., Gautier, E.L., Jojic, V., Cohain, A., Pandey, G., Leboeuf, M., Elpek, K.G., Helft, J., et al.; Immunological Genome Consortium (2012). Deciphering the transcriptional network of the dendritic cell lineage. Nat. Immunol. *13*, 888–899.

Miyake, Y., Asano, K., Kaise, H., Uemura, M., Nakayama, M., and Tanaka, M. (2007). Critical role of macrophages in the marginal zone in the suppression of immune responses to apoptotic cell-associated antigens. J. Clin. Invest. *117*, 2268–2278.

Nonaka, M., Ma, B.Y., Murai, R., Nakamura, N., Baba, M., Kawasaki, N., Hodohara, K., Asano, S., and Kawasaki, T. (2008). Glycosylation-dependent interactions of C-type lectin DC-SIGN with colorectal tumor-associated Lewis glycans impair the function and differentiation of monocyte-derived dendritic cells. J. Immunol. *180*, 3347–3356.

Parker, K.H., Sinha, P., Horn, L.A., Clements, V.K., Yang, H., Li, J., Tracey, K.J., and Ostrand-Rosenberg, S. (2014). HMGB1 enhances immune suppression by facilitating the differentiation and suppressive activity of myeloid-derived suppressor cells. Cancer Res. *74*, 5723–5733.

Rolink, A., Melchers, F., and Andersson, J. (1996). The SCID but not the RAG-2 gene product is required for S mu-S epsilon heavy chain class switching. Immunity *5*, 319–330.

Schoenberger, S.P., Toes, R.E., van der Voort, E.I., Offringa, R., and Melief, C.J. (1998). T-cell help for cytotoxic T lymphocytes is mediated by CD40-CD40L interactions. Nature *393*, 480–483.

Smits, H.H., Engering, A., van der Kleij, D., de Jong, E.C., Schipper, K., van Capel, T.M., Zaat, B.A., Yazdanbakhsh, M., Wierenga, E.A., van Kooyk, Y., and Kapsenberg, M.L. (2005). Selective probiotic bacteria induce IL-10-producing regulatory T cells in vitro by modulating dendritic cell function through dendritic cell-specific intercellular adhesion molecule 3-grabbing nonintegrin. J. Allergy Clin. Immunol. *115*, 1260–1267.

Soilleux, E.J., Morris, L.S., Leslie, G., Chehimi, J., Luo, Q., Levroney, E., Trowsdale, J., Montaner, L.J., Doms, R.W., Weissman, D., et al. (2002). Constitutive and induced expression of DC-SIGN on dendritic cell and macrophage subpopulations in situ and in vitro. J. Leukoc. Biol. *71*, 445–457.

Sudo, T., Nishikawa, S., Ogawa, M., Kataoka, H., Ohno, N., Izawa, A., Hayashi, S., and Nishikawa, S. (1995). Functional hierarchy of c-kit and c-fms in intramarrow production of CFU-M. Oncogene *11*, 2469–2476.

Takahara, K., Yashima, Y., Omatsu, Y., Yoshida, H., Kimura, Y., Kang, Y.S., Steinman, R.M., Park, C.G., and Inaba, K. (2004). Functional comparison of the mouse DC-SIGN, SIGNR1, SIGNR3 and Langerin, C-type lectins. Int. Immunol. *16*, 819–829.

van Gisbergen, K.P., Aarnoudse, C.A., Meijer, G.A., Geijtenbeek, T.B., and van Kooyk, Y. (2005). Dendritic cells recognize tumor-specific glycosylation of carcinoembryonic antigen on colorectal cancer cells through dendritic cell-specific intercellular adhesion molecule-3-grabbing nonintegrin. Cancer Res. *65*, 5935–5944.

van Kooyk, Y., and Geijtenbeek, T.B. (2003). DC-SIGN: escape mechanism for pathogens. Nat. Rev. Immunol. *3*, 697–709.

van Liempt, E., Bank, C.M., Mehta, P., Garciá-Vallejo, J.J., Kawar, Z.S., Geyer, R., Alvarez, R.A., Cummings, R.D., Kooyk, Yv., and van Die, I. (2006). Specificity of DC-SIGN for mannose- and fucose-containing glycans. FEBS Lett. *580*, 6123–6131.

Walker, W.E., Nasr, I.W., Camirand, G., Tesar, B.M., Booth, C.J., and Goldstein, D.R. (2006). Absence of innate MyD88 signaling promotes inducible allograft acceptance. J. Immunol. *177*, 5307–5316.

Wu, H., Chen, G., Wyburn, K.R., Yin, J., Bertolino, P., Eris, J.M., Alexander, S.I., Sharland, A.F., and Chadban, S.J. (2007). TLR4 activation mediates kidney ischemia/reperfusion injury. J. Clin. Invest. *117*, 2847–2859.

Zhang, W., Liang, S., Wu, J., and Horuzsko, A. (2008). Human inhibitory receptor immunoglobulin-like transcript 2 amplifies CD11b+Gr1+ myeloid-derived suppressor cells that promote long-term survival of allografts. Transplantation *86*, 1125–1134.

Curr Transpl Rep
DOI 10.1007/s40472-015-0054-9

CELLULAR TRANSPLANTS (A PILEGGI, SECTION EDITOR)

Monocyte-Derived Suppressor Cells in Transplantation

Jordi Ochando[1] · **Patricia Conde**[1] · **Vincenzo Bronte**[2]

Abstract Myeloid-derived suppressor cells (MDSC) are cells of myeloid origin with enhanced suppressive function. They are negative regulators of the immune responses and comprise a heterogeneous mixture of immunosuppressive cells of monocytic (M-MDSC) and granulocytic (G-MDSC) origin. A more recent nomenclature proposes the term "suppressive monocyte derived cells" (suppressive MCs) to define CSF1/CSF2-dependent mouse suppressor cells that develop from common monocyte progenitors (cMoPs) after birth. Here, we review the literature about monocytic-derived cells with demonstrated suppressor function in vitro and in vivo within the context of solid organ transplantation.

Keywords MDSC · Suppressor MCs · Transplantation · Immune regulation

Introduction

The mononuclear phagocyte system (MPS) comprises monocytes, macrophages, and dendritic cells (DCs). The terminology to define cell subsets that belong to the MPS is currently confusing, and a new classification of macrophages, monocytes, and DCs was recently proposed. In mice, two main subsets of monocytes (Ly6C^{hi}/CX3CR1^{lo} and Ly6C^{lo}/CX3CR1^{hi}) [1]; three main subsets of DCs (BATF3 dependent cDC1, IRF4 dependent cDC2, and E2-2 dependent pDC) [2]; and various types of tissue resident macrophages that originate during embryogenesis (Kupffer cells—liver, microglia—brain, Langerhans cells—epidermis, alveolar macrophages—lung) [3] have been defined. Upon inflammation, monocytes and DCs infiltrate the injured tissue and, along with the resident macrophages undergo activation, acquiring an inflammatory phenotype. This results in an overlapping expression of phenotypic markers, such as CD11c, F4/80, and MHC-II among these cell subsets, which makes it difficult to characterize specific myeloid cells under inflammatory conditions [4]. In an attempt to exploit immune regulatory mechanisms that take place during cancer progression and under other inflammatory pathological conditions, the term myeloid-derived suppressor cells (MDSC) was originally proposed to describe CD11b^{+}Gr-1^{+} expressing myeloid cells with the ability to suppress the immune response [5]. The terminology was widely accepted by the research community, including transplant immunologists, which reported the critical implication of monocytic MDSC (M-MDSC) in the prolongation of allograft survival. A more recent nomenclature of the MPS has been proposed based on ontogeny, location, function, and phenotype [2]. This latest classification provides a criterion to define new myeloid subsets and recommends the term suppressive monocyte-derived cells (suppressive MCs) as CSF1/CSF2-dependent suppressor cells that develop from common monocyte progenitors (cMoPs) after birth. Here, we provide a historical overview of monocyte-derived cells with demonstrated suppressive function in the context of solid organ transplantation.

This article is part of the Topical Collection on *Cellular Transplants*

✉ Jordi Ochando
jordi.ochando@mssm.edu

[1] Department of Medicine, Icahn School of Medicine at Mount Sinai, New York, USA

[2] Department of Pathology and Diagnostics, Verona University Hospital, Verona, Italy

Published online: 27 March 2015

Suppressive MCs in Solid Organ Transplantation

Allograft immunological unresponsiveness is associated with presence of suppressor cells in the transplanted recipients, which include cells of the lymphoid and the myeloid lineage [6]. In solid organ transplantation, Nicholas Tilney and Terry Strom first suggested the suppressive activity of graft infiltrating, monocyte-derived cells in 1977 [7]. The suppressive capacity of acute rejecting and enhanced rat cardiac allograft infiltrating cells (in which macrophages account for 10 % of the total) were analyzed by spontaneous blastogenesis using ^{3}H-thymidine incorporation. Using fractionation approaches, the authors reported that the greatest suppressive activity corresponded to adherent cells of enhanced recipients (90 %), in contrast to non-adherent cells obtained from rejecting recipients (15 %) [7]. Further analysis of the adherent cells present in the spleen confirmed the above results, suggesting that monocyte-derived inflammatory macrophages, which accumulate in the enhanced allografts early after transplantation, possessed suppressive function.

In 1979, seminal work from Hyung Mo Lee and colleagues reported macrophage-related suppressor cell function in human renal transplant recipients [8•]. The study delineated the immune reactivity of cells obtained from 66 renal transplant recipients under routine immunosuppressive therapy with prednisone and azathioprine. The suppressive activity of mononuclear cells from renal transplant recipients was assayed by adding recipient mononuclear cells to donor stimulated, third-party cytotoxic T lymphocytes responding against ^{51}Cr-labeled donor target cells. The percentage of lysis of target cells measured by ^{51}Cr release into the medium demonstrated that addition of mononuclear cells from renal transplant recipients suppressed cell-mediated lympholysis (CML) of donor cells in vitro. As controls for the suppressive function, the authors used non-donor fourth-party stimulated cytotoxic T lymphocytes and non-donor (recipient or irrelevant) ^{51}Cr-labeled target cells, showing no suppressive activity. This experiment confirmed the antigen-specific suppressive function of transplant recipient mononuclear cells. Further, the authors went onto demonstrate that the adherent cell fraction of the mononuclear cells from renal transplant patients, containing 54–82 % esterase positive monocytes/macrophages, was responsible for the donor specific suppression.

Shortly afterwards, Judith and Francis Thomas extended their findings using an experimental skin allograft transplant model in rhesus monkey recipients that received a 5-day course of anti-thymocyte globulin (ATG) treatment [9]. The in vitro mitogen-induced lymphoproliferative response was reduced by the adherent fraction of the peripheral blood mononuclear cells (PBMC) from ATG-treated versus untreated rhesus monkeys skin allograft recipients. Both concanavalin A (Con A)- and phytohemagglutinin (PHA)-induced lymphocyte blastogenesis were reduced significantly when prostaglandin synthetase-dependent adherent cells were added to the cultures, suggesting that suppressive macrophages mediated part of the ATG induced immunosuppressive function. These experiments confirmed in vitro previous findings linking the immunosuppressive function of ATG with the ability of macrophages to phagocyte lymphocytes. In 1969, Ivan Roitt and colleagues reported that the immunosuppressive capacity of anti-lymphocyte sera (ALS) and its ability to prolong skin graft survival was associated with the capacity of macrophages to opsonize lymphocytes in vitro [10]. The authors reported that cytoadherence represented an early step in the process of opsonization, which suggested that the immunosuppressive function of ALS was in part due to macrophage-mediated in vitro lymphocyte phagocytosis [11]. Similar results associated the suppressive function anti-lymphocyte globulin (ALG) with the rosette formation of lymphocytes around monocytes [12].

In 1983, an elegant study from Deborah Cameron further validated the suppressive function of macrophages present in transplant recipients [13]. Macrophages obtained from prednisone plus azathioprine treated human kidney transplant patients mediated cell cytotoxicity, as measured by release of ^{3}H-thymidine labeled target cells in vitro. Later in 1991, Kamada and colleagues reported two phases of cell-mediated suppressor activity, involving macrophages and regulatory T cells, respectively, in an experimental rat liver transplant model [14]. Early after transplantation (4–34 days), adherent suppressor macrophages present in the spleen of tolerant recipients mediated the in vitro inhibitory function measured by suppression of mixed leukocyte reactions, while late after transplantation (20 weeks), non-adherent suppressor T cells were responsible for the suppressive function of recipient splenic cells. Moreover, macrophage-mediated suppression was dependent on prostaglandins, since indomethacin inhibited their suppressive function [14]. These results suggested that non-specific suppressor macrophages develop in the spleens of tolerant liver transplant recipients.

The first report describing the suppressive activity of CD11b expressing monocytic cells was from by Myburgh and colleagues in 1995 [15]. Using non-human primates treated with total lymphoid irradiation as tolerogenic therapy, the authors characterized the antigen non-specific suppressor cells present in renal allograft recipients that inhibited in vitro mixed lymphocyte cultures. Depletion of CD11b or CD38 expressing cells resulted in loss of suppressive function of mononuclear cells obtained from the blood of transplanted baboons indicating that monocytes and NK cells mediated inhibition of cell proliferation. Suppression was mediated by a soluble factor, as inhibition of mixed lymphocyte cultures (MLC) separation of suppressor macrophages from responding T cells by a transwell cellulose membrane abrogated the in vitro suppressive activity. The authors went on to demonstrate that suppression was not mediated by PGE2 or by

de novo protein synthesis since neither indomethacin nor cycloheximide had any effect on macrophage-mediated T cell hyporesponsiveness. On the contrary, the lysosome-destabilizing adjuvant Leu-Leu-OMe (LLOMe), which induces lysosome rupture, degradation of inflammatory proteins, and necrotic cell death, revealed that LLOMe treatment abrogated the macrophage inhibitory effect.

MDSC in Solid Organ Transplantation

Using the MDSC terminology [5], Vanhove and colleagues were the first to report the critical role of MDSC in solid organ transplantation using an experimental kidney transplant model in rats [16]. Tolerance was induced by a costimulatory blockade with anti CD28 antibodies and $CD11b^+CD80/86^+Sirp\alpha^+$ expressing MDSC cells accumulated in the recipient allografts. The $CD11b^+Sirp\alpha^+$ expressing MDSC present in the blood and bone marrow inhibited proliferation of anti-CD3/CD28 stimulated T cells in a contact-dependent manner, while the same cells obtained from the lymph nodes or the spleen did not. The suppressive mechanisms of tolerance was in part mediated by the inducible nitric oxide synthase (iNOS), since in vivo treatment with the iNOS inhibitor aminoguanidine abrogated tolerance in long-term allograft survival recipients (<120 days post-transplantation), and all grafts were rejected acutely. The critical role for iNOS in MDSC-mediated T cell suppression was reported by Segal and colleagues in experiments using inducible NO synthase knockout mice, which demonstrated that NO inhibited of T cell proliferation in an antigen-specific and cell contact-dependent manner [17]. In a separate report, Vanhove's laboratory demonstrated that graft infiltrating $CD11b^+CD80/86^+Sirp\alpha^+$ expressing MDSC were responsible for the CCL5 gradient that directs Treg into the tolerized allograft during the induction of kidney allograft survival in rats [18].

In mice, MDSC express the cell surface markers CD11b (Mac-1) and Gr-1 [19, 20], and using these markers, Horuzsko and colleagues described a different mechanism by which MDSC mediated prolonged allograft survival [21]. Using an MHC-II mismatched bm12 skin transplants, which varies from its parental strain C57BL/6 at the I-A beta locus but are matched at all other major and minor histocompatibility antigens, the authors demonstrated that binding of HLA-G to the immunoglobulin-like transcript 2 (ILT-2) expressed in suppressive $CD11b^+Gr\text{-}1^+$ expanded MDSC in vivo. This expansion was associated to indefinite allograft survival of MHC-II mismached skin graft recipients. The data is consistent with a previous report from Suciu-Foca and colleagues, which reported that expression of the ILT2/3 mice homologue paired immunoglobulin-like receptor B (PIR-B) in myeloid cells associated with prolonged allograft survival a rat transplant model [22].

Le Moine and colleagues reported the critical role of heme oxygenase-1 (HO-1) in MDSC-mediated alloreactivity suppression [23]. Using the skin transplant system described above (bm12 MHC-II disparate skin grafts into C57BL/6 recipients), the authors reported that in vivo treatment with LPS resulted in the development of HO-1 expressing $CD11b^+GR\text{-}1^+$ MDSC that produced large amounts of IL-10. These LPS-induced MDSC were able to inhibit polyclonally activated $CD4^+$ and $CD8^+$ T cell proliferation in an antigen-specific dependent manner. The authors went on to demonstrate that HO-1 inhibition abrogated and prevented IL-10 production by MDSC. Further, they demonstrated the potential therapeutic applications of MDSC in prolonging allograft survival using adoptive transfer experiments. This is to our knowledge the first report of MDSC transfer to unmanipulated recipients to prolong graft survival. These findings are consistent with previous reports suggesting the critical role of HO-1 in the modulation of IL-10 and the promotion of tolerance to transplanted organs. Bach and colleagues reported that, while long-term tolerance was not achieved in HO-1 deficient recipients, induction of HO-1 expression by cobalt protoporphyrin IX led to a significant up-regulation of Foxp3, TGF-beta, IL-10, and CTLA4 associated with prolonged graft survival [24]. Specific overexpression of HO-1 following adenovirus-mediated (AdHO-1) gene transfer has been reported to prolong graft survival [25].

In a mouse heart transplantation model under costimulatory blockade with anti-CD40L mAb, Ochando and colleagues demonstrated the tolerogenic role of MDSC in solid organ transplantation [26••]. Using different depletional approaches, including antibodies against Gr-1 and Ly6G, CD11b-DTR mice, Macrophage Fas-Induced Apoptosis (MAFIA) mice, and clodronate liposomes, the authors reported that transplantation tolerance was dependent on $CD11b^+CD115^+GR\text{-}1^+$ MDSC that migrated from the bone marrow to the transplant organ shortly after transplantation, where they prevented the initiation of adaptive immune responses that lead to allograft rejection and participated in the development of Tregs. The authors further proposed that both iNOS and arginase-1 (Arg-1) mediated the suppressive function of monocytic $CD11b^+CD115^+GR\text{-}1^+$ suppressive cells. MDSC use these enzymes to mediate their suppressive function, both of which are implicated in the L-arginine metabolism: iNOS, leading to suppressive NO production and Arg-1, which causes a direct starvation of arginine within the microenvironment [27]. This study is consistent with a previous report which demonstrated that CD115 expressing MDSC induced antigen-specific Treg expansion and iNOS dependent T cell suppression in tumor-bearing mice [28].

Using a pancreatic islet transplantation in a diabetic mice, Bronte and colleagues described for the first time that organ rejection could be prevented by MDSC generated in vitro [29••]. Using a model of subcapsular islet transplantation in

diabetic mice, the authors demonstrated that transfer of MDSC generated with GM-CSF and IL-6 inhibited $CD8^+$ T cell priming and induced long-term acceptance of allogeneic islet allografts in the absence of immunosuppressive drug treatment. In the GM-CSF+IL-6 induced MDSCs treatment group, about 75 % of mice remained normoglycemic and healthy for the entire observation period of 200 days, analogously to all the control mice transplanted with syngeneic islets. Graft histology indicated a histological pattern not compatible with insulitis in the MDSC-treated group and demonstrated that the lymphocytic infiltration (comprising $CD4^+$, $CD8^+$ T cells, and $CD49b^+$ cells) was usually confined to the areas surrounding the insulin-positive graft. Tolerance was due the inhibition of IFN-γ production by T cells and was dependent on the expression of CCAAT/enhancer-binding protein β (C/EBPβ), which regulates myelopoiesis during emergency myelopoiesis and has a crucial role in controlling the differentiation of myeloid progenitors to MDSC. This results have been recently confirmed by Louvet and colleagues, which evaluated the potential of GM-CSF/IL-6 and LPS-induced MDSC to control auto- and allo-immunity [30].

Using MHC class II disparate skin allograft model, Inverardi and colleagues demonstrated the ability of the colony-stimulating factor 3 (CSF3) to induce IL-4Rα$^+$ MDSC in vivo following a short course of Neupogen treatment [31]. The authors further demonstrated that Neupogen mediated expansion of MDSC together with interleukin-2 complex (IL-2C) mediated expansion of Treg in vivo prolong allograft survival (MST=74 days). When looking into the mechanisms that were responsible for prolonged allograft survival, the authors indicated that synergistic treatment with Neupogen plus IL2-C resulted in an attenuated T cell response and reduction of cellular infiltrates into the allografts.

In addressing the involvement of alarmins in MDSC immunobiology, Thomson and Turnquist reported the crucial role for IL-33 in prolonging heart allograft survival in mice [32]. The authors demonstrated that IL-33 induces an increase in suppressive $CD11b^+Gr\text{-}1^+$ MDSC, together with an expansion of suppressive $ST2^+Foxp3^+$ regulatory T cells in an ST2 (IL-1R-like-1)-dependent-manner in vivo. These findings revealed a new immunoregulatory activity of IL-33 with cardioprotective properties, as it limits ST2 expression and cardiovascular pathology. A recent report from this group confirms the potential role of IL-33 in the generation of activated IL-33R/$ST2^+ICOS^{high}CD44^{high}Foxp3^+$ Treg [33]. In human kidney transplant recipients, IL-33 represents an innate inflammatory mediator that activates iNK cells during ischemia reperfusion injury, and neutralization of IL-33 has been proposed as a potential therapeutic target [34]. These results contrast previous murine findings suggesting that IL-33 increase CD11bhigh Gr-1int MDSC that favors immune deviation, Foxp3+ Treg expansion, reduces antibody-mediated rejection, and prolongs allograft survival during acute and chronic cardiac rejection [35, 36].

An elegant study from Zhao and colleagues elucidated part of the signaling pathway mediated in iNOS-dependent prolongation of allograft survival mediated by MDSC [37]. $CD11b^+Gr\text{-}1^+$ myeloid cells obtained from Smad3-deficient mice were shown to significantly inhibit alloantigen specific T cell responses, which resulted in a delayed allograft rejection in both skin and heart transplantation model in mice. These results reinforce the concept that transforming growth factor-β (TGF-β)/Smad3 signaling plays a complex role in the immune system, as TGF-β directly suppresses both the clonal expansion of $CD8^+$ T cells and their cell cytotoxicity in vivo [38]. The authors further demonstrated that Smad3-deficient MDSC were responsible for skewing T cells towards Th2-type immunity in transplanted Smad3−/− mouse recipients. Therefore, this study demonstrated that Smad3 is an intrinsic factor that inhibits the differentiation and immunosuppressive function of $CD11b^+Gr\text{-}1^+$ MDSC in mouse transplant models.

Luo and colleagues reported that infusions of donor splenocytes treated with 1-ethyl-3(3′-dimethylaminopropyl)-carbodiimide (ECDI-SPs) induced permanent donor-specific protection of islet allografts and prolonged cardiac allograft survival associated with intragraft accumulation of $CD11b^+IDO^+$ MDSC [39, 40]. Indoleamine 2,3 dioxygenase (IDO) activity limits T cell growth by depleting L-tryptophan and promotes T cell apoptosis by generating L-tryptophan-derived metabolites (i.e., kynurenins). Presence of intragraft $CD11b^+IDO^+$ population was dependent on $GR\text{-}1^+$ cells and either depletion of $GR\text{-}1^+$ cells or inhibition of IDO activity abrogated graft protection by ECDI-SPs. Additionally, the authors reported that induction of tolerance is critically dependent on PD1/PDL1 signaling pathway, $Foxp3^+$ Treg, and associated with increased IL-10 levels from in vitro stimulated T cells from ECDI-SPs treated recipients. In combination with a short course of rapamycin (day −1 to +8) ECDI-SPs induced long-term allograft survival (>150 days) in 100 % of the recipients. These results extend previous finding demonstrating that ECDI-fixed allogeneic splenocytes induced reduced CD8 T cell-mediated cytotoxicity in mixed lymphocyte reactions and in vivo CD4 T cell anergy [41, 42].

Lina Lu and colleagues reported the importance of stromal cells in the generation of graft protective MDSC [43]. Using an islet transplant model, the authors demonstrated that transfer of $CD11b^+$ and hepatic stellate cells (HSC) into the renal capsule of diabetic recipients differentiated $CD11b^+$ myeloid cells into potent MDSC that protected islet allograft and promoted long-term graft survival. MDSC protected the allografts by attenuating $CD8^+$ T cell alloreactivity and promoting antigen-specific Treg cell development through the B7-H1 pathway. Both in vitro and in vivo data demonstrated that B7-H1 was required for MDSC to exert immune regulatory

activity. The data extends previous findings from this group, which documented the induction of MDSC by HSC [44]. HSC-induced MDSC co-transplanted into the allografts expressed high levels of iNOS and Arg-1 and suppressed the proliferative response of both $CD4^+$ and $CD8^+$ T cells. Mechanistically, the authors showed that HSC lost their ability to induce MDSC when using HSC from IFNγR1 deficient mice, and suggested that MDSC induction was mediated by soluble factors produced by HSC, such as complement 3 [45]. A recent report from this group reported the beneficial effects of GM-CS and HSC in the generation of $iNOS^+$ MDSC [46].

Strober and colleagues elucidated the cellular and molecular mechanisms by which a conditioning regimen with total lymphoid irradiation, anti-thymocyte serum (ATS), and donor bone marrow transplant induced the expansion of IL-4Rα expressing MDSC that mediated the acceptance of cardiac allografts [47]. Specifically, the authors established that this conditioning regimen generates a tolerogenic environment with augmented numbers of IL-4Rα expressing MDSC and IL-4 secreting iNKT. Using iNKT-deficient ($CD1day^{-/-}$ and $Ja18^{-/-}$) and IL-4-deficient mice, the authors concluded that transplantation tolerance depended on MDSC-iNKT interaction and further implicated the possible role for Arg-1 in this clinically relevant conditioning regimen with the concomitant therapeutic applications. L-arginine is an amino acid essential for lymphocyte growth and differentiation, and depletion of L-arginine through Arg-1 inhibits T cell proliferation. The critical role for IL-4R expressing MDSC and Arg-1 dependent T cell suppression was initially described by Bronte and colleagues, who demonstrated that arginase mediated suppression by IL-4R expressing MDSC required IL-4 [48]. These findings are consistent with Myburgh's report [15], which suggested an interplay between MDSC and NK in the establishment of transplantation tolerance mediated by total lymphoid irradiation as induction therapy [49].

In human kidney transplant recipients, Murphy and colleagues reported for the first time that $CD11b^+CD33^+HLA\text{-}DR^-$ MDSC were capable of expanding Treg in vitro and their accumulation after transplantation correlated with an increase in Treg in vivo [50•]. MDSC-dependent expansion of Treg was suggested to be mediated by the production of soluble factors such as TGFβ and IL10. Consistent with this hypothesis, it has been reported that human $CD14^+HLA^-DR^{low/-}$ MDSCs favor the development of $Foxp3^+$ Treg through the production of TGFβ [51]. Interestingly, kidney transplant recipients of this study were treated with the synthetic corticosteroid prednisone. Glucocorticoids are given routinely to transplant recipient patients and induce IL-10 expression in $CD11b^+Gr\text{-}1^+$ MDSC [52]. A recent report in mice by Liu and colleagues confirmed the above results and extended Sunderkoetter's findings to demonstrate that dexamethasone induced MDSC prolong skin allograft survival though glucocorticoid receptor, IL-10 and iNOS dependent manner [49, 53].

Conclusions

One of the major goals in solid organ transplantation is the induction of long-term allograft survival in a mature immune system that is free from chronic rejection and lifelong treatment with immunosuppressive drugs and their side effects. The use of MDSC in transplantation therapy is moving forward, and current literature indicates that MDSC favor allograft tolerance in many ways (Fig. 1 highlights MDSC-dependent suppressive mechanisms that mediate graft survival). MDSC suppress inflammation and promote tissue repair in the allografts, exert immunosuppressive effects by secreting anti-inflammatory mediators, and induce alloantigen-specific Tregs, anergizing, and/or depleting recipient effector T cells. However, the complexity of the in vivo myeloid system in solid organ transplantation that regulates the immune response during strong sterile inflammatory conditions due to ischemia reperfusion injury of the donor organ and surgical anastomosis in the recipient makes it difficult to determine the specific mechanisms by which myeloid-derived subsets exert their inhibitory function. The original MDSC terminology includes multiple cell subsets as myelopoiesis refers to the differentiation of a myeloid progenitor into granulocytes, macrophages, mast cells, and dendritic cells. Myeloid cell subsets have been historically proposed based on morphology, cytochemistry, and flow cytometry, but the latest technological revolution in deep-sequencing, mass cytometry, and fate mapping experiments in vivo will enable us to classify myeloid cell subsets more appropriately. Using some of these novel approaches, Guilliams and collaborators have proposed the term monocyte-derived suppressive cells [2]. This recent classification may be more comprehensive in solid organ transplantation as it would include seminal studies from different laboratories that investigated the suppressive function of monocyte-derived cells. Hutchinson and colleagues reported the therapeutic potential of regulatory macrophages in human kidney transplant recipients and cardiac allograft transplanted mice

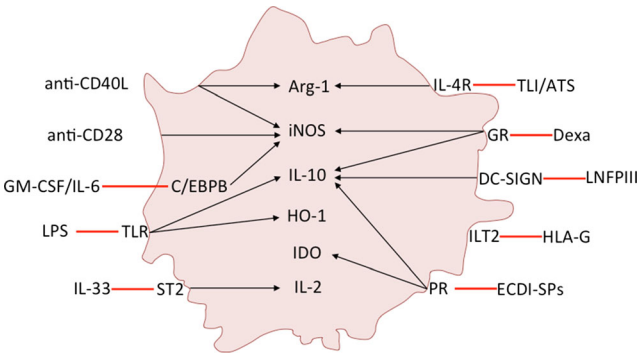

Fig. 1 Monocyte-derived suppressor cells in transplantation. The figure summarizes induction therapies and mechanisms of action of monocyte-derived suppressor cells in organ transplantation. *GR* glucocorticoid receptor, *PR* phagocytic receptor, *TLI/ALS* total lymphoid irradiation/anti-thymocyte serum

([54•], [55••]), and Burlingham and colleagues reported graft survival prolongation using Lacto-N-fucopentaose III activated macrophages [56]. On the other hand, and in contrast to G-MDSC depletional studies in tumor bearing mice [57], we demonstrated that depletion of Ly6G expressing granulocytic cells (clone A18) had no effect in tolerance, suggesting that only monocyte-derived cells are responsible for the induction of indefinite allograft survival in solid organ transplantation. In conclusion, clarification on how suppressive cells of the mononuclear phagocyte system are classified, consensus on which markers should be used for subset identification, and unified guidelines to characterize future suppressive cell subsets in solid organ transplantation is urgently needed.

Acknowledgments This work was supported by grants from the Italian Ministry of Health; Italian Ministry of Education (FIRB cup: B31J11000420001), Universities, and Research; Italian Association for Cancer Research (AIRC, grants 6599, 12182 and 14103) to Vincenzo Bronte and the Spanish Ministry of Education (SAF2013-48834-R) to Jordi Ochando.

Compliance with Ethics Guidelines

Conflict of Interest Jordi Ochando and Patricia Conde declare that they have no conflict of interest.

Vincenzo Bronte reports he has been a consultant/independent contract for Jounce Therapeutics Inc., and an advisor/board member for F. Hoffmann - La Roche LTD.

Human and Animal Rights and Informed Consent This article does not contain any studies with human or animal subjects performed by any of the authors.

References

Papers of particular interest, published recently, have been highlighted as:
- • Of importance
- •• Of major importance

1. Geissmann F, Jung S, Littman DR. Blood monocytes consist of two principal subsets with distinct migratory properties. Immunity. 2003;19(1):71–82.
2. Guilliams M, Ginhoux F, Jakubzick C, Naik SH, Onai N, Schraml BU, et al. Dendritic cells, monocytes and macrophages: a unified nomenclature based on ontogeny. Nat Rev Immunol. 2014;14(8):571–8.
3. Perdiguero EG, Klapproth K, Schulz C, Busch K, Azzoni E, Crozet L, et al. Tissue-resident macrophages originate from yolk-sac-derived erythro-myeloid progenitors. Nature. 2015;518(7540):547-51.
4. Ferenbach D, Hughes J. Macrophages and dendritic cells: what is the difference? Kidney Int. 2008;74(1):5–7.
5. Gabrilovich DI, Bronte V, Chen SH, Colombo MP, Ochoa A, Ostrand-Rosenberg S, et al. The terminology issue for myeloid-derived suppressor cells. Cancer Res. 2007;67(1):425. *author reply 426*.
6. Furuzawa-Carballeda J, Lima G, Simancas P, Ramos-Bello D, Simancas M, Bostock IC, et al. Peripheral regulatory cells immunophenotyping in kidney transplant recipients with different clinical profiles: a cross-sectional study. J Transplant. 2012;2012:256960.
7. Tilney NL, Strom TB, Booth DB, Finnegan A, Lundin P, Carpenter CB. Identification, cytotoxicity, and suppressor activity of infiltrating cells from enhanced organ allografts. Transplant Proc. 1977;9(1):713–5.
8.• Thomas J, Thomas F, Hoffmann S, Johns C, Lee HM. Macrophage-related suppressor cells in human renal transplant recipients. Surgery. 1979;86(2):266–74. *This seminal manuscript provided the first evidence that long-term acceptance of histoincompatible allografts with an adaptation of the host immune response was mediated by suppressor macrophages that inhibited effector mechanisms of graft rejection.*
9. Thomas JM, Carver FM, Haisch CE, Fahrenbruch G, Deepe RM, Thomas FT. Suppressor cells in rhesus monkeys treated with antithymocyte globulin. Transplantation. 1982;34(2):83–9.
10. Greaves MF, Tursi A, Playfair JH, Torrigiani G, Zamir R, Roitt IM. Immunosuppressive potency and in-vitro activity of antilymphocyte globulin. Lancet. 1969;1(7585):68–72.
11. Martin WJ. Assay for the immunosuppressive capacity of antilymphocyte serum. 3. Opsonizing activity of anti-human lymphocyte serum. J Immunol. 1969;103(5):1000–5.
12. Huber H, Michlmayr G, Fudenberg HH. The effect of antilymphocyte globulin on human monocytes in vitro. Clin Exp Immunol. 1969;5(6):607–17.
13. Cameron DJ. Macrophage mediated tumor cytotoxicity–function of macrophages in human renal allograft recipients. Jpn J Exp Med. 1983;53(1):19–26.
14. Yoshimura S, Gotoh S, Kamada N. Immunological tolerance induced by liver grafting in the rat: splenic macrophages and T cells mediate distinct phases of immunosuppressive activity. Clin Exp Immunol. 1991;85(1):121–7.
15. Gray CM, Smit JA, Myburgh JA. Identification of non-T suppressor cells with possible contra-interleukin-2 properties in non-human primates tolerant to their renal allograft. Afr J Health Sci. 1995;2(3):354–8.
16. Dugast AS, Haudebourg T, Coulon F, Heslan M, Haspot F, Poirier N, et al. Myeloid-derived suppressor cells accumulate in kidney allograft tolerance and specifically suppress effector T cell expansion. J Immunol. 2008;180(12):7898–906.
17. Mazzoni A, Bronte V, Visintin A, Spitzer JH, Apolloni E, Serafini P, et al. Myeloid suppressor lines inhibit T cell responses by an NO-dependent mechanism. J Immunol. 2002;168(2):689–95.
18. Dilek N, Poirier N, Usal C, Martinet B, Blancho G, Vanhove B. Control of transplant tolerance and intragraft regulatory T cell localization by myeloid-derived suppressor cells and CCL5. J Immunol. 2012;188(9):4209–16.
19. Bronte V, Apolloni E, Cabrelle A, Ronca R, Serafini P, Zamboni P, et al. Identification of a CD11b(+)/Gr-1(+)/CD31(+) myeloid progenitor capable of activating or suppressing CD8(+) T cells. Blood. 2000;96(12):3838–46.
20. Bronte V, Wang M, Overwijk WW, Surman DR, Pericle F, Rosenberg SA, et al. Apoptotic death of CD8+ T lymphocytes after immunization: induction of a suppressive population of Mac-1+/Gr-1+ cells. J Immunol. 1998;161(10):5313–20.
21. Zhang W, Liang S, Wu J, Horuzsko A. Human inhibitory receptor immunoglobulin-like transcript 2 amplifies CD11b+Gr1+ myeloid-derived suppressor cells that promote long-term survival of allografts. Transplantation. 2008;86(8):1125–34.
22. Liu J, Liu Z, Witkowski P, Vlad G, Manavalan JS, Scotto L, et al. Rat CD8+ FOXP3+ T suppressor cells mediate tolerance to allogeneic heart transplants, inducing PIR-B in APC and rendering the graft invulnerable to rejection. Transpl Immunol. 2004;13(4):239–47.

23. De Wilde V, Van Rompaey N, Hill M, Lebrun JF, Lemaitre P, Lhomme F, et al. Endotoxin-induced myeloid-derived suppressor cells inhibit alloimmune responses via heme oxygenase-1. Am J Transplant. 2009;9(9):2034–47.
24. Yamashita K, Ollinger R, McDaid J, Sakahama H, Wang H, Tyagi S, et al. Heme oxygenase-1 is essential for and promotes tolerance to transplanted organs. Faseb J. 2006;20(6):776–8.
25. Braudeau C, Bouchet D, Tesson L, Iyer S, Remy S, Buelow R, et al. Induction of long-term cardiac allograft survival by heme oxygenase-1 gene transfer. Gene Ther. 2004;11(8):701–10.
26.•• Garcia MR, Ledgerwood L, Yang Y, Xu J, Lal G, Burrell B, et al. Monocytic suppressive cells mediate cardiovascular transplantation tolerance in mice. J Clin Invest. 2010;120(7):2486–96. *This is the first demonstration that monocyte-derived suppressor cells are required for the induction of transplantation tolerance.*
27. Bronte V, Zanovello P. Regulation of immune responses by L-arginine metabolism. Nat Rev Immunol. 2005;5(8):641–54.
28. Huang B, Pan PY, Li Q, Sato AI, Levy DE, Bromberg J, et al. Gr-1+ CD115+ immature myeloid suppressor cells mediate the development of tumor-induced T regulatory cells and T-cell anergy in tumor-bearing host. Cancer Res. 2006;66(2):1123–31.
29.•• Marigo I, Bosio E, Solito S, Mesa C, Fernandez A, Dolcetti L, et al. Tumor-induced tolerance and immune suppression depend on the C/EBPbeta transcription factor. Immunity. 2010;32(6):790–802. *This is the first demonstration that adoptive transfer of MDSC can be use in the absence of immunosuppressive therapy to induce transplantation tolerance.*
30. Drujont L, Carretero-Iglesia L, Bouchet-Delbos L, Beriou G, Merieau E, Hill M, et al. Evaluation of the therapeutic potential of bone marrow-derived myeloid suppressor cell (MDSC) adoptive transfer in mouse models of autoimmunity and allograft rejection. PLoS One. 2014;9(6):e100013.
31. Adeegbe D, Serafini P, Bronte V, Zoso A, Ricordi C, Inverardi L. In vivo induction of myeloid suppressor cells and CD4(+)Foxp3(+) T regulatory cells prolongs skin allograft survival in mice. Cell Transplant. 2011;20(6):941–54.
32. Turnquist HR, Zhao Z, Rosborough BR, Liu Q, Castellaneta A, Isse K, et al. IL-33 expands suppressive CD11b+ Gr-1(int) and regulatory T cells, including ST2L+ Foxp3+ cells, and mediates regulatory T cell-dependent promotion of cardiac allograft survival. J Immunol. 2011;187(9):4598–610.
33. Matta BM, Lott JM, Mathews LR, Liu Q, Rosborough BR, Blazar BR, et al. IL-33 is an unconventional Alarmin that stimulates IL-2 secretion by dendritic cells to selectively expand IL-33R/ST2+ regulatory T cells. J Immunol. 2014;193(8):4010–20.
34. Thierry A, Giraud S, Robin A, Barra A, Bridoux F, Ameteau V, et al. The alarmin concept applied to human renal transplantation: evidence for a differential implication of HMGB1 and IL-33. PLoS One. 2014;9(2):e88742.
35. Yin H, Li XY, Jin XB, Zhang BB, Gong Q, Yang H, et al. IL-33 prolongs murine cardiac allograft survival through induction of TH2-type immune deviation. Transplantation. 2010;89(10):1189–97.
36. Brunner SM, Schiechl G, Falk W, Schlitt HJ, Geissler EK, Fichtner-Feigl S. Interleukin-33 prolongs allograft survival during chronic cardiac rejection. Transpl Int. 2011;24(10):1027–39.
37. Wu T, Sun C, Chen Z, Zhen Y, Peng J, Qi Z, et al. Smad3-deficient CD11b(+)Gr1(+) myeloid-derived suppressor cells prevent allograft rejection via the nitric oxide pathway. J Immunol. 2012;189(10):4989–5000.
38. Thomas DA, Massague J. TGF-beta directly targets cytotoxic T cell functions during tumor evasion of immune surveillance. Cancer Cell. 2005;8(5):369–80.
39. Luo X, Pothoven KL, McCarthy D, DeGutes M, Martin A, Getts DR, et al. ECDI-fixed allogeneic splenocytes induce donor-specific tolerance for long-term survival of islet transplants via two distinct mechanisms. Proc Natl Acad Sci U S A. 2008;105(38):14527–32.
40. Chen G, Kheradmand T, Bryant J, Wang S, Tasch J, Wang JJ, et al. Intragraft CD11b(+) IDO(+) cells mediate cardiac allograft tolerance by ECDI-fixed donor splenocyte infusions. Am J Transplant. 2012;12(11):2920–9.
41. Corlett L, Davies DH. Reduced lysis by CD8+ cytotoxic T cells in mixed lymphocyte reactions induced via CD4+ T cells exposed to chemically modified antigen presenting cells. Immunology. 1995;84(3):488–94.
42. Karpus WJ, Peterson JD, Miller SD. Anergy in vivo: down-regulation of antigen-specific CD4+ Th1 but not Th2 cytokine responses. Int Immunol. 1994;6(5):721–30.
43. Chou HS, Hsieh CC, Charles R, Wang L, Wagner T, Fung JJ, et al. Myeloid-derived suppressor cells protect islet transplants by B7-H1 mediated enhancement of T regulatory cells. Transplantation. 2012;93(3):272–82.
44. Chou HS, Hsieh CC, Yang HR, Wang L, Arakawa Y, Brown K, et al. Hepatic stellate cells regulate immune response by way of induction of myeloid suppressor cells in mice. Hepatology. 2011;53(3):1007–19.
45. Hsieh CC, Chou HS, Yang HR, Lin F, Bhatt S, Qin J, et al. The role of complement component 3 (C3) in differentiation of myeloid-derived suppressor cells. Blood. 2013;121(10):1760–8.
46. Arakawa Y, Qin J, Chou HS, Bhatt S, Wang L, Stuehr D, et al. Cotransplantation with myeloid-derived suppressor cells protects cell transplants: a crucial role of inducible nitric oxide synthase. Transplantation. 2014;97(7):740–7.
47. Hongo D, Tang X, Baker J, Engleman EG, Strober S. Requirement for interactions of natural killer T cells and myeloid-derived suppressor cells for transplantation tolerance. Am J Transplant. 2014;14(11):2467–77.
48. Bronte V, Serafini P, De Santo C, Marigo I, Tosello V, Mazzoni A, et al. IL-4-induced arginase 1 suppresses alloreactive T cells in tumor-bearing mice. J Immunol. 2003;170(1):270–8.
49. Liao J, Wang X, Bi Y, Shen B, Shao K, Yang H, et al. Dexamethasone potentiates myeloid-derived suppressor cell function in prolonging allograft survival through nitric oxide. J Leukoc Biol. 2014;96(5):675–84.
50.• Luan Y, Mosheir E, Menon MC, Wilson D, Woytovich C, Ochando J, et al. Monocytic myeloid-derived suppressor cells accumulate in renal transplant patients and mediate CD4(+) Foxp3(+) Treg expansion. Am J Transplant. 2013;13(12):3123–31. *This is the first report that demonstrated that CD11b+CD33+HLA-DR- myeloid derived suppressor cells from human transplant recipients expand Treg in vitro and correlate with in vivo presence of Treg.*
51. Hoechst B, Gamrekelashvili J, Manns MP, Greten TF, Korangy F. Plasticity of human Th17 cells and iTregs is orchestrated by different subsets of myeloid cells. Blood. 2011;117(24):6532–41.
52. Varga G, Ehrchen J, Tsianakas A, Tenbrock K, Rattenholl A, Seeliger S, et al. Glucocorticoids induce an activated, anti-inflammatory monocyte subset in mice that resembles myeloid-derived suppressor cells. J Leukoc Biol. 2008;84(3):644–50.
53. Ochando JC, Conde P. Editorial: Dexamethasone and MDSC in transplantation: yes to NO. J Leukoc Biol. 2014;96(5):669–71.
54.• Riquelme P, Tomiuk S, Kammler A, Fandrich F, Schlitt HJ, Geissler EK, et al. IFN-gamma-induced iNOS expression in mouse regulatory macrophages prolongs allograft survival in fully immunocompetent recipients. Mol Ther. 2013;21(2):409–22. *This manuscript evaluates the ability of different in vitro generated macrophage subsets to prolong allograft survival in cardiac allograft recipient mice.*
55.•• Hutchinson JA, Riquelme P, Sawitzki B, Tomiuk S, Miqueu P, Zuhayra M, et al. Cutting edge: immunological consequences and trafficking of human regulatory macrophages administered to renal transplant recipients. J Immunol. 2011;187(5):2072–8. *This is the*

first report investigating the clinical applications of regulatory macrophages as an adjunct immunosuppressive therapy in human kidney transplant recipients.

56. Dutta P, Hullett DA, Roenneburg DA, Torrealba JR, Sollinger HW, Harn DA, et al. Lacto-N-fucopentaose III, a pentasaccharide, prolongs heart transplant survival. Transplantation. 2010;90(10): 1071–8.
57. Srivastava MK, Zhu L, Harris-White M, Kar UK, Huang M, Johnson MF, et al. Myeloid suppressor cell depletion augments antitumor activity in lung cancer. PLoS One. 2012;7(7):e40677.

JLB

Editorial

Editorial: **Dexamethasone and MDSC in transplantation: yes to NO**

J. C. Ochando[1] *and P. Conde*

Department of Nephrology, Icahn School of Medicine at Mount Sinai, New York, New York, USA

RECEIVED MAY 29, 2014; REVISED JULY 8, 2014; ACCEPTED JULY 25, 2014. DOI: 10.1189/jlb.3CE0514-272R

SEE CORRESPONDING ARTICLE ON PAGE 675

The progress of immunosuppressive therapy has dramatically improved the short-term results of organ transplantation. However, no immunosuppressive drug is devoid of side-effects, and despite multiple therapeutic strategies to use immunosuppressive drugs in a less toxic manner, no alternative regimen has seriously challenged the universal use of these drugs in transplantation until recently. Immune cells with suppressive function have newly emerged as potential therapeutic approaches for the induction of prolonged allograft survival in a mature immune system that is free from immune suppression and chronic rejection. In this respect, manipulation of myeloid cells with potent inhibitory activity represents an innovative therapeutic methodology to achieve this goal, and the term MDSC has been proposed recently to define cells of myeloid origin with suppressor function [1].

As negative regulators of the immune response, MDSC includes a morphologically and functionally heterogeneous population of myeloid progenitor cells, which consist of monocytes, macrophages, granulocytes, DCs, and immature myeloid cells at different stages of differentiation. Given the wide range of cell types that may be included in this category, finding a phenotypic profile that characterizes all of them has been a difficult task. In mice, all MDSCs express the cell-surface markers $CD11b^+Gr1^+$ [2]. CD11b is a subunit of the b2 integrin macrophage receptor 1, which is expressed in granulocytes, DCs, monocytes, and macrophages and regulates leukocyte adhesion and cell migration. The Gr1 antigen is expressed predominantly on the surface of monocytes/macrophages and granulocytes and is recognized by the RB6-8C5 antibody, which binds to the cell-surface molecules Ly6C and Ly6G.

The most important function of MDSC is to inhibit the cytotoxic response mediated by T lymphocytes and NK cells. However, as a result of their heterogeneous phenotype, MDSCs can use diverse mechanisms to control immune responses. Tumor-derived MDSCs inhibit T cell responses though reactive oxygen species. In addition, MDSC-mediated depletion of nutrients required by T cell growth and differentiation, such as of L-arginine and L-cysteine, has been reported to inhibit T cell responses via iNOS [2].

Although described initially in cancer patients, MDSCs are also present in other inflammatory settings, including solid organ transplantation. MDSCs accumulate in the allografts of tolerant recipients and mediate the induction of indefinite allograft survival by inhibiting T cell proliferation and expanding the numbers of graft-infiltrating regulatory T cells [3]. As a result of their ability to manipulate the immune response effectively, several culture conditions for the generation of MDSCs in vitro have been developed. Whereas most methods use a combination of cytokines (IL-4, IL-6, IL-13, and IL-33), growth factors (vascular endothelial growth factor), and inflammatory mediators (PGE2, cyclooxygenase, and hypoxia-inducible factor 1α) [2], the effects of common immunosuppressive drugs in MDSC development, such as glucocorticoids, are largely unknown. Glucocorticoids are steroid drugs with anti-inflammatory and immunosuppressant effects that are given routinely to transplant recipient patients. Whereas the beneficial effects of glucocorticoids have been long demonstrated, the mechanisms of action by which steroid hormones mediate their suppressive function in transplant recipients are not fully understood.

In this issue of the *Journal of Leukocyte Biology*, Liao et al. [4]. report that the glucocorticoid Dex significantly prolongs skin-graft survival to fully mismatched allografts. Mechanistically, the authors show that in vivo Dex treatment in transplant recipients results in a significant increase in the number of $CD11b^+Gr1^+$ MDSCs systemically (allograft, draining lymph node, spleen, blood, and bone marrow). Interestingly, Dex treatment induces the expression the chemokine receptor CXCR2 in MDSCs, which is necessary for their migration into the allograft. Interestingly, the interference with CXCR2, using an in vivo blocking mAb, prevents graft-survival prolongation despite Dex treatment. This finding unmasks a previously unrecognized mechanism of action of glucocorticoids and is consistent with an

Abbreviations: DC=dendritic cell, Dex=dexamethasone, GR=glucocorticoid receptor, Gr1=granulocyte differentiation antigen 1, L-NMMA=NOS inhibitor N^G-monomethyl-L-arginine, MDSC=myeloid-derived suppressor cell

1. Correspondence: Icahn School of Medicine at Mount Sinai, Hess Center for Science and Medicine, 1470 Madison Ave., New York, NY 10029, USA. E-mail: jordi.ochando@mssm.edu

earlier report, which demonstrated that MDSC migration to the allografts was required for the induction of indefinite allograft survival [3]. It also extends the findings from the Bernard Vanhove laboratory [5], which described the critical role for chemokine and chemokine receptor expression by MDSCs (CCL5/CCR5) in the control of kidney transplantation tolerance. Interestingly, Liao et al. [4] associate the up-regulation of CXCR2 expression with GR expression, as blocking GR with RU486 diminishes CXCR2 expression, reduces MDSC recruitment to the allografts, and diminishes graft survival.

Liao et al. [4] also demonstrate that Dex-induced MDSCs produce lower levels of TNF-α and higher levels of the immune modulatory cytokine IL-10. This is consistent with a previous report, which showed that LPS-induced MDSCs produce large amounts of IL-10 that were able to prolong graft survival in a skin-transplant model. In their study, Le Moine and colleagues [6] demonstrated that blocking IL-10 inhibited the suppressive function of MDSC, which resulted in early skin-graft rejection. This is consistent with a previous study, which demonstrated that Dex induces an anti-inflammatory monocyte that resembles MDSC. In their study, Sunderkoetter and colleagues [7] demonstrated that $CD11b^+Gr1^+$ myeloid cells up-regulate the expression of anti-inflammatory cytokine IL-10 and down-regulate the expression of the inflammatory cytokine IL-6 following 48 h of Dex treatment. In addition, Dex-treated monocytes were shown to increase motility and transmigration capacity, indicating that glucocorticoid-induced monocytes not only have an anti-inflammatory activity, but they can also migrate more rapidly to the inflammation site in vivo. On the contrary, the ability of glucocorticoid-treated $CD11b^+Gr1^+$ myeloid cells to suppress T cell proliferation was not investigated by Sunderkoetter and colleagues [7].

The main finding of Liao and colleagues [4] is that Dex-induced MDSCs produce large amounts of NO in the recipient allografts. Treatment with L-NMMA, which competitively inhibits the generation of NO from arginine and is a useful tool for inhibition of NO-mediated effects, results in MDSC loss of suppression function and abrogation of prolonged allograft survival. Furthermore, the authors demonstrated the critical role for NO in Dex-induced MDSC in a very elegant experiment. Adoptive transfer of Dex-treated MDSC but not Dex + L-NMMA-treated MDSCs was able to prolong allograft survival in MDSC-depleted recipients. These results are in agreement with previous literature described, which demonstrated that MDSCs, required for the induction of indefinite allograft survival, express high levels of iNOS. The critical role of NO in transplantation was demonstrated by blocking iNOS with aminoguanidine in vivo, which results in rapid rejection of all kidney donor allografts in long-term, tolerant recipients (>120 days post-transplant) [8]. The reported allograft protection mediated by iNOS may be a result of direct inhibitory effects of NO or through its reaction with the superoxide anion to form peroxynitrite, which is highly toxic [2] (**Fig. 1**).

In summary, the findings by Liao et al. [4] (in this issue) provide novel, mechanistic insights linking the necessary role of MDSCs in transplantation and Dex. The present study unveils a novel protocol to induce MDSCs in vivo, which compliments previous studies aiming at preventing MDSC function. As MDSCs were described initially in cancer patients and tumor-bearing mice and are, in part, responsible for the inhibition of the cell-mediated immune response against the tumor, most therapeutic application with MDSCs proposes to reduce their expansion and inhibit their activation [2]. However, MDSCs have considerable relevance to the crucial problem as to why a growing tumor

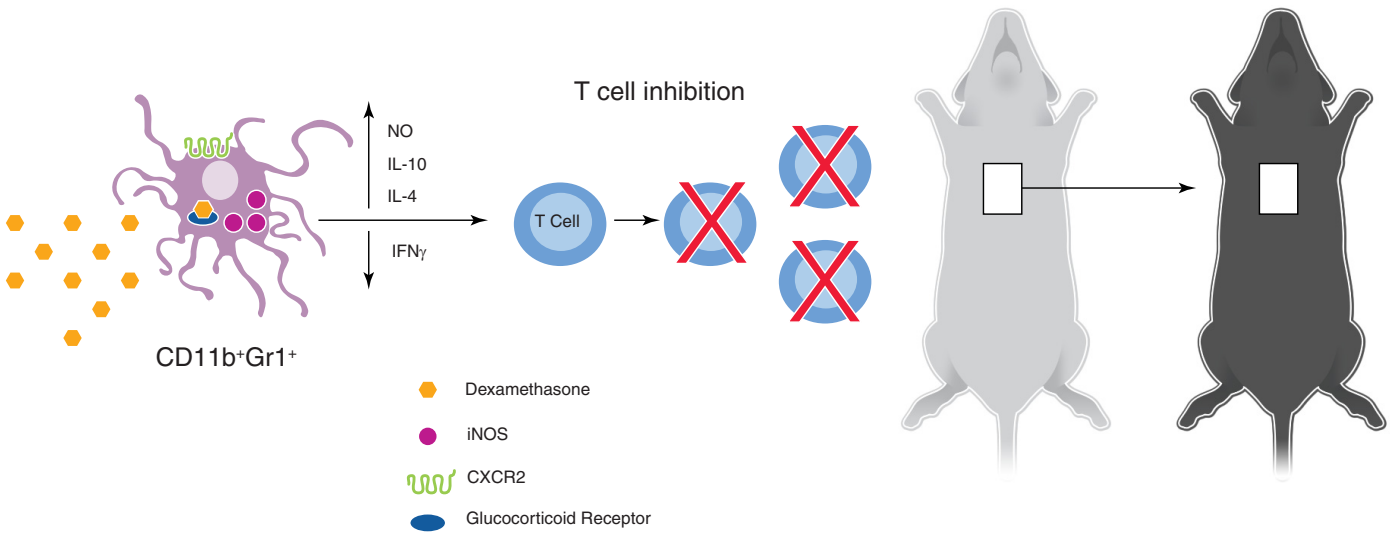

Figure 1. Dex-induced MDSCs mediate T cell suppression and prolong skin allograft survival. In vivo-induced $CD11b^+Gr1^+$ MDSCs secrete IL-4 and IL-10 in transplant recipients following Dex treatment. Dex-induced $CD11b^+Gr1^+$ MDSCs inhibit T cell proliferation and prolong fully allogeneic skin-graft survival through NO-dependent mechanisms.

cannot be rejected despite the recognition of tumor-associated antigens, and manipulation of MDSCs has been used to prevent allograft rejection. The Vincenzo Bronte laboratory [9] generated fully competent MDSCs, based on the analysis of cytokines and soluble factors released within the tumor, and used these in vitro-generated, bone marrow-derived MDSCs to induce tolerance to islet allografts in mice.

Future studies that investigate the glucocorticoid-dependent mechanisms of MDSC development represent a novel, therapeutic approach to achieve long-term allograft survival in the clinic. A recent report identified and characterized IL-10-expressing MDSCs that accumulate in glucocorticoid-treated human kidney transplant recipients [10]. Additional studies that investigate the effects of glucocorticoids in human MDSCs in other immune settings are needed.

ACKNOWLEDGMENTS

Grant support is provided by the American Society of Transplantation/Pfizer Basic Science Faculty Development Grant, Ministerio de Economia y Competitividad SAF2010-15062, and Fundación Mutua Madrileña.

DISCLOSURES

The authors of this manuscript have no conflicts of interest to disclose.

REFERENCES

1. Gabrilovich, D. I., Bronte, V., Chen, S. H., Colombo, M. P., Ochoa, A., Ostrand-Rosenberg, S., Schreiber, H. (2007) The terminology issue for myeloid-derived suppressor cells. *Cancer Res.* **67,** 425; author reply 426.
2. Ochando, J. C., Chen, S. H. (2012) Myeloid-derived suppressor cells in transplantation and cancer. *Immunol. Res.* **54,** 275–285.
3. Garcia, M. R., Ledgerwood, L., Yang, Y., Xu, J., Lal, G., Burrell, B., Ma, G., Hashimoto, D., Li, Y., Boros, P., Grisotto, M., van Rooijen, N., Matesanz, R., Tacke, F., Ginhoux, F., Ding, Y., Chen, S. H., Randolph, G., Merad, M., Bromberg, J. S., Ochando, J. C. (2010) Monocytic suppressive cells mediate cardiovascular transplantation tolerance in mice. *J. Clin. Invest.* **120,** 2486–2496.
4. Liao, J., Wang, X., Bi, Y., Shen, B., Shao, K., Yang, H., Lu, Y., Zhang, Z., Chen, X., Liu, H., Wang, J., Chu, Y., Xue, L., Liu, G. (2014) Dexamethasone potentiates myeloid-derived suppressor cell function in prolonging allograft survival through nitric oxide. *J. Leukoc. Biol.* **96,** 675–684.
5. Dilek, N., Poirier, N., Usal, C., Martinet, B., Blancho, G., Vanhove, B. (2012) Control of transplant tolerance and intragraft regulatory T cell localization by myeloid-derived suppressor cells and CCL5. *J. Immunol.* **188,** 4209–4216.
6. De Wilde, V., Van Rompaey, N., Hill, M., Lebrun, J. F., Lemaitre, P., Lhomme, F., Kubjak, C., Vokaer, B., Oldenhove, G., Charbonnier, L. M., Cuturi, M. C., Goldman, M., Le Moine, A. (2009) Endotoxin-induced myeloid-derived suppressor cells inhibit alloimmune responses via heme oxygenase-1. *Am. J. Transplant.* **9,** 2034–2047.
7. Varga, G., Ehrchen, J., Tsianakas, A., Tenbrock, K., Rattenholl, A., Seeliger, S., Mack, M., Roth, J., Sunderkoetter, C. (2008) Glucocorticoids induce an activated, anti-inflammatory monocyte subset in mice that resembles myeloid-derived suppressor cells. *J. Leukoc. Biol.* **84,** 644–650.
8. Dugast, A. S., Haudebourg, T., Coulon, F., Heslan, M., Haspot, F., Poirier, N., Vuillefroy de Silly, R., Usal, C., Smit, H., Martinet, B., Thebault, P., Renaudin, K., Vanhove, B. (2008) Myeloid-derived suppressor cells accumulate in kidney allograft tolerance and specifically suppress effector T cell expansion. *J. Immunol.* **180,** 7898–7906.
9. Marigo, I., Bosio, E., Solito, S., Mesa, C., Fernandez, A., Dolcetti, L., Ugel, S., Sonda, N., Bicciato, S., Falisi, E., Calabrese, F., Basso, G., Zanovello, P., Cozzi, E., Mandruzzato, S., Bronte, V. (2010) Tumor-induced tolerance and immune suppression depend on the C/EBPbeta transcription factor. *Immunity* **32,** 790–802.
10. Luan, Y., Mosheir, E., Menon, M. C., Wilson, D., Woytovich, C., Ochando, J., Murphy, B. (2013) Monocytic myeloid-derived suppressor cells accumulate in renal transplant patients and mediate CD4(+) Foxp3(+) Treg expansion. *Am. J. Transplant.* **13,** 3123–3131.

KEY WORDS:
transplantation tolerance · immune regulation

Editorial: **The intricacy of choice: can bacteria decide what type of myeloid cells to stimulate?**

By Dmitry I. Gabrilovich[1]

The Wistar Institute, Philadelphia, Pennsylvania, USA

RECEIVED MAY 28, 2014; REVISED JULY 8, 2014; ACCEPTED JULY 25, 2014. DOI: 10.1189/jlb.4CE0514-271R

SEE CORRESPONDING ARTICLE ON PAGE 685

Sepsis is a major cause of death in the Western world with high mortality rates in ICUs. The disease is characterized by an excessive and dysregulated immune response to microbial infections, coagulation abnormalities leading to capillary leakage, lung damage, and finally, multiple organ failure [1]. It is known that most septic patients in ICUs, in addition to hyperinflammatory response, suffer from a hypoinflammatory state, which often leads to sepsis-induced multiorgan dysfunction and death. This suggests that sepsis-induced immunosuppression is a significant factor contributing to these deaths. MDSCs may be a critical element in the development of such a hypoinflammatory state and thus, in the outcome of the disease.

Although MDSCs were described originally in cancer [2], it has now become increasingly clear that MDSCs play an important role in the regulation of immune responses in many pathological conditions not directly associated with

Abbreviations: G^-=gram-negative, G^+=gram-positive, ICU=intensive care unit, M-MDSC=monocytic-myeloid-derived suppressor cell, MDSC=myeloid-derived suppressor cell, PMN=polymorphonuclear neutrophil, PMN-MDSC=polymorphonuclear neutrophil-myeloid-derived suppressor cell

1. Correspondence: The Wistar Institute, 3601 Spruce St., Rm. 118, Philadelphia, PA 19104, USA. E-mail: dgabrilovich@wistar.org